



ΠΑΝΕΠΙΣΤΗΜΙΟ ΙΩΑΝΝΙΝΩΝ  
ΣΧΟΛΗ ΘΕΤΙΚΩΝ ΕΠΙΣΤΗΜΩΝ  
ΤΜΗΜΑ ΧΗΜΕΙΑΣ

**Khalid Mahmud**

**ΠΑΡΑΣΚΕΥΗ ΚΑΙ ΧΑΡΑΚΤΗΡΙΣΜΟΣ  
ΔΙΦΑΣΙΚΩΝ ΦΩΣΦΟΡΙΚΩΝ ΥΛΙΚΩΝ ΓΙΑ ΤΗΝ  
ΑΠΟΜΑΚΡΥΝΣΗ ΟΡΓΑΝΙΚΩΝ ΧΡΩΣΤΙΚΩΝ  
ΑΠΟ ΥΔΑΤΙΚΑ ΔΙΑΛΥΜΑΤΑ**

**Διδακτορική Διατριβή**

Ιωάννινα 2009



UNIVERSITY OF IOANNINA  
SCHOOL OF NATURAL SCIENCE  
DEPARTMENT OF CHEMISTRY

**PREPARATION AND CHARACTERIZATION OF  
BIPHASIC PHOSPHATE MATERIALS FOR  
REMOVAL OF ORGANIC DYES FROM  
AQUEOUS SOLUTION**

**By**

**Khalid Mahmud**

**Supervised by Associate Professor Tiverios Vaimakis**

University of Ioannina, Greece (Hellas)

This thesis submitted to Department of Chemistry, University of  
Ioannina in partial fulfillment of the requirements of the degree

of

**DOCTOR OF PHILOSOPHY (PhD)**

Ioannina, June, 2009



ΠΑΝΕΠΙΣΤΗΜΙΟ ΙΩΑΝΝΙΝΩΝ  
ΣΧΟΛΗ ΘΕΤΙΚΩΝ ΕΠΙΣΤΗΜΩΝ  
ΤΜΗΜΑ ΧΗΜΕΙΑΣ

**Khalid Mahmud**

**ΠΑΡΑΣΚΕΥΗ ΚΑΙ ΧΑΡΑΚΤΗΡΙΣΜΟΣ  
ΔΙΦΑΣΙΚΩΝ ΦΩΣΦΟΡΙΚΩΝ ΥΛΙΚΩΝ ΓΙΑ ΤΗΝ  
ΑΠΟΜΑΚΡΥΝΣΗ ΟΡΓΑΝΙΚΩΝ ΧΡΩΣΤΙΚΩΝ  
ΑΠΟ ΥΔΑΤΙΚΑ ΔΙΑΛΥΜΑΤΑ**

**Διδακτορική Διατριβή**

ΕΠΤΑΜΕΛΗΣ ΕΞΕΤΑΣΤΙΚΗ ΕΠΙΤΡΟΠΗ

- Τ. ΒΑΪΜΑΚΗΣ, Αναπλ. Καθηγητής (Τμ. Χημείας, ΠΙ, Επιβλέπων Καθηγητής)  
Μ. ΚΑΡΑΚΑΣΙΔΗΣ, Αναπλ. Καθηγητής (Τμ. Μηχανικών Επιστήμης Υλικών, ΠΙ,  
Μέλος συμβουλευτικής επιτροπής)  
Χ. ΤΡΑΠΑΛΗΣ, Ερευνητής ΕΚΕΦΕ (Μέλος συμβουλευτικής επιτροπής)  
Φ. ΠΟΜΩΝΗΣ, Καθηγητής (Τμήμα Χημείας, ΠΙ)  
Τ. ΑΛΜΠΙΑΝΗΣ, Καθηγητής (Τμήμα Χημείας, ΠΙ)  
Θ. ΜΠΑΚΑΣ, Καθηγητής (Τμήμα Φυσικής, ΠΙ)  
Δ. ΠΕΤΡΑΚΗΣ, Επίκουρος Καθηγητής (Τμήμα Χημείας, ΠΙ)

**Εξεταστική Επιτροπή για την υποστήριξη της Διδακτορικής Διατριβής  
του κ. Khalid Mahmud**

Προς  
Το Τμήμα Χημείας  
Παν/μίου Ιωαννίνων

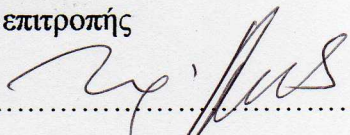
**Θέμα:** «Απόφαση Επταμελούς Εξεταστικής επιτροπής ενώπιον της οποίας ο κ. Khalid Mahmud υποστήριξε τη Διδακτορική του Διατριβή»


Σήμερα 9/10/2009 και ώρα 5μ.μ. έγινε δημόσια παρουσίαση της Διδακτορικής Διατριβής με θέμα: «ΠΑΡΑΣΚΕΥΗ ΚΑΙ ΧΑΡΑΚΤΗΡΙΣΜΟΣ ΔΙΦΑΣΙΚΩΝ ΦΩΣΦΟΡΙΚΩΝ ΥΛΙΚΩΝ ΓΙΑ ΤΗΝ ΑΠΟΜΑΚΡΥΝΣΗ ΟΡΓΑΝΙΚΩΝ ΧΡΩΣΤΙΚΩΝ ΑΠΟ ΥΔΑΤΙΚΑ ΔΙΑΛΥΜΑΤΑ», από τον υποψήφιο διδάκτορα Khalid Mahmud. Η παρουσίαση έλαβε χώρα στην αίθουσα Συνεδριάσεων (X2-090) του Τμήματος Χημείας, Πανεπιστημίου Ιωαννίνων, ενώπιον της, κατά τον νόμο, επταμελούς εξεταστικής επιτροπής.

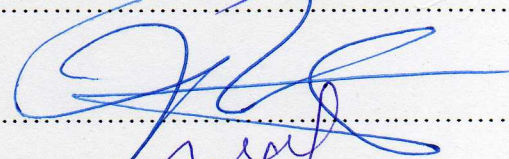
Ο κ. Khalid Mahmud, ανέπτυξε επί μία ώρα τα κυριότερα αποτελέσματα της Διατριβής του και στη συνέχεια απάντησε σε σειρά ερωτημάτων της εξεταστικής επιτροπής και του ακροατηρίου.

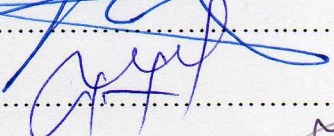
Κατόπιν αποχώρησε ο υποψήφιος και το ακροατήριο και ακολούθησε σύσκεψη μεταξύ των μελών της επταμελούς εξεταστικής επιτροπής. Η επιτροπή έκρινε ότι η Διατριβή είναι πρωτότυπη και συμβάλει στην πρόοδο της επιστήμης. Προχώρησε δε στην έγκριση αυτής με βαθμό «**Άριστα**» και αποφάσισε να προτείνει την απονομή του Τίτλου του Διδάκτορα στον Khalid Mahmud από το Τμήμα Χημείας του Πανεπιστημίου Ιωαννίνων.

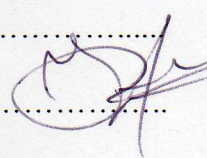
Τα μέλη της εξεταστικής επιτροπής

Τ. ΒΑΪΜΑΚΗΣ, Αναπλ. Καθηγητής  
(Τμ. Χημείας, Π.Ι., Επιβλέπων Καθηγητής)..... 

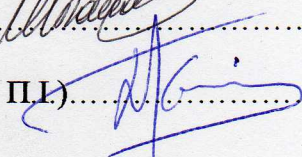
Μ. ΚΑΡΑΚΑΣΙΔΗΣ, Αναπλ. Καθηγητής  
(Τμ. Μηχανικών Επιστήμης Υλικών, Π.Ι., Μέλος συμβουλευτικής επιτροπής)..... 

Χ. ΤΡΑΠΑΛΗΣ, Ερευνητής ΕΚΕΦΕ  
(Μέλος συμβουλευτικής επιτροπής)..... 

Φ. ΠΟΜΩΝΗΣ, Καθηγητής (Τμήμα Χημείας, Π.Ι.)..... 

Τ. ΑΛΜΠΙΑΝΗΣ, Καθηγητής (Τμήμα Χημείας, Π.Ι.)..... 

Θ. ΜΠΑΚΑΣ, Καθηγητής (Τμήμα Φυσικής, Π.Ι.)..... 

Δ. ΠΕΤΡΑΚΗΣ, Επίκουρος Καθηγητής (Τμήμα Χημείας, Π.Ι.)..... 

---

# TABLE OF CONTENTS

---

<b>Title</b>	<b>Page</b>
<b>Περίληψη</b>	1
<b>Abstract</b>	4
<b>Acknowledgement</b>	7
<b>1. GENERAL INTRODUCTION</b>	9
1.1 General description of phosphate materials	9
1.2 Phosphate materials as an adsorbent of dye	11
1.3 Objectives of the present study	12
<b>PART 1</b>	
<b>2. LITERATURE REVIEW</b>	13
2.1 Structure of phosphate material	13
2.2 Chemical properties	13
2.3 Cellular function	16
2.4 Characteristics of inorganic phosphate materials	16
2.5 General description of calcium orthophosphates	17
2.5.1 Amorphous Calcium Phosphate (ACP)	19
2.5.2 Thermal Changes	21
2.6 Tricalcium Phosphate	22
2.6.1 Structure of some calcium phosphate materials	23
2.6.2 Reaction with H <sub>2</sub> O	23
2.7 Calcium pyrophosphate	24
2.8 Octacalcium Phosphate (OCP)	25
2.8.1 A Survey on Different Methods for Synthesizing OCP	27

2.8.2	Thermal transformation of Octacalcium phosphate	33
2.8.3	Solubility and hydrolysis of OCP	34
2.8.4	Stability in aqueous solution	35
2.8.5	Catalytic property	35
2.9	General description of hydroxyapatite	35
2.9.1	Medical uses of hydroxyapatite	37
2.9.2	Hydroxyapatite uses in chromatography	38
2.9.3	Background	39
2.9.4	Key properties	40
2.9.5	Applications	40
2.9.6	Thermal Transformation of Hydroxyapatite	40
2.9.7	The Apatitic Family and Its Importance in the Biomedical Field	42
2.9.8	The role of impurities present in a hydroxyapatite powder	45
2.9.9	Transformations Induced at High Temperature by Plasma Spraying	48
2.9.10	A Survey on Different Methods for Synthesizing Hydroxyapatite	49
2.9.10.1	Wet Preparation	49
2.9.10.2	Sol-gel preparation	52
2.9.10.3	Mechanochemical preparation	58
2.9.10.4	Other methods	59
	<b>REFERENCES</b>	68
3	<b>MATERIALS AND METHODS</b>	87
3.1	Reagents and solutions	88
3.2	Synthesis of Hydroxyapatite	89
3.3	Synthesis of octacalcium phosphate	90
3.4	Characterization	91

3.4.1	XRD	91
3.4.2	FT-IR	92
3.4.3	SEM	92
3.4.4	TG-DTG	92
3.4.5	N <sub>2</sub> Porosimetry	92
4.	<b>RESULTS AND DISCUSSION</b>	93
4.1	XRD analysis of HA	93
4.2	XRD analysis of OCP	95
4.3	FT-IR analysis of HA	98
4.4	FT-IR analysis of OCP	99
4.5	Mechanism of OCP and monetite formation	101
4.6	SEM analysis of HA	102
4.7	SEM analysis of OCP	103
4.8	Thermal analysis of material	108
4.9	Peak separation of material	111
4.10	BET analysis of HA	116
4.11	BET analysis of OCP	117
4.12	Determination of activation energy	123
4.13	Compensation effect and isokinetic temperature	134
4.14	Conclusion	140
	<b>REFERENCES</b>	141

## **PART 2**

5.	Adsorption theory	144
5.1	Isotherms	144
5.2	Adsorbent Characteristics and general requirements	145

5.3	Langmuir Adsorption Isotherm	145
5.3.1	Equation Derivation	146
5.3.2	Equation Fitting	147
5.4	Freundlich equation	148
5.4.1	Freundlich adsorption isotherm	148
5.5	A survey on different methods of adsorption	148
6.	<b>Materials and methods</b>	
6.1	Reagents and solutions	153
6.2	Choice of dye	153
6.3	Choice of adsorbent	155
6.4	Adsorption experiments	156
7.	<b>Results and discussion</b>	
7.1	Zeta potential measurement	158
7.2	Effect of contact time	160
7.3	Effect of concentration	160
7.4	Effect of adsorbent amount	161
7.5	Effect of pH	163
7.6	Kinetic study	165
7.7	Adsorption isotherms	167
7.8	Conclusion	170
	<b><i>REFERENCES</i></b>	171



## Περίληψη:

Η παρούσα μελέτη χωρίζεται σε δυο πειραματικά μέρη. Στο πρώτο μέρος μελετάται η παρασκευή των φωσφορικών υλικών του ασβεστίου με ατομικό λόγο Ca/P ίσο με 1,67 και 1,33, που αντιστοιχούν στο στοιχειομετρικό υδροξυαπατίτη (HA) και φωσφορικό οκτασβέστιο (octacalcium phosphate, OCP), αντίστοιχα. Στο ίδιο μέρος μελετάται η επίδραση της συγκέντρωσης της θρεονίνης, στο σχηματισμό του OCP και της πύρωσης στους 900 °C αυτών. Στο δεύτερο μέρος μελετάται η απομάκρυνση όζω-χρωμάτων από διαλύματά τους, με τη βοήθεια των παρασκευασθέντων φωσφορικών υλικών.

Για την παρασκευή των φωσφορικών υλικών HA και OCP χρησιμοποιήθηκε η τροποποιημένη μέθοδος καταβύθισης (pH shock-wave method) που αναπτύχθηκε στο Εργαστήριο Βιομηχανικής Χημείας, σε συνδυασμό με συσκευή διασκορπισμού υψηλής ενέργειας. Σε διάλυμα 800 mL που περιείχε 0,0538 mol  $\text{Ca}(\text{H}_2\text{PO}_4)_2 \cdot \text{H}_2\text{O}$  και 0,1254 mol  $\text{CaCl}_2$  με Ca/P = 1,67 για την παρασκευή HA ή 0,0538 mol  $\text{Ca}(\text{H}_2\text{PO}_4)_2 \cdot \text{H}_2\text{O}$  και 0,0891 mol  $\text{CaCl}_2$  με Ca/P = 1,33 για την παρασκευή των υλικών OCP. Στο παρασκευασθέν υλικό HA υπολογίστηκαν, με την τεχνική XRD, οι κρυσταλλογραφικοί παράμετροι  $a = 9.427 \text{ \AA}$  and  $c = 6.930 \text{ \AA}$  (εξαγωνικό  $P6_3/m$ ). Η αντίστοιχη ανάλυση για τα υλικά OCP, έδειξε ότι υπάρχουν τρεις φάσεις OCP, monetite και HA. Οι υπολογισθείσες κρυσταλλογραφικές παράμετροι για το OCP έδωσαν  $a = 10,733 \text{ \AA}$ ,  $b = 13,753 \text{ \AA}$  and  $c = 5,832 \text{ \AA}$  (ορθορομβικό  $Pna-21$ ). Οι τιμές αυτές είναι ελαφρός διαφορετικές από αυτές του καθαρού OCP, λόγω της παρουσίας και άλλων φάσεων στη δομή του. Μετά την πύρωσή τους στους 900 °C, δυο φάσεις ανιχνεύονται οι  $\beta$ -TCP (μονοκλινές  $p2/c$ ) και  $\beta$ - $\text{Ca}_2\text{P}_2\text{O}_7$ .

Τα φάσματα FT-IR έδωσαν τις χαρακτηριστικές απορροφήσεις των HA, OCP and  $\beta$ -TCP. Οι μικροφωτογραφίες SEM έδειξαν την διαφορετική μορφολογία των δειγμάτων. Ο HA αποτελείται από μεγάλα συσσωματώματα σφαιρικών σωματιδίων. Τα σωματίδια του δείγματος TH0 ήταν ανομοιόμορφα. Η χρήση θρεονίνης έχει σαν αποτέλεσμα την αλλαγή του σχήματος των σωματιδίων αναλόγως με τη συγκέντρωση, από βελονοειδή για το δείγμα TH2, σε στρογγυλά για το δείγμα TH4 και σφαιρικά για το δείγμα TH6. Τα πυρωμένα δείγματα έδειξαν σωματίδια βοστρυχοειδούς σχήματος.

Η θερμική μετατροπή λαμβάνει χώρα σε τέσσερα διαδοχικά βήματα. Το πρώτο εξώθερμο βήμα (20-400 °C) αποδίδεται κυρίως στην απομάκρυνση μέρους των κρυσταλλικών νερών και του προσροφημένου νερού. Το δεύτερο ενδόθερμο βήμα (400-750 °C) αποδίδεται στην διάσπαση του OCP και monetite σε πυροφωσφορικό ασβέστιο. Το τρίτο εξώθερμο βήμα λαμβάνει χώρα στην περιοχή θερμοκρασιών 750-1100 °C. Οι κύριες μεταβολές που παρατηρούνται είναι η μετατροπή του  $\gamma$ -Ca<sub>2</sub>P<sub>2</sub>O<sub>7</sub> σε  $\beta$ -Ca<sub>2</sub>P<sub>2</sub>O<sub>7</sub> και η αντίδραση του πυροφωσφορικού ασβεστίου με τον HA και ο σχηματισμός  $\beta$ -TCP. Η μερική αφυδάτωση του HA και η μετατροπή του  $\beta$ -TCP σε  $\alpha$ -TCP λαμβάνει χώρα στο τέταρτο βήμα (1100-1400 °C). Στο τέλος του βήματος αυτού παρατηρείται η μερική πυροσυσσώματωση των δειγμάτων εξ αιτίας της τήξης του πυροφωσφορικού ασβεστίου.

Από τις ισόθερμες απορρόφησης-εκρόφησης N<sub>2</sub>, υπολογίζεται με τη χρήση της εξίσωσης BET, η ειδική επιφάνεια (ssa), η οποία ήταν 45-53 m<sup>2</sup>/g για τα μη πυρωμένα δείγματα και 5-6 m<sup>2</sup>/g για τα πυρωμένα.

Στο δεύτερο μέρος της μελέτης μας, πραγματοποιήσαμε πειράματα προσρόφησης για την απομάκρυνση της χρωστικής direct yellow 27 από διαλύματα. Βρέθηκε ότι ο HA έχει την μεγαλύτερη ικανότητα προσρόφησης σε σύγκριση με τα

δείγματα OCP. Στα πειράματα προσρόφησης μελετήθηκε η επίδραση: α) της συγκέντρωσης της χρωστικής, η οποία ήταν 20, 30, 40, 50 and 60 mg/L, β) η ποσότητα του προσροφητικού, η οποία ήταν 0,025, 0,50, 0,1, 0,2 and 0,3 g και το pH, με μεταβολή κατά 1 στην τιμή του από 3,5 έως 11,5. Τα πειράματα έδειξαν ότι η προσρόφηση της χρωστικής αυξάνει με την αύξηση της ποσότητας του προσροφητικού, λόγω της μεγαλύτερης διαθέσιμης επιφάνειας και συνεπώς της μεγαλύτερης ικανότητας προσρόφησης. Η προσρόφηση εξαρτάται σε μεγάλο βαθμό από το pH. Μεγαλύτερη απομάκρυνση της χρωστικής παρατηρείται σε μικρές τιμές pH και αντίστροφα μικρές τιμές απομάκρυνσης σε μεγάλες τιμές pH. Π.χ. για συγκέντρωση χρωστικής 20 mg/L και ποσότητα προσροφητικού 0,2g οι απομάκρυνση ήταν 92% σε pH 3,5 και 24% σε pH 11,5. Οι πειραματικές τιμές της ισόθερμης προσρόφησης δείχνουν να περιγράφονται σε μεγαλύτερο βαθμό από την εξίσωση Langmuir παρά την Freundlich. Με βάση την ισόθερμο Langmuir η μέγιστη ικανότητα προσρόφησης είναι 89,28 mg/g. Συμπερασματικά μπορούμε να πούμε ότι ο υδροξυαπατίτης, ένα υλικό με χαμηλό κόστος παραγωγής, έδειξε εξαιρετική προσροφητική ικανότητα για την απομάκρυνση της χρωστικής direct yellow 27.

## Summary:

The present study was designed for two experimental parts. The first part was constructed to synthesize phosphate materials of Ca/P atomic ratio of 1.67 and 1.33, which are stoichiometry of hydroxyapatite (HA) and octacalcium phosphate (OCP). This part also showed the effect of different concentrations of threonine and calcination effect at 900 °C on octacalcium phosphate. The second part of this study deals with the application of these synthesized phosphate materials, at which we removed azo-dye from aqueous solution.

The high-energy dispersing equipment used in combination with a pH shock-wave method to synthesize HA and OCP. An 800 mL solution of 0.0538 mol of  $\text{Ca}(\text{H}_2\text{PO}_4)_2 \cdot \text{H}_2\text{O}$  and 0.1254 mol of  $\text{CaCl}_2$  with a Ca/P molar ratio of 1.67 (stoichiometry of HA) used for synthesize HA and for the synthesize of OCP, 0.0538 mol of  $\text{Ca}(\text{H}_2\text{PO}_4)_2 \cdot \text{H}_2\text{O}$  and 0.0891 mol of  $\text{CaCl}_2$  with a Ca/P molar ratio of 1.33 (stoichiometry of OCP) used. The obtained powders of HA was detected single phase in XRD analysis and the calculated lattice parameters were  $a = 9.427 \text{ \AA}$  and  $c = 6.930 \text{ \AA}$  (hexagonal  $P6_3/m$ ). From XRD pattern of uncalcination samples of OCP, three phases of OCP, monetite and HA were structurally analyzed. The calculated lattice parameters for OCP were  $a = 10.733 \text{ \AA}$ ,  $b = 13.753 \text{ \AA}$  and  $c = 5.832 \text{ \AA}$  (orthorhombic  $Pna-21$ ). These values were slightly different from standard values, these differences is due to the presence of multiphase and the element content on unit cell. After calcination at 900 °C, two phases of  $\beta$ -TCP (monoclinic  $p2_1/c$ ). and  $\beta$ - $\text{Ca}_2\text{P}_2\text{O}_7$  were detected.

FT-IR analysis showed all the characteristic peaks of HA, OCP and  $\beta$ -TCP. SEM micrograph showed the different morphology of samples. For HA, the observed particles were spherical in shape and highly agglomerated. For TH0 the shape was

ununiform. After used different concentration of threonine the shape changed to needle-like for TH2, spheroidal for TH4 and spherical for TH6. The calcined samples showed the particles of botryoidal shape.

The thermal transformation takes place through four consecutive steps. The first exothermic step (20-400 °C), mainly assigned removal of part of crystalline and adsorbed water. The second step is endothermic (400-750 °C) and this step OCP and monetite decompose to calcium pyrophosphate. The third exothermic step happen between temperature 750-1100 °C. The main transformation observed here  $\gamma\text{-Ca}_2\text{P}_2\text{O}_7$  to  $\beta\text{-Ca}_2\text{P}_2\text{O}_7$  and the reaction between hydroxyapatite and calcium pyrophosphate to form  $\beta\text{-TCP}$ . The partial dehydration of hydroxyapatite and the transformation of  $\beta\text{-TCP}$  to  $\alpha\text{-TCP}$  occurred in fourth step (1100-1400 °C). At the end of the thermal experiment, we observed partial sintering of materials due to melting of pyrophosphate.

The  $\text{N}_2$  adsorption-desorption isotherms for the samples were measured by using BET equation and the observed specific surface areas (ssa) were 45-53  $\text{m}^2/\text{g}$  for uncalcination samples and 5-6  $\text{m}^2/\text{g}$  for calcination samples.

In the second part of our study, batch adsorption experiments were conducted to investigate the removal of dye direct yellow 27, from aqueous solution. We have found that hydroxyapatite has higher adsorption capacity comparing other samples of OCP. The adsorption experiments were carried out to investigate the factors that influence the dye uptake by the adsorbent, such as contact time, dye concentration, adsorbent dosage and effect of pH. The concentration of dye solutions used were 20, 30, 40, 50 and 60 mg/L, adsorbent dosage were 0.025, 0.50, 0.1, 0.2 and 0.3 g and solution pH values were 3.5 until 11.5 with the regular pH difference of 1. The experimental results showed that the percentage of dye removal increases with

increasing the amount of adsorbent. An increase in the adsorption with the adsorbent dosage can attributed to a greater surface area and the availability of more adsorption capacity. The adsorption was greatly pH dependent. The high uptake of the dye observed at low pH and low uptake at high pH. The experimental values were 92% at pH 3.5 and 24% at pH 11.5 for 20 mg/L dye concentration and 0.2g of adsorbent. The adsorption data followed the Langmuir model better than the Freundlich model and the adsorption equilibrium was described well by the Langmuir isotherm model with maximum adsorption capacity 89.28 mg/g. Finally, we can say that, hydroxyapatite showed an excellent adsorptive characteristics for the removal of direct yellow 27 due to its good adsorption capacity and its low production cost.

## ACKNOWLEDGEMENTS

Many thanks to Almighty Allah, who has given me the persuasiveness to successfully complete this work.

My warm thanks to Mr T. Vaimakis, who has given me this broad opportunity by his kind supervision. Not only academically, even many other cases his guideline never feels me far away from home. His helping hand and valuable time really help me a lot. Without his kind cooperation, this work would likely not have matured.

I would like to thanks Mr. Albanis for his kind permission to work his laboratory. One important part of this work has done in his laboratory, which could not be fulfill without his kind permission.

I would like to thanks Mr. P. J Pomonis and Mr. Petrakis for their kind help for SEM and porosimetry. They really gave me their kind suggestion about SEM and porosimetry analysis even their busy time.

I would like to thanks Mr. M. Karakasidis and Mr. C. Trapalis to be my co supervisor and their valuable time to discuss my work.

Many thanks to Mr. Thomas Bakas. I am very grateful to him. One important analysis of XRD, he gave a lot of his valuable time to me and his kind opinion really help me a lot to prepare this part of my work. Like him, Mr. Nikos Kourkoumelis also help me a lot for XRD software to find solution of my material. Many thanks to Nikos for his time and kind behavior to me.

Many thanks to Vasilios Sakkas and his laboratory team for their helping hand during my adsorption work in their lab.

Many many thanks to Dr. Azharul Islam, who has given me a broad idea for adsorption part of my study. His shadow helping during the whole work really makes it possible. His helping had and kind help unforgettable.

I also do many thanks to Angelos, Thsos, Dionisia, Eleni, Christos, Aki and Eleftheria. They did a lot of support and help from beginning till end of my work and their friendly time to me.

I would like to thank Greek State Scholarship Foundation (IKY) for providing me financial support to complete this work.

Finally, I am very grateful to all of these personnel having attached during my work and living in Greece. I wish very happy and healthy life to all of them.



## GENERAL INTRODUCTION

### 1.1. General description of phosphate materials:

Phosphates are naturally present in all soils at varying levels. Much progress in phosphate chemistry and technology has been made in recent years. The name phosphorus came from Greek word which mean “light bearer”. It is discovered in 1669 by an alchemist, H. Brandt. At the end of the 17<sup>th</sup> century, Boyle obtained phosphoric acid by dissolving phosphorous oxide in water. In 1770, phosphorus was recognized to be a main component in animal bone and teeth. In 1840, Liebig clarified the availability of calcium superphosphate for plant nutrition. Phosphate fertilizer represented by calcium superphosphate was the most important material among the inorganic phosphate chemicals.

Phosphate salts are inorganic compounds containing the phosphate ion ( $\text{PO}_4^{3-}$ ), the hydrogen phosphate ion ( $\text{HPO}_4^{2-}$ ), or the dihydrogen phosphate ion ( $\text{H}_2\text{PO}_4^-$ ), along with any cation. Phosphate esters are organic compounds in which the hydrogens of phosphoric acid are replaced by organic groups (e.g., methyl, ethyl, phenyl), with one of their carbon atoms bonding to an oxygen atom in the phosphate group. Nucleic acids and ATP both contain phosphate, bones and teeth contain calcium phosphate. Phosphate rock (mainly calcium phosphate) is one of the four most important basic chemical commodities. Phosphates were formerly used in detergents, which washed into rivers and lakes, causing water blooms of algae and bacteria, such use is now generally outlawed or regulated. Phosphates are still used in fertilizers, baking powder, and toothpaste.

Anthropogenically derived phosphates have their sources in a wide range of organic materials with the result that in occupation areas, burials, food processing areas, latrine areas and animal compounds and driveways the phosphate levels in the soil can be considerably enhanced. Once in the soil, phosphate is generally fixed in an insoluble form to inorganic aluminium, calcium, and iron components, or associates with organic molecules to form insoluble complexes. Fixed in this way it can survive for long periods. In archaeology, identifying concentrations of phosphates through phosphate analysis is extremely useful for the recognition and definition of settlement

sites, and mapping the different levels of activity within a site. Phosphates can also be used to identify the presence of burials in ground where all physical traces have vanished.

Calcium phosphates are used as bone substitutes because of its high compatibility with bone tissues as well as adsorbents because of specific adsorption properties against organic substances. There are many types of calcium phosphate materials such as, hydroxyapatite, octacalcium phosphate, tetracalcium phosphate, tricalcium phosphate, etc. Octacalcium phosphate,  $(Ca_8H_2(PO_4)_6 \cdot 5H_2O)$ , OCP: Ca/P molar ratio= 1.33), often occurs as a transient intermediate in the precipitation of the thermodynamically more stable hydroxyapatite  $(Ca_{10}(PO_4)_6(OH)_2)$ , HA: Ca/P molar ratio=1.67), and has been suggested to be involved in the mineralization of biological tissues, such as bone and dentine. Both OCP and HA are of great scientific interest in the field of biomaterials due to their importance in the formation of mineralized tissue.

In our present study, we used Ca/P molar ratio 1.67 and 1.33, which is stoichiometry of HA and OCP. The method used here pH shock wave method with high speed dispersing equipment. At the same time, we used different concentration of threonine in order to see the effect on calcium phosphate material. Threonine is an essential amino acid, serving as a carrier for phosphate in phosphoproteins. Threonine is present in the heart, central nervous system, and skeletal muscle. It assists in maintaining protein balance in the body and is important in the formation of collagen and elastin. When combined with aspartic acid, methionine aids liver and lipotropic function. Other names for threonine include: THR, amino acid T, and 2-amino-3-hydroxy-butanoic acid. Some spectroscopic measurements, including X-ray diffraction (XRD), fourier transformed infrared spectroscopy (FTIR), scanning electron microscopy (SEM), differential thermal analysis-thermo gravimetric analysis

(DTG-TG) and nitrogen adsorption-desorption porosimetry used for the characterization of material.

## **1.2. Phosphate materials as an adsorbent of dye:**

Modern society cannot ignore the grandness of dye in everyday needs as an aesthetic point of view. Dyes are applied to numerous substrates for example to textiles, leather, cosmetics, plastic, paper, carpet etc. in order to bringing color into our lives. One of the main characteristic of dye is that it must get completely or at least partially soluble in which it is being put to and produce considerable amount of colored wastewater. However, certain kind of dyes can be toxic, carcinogenic or mutagenic and can pose as a hazard to health. The nature of pollution that accompanies different textile and dyeing based industry is primarily due to the non-biodegradable nature of the dyes along with the strong presence of toxic trace metals or acid or alkali carcinogenic aromatic amines traceable in the effluents. The presence of these species in aquatic systems reduces light penetration, which cause to move more slowly photosynthetic activity and also has a tendency to chelate metal ions producing microtoxicity to fish and other organisms.

It is very important that dyes need to be removed before the effluents are discharged into water. It has always been a major problem due to the difficulty of treating such wastewaters by conventional methods. Biological procedures, which are widely utilized in the removal of dye, are very inefficient because of the low biodegradability of dyes. To decontaminate the dying waste water, a variety of methods such as coagulation, chemical oxidation and reduction, photocatalysis, adsorption, ion pair extraction and electrochemical techniques has been examined.

Adsorption techniques have been widely applied to the treatment of industrial wastewater containing dyes, heavy metals and other inorganic and organic impurities.

Hydroxyapatite is an important inorganic material in biology and chemistry. Since many years, calcium phosphate materials were suitable used for a number of biomedical applications, e.g., artificial bone and teeth, as well as a carrier for drug delivery. However, in the recent years, there has been increasing interest for calcium phosphate materials as an adsorbent due to their ionic exchange property, adsorption affinity, characteristic to establish bonds with organic molecules, low water solubility, high stability under reducing and oxidizing conditions, availability and low cost.

### **1.3. Objectives of the present study:**

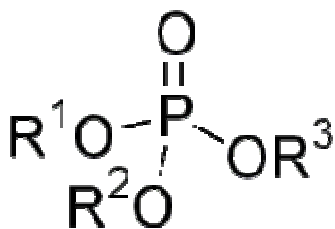
The broad objectives of the present study were,

- (i) To prepare the calcium phosphate materials with economically convenient.
- (ii) To investigate the effect of amino acid (threonine) on it.
- (iii) To observe the characteristic change after calcination of 900 °C.
- (iv) To investigate the adsorption capacity for some selected dye.

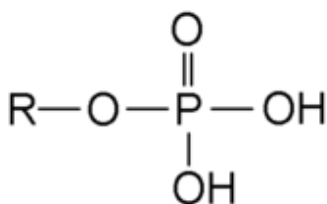
## Part 1

### LITERATURE REVIEW

#### 2.1. Structure of phosphate material:



The general chemical structure of a phosphate



This is the structural formula of the phosphoric acid functional group as found in a weakly acidic aqueous solution. In more basic aqueous solutions, the group donates the two hydrogen atoms and ionizes as a phosphate group with a negative charge of 2. [1-3]

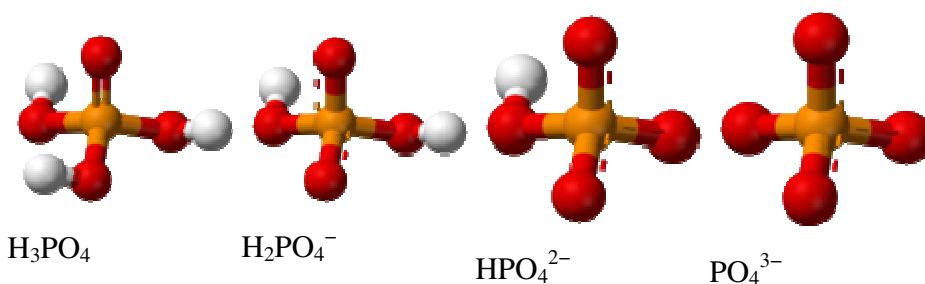
#### 2.2. Chemical properties:

The phosphate ion is a polyatomic ion with the empirical formula  $\text{PO}_4^{3-}$  and a molar mass of 94.973 g/mol; it consists of one central phosphorus atom surrounded by four identical oxygen atoms in a tetrahedral arrangement. The phosphate ion carries a negative three formal charge and is the conjugate base of the hydrogen phosphate ion,  $\text{HPO}_4^{2-}$ , which is the conjugate base of  $\text{H}_2\text{PO}_4^-$ , the dihydrogen phosphate ion, which in turn is the

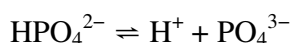
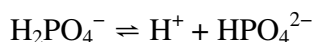
conjugate base of  $\text{H}_3\text{PO}_4$ , phosphoric acid. It is a hypervalent molecule (the phosphorus atom has 10 electrons in its valence shell). Phosphate is also an organophosphorus compound with the formula  $\text{OP}(\text{OR})_3$ .

A phosphate salt forms when a positively-charged ion attaches to the negatively-charged oxygen atoms of the ion, forming an ionic compound. Many phosphates are not soluble in water at standard temperature and pressure. The sodium, potassium, rubidium, caesium and ammonium phosphates are all water soluble. Most other phosphates are only slightly soluble or are insoluble in water. As a rule, the hydrogen phosphates and the dihydrogen phosphates are slightly more soluble than the corresponding phosphates. The pyrophosphates are mostly water soluble.

In dilute aqueous solution, phosphate exists in four forms. In strongly-basic conditions, the phosphate ion ( $\text{PO}_4^{3-}$ ) predominates, whereas in weakly-basic conditions, the hydrogen phosphate ion ( $\text{HPO}_4^{2-}$ ) is prevalent. In weakly-acid conditions, the dihydrogen phosphate ion ( $\text{H}_2\text{PO}_4^-$ ) is most common. In strongly-acid conditions, aqueous phosphoric acid ( $\text{H}_3\text{PO}_4$ ) is the main form.



More precisely, considering the following three equilibrium reactions:



The corresponding constants at  $25^\circ\text{C}$  (in mol/L) are

$$K_{a1} = \frac{[\text{H}^+][\text{H}_2\text{PO}_4^-]}{[\text{H}_3\text{PO}_4]} \simeq 6.92 \times 10^{-3}$$

$$K_{a2} = \frac{[\text{H}^+][\text{HPO}_4^{2-}]}{[\text{H}_2\text{PO}_4^-]} \simeq 6.17 \times 10^{-8}$$

$$K_{a3} = \frac{[\text{H}^+][\text{PO}_4^{3-}]}{[\text{HPO}_4^{2-}]} \simeq 4.79 \times 10^{-13}$$

For a strongly-basic pH (pH=13),

$$\frac{[\text{H}_2\text{PO}_4^-]}{[\text{H}_3\text{PO}_4]} \simeq 7.5 \times 10^{10}, \quad \frac{[\text{HPO}_4^{2-}]}{[\text{H}_2\text{PO}_4^-]} \simeq 6.2 \times 10^5, \quad \frac{[\text{PO}_4^{3-}]}{[\text{HPO}_4^{2-}]} \simeq 2.14$$

showing that only  $\text{PO}_4^{3-}$  and  $\text{HPO}_4^{2-}$  are in significant amounts.

For a neutral pH (for example the cytosol pH=7.0),

$$\frac{[\text{H}_2\text{PO}_4^-]}{[\text{H}_3\text{PO}_4]} \simeq 7.5 \times 10^4, \quad \frac{[\text{HPO}_4^{2-}]}{[\text{H}_2\text{PO}_4^-]} \simeq 0.62, \quad \frac{[\text{PO}_4^{3-}]}{[\text{HPO}_4^{2-}]} \simeq 2.14 \times 10^{-6}$$

so that only  $\text{H}_2\text{PO}_4^-$  and  $\text{HPO}_4^{2-}$  ions are in significant amounts (62%  $\text{H}_2\text{PO}_4^-$ , 38%  $\text{HPO}_4^{2-}$ ). Note that in the extracellular fluid (pH=7.4), this proportion is inverted (61%  $\text{HPO}_4^{2-}$ , 39%  $\text{H}_2\text{PO}_4^-$ ).

For a strongly-acid pH (pH=1),

$$\frac{[\text{H}_2\text{PO}_4^-]}{[\text{H}_3\text{PO}_4]} \simeq 0.075, \quad \frac{[\text{HPO}_4^{2-}]}{[\text{H}_2\text{PO}_4^-]} \simeq 6.2 \times 10^{-7}, \quad \frac{[\text{PO}_4^{3-}]}{[\text{HPO}_4^{2-}]} \simeq 2.14 \times 10^{-12}$$

showing that  $\text{H}_3\text{PO}_4$  is dominant with respect to  $\text{H}_2\text{PO}_4^-$ .  $\text{HPO}_4^{2-}$  and  $\text{PO}_4^{3-}$  are practically absent.

Phosphate can form many polymeric ions such as diphosphate (also pyrophosphate),  $P_2O_7^{4-}$ , and triphosphate,  $P_3O_{10}^{5-}$ . The various metaphosphate ions have an empirical formula of  $PO_3^-$  and are found in many compounds.

Phosphate deposits can contain significant amounts of naturally occurring uranium. Uptake of these substances by plants can lead to high uranium concentrations in crops.

### **2.3. Cellular function:**

Phosphate is useful in animal cells as a buffering agent. Phosphate salts that are commonly used for preparing buffer solutions at cell pHs include  $Na_2HPO_4$ ,  $NaH_2PO_4$ , and the corresponding potassium salts.

### **2.4. Characteristics of inorganic phosphate materials:**

Outstanding characteristics of solid phosphates are listed below.

- (1) Many phosphates have water-affinity.
- (2) Many phosphates hydrolyze easily.
- (3) One-dimensional chain polymers are easily formed.
- (4) The P-O ion structure is anisotropic.
- (5) The volatility of P component in phosphate is high at high temperatures.
- (6) Phosphates are easily fusible at low temperatures.
- (7) Many phosphates are corrosive.
- (8) Many phosphates are highly soluble in acidic solution.
- (9) Phosphates, especially calcium phosphates, are closely related to biological materials.
- (10) Rock phosphates are necessary as a raw material of various phosphates.



These characteristics can be understood if the phosphate compounds are compared with solid silicate compounds. [4-7] are due to the anti-branching-rule[5] of the phosphate ion. Bonding energy between M, where M is Si, P or S, and oxygen, follows the order (S-O)>(P-O)>(Si-O).[6] Thus the P-O bond is seen to be intermediate between Si-O and S-O bonds. Roughly speaking, a sulfate is chemical-agent-like, while a silicate is mineral-like, therefore a phosphate is intermediate and ambiguous.[8-11]

## **2.5. General description of calcium orthophosphates:**

The calcium orthophosphates are conventionally classified according to their ca/P molar ratio, which varies from 0.5 to 2. These salts are insoluble except for  $\text{Ca}(\text{HPO}_4)_2$  and  $\text{Ca}(\text{HPO}_4) \cdot \text{H}_2\text{O}$ . Hydroxyapatite is the most insoluble salt in the neutral and alkaline solutions. Therefore, all of the calcium orthophosphate salts in table :1 can be converted into hydroxyapatite at a pH higher than 5 [12]. Except for tricalcium and tetracalcium phosphates, these salts can be formed in aqueous solutions. However, when a small amount of divalent cation with an ionic radius of 0.07 nm, typically magnesium, is present in solution such as body fluid, whitlockite, that has a structure very similar to  $\beta$ -tricalcium phosphate, is precipitated [13].

Dicalcium phosphate dehydrate (DCPD) with the formula  $\text{CaHPO}_4 \cdot 2\text{H}_2\text{O}$  and dicalcium phosphate anhydrous (DCPA) with the formula  $\text{CaHPO}_4$  are stable phases at a pH lower than 4.5-4.3 at  $25^\circ\text{C}$  [14]. Dicalcium phosphate anhydrous is 0.680 times less soluble than dicalcium phosphate dehydrate. Dicalcium phosphate dehydrate gradually dehydrated in water at  $60\text{-}100^\circ\text{C}$  resulting in the formation of dicalcium phosphate anhydrous.

The calcium orthophosphates are salts of the tribasic phosphoric acid,  $\text{H}_3\text{PO}_4$ , and thus can form compounds that contain  $\text{H}_2\text{PO}_4^{-1}$ ,  $\text{HPO}_4^{2-}$  or  $\text{PO}_4^{3-}$  ions. Those with  $\text{H}_2\text{PO}_4^{-1}$  ions only form under rather acidic conditions, and are therefore not normally found in biological systems. However, both  $\text{HPO}_4^{2-}$  and  $\text{PO}_4^{3-}$  ions occur in the mineral of bones and teeth and in various pathological calcifications. Some calcium phosphates are

hydrated and those that belong to the basic apatitic calcium phosphate family contain OH<sup>-</sup> ions.

**Table 2.5:** Calcium Orthophosphate Family

Abbreviation	Explanation	Chemical formula	Ca/P molar ratio
MCPA	Monocalcium phosphate anhydrous	Ca(PO <sub>4</sub> ) <sub>2</sub>	0.50
MCPM	Monocalcium phosphate monohydrate	Ca(HPO <sub>4</sub> ).H <sub>2</sub> O	0.50
DCPD	Dicalcium phosphate dihydrate	CaHPO <sub>4</sub> .2H <sub>2</sub> O	1.00
D CPA	Dicalcium phosphate anhydrous	CaHPO <sub>4</sub>	1.00
OCP	Octacalcium Phosphate	Ca <sub>8</sub> H <sub>2</sub> (PO <sub>4</sub> ) <sub>6</sub> .5H <sub>2</sub> O	1.33
ACP	Amorphous calcium phosphate	Ca <sub>3</sub> (PO <sub>4</sub> ) <sub>2</sub> .nH <sub>2</sub> O	1.50
TCP	Tricalcium phosphate	Ca <sub>3</sub> (PO <sub>4</sub> ) <sub>2</sub>	1.50
α-TCP	α-Tricalcium phosphate	α-Ca <sub>3</sub> (PO <sub>4</sub> ) <sub>2</sub>	1.50
β-TCP	β-Tricalcium phosphate	β-Ca <sub>3</sub> (PO <sub>4</sub> ) <sub>2</sub>	1.50
HA	Hydroxyapatite	Ca <sub>10</sub> (PO <sub>4</sub> ) <sub>6</sub> (OH) <sub>2</sub>	1.67

Pyrophosphates (P<sub>2</sub>O<sub>7</sub><sup>4-</sup>, dipolyphosphates) and polyphosphates, which contain P-O-P bonds, are of less biological importance than the orthophosphates, although calcium pyrophosphates occur in some pathological calcifications. Pyrophosphates are potent inhibitors of nucleation and crystal growth of CaPs in aqueous systems, and are also sometimes formed on ignition of hydrogen orthophosphates. In addition to their biological importance many CaPs occur as minerals [15-18], the most important of these being the apatites whose mineralogy will be briefly mentioned below.

The CaPs are all white solids (unless doped with a coloured ion), most are sparingly soluble in water, and some are very insoluble, but all dissolve in acids. The preparation and chemistry of the CaPs [19-21], ortho- and polyphosphates [9, 10], and the alkaline earth ortho- and polyphosphates [22-24] have been reviewed. Structural aspects of biological CaPs have been discussed [25]. Details of the preparation and characteristics

of the calcium pyrophosphates [26], and the preparation, X-ray, optical and IR characteristics of alkaline earth and other ortho- and pyrophosphates [27] have been published.

Well-known calcium orthophosphates other than apatite are  $\text{Ca}_3(\text{PO}_4)_2$  (TCP),  $\text{Ca}_4(\text{PO}_4)_2\text{O}$  (hilgenstockite),  $\text{Ca}(\text{H}_2\text{PO}_4)_2$ ,  $\text{Ca}(\text{H}_2\text{PO}_4)_2 \cdot \text{H}_2\text{O}$ ,  $\text{CaHPO}_4$  (monetite),  $\text{CaHPO}_4 \cdot 2\text{H}_2\text{O}$  (brushite),  $\text{Ca}_5\text{H}_2(\text{PO}_4)_6 \cdot 5\text{H}_2\text{O}$  (octacalcium phosphate; OCP) and  $\text{Ca}_3(\text{PO}_4)_2 \cdot 3-4.5\text{H}_2\text{O}$  (amorphous calcium phosphate; ACP). The dihydrogen phosphates are water-soluble and important fertilizer salts.  $\beta$ -TCP is often called whitlockite. However natural whitlockite is considered to be a compound with hydrogen phosphate like  $6\text{Ca}_3(\text{PO}_4)_2 \cdot 2\text{MHP0}_4$  ( $\text{M} = \text{Mg}, \text{Mn}, \text{Fe}$ ). Both OCP and ACP are interesting biologically and crystallographically as precursors during the course of HAp formation in vivo. The other calcium phosphates, some of which have industrial uses, are employed mainly as sources or reagents for the preparation of various calcium phosphate-containing materials.

Precipitates, especially HA and related calcium phosphates such as ACP and OCP, from calcium phosphate solution have been studied in detail with respect to various reaction factors, e.g., degree of super saturation, concentration of solution, pH, mixing ratio of Ca/P, temperature, ripening duration and coexistent ions. The ACP has been thought to change in neutral to alkaline media into apatite in the course of  $\text{ACP} \rightarrow \text{HA}$  ( $\text{Ca/p} < 1.67$ )  $\rightarrow \text{HA}$  ( $\text{Ca/p} = 1.67$ ). Recently, it has been suggested that ACP changes to HAp through two processes, *i.e.*,  $\text{ACP} \rightarrow \text{OCP} \rightarrow \text{HA}$  ( $\text{Ca/p} < 1.67$ )  $\rightarrow \text{HA}$  ( $\text{Ca/p} = 1.67$ ), and  $\text{ACP} \rightarrow \text{HA}$  ( $\text{Ca/p} = 1.67$ ) directly [28].

### 2.5.1. Amorphous Calcium Phosphate (ACP):

ACP is amorphous with the composition of  $\text{Ca}_3(\text{PO}_4)_2 \cdot n\text{H}_2\text{O}$  ( $n=3-4.5$ ), which corresponds compositionally to a calcium deficient Ha. ACP forms mostly as spherical particles of ca. 300-1000 Å in diameter and has a surface area of ca. 30-120 m<sup>2</sup>/g [28]. X-ray diffraction of ACP gives an amorphous pattern as shown in figure 2.5.1 (a)

[29,30]. IR and ESR results show a lowering of the symmetry of  $\text{PO}_4$  tetrahedra and the absence of a strong crystalline field in ACP [31,32].

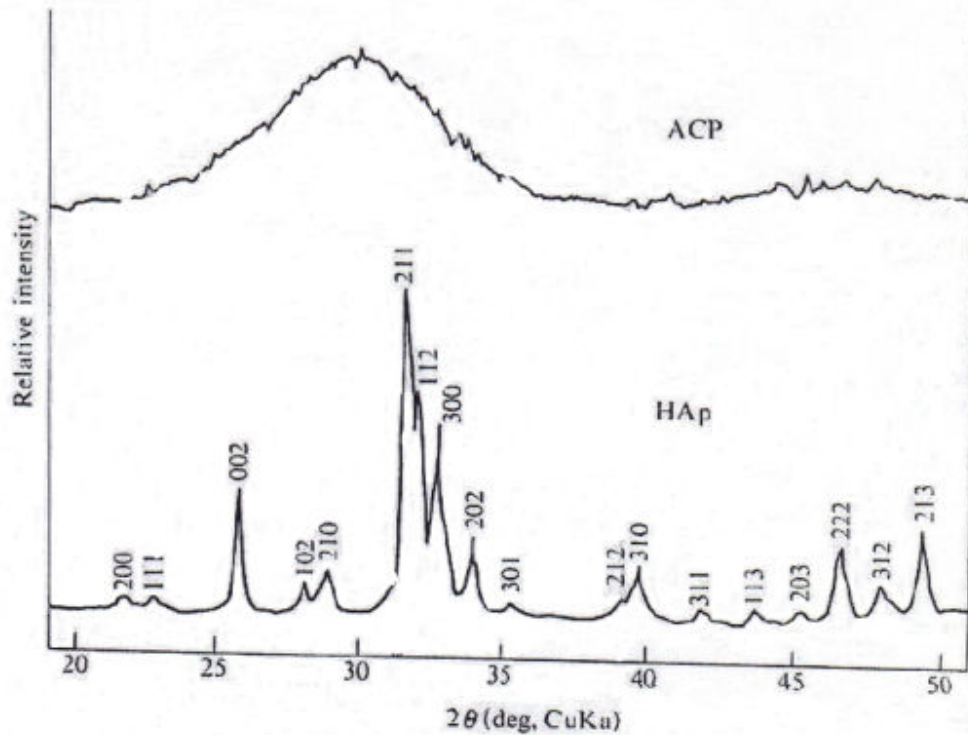
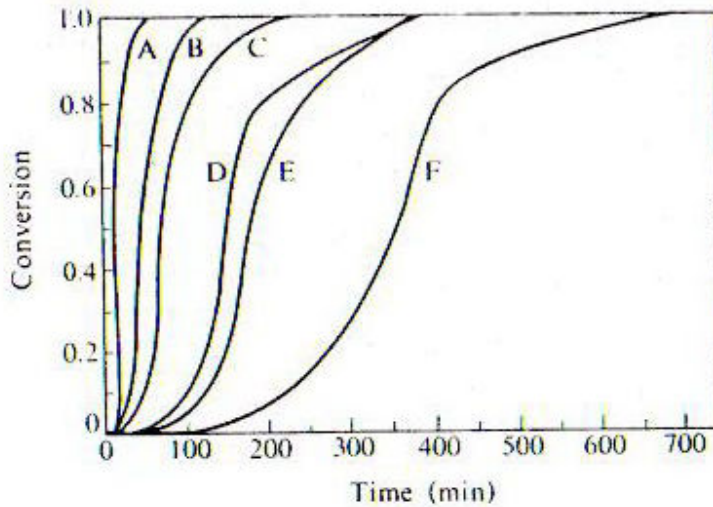


**Figure 2.5.1 (a):** Comparison of X-ray diffraction patterns of ACP and well crystallized HA.

(Reproduced with permission by Posner, A.S and Betts, F., *Accounts Chem. Res.*, 8, 274 (1975)).

The formation of ACP from solution involves an induction period or formation time ( $t_{\text{ACP}}$ ), with increases in initial  $[\text{Ca}] \times [\text{P}]$  solution product, Ca/P mixing ratio, temperature and pH,  $t_{\text{ACP}}$  becomes shorter.[33]



A: pH 6.8, B: pH 7, C: pH 7.5, D: pH 8

**Figure 2.5.1 (b):** Effect of pH on the transformation of ACP to HA at 26 °C.

(After Boskey, A.L. and Posner, A.S. J. Phys. Chem. 77, 2314(1973)).

At values below pH 6.6, CaHPO<sub>4</sub>·2H<sub>2</sub>O formed instead of ACP, and was gradually converted to OCP or HA [34] (Fig. 2.5.1 (b)). ACP forms in vitro over a wide range of initial [Ca] X [P] mM<sup>2</sup> from 2.5 X 10 to 5 X 10<sup>5</sup> as long as the precipitation is carried out in alkaline medium [35]. Coexistence of Na<sup>+</sup> and K<sup>+</sup> does not change t<sub>ACP</sub>, however EDTA and citrates increase t<sub>ACP</sub>, Trace amounts of CO<sub>3</sub><sup>2-</sup>, Mg<sup>2+</sup>, F<sup>1-</sup> and P<sub>2</sub>O<sub>7</sub><sup>4-</sup> decrease t<sub>ACP</sub> longer in this order, and polymer electrolytes also tend to increase t<sub>ACP</sub> [33].

### 2.5.2. Thermal Changes:

ACP crystallizes to OCP or HA in aqueous solution, whereas in dry atmosphere it crystallizes to TCP with heating. An endothermic peak around 150 °C corresponds to dehydration of ACP, and an exothermic peak at about 660 °C to crystallization into α-TCP, and the α form converts exothermically into β-TCP at about 870 °C. With further heating, the β form transforms into the α form at about 1180 °C. Apparent activation energies for the dehydration were 10.5 and 20.0 kcal/mol for loosely held water and tightly bound hydrate water, respectively [36]. The formation of the α form at such a thermodynamically unstable temperature range was studied in detail [35,37,38].

Complicating features of the crystallization were observed depending on preparative conditions as shown in figure 2.5.2 [37]. ACP samples prepared from solution with low initial  $[Ca] \times [P]$  products tended to first crystallize  $\beta$ -TCP only or an  $\alpha$  and  $\beta$ -TCP mixture.

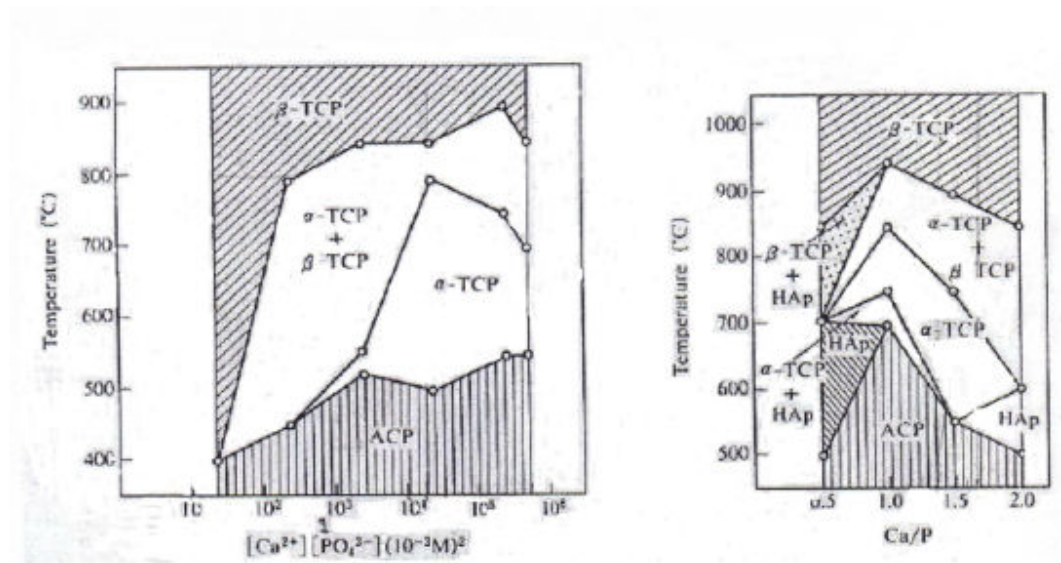


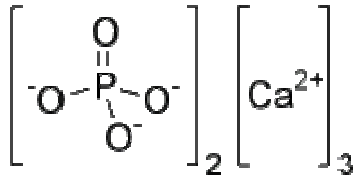
**Figure 2.5.2:** Thermal changes of ACP at different  $[Ca] \times [P]$  products (left) and Ca/P mixing ratios (right).

## 2.6. Tricalcium Phosphate (TCP):

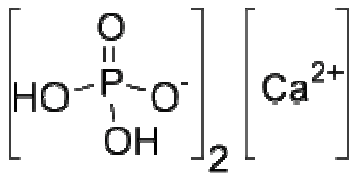
Tricalcium phosphate is a compound with formula  $Ca_3(PO_4)_2$ . It is also known as calcium orthophosphate, tertiary calcium phosphate, tribasic calcium phosphate, or "bone ash" (calcium phosphate being one of the main combustion products of bone). TCP is typically more soluble and less crystalline than hydroxyapatite. TCP is extremely biocompatible and act as an osteoconductive scaffold. Tricalcium phosphate comes in two forms, alpha ( $\alpha$ ) and beta ( $\beta$ ) TCP. The  $\alpha$ -TCP is more soluble than  $\beta$ -TCP and has a faster bioresorbable profile in vivo. In minerals, "calcium phosphate" refers to minerals containing calcium ions ( $Ca^{2+}$ ) together with orthophosphates ( $PO_4^{3-}$ ), metaphosphates or pyrophosphates ( $P_2O_7^{4-}$ ) and occasionally hydrogen or hydroxide ions. Especially, the common mineral apatite has formula  $Ca_5(PO_4)_3X$ , where X is F, Cl, OH, or a mixture; it is

hydroxyapatite if the extra ion is mainly hydroxide. Much of the "tricalcium phosphate" on the market is actually powdered hydroxyapatite.

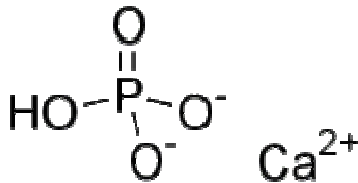
### 2.6.1. Structure of some calcium phosphate materials:



Tricalcium phosphate -  $\text{Ca}_3(\text{PO}_4)_2$



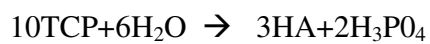
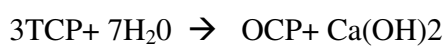
Calcium dihydrogen phosphate



Calcium hydrogen phosphate

### 2.6.2. Reaction with $\text{H}_2\text{O}$ :

TCP has been found to react with  $\text{H}_2\text{O}$  below  $100^\circ\text{C}$  [39]. The reactions are expressed as follows, depending on pH.



Formation field of the products was obtained with respect to pH and temperature as shown in figure 2.10 compared with that from  $\text{CaHPO}_4 \cdot 2\text{H}_2\text{O}$  [40]. These hydrolysis

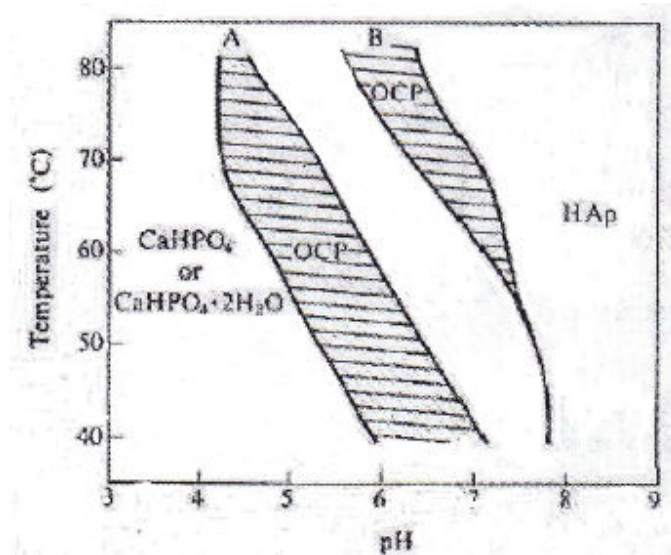
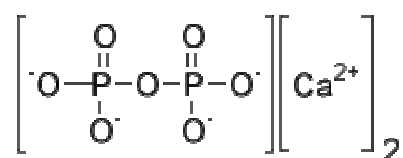


**Figure 2.6.2:** Hydrolysis products of  $\alpha$ -TCP (A) and  $\text{CaHPO}_4 \cdot 2\text{H}_2\text{O}$  (B)

reactions are used in the preparation of OCP and HA. In particular, the hydrolysis reaction of TCP is unique in that the reaction of powdery TCP carried out without stirring is accompanied by a hardening or solidification phenomenon [39,41]. Similar phenomena are well known for calcium sulfate hemihydrates and Portland cement. The solidification occurs with entanglement of produced microcrystals of OCP or HA.

### 2.7. Calcium pyrophosphate:

Calcium pyrophosphate ( $\text{Ca}_2\text{O}_7\text{P}_2$ ) is a chemical compound that can be formed by the reaction of pyrophosphoric acid and a calcium base or by strongly heating calcium hydrogen orthophosphate or calcium ammonium orthophosphate. It is commonly used as a mild abrasive agent in toothpastes. Deposition of CPPD in articular joints causes an arthritis condition called pseudogout.





Structure of calcium pyrophosphate.

## 2.8. Octacalcium Phosphate (OCP):

Octacalcium phosphate,  $\text{Ca}_8\text{H}_2(\text{PO}_4)_6 \cdot 5\text{H}_2\text{O}$  (OCP), often occurs as a transient intermediate in the precipitation of the thermodynamically more stable hydroxyapatite (HA) [42], and has been suggested to be involved in the mineralization of biological tissues, such as bone and dentine [42-44]. The inorganic phase in these calcified tissues is a poor crystalline carbonated apatite, which, however, could be just the final phase of a process where OCP acts as a precursor phase.

HA crystallizes in the hexagonal space group  $\text{P6}_3/\text{m}$ . Biogenic apatite crystals from bone, dentine and calcifying enamel exhibit or ribbon-like shapes and are elongated along the c-axis [45-47]. The plate like habit, which is not consistent with apatite symmetry, is one of the reason why OCP is thought to be involved in the first stages of mineralization of bone and tooth tissues [48]. In fact, crystallizes as {100} blades of triclinic pinacoidal symmetry, elongated along the c-axis and bordered by the forms {010}, {001} and {011} [44]. Although the triclinic structure of OCP, space group P1, does not exhibit any sixfold symmetry relation, its similarity with HA structure is remarkable. The unit cell consists of a layer practically identical to the unit cell of HA and a layer with more widely spaced  $\text{PO}_4^{3-}$  and  $\text{Ca}^{2+}$  ions and  $\text{H}_2\text{O}$  molecules interdispersed. Apatitic layers, about 1.1 nm thick alternate with hydrated layers, about 0.8 nm thick, parallel to the (100) face [49]. Figure 2.8 shows the projections along the (100) plane of the structures of OCP and HA, together with a tridimensional scheme of the layered OCP structure. OCP hydrolyzes in water to HA. It has been suggested that the transformation of OCP to HA takes place through in situ hydrolysis of OCP, and/or dissolution of OCP followed by HA precipitation [42, 49-51]. The involvement of the exchange of ions and water molecules between solid and solution phases

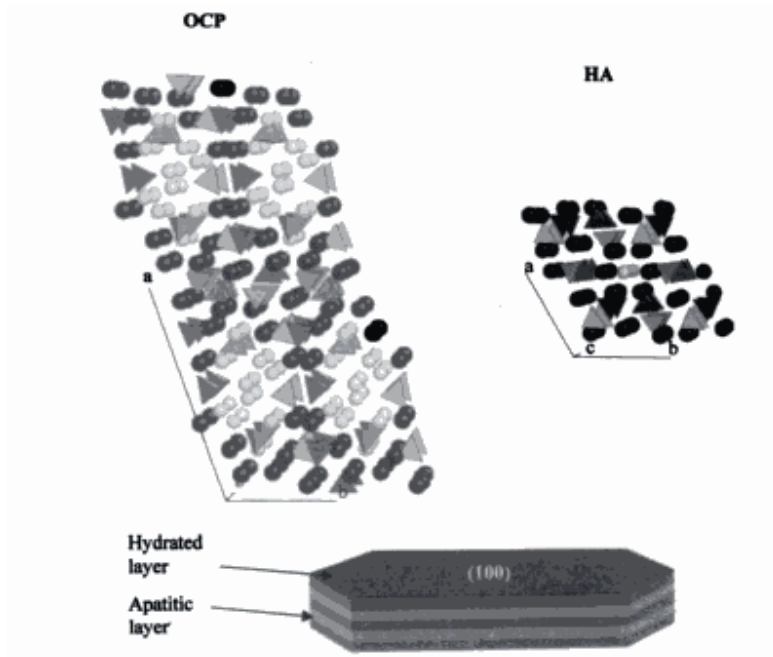


**Figure 2.8:** Projections along the (100) face of the structures of OCP and HA, together with a tridimensional scheme showing the alternating apatitic and hydrated layers parallel to the (100) face of OCP. The dark spheres indicate the Ca atoms, the white spheres show the oxygen atoms of water molecules in OCP, as well as of OH group in HA, and the shadowed tetrahedral indicate the phosphate groups.

[49], as well as the great influence of pH on the transition rate [50-51], suggests that the dissolution/reprecipitation process is the most probable. Fluoride, carbonate, citrate, as well as several mono and divalent cations, have been found to influence the conversion of OCP to HA [51-56]. Furthermore, the same ions, when present during the synthesis of OCP, can affect its growth and morphology, the presence of magnesium, carbonate and fluoride, for instance, suppresses the growth of OCP along the c-axis under most conditions [57-59].

OCP structure can incorporate a large variety of inorganic and organic species [60]. Thus, the presence of impurities which stabilize or destabilize OCP [61-62] could affect not only the relative rate of crystallization and hydrolysis but also the composition and structure of the calcium phosphate finally formed [53,63]. Ionic incorporation during OCP transformation into HA could account also for the nonstoichiometry and poor

crystallinity of biological apatites [43]. OCP has been found in dental calculi [64,65], as well as in other pathological calcifications [66]. Furthermore, high resolution electron microscopy images of calcifying dentine revealed the presence of OCP in the central part and of HA at the extremities of the same crystal [47].

It must be remembered that the process of mineralization of biological tissues takes place in an environment rich in acidic macromolecules, which can affect crystallization and growth of the mineral phase [67]. Because of the presence of many charged groups, such as carboxylate, phosphate and sulphate groups, the acidic macromolecules can interact with the charge crystal surfaces. The interaction can be specific, with the protein adopting a conformation and exhibiting charge distribution and repeating distances matching some structural motif of the mineral crystal, or even non-specific, due to multiple electrostatic interaction [68]. The results of *in vitro* experiments carried out on OCP crystallization suggest a specific interaction of the highly phosphorylated acidic protein, phosphophoryn, with the (010) face, whereas carboxylate rich proteins seem to interact preferentially with the hydrated layer of the (100) face [68]. It has been verified that some synthetic polyelectrolytes can affect the nucleation and growth of calcium phosphates playing a role similar to that played *in vivo* by biological macromolecules [69]. In particular it has been verified that the presence of polyacrylic acid, as well as its sodium salt, inhibits the synthesis of hydroxyapatite [69-70]. The presence of the carboxylate-rich polyelectrolyte affects also the morphology of the crystals, suggesting that its significant adsorption on HA crystals takes place through interaction with the phosphate sites on the (100) faces [71]. Furthermore, polyacrylic acid, as well as its sodium salt, is easily and irreversibly adsorbed on HA through a process which has been ascribed to electrostatic interactions and/or hydrogen bonding forces [72].

### **2.8.1. A Survey on Different Methods for Synthesizing OCP:**

OCP is one of the most important calcium phosphates and has a high compatibility with bone tissues as well as HAp. *In vitro* crystal growth studies have been reported in which

dicalcium phosphate dehydrate (DCPD) and amorphous calcium phosphate (ACP) could be hydrolyzed to HAp via OCP [73-75]. Thus, the basic study of OCP offers useful information about biological mineralization processes [76-79]. Furthermore, OCP is paid much attention as a functional material with a large potential for being applied as calcium phosphate compound containing organic substances like medicine. This is because only OCP in many kinds of calcium phosphates has a unique layered structure composed of alternative layers of apatitic and hydrate. In addition, some organic matter, especially with a di-carboxylic group, can be intercalated between these uniquely alternative layers. However, it is well known that synthesizing pure OCP is difficult because the crystalline structure of OCP is unstable and can be easily hydrolyzed to HAp near room temperature [80-82].

Nakahira et al. successfully synthesized OCP by a hydrolysis of  $\beta$ -tricalcium phosphate ( $\text{Ca}_3(\text{PO}_4)_2$ ,  $\alpha$ -TCP: Ca/P molar ratio = 1.50) [83,84]. However, the formation of OCP by the hydrolysis of  $\alpha$ -TCP was limited within narrow processing conditions, and this restriction makes the synthesis of OCP difficult. Additionally, OCP could not be sintered as ceramic because of its thermal dehydration property. In the case of organic substances being added to OCP for developing new functional properties, organic matter could be easily decomposed at relatively low temperature [85,86]. The above features inhibit new application of OCP as potential biomaterial, artificial bone. Few studies have been reported about how OCP was used as a new material [87,88]. Therefore, it is expected that OCP ceramic can be used as an important material like artificial bone for the following reasons: (1) if OCP ceramic had an improved mechanical property, this can support to the body as artificial bone; (2) OCP is believed to be more bioactive than HAp when used clinically to fill bone defects because OCP is transformed into HAp in vivo [89].

Shiho et al. [90]. showed hydrothermal hot-pressing (HHP) method can achieve densification of dissolvable powder materials at extremely low temperatures below 200°C. It has been reported that with the HHP processing technique, it is possible to promote the solubility of particles and connect with these particles under the low temperature condition [91-104]. In this process, not only OCP but also adipic acid-

intercalated OCP (*Adi-OCP*) as an organic-inorganic hybrid for the development of functional biomaterials were synthesized and used as starting materials. Then, fabrications of OCP bulk ceramics with mono phase of OCP and *Adi-OCP* were attempted by HHP. The hydrothermal hot-pressing method was a feasible way to fabricate OCP ceramics without thermal dehydration and thermal decomposition. Mechanical properties of the OCP ceramics could be improved by HHP treatment as low as 110°C. The OCP ceramics showed good bioactivity in the SBF immersion test.

Recent studies demonstrated that OCP could stimulate osteoblastic cell differentiation in vitro [105-108]. In vivo studies showed biodegradability and replacement by newly formed bone [109-112]. Also, OCP coating on metallic implants promoted osteoconductivity [113], osteoblastic cell proliferation [114] and ectopic osteoinduction in some cases [111,115]. There is a general consensus that OCP is a metastable calcium phosphate salt at physiological pH and temperature. The transition of OCP to HA is thermodynamically favored. This transition proceeds spontaneously and irreversibly once initiated [116,117]. Also, this conversion is accompanied by changes in the physicochemical aspects including: 1) base consumption if converted from amorphous calcium phosphate to HA via OCP-like phase [118,119]; 2) calcium consumption and phosphate release [120,121]; 3) progressive increase of the Ca/P molar ratio [122-124]; 4) progressive decrease of acid phosphate in total phosphorus [105,125]; 5) modification of the adsorption affinity of serum proteins [126]. It is also becoming clear that major incorporation of impurities, such as carbonate and fluoride ions, into biominerals occurs during the hydrolysis [122,127].

Mathew et al. [128] proposed an example of the non-stoichiometric formula of OCP,  $\text{Ca}_{16}\text{H}_4 + \text{X}(\text{P}_0_4)_d(\text{OH})_x - (10 - \text{X})\text{H}_2\text{O}$  with excess hydrogen in the structure. In fact, the non-stoichiometric OCP has been shown to have approximately 40%  $\text{HP}_0_4$  that excess proton can release if extracted in an alkaline condition without disruption of the OCP structures and its labile  $\text{HP}_0_4$  can be reordered in its stoichiometric 33% if re-extracted in a neutral condition [125]. A previous study suggested that partially hydrolyzed OCP has a common structural feature with partially dehydrated OCP which is derived from disordered structure in the hydrated layer of OCP [129]. Thus, OCP exhibits a variety of

stoichiometries in composition and structure, most probably due to the existence of the hydrated layers which stack alternately with the apatitic layers [130].

Naohisa et al. [131] investigated whether subtle compositional and structural changes of OCP, caused by partial hydrolysis, affect its osteoconductive characteristics when implanted in rat bone marrow. Furthermore, the biodegradability of the OCP was compared to the typical, biodegradable bioceramic  $\beta$ -tricalcium phosphate ( $\beta$ -TCP). Ca-P ceramic biodegradation is the highest in marrow tissue, and higher in cancellous bone than in cortical bone, hence marrow tissue has been suggested to be better for testing material biocompatibility in vivo [132]. They have found that the stoichiometry of OCP, controlled by the partial hydrolysis of OCP in the synthetic preparation, influences the osteoconductivity, biodegradable characteristics and immune response of this material in bone marrow. The partial hydrolysis, observed as the onset of the conversion to HA, decreased the crystallinity with the formation of a very small amount of HA in the OCP crystals.

Arellano et al. [133] produced octacalcium phosphate (OCP) powder by precipitating 250 mL Ca(CH<sub>3</sub>COOH 0.04 M into 750 L of phosphate solution (5 mmol Na<sub>2</sub>HPO<sub>4</sub> and 5 mmol NaH<sub>2</sub>PO<sub>4</sub>) at a constant temperature of 60 °C and pH 5, which resulted in a dry white powder. X-ray diffraction (XRD), transmission electron microscopy (TEM) analysis, and the electron diffraction pattern (SAED) all showed only OCP. Hydroxyapatite (HAP) was directly obtained through hydrolysis of the powder. The total transformation of OCP into HAP was registered over a period of 6 h. During the first 30 min of hydrolysis both phases coexisted. The two phases and the OCP-HAP interface were structurally analyzed through XRD and TEM. Xin et al. [134] reported the formation of OCP into HAP by electron beam radiation in situ observations in the transmission electron microscope (TEM) also observing OCP and HAP domains as a result of solid-state-transformation mechanism in the OCP crystals. Recent intensive studies on the experimental application of synthetic OCP have shown that it has the potential to enhance new bone formation [135-141].

The osteoconductive nature of synthetic OCP was found first by its subperiosteal implantation in mouse calvaria in comparison with synthetic hydroxyapatite [135,142]. Several studies have been conducted to investigate the possible use of synthetic OCP as a bone regenerative scaffold in various forms, such as coatings on metallic implants [138-140,143], micro scaffold self-assembled [144,145] and granules [135,137,141,142,146]. Recent in vitro studies disclosed that OCP facilitates osteoblastic cell differentiation [141,144,145], and that marked increase in osteoblast-related gene expression, such as osterix and alkaline phosphatase (ALP), was observed depending on the dose of OCP [147]. It has been shown that synthetic OCP is converted into HA both in vivo [135,141,142,148] and in vitro [141,149-151]. Previous studies showed that a process of OCP-HA conversion involves exchanges of calcium and phosphate ions with surrounding tissue milieu [141,152,153] and is involved in promoting osteoblastic cell differentiation [141,147] and bone regeneration [135,141,142]. OCP can be converted topotaxially without changing its original morphology [150,154,2155] even in vivo, where bone formation was accelerated by its implantation [156] thereby providing a scaffold for osteoblast attachment, proliferation and subsequent differentiation.

It is known that solubility at physiological pH decreases in the order of OCP,  $\beta$ -tricalcium phosphate ( $\beta$ -Ca<sub>3</sub>(PO<sub>4</sub>)<sub>2</sub>;  $\beta$ -TCP) and HA [152].  $\beta$ TCP is widely accepted as a biodegradable bioceramic and used clinically [157-159]. Thus, OCP is the most soluble salt among them. So a lot of attention has been paid to the use of synthetic OCP with the expectation of it acting as potentialloci for the nucleation of bone induction in orthotopic sites, which could be replaced with a significantly higher volume of newly formed bone compared with the other calcium phosphate phases such as HA [157,158] or amorphous carbonated apatite [143]. It has been explained that the biodegradable characteristics of OCP are acquired via its resorption by osteoclast-like multinucleated giant cells (MNGCs) in bone marrow spaces [136,146,160] after a larger amount of new bone deposition compared with the amount by HA [146], in addition to its soluble nature in physiological condition. However, it is still uncertain whether the enhanced bone formation is induced coupled with osteoclastic resorption of OCP in not only bone marrow spaces but also in an environment near to intramembranous bone, such as the

calvaria. The subperiosteal region of intramembranous bone is considered to be a less reactive site compared with the bone marrow site regarding bone formation [161,162].

Kikawa et.al [163] designed to investigate whether synthetic OCP in granule form has biodegradable characteristics when implanted in the subperiosteal area of mouse calvaria in comparison with non-sintered stoichiometric HA, especially in relatively short periods after implantation. OCP crystals exhibited plate-like morphology, whereas HA crystals had a sphere-like structure. Both crystals had large pore volumes >75% in total, with micropores within the granules. Direct bonding of newly formed bone was discernible in HA until 35 days after implantation by element analysis for calcium and phosphorus. However, histomorphometric analysis demonstrated that bone formation was facilitated on OCP surfaces with greater alkaline phosphatase activity than on HA up to 21 days. The surfaces attacked by tartrate-resistant acid phosphatase positive osteoclast-like cells were significantly greater than those of HA. OCP became encapsulated and replaced with new bone with prolonged implantation periods up to 180 days. The results suggest that the enhanced bone formation in mouse calvaria could be associated with the biodegradable nature of OCP, and that OCP could be used in augmenting intramembranous bone volume.

There is a general consensus that the OCP structure stacks apatitic layers alternatively with hydrated layers, and that the transition of OCP to hydroxyapatite ( $\text{Ca}_{10}(\text{PO}_4)_6(\text{OH})_2$ ; (HA) is thermodynamically favored [166,167]. Because of the transitory characteristics of OCP in the physiological condition [165-167], the detection of OCP in these calcified tissues is not easy. The direct evidence of the presence of OCP, however, was obtained as the inclusion in the central part of a dentin crystal and apatite in the outer most layers of the same crystal [168]. The mineral prototype of bones and teeth is usually considered to be basic calcium phosphate HA [169-171]. The biomineral displays better crystallinity and a higher molar ratio with mineral development [169-171]. The final biological apatite crystals are constituted of poorly crystalline HA with a low Ca/P molar ratio, i.e. Ca-deficient HA, containing foreign ions, such as carbonate and fluoride. Conversion of synthetic OCP into HA has been investigated in various physiological media, such as simulated body fluid [172] and ultrafiltered human serum [173], and by murine tissue

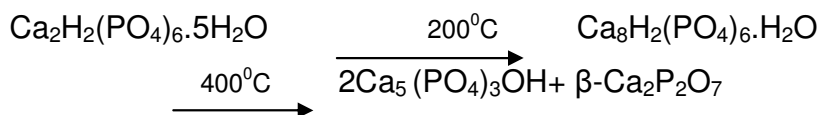


implantation [164,174,175]. It has been shown that the apatite converted from OCP in in vitro physiological conditions was a Ca-deficient HA, which has a chemical composition with a lower Ca/P molar ratio and a higher acid phosphate content [176].

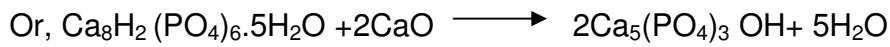
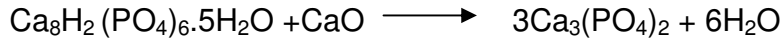
Suzuki et. al [177] demonstrated that the implantation of OCP markedly enhanced bone formation compared to the implantation of hydrolyzed Ca-deficient HA from OCP. Osteoblastic cell proliferation and the differentiation were also facilitated on OCP in vitro. Since OCP tended to convert to apatite both in vivo and in vitro, it is conceivable that OCP supports not only appositional bone formation but OCP-apatite conversion may be involved in this stimulatory effect of OCP. Their results reconfirmed one of the attractive aspects of OCP as a bone substitute material that enhances bone regeneration. Since OCP is thought to be a precursor of biological apatite crystals in bones and teeth [178-180], studies of the mechanism of bone formation by synthetic OCP implantation may lead to the elucidation of the mechanism of biomineralization during bone formation, in addition to the understanding of OCP as a bone substitute material.

### 2.8.2. Thermal transformation of Octacalcium phosphate:

The thermal decomposition of OCP is complex. OCP with partial loss of water of hydration, collapsed OCP, DCPA ( $\text{CaHPO}_4$ ), HA,  $\beta\text{-Ca}_2\text{P}_2\text{O}_7$  and tripolyphosphate are formed as the temperature increases, with these compounds persisting over different temperature ranges. The products also often depend on the duration of heating. Octacalcium phosphate (OCP),  $\text{Ca}_8\text{H}_2(\text{PO}_4)_6 \cdot 5\text{H}_2\text{O}$  undergoes a thermal evolution represented by the following canonical chain of reaction:



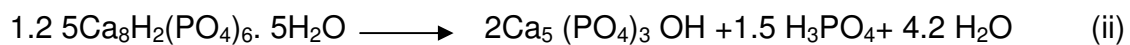
However, the production of pyrophosphate is a negative factor. Therefore, the OCP is not a thermally stable compound and it is therefore an unsuitable constituent of a material designed ceramic bodies. When this substance occurs, either originally or through formation, it may react with calcium oxide or calcium carbonate (originating from the breaking up of other phosphates) to give rise to the reaction:



### 2.8.3. Solubility and hydrolysis of OCP:

The effects of solution Ca/P ratio and degree of saturation on the dissolution kinetics of OCP at constant pH 5.75 and 25 °C have been studied [181]. The results indicated that the dissolution of OCP can apparently be controlled by two processes (probably transport and nucleation), depending on the undersaturation and Ca/P ratio. The dissolution has also been investigated [182] at constant undersaturation using constant composition methods. The kinetic data were analyzed in terms of recent crystal growth theories using a nonlinear least squares procedure. A rate equation was derived for a spiral dissolution, following detachment-desorption-volume diffusion mechanism at very low kink densities. The results indicated that processes at the crystal surface were much more important than volume diffusion in determining the rate of dissolution.

OCP hydrolyses in water to HA with contributions from both the reactions:



The hydrolysis of OCP to HA at different calcium and phosphate concentrations has been studied [183]. Carbonate ions slow the rate [184] and are retained in the solid [185,186]. The amount of carbonate incorporated depends markedly on which alkali carbonate is used [187]. These results have led to the suggestion that it might be possible for part of the carbonate to be situated in some type of gross defects introduced during hydrolysis, rather than on true lattice sites [188,187,189]. Na<sup>+</sup> ions can also be retained during hydrolysis [185]. Mg<sup>2+</sup> ions inhibit the reaction [186]. A recent study [190] of the transformation of OCP to apatite using scanning and transmission electron microscopy and IR demonstrated the inhibiting effect of Mg<sup>2+</sup>, citrate and pyrophosphate ions and

facilitation by  $F^{1-}$ ,  $CO_3^{2-}$ ,  $HPO_4^{2-}$ , and  $Ca^{2+}$  ions. Solution pH, ionic concentrations and OCP crystal size also influenced the rate of transformation.

#### **2.8.4. Stability in aqueous solution:**

OCP is thermodynamically metastable with respect to  $CaHPO_4 \cdot 2H_2O$  in acidic solutions and to HA in slightly acidic to alkaline solutions. Stability of OCP is strongly affected by solution conditions. For instance, OCP is stable in water, at pH 6 and  $40^\circ C$  for up to 9 days. The addition of  $F^{1-}$  ions markedly the conversion to fluoridated apatite (FAP). This reaction is applied in the preparation of FAP. OCP converts to FAP with 4.0 % F content by treatment in 0.1M NaF or KF solution at  $45^\circ$  or  $40^\circ C$  for 7 or 21 days [191-192]. Even in dilute solutions of  $F^{1-}$ , OCP converts easily into a partially fluoridated HA [193]. In an alkaline solution of pH 12, about 50% OCP converts to HA at  $40^\circ C$  for 3 hours [193]. When OCP is boiled in water, it converts to HA after 3 days [194].

#### **2.8.5. Catalytic property:**

OCP shows typical acidic behavior as a catalyst, i.e., strong dehydration character for the thermal decomposition of alcohols as well as nonstoichiometric HA and  $CaHPO_4 \cdot 2H_2O$ . Increases and decreases in acidity and acid strength are considered to be correlated to various thermal changes in  $HPO_4$  groups, lattice and adsorptive water contained in OCP [195].

### **2.9. General description of hydroxyapatite (HA):**

Hydroxyapatite is a mineral which is a naturally occurring form of calcium apatite with the formula  $Ca_5(PO_4)_3(OH)$ , but is usually written  $Ca_{10}(PO_4)_6(OH)_2$  to denote that the crystal unit cell comprises two entities. Hydroxylapatite is the hydroxyl end member of the complex apatite group. The  $OH^-$  ion can be replaced by fluoride, chloride or carbonate. It crystallizes in the hexagonal crystal system. It has a specific gravity of 3.08 and is 5 on the Mohs hardness scale. Pure hydroxyapatite powder is white. Naturally occurring apatites can however also have brown, yellow or green colorations, comparable to the discolorations of dental fluorosis.

Substitutions in the HA structure is possible. Substitutions for Ca, PO<sub>4</sub> and OH groups results in the change in the lattice parameter as well as changes in some of the properties of the crystal, such as solubility. If the OH<sup>1-</sup> groups in HA are replaced by F<sup>1-</sup> the anions are closer to the neighboring Ca<sup>2+</sup> ions. This substitution helps to further stabilize the structure and is proposed as one of the reasons that fluoridation helps reduced tooth decay as shown by the study of the incorporation of F into HA and its effect on solubility. Biological apatites, which are the mineral phases of bone, enamel and dentin, are usually referred to as HA. Actually, they differ from pure HA in stoichiometry, composition. Crystallinity, as well as in other physical and mechanical properties.

Hydroxyapatite constitutes ~65% of human bone by weight. There is another 18% collagen fiber, which makes the bone flexible and more durable. Then there is ~10% genetic tissue (mostly living bone cells). This tissue carries the genetic code of the person or animal and unless it is in a denatured form, which also kills the bone, it is likely to be rejected in the body as bone graft. Therefore, it is impossible to be successfully implant living bone even closely related donors. The remainder of bone is composed capillaries, nerves and so on.

Hydroxyapatite is a very strong material. Tooth enamel is nearly 100% hydroxyapatite. For the last two or three decades, researchers have tried to produce strong bioceramics starting with hydroxyapatite powder that can be obtained from geological sites or obtained in a white powder form from a number of chemical manufacturers. In the past, it has been mostly ceramicists who attempted to create strong hydroxyapatites. Although ceramicists now have advanced techniques such as solgel technology, most often ceramicists use molds to heat and press. Unfortunately, hydroxyapatite is only stable ~1200 °C. At the point, the OH<sup>1-</sup> comes off as steam (H<sub>2</sub>O) leaving behind mixtures of calcium phosphate compounds that are not very strong and are also somewhat water soluble. Obviously, it would not be a good idea to have water soluble teeth and bones.

Seventy percent of bone is made up of the inorganic mineral hydroxyapatite. Carbonated-calcium deficient hydroxyapatite is the main mineral of which dental enamel and dentin

are comprised. Hydroxyapatite crystals are also found in the small calcifications (within the pineal gland and other structures) known as corpora arenacea or 'brain sand'.

### **2.9.1. Medical uses of hydroxyapatite:**

Hydroxyapatite can be found in teeth and bones within the human body. Thus, it is commonly used as a filler to replace amputated bone or as a coating to promote bone in growth into prosthetic implants. Although many other phases exist with similar or even identical chemical makeup, the body responds much differently to them. Coral skeletons can be transformed into hydroxyapatite by high temperatures, their porous structure allows relatively rapid in growth at the expense of initial mechanical strength. The high temperature also burns away any organic molecules such as proteins, preventing graft-versus-host disease (GVHD) and rejection.

Many modern implants, e.g. hip replacements and dental implants, are coated with hydroxyapatite. It has been suggested that this may promote Osseo integration and there is strong supporting evidence for this [196]. In orthopedic surgery and dental applications, there is a great need for biocompatible and bioresorbable implant materials which can be used as a bone substitute. This includes bone lost due to periodontal disease, ridge augmentation, bone defect or bone cavities due to trauma or surgery, and spinal fusion. After implantation, the bone substitute is resorbed and replaced by the formation of new bone.

In orthopedic surgery, autogenous bone has been used quite often for bone repair or bone substitute. Autogenous bone has good biocompatibility, is not subject to immunological rejection, and induces bone growth. However, it requires a secondary surgery and thus increases the burden on the patient while delaying recovery. On the other hand, both homogeneous bone from other human sources and heterogeneous bone from animal sources always suffer the disadvantages of adverse immunological reactions. This will result in an inflammatory reaction and rejection after implantation.

The major inorganic composition of hard tissue is a calcium phosphate compound called biological apatite. Bone has 65% to 70% of biological apatite and teeth contain near 98% biological apatite. Hydroxyapatite and other apatite compounds have the same crystal structure as biological apatite. In principle, these apatite materials should be ideal candidates for bone replacement. However, the precipitated hydroxyapatite and other apatite compounds have very fine particle size. The difficulty in manipulating these fine powders renders them useless as materials for bone replacement.

Recently, many attempts have been made to prepare artificial bone substitute materials. Among these are metal, plastics and ceramics. In the past, several types of ceramics have been developed. These included aluminum oxide, calcium sulfate dihydrate, a glass containing calcium phosphate, and a variety of calcium phosphate ceramics.

The advancement of ceramics technology to prepare different types of calcium phosphate ceramics makes the medical application of calcium phosphate realized. In fact, clinical studies confirmed that apatite ceramic has the best biocompatibility among the artificial bone substitutes. Other calcium phosphate compounds or ceramics such as dicalcium phosphate, tricalcium phosphate, octacalcium phosphate and tetracalcium phosphate also show excellent biocompatibility.

Previous studies indicated that dense hydroxyapatite is not bioresorbable, while porous  $\beta$ -tricalcium phosphate and other calcium phosphates are bioresorbable. The bioresorption rate of  $\beta$ -tricalcium phosphate is rather difficult to predict. Plaster of Paris has been studied as a hard tissue replacement material for many years. In general, Plaster of Paris has acceptable biocompatibility. However, its resorption rate is too fast to match the in growth of new bone formation. In orthopedic surgery, particularly in bone defect repair, there is a great need for an implant material with good biocompatibility and a controllable resorption rate.

### **2.9.2. Hydroxyapatite uses in chromatography:**

The mechanism of hydroxyapatite (HA) chromatography is complicated and has been described as "mixed-mode" ion exchange. It involves nonspecific interactions between

positively charged calcium ions and negatively charged phosphate ions on the stationary phase HA resin with protein negatively charged carboxyl groups and positively charged amino groups. It may be difficult to predict the effectiveness of HA chromatography based on physical and chemical properties of the desired protein to be purified. For elution, a buffer with increasing phosphate concentration is typically used.

Microcrystalline hydroxyapatite (MH) is marketed as a "bone-building" supplement with superior absorption than calcium. It is a second-generation calcium supplement derived from bovine bone. In the 1980s, bone meal calcium supplements were found to be contaminated with heavy metals, and although the manufacturers claim their MH is free from contaminants, people are advised to avoid it because it has not been well-tested. However, the limited tests seem to show positive results. A 1995 randomized placebo-controlled study of 40 people in Europe found that it was more effective than calcium carbonate in slowing bone loss. A 2007 randomized double-blind controlled study of an MH supplement called the Bone Builder found significant positive effects in bone mineral density (BMD) [197].

### **2.9.3. Background:**

Hydroxyapatite is chemically similar to the mineral component of bones and hard tissues in mammals. It is one of few materials that are classed as bioactive, meaning that it will support bone in growth and Osseo integration when used in orthopedic, dental and maxillofacial applications. The chemical nature of hydroxyapatite lends itself to substitution, meaning that it is not uncommon for non-stoichiometric hydroxyapatites to exist. The most common substitutions involve carbonate, fluoride and chloride substitutions for hydroxyl groups, while defects can also exist resulting in deficient hydroxyapatites.

#### **2.9.4. Key properties:**

- I) The ability to integrate in bone structures and support bone ingrowth, without breaking down or dissolving (i.e it is bioactive).
- ii) Hydroxyapatite is a thermally unstable compound, decomposing at temperature from about 800-1200 °C depending on its stoichiometry .
- iii) Generally speaking dense hydroxyapatite does not have the mechanical strength to enable it to succeed in long term load bearing applications.

#### **2.9.5. Applications:**

- i) Bioceramic Coatings: Coatings of hydroxyapatite are often applied to metallic implants (most commonly titanium/titanium alloys and stainless steels) to alter the surface properties. In this manner, the body sees hydroxyapatite-type material, which it is happy to accept. Without the coating, the body would see a foreign body and work in such a way as to isolate it from surrounding tissues. To date, the only commercially accepted method of applying hydroxyapatite coatings to metallic implants is plasma spraying.
- ii) Bone Fillers: Hydroxyapatite may be employed in forms such as powders, porous blocks or beads to fill bone defects or voids. These may arise when large sections of bone have had to be removed (e.g. bone cancers) or when bone augmentations are required (e.g. maxillofacial reconstructions or dental applications). The bone filler will provide a scaffold and encourage the rapid filling of the void by naturally forming bone and provides an alternative to bone grafts. It will also become part of the bone structure and will reduce healing times compared to the situation, if no bone filler was used.

#### **2.9.6. Thermal Transformation of Hydroxyapatite:**

Each denomination (TCP, OCP, HA, etc.) refers to a chemical compound with a defined stoichiometric formula. Most of the compounds crystallize and have many crystallization



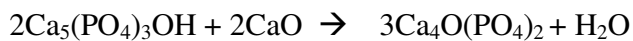
phases. The crystallized phases generally have different names. Sometimes the name used is the chemical one, and a Greek letter is adopted to distinguish the different phases.

Hydroxyapatite is a well-defined chemical compound with formula  $\text{Ca}_5(\text{PO}_4)_3 \text{OH}$  (though the term apatite, in this case calcium hydroxyapatite, derives from a mineralogical definition). It belongs to a family of homologous compositions, crystallizing in the same spatial group, defined as apatites. The  $\text{OH}^-$  group can be replaced, for example, by  $\text{F}^-$  and  $\text{Cl}^-$ , so that fluorapatite and chlorapatite are obtained, respectively. Also, the cation can be replaced by other bivalent ions (such as  $\text{Sr}^{2+}$ ,  $\text{Ba}^{2+}$ ,  $\text{Pb}^{2+}$ ) to give rise to strontium, barium, and lead hydroxyapatites. All these apatitic compounds crystallize with only one phase, with the specific lattice group  $\text{P6}_3/\text{m}$ .

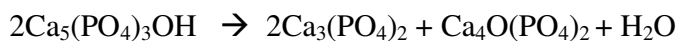
Stoichiometric (calcium) hydroxyapatite is a very stable compound up to  $1400^\circ\text{C}$ . At temperatures over  $1200^\circ\text{C}$  the following reaction can occur:



particularly if associated with a CaO-consuming one. If calcium oxide is present, the following transformation can take place:



By combining both equations, the following is obtained:



The main transformations under consideration are:

- i) Formation of oxyapatite  $[\text{Ca}_{10}(\text{PO}_4)_6\text{O}]$  - through condensation of hydroxyapatite, particularly above  $1400^\circ\text{C}$ .
- ii) Of great importance is the transformation that can take place in  $\alpha$ -TCP and  $\text{Ca}_4\text{O}(\text{PO}_4)_2$  at  $1550^\circ\text{C}$ .

At  $1550^\circ\text{C}$ , the last reaction is completely shifted to the right side.

There are also other cations and anions which, though unable to reach a complete substitution, may be available for playing a role in the formation of solid solutions confined within the apatitic crystal lattice. As regards the  $Mg^{2+}$ , it was ascertained to be a characteristic ion not favoring the apatitic structure (LeGeros, 1991). This ion can be incorporated into synthetic apatites in quantities lower than 0.4%. Similar ions are  $P_2O_7^{4-}$ ,  $Sn^{2+}$ , and  $Al^{3+}$ , all of which tend to divert the formation of amorphous calcium phosphatic compounds (ACP).

Other ions, such as  $CO_3^{2-}$ , may be contained in the apatitic lattice in sufficiently large percentages on condition that  $Mg^{2+}$  is not present. A further ion that may occur in sufficiently large percentage proportions is  $HPO_4^{2-}$ .

In these cases, we deal with the so-called nonstoichiometric hydroxyapatites which are, in reality, different solid solutions belonging to the same large family isomorphous compounds, better defined by the general term of apatites. If the starting powders are not stoichiometric, the formation of other compounds, such as mainly CaO or amorphous phosphates, is expected.

### **2.9.7. The Apatitic Family and Its Importance in the Biomedical Field:**

The term hydroxyapatite commonly refers in the biomedical field to calcium hydroxyapatite, the chemical compound with stoichiometric formula  $Ca_5(PO_4)_3OH$ . The term comes from the mineralogical class of apatites to which the crystallized minerals of this compound belong (with the same name).

In many cases an imperfect understanding of the chemistry has produced confusion about the utilized terminology and, in particular, about the meaning of the term hydroxyapatite. This led, for example, to the erroneous concept that there are different calcium hydroxyapatites, as this term was intended to indicate a commercial name and not a chemical compound. Even a large number of experiments, once considered exhaustive, were carried out on numerous nonchemical aspects, but in some cases the results of these

studies are improper because no distinction was made between the differences in chemical nature. It frequently happens that different laboratories have used powders of different origin (whether from the market or produced individually), with the result that there is an imperfect correspondence between the obtained data.

Considering all this, it would be more proper to speak of defective apatites, apatites containing substituting ions, or other apatites stable in their own right. In the past, many measurements used to be conducted on samples believed to be identical while in reality they were different in nature. This was due to the difficulty of dealing with a system made up of a myriad of equicomponent compounds existing in an equilibrium relationship to each other, not just individually but more than one at a time. Hence the difficulty of a deliberately systematic study, and also the ease with which they are spoken of in an improper way.

Various arrangement mechanisms are adopted by different ions that try to occupy sites, which are more congenial to their requirements in terms of charge, volume and molecular shape, or specific chemical properties. The greater the number and quantity of species substituting the original groups (bivalent cation, or site C; OH<sup>-</sup> group, or site A; PO<sub>4</sub><sup>3-</sup> group, or site B), the more numerous are the possible combinations of solid apatitic solutions. Account must also be taken of sites that must remain empty in order to respect charge neutrality even at short distance. Such sites may involve each of the three original groups. The following table lists the most common, or regular, ions which can form specific apatitic molecules by filling the three sites. Some other ions are included in the list in parentheses, but they are not typical for the formation of apatitic compounds and can substitute regular ones in their own crystallographic site as vicarious.

**Table 2.9.7:** Main components that can fill the three sites of hydroxyapatite

Site of Ca <sup>2+</sup>	Site of PO <sub>4</sub> <sup>3-</sup>	Site of OH <sup>-</sup>
(C)	(B)	(A)
Ca <sup>2+</sup>	PO <sub>4</sub> <sup>3-</sup>	OH <sup>-</sup>
Sr <sup>2+</sup>	HPO <sub>4</sub> <sup>2-</sup>	CO <sub>3</sub> <sup>2-</sup>
Ba <sup>2+</sup>	CO <sub>3</sub> <sup>2-</sup>	F <sup>-</sup>
Cd <sup>2+</sup>	(SiO <sub>4</sub> <sup>2-</sup> )	Cl <sup>-</sup>
Pb <sup>2+</sup>	(HCO <sub>3</sub> <sup>-</sup> )	(S <sup>2-</sup> )
Eu <sup>2+</sup>	(P <sub>2</sub> O <sub>7</sub> <sup>4-</sup> )	O <sup>2-</sup>
(M <sup>+</sup> ) <sup>b</sup>	(H <sub>2</sub> O)	----
(D <sup>2+</sup> ) <sup>b</sup>	-----	----
(T <sup>3+</sup> ) <sup>b</sup>	-----	-----
(Mg <sup>2+</sup> )	-----	-----

<sup>b</sup>M= Monovalent ions (Na<sup>+</sup>, K<sup>+</sup>), D= Divalent ions (Fe<sup>2+</sup>, Mn<sup>2+</sup>), T= Tetravalent ions (Al<sup>3+</sup>, Fe<sup>3+</sup>, Mn<sup>3+</sup>).

Classical vicarious substitutions are, e.g. HPO<sub>4</sub><sup>2-</sup> and CO<sub>3</sub><sup>2-</sup> for PO<sub>4</sub><sup>2-</sup>. However, it must be emphasized that, for example, incorporation of CO<sub>3</sub><sup>2-</sup> is extremely difficult in high-temperature syntheses, while at the same temperatures it is very much possible to incorporate P<sub>2</sub>O<sub>7</sub><sup>4-</sup> groups (e.g. originating from the condensation of HPO<sub>4</sub><sup>2-</sup>) into the apatitic groups.

### 2.9.8. The role of impurities present in a hydroxyapatite powder:

Impurities can play an important role during thermal transformation of hydroxyapatite. They can be divided into two categories:

**(i) Ionic impurities:** As previously noted in relation to hydroxyapatite substitutions, some ionic species may penetrate into the lattice and take the place of each of the three groups: cation ( $\text{Ca}^{2+}$ ), phosphate ( $\text{PO}_4^{-3}$ ), and even hydroxyl ( $\text{OH}^-$ ). Each kind of substitution modifies in a specific way the behavior of the resulting apatite in terms of its chemical and thermal stability. In the thermal evolution, in particular, these ionic impurities may (depending on their nature and quantity) lead to the existence of other phosphatic phases. Some possible cations which substitute  $\text{Ca}^{2+}$  in its site can be toxic (such as  $\text{Ba}^{2+}$ ,  $\text{Pb}^{2+}$ ), and this has induced authorities to introduce normative regulations and standards of production to prevent particular kinds of contaminants. Other impurities may be  $\text{Sr}^{2+}$ ,  $\text{Mg}^{2+}$  alkaline ions, etc., which may even influence - by their nature and quantity - the stability of the phosphates in question.

**(ii) Foreign phases:** These may either occur in the starting powders or may develop as a result of thermal decomposition of the different phosphates. The latter aspect is particularly important in regard to thermal decomposition of defective hydroxyapatite. The foreign phases and more stoichiometric hydroxyapatite remain in physicochemical equilibrium between themselves at every temperature.

**(a) Ionic Impurities.** X-ray analysis sometimes shows apatite peaks at a large band. This kind of compound appears to give rise to sudden transformations from 550 °C to 650 °C. Within this range there is a decrease in the crystallinity shown by X-ray, while at a higher temperature separate phases form such as primarily, hydroxyapatite, TCP (in  $\beta$ - and  $\alpha$ -phases), and OCP. In addition, the more different the compositions and physicochemical methods for obtaining the powders, the more variations will there be in the thermal story of hydroxyapatite following the disruption of the apatite lattice.

Regarding the behavior of elementary cells, there is seen in the original lattice a general tendency to high volumes, a circumstance that illustrates the difficulty of molecular rearrangement. An increase in thermal mobility brings about a collapse of the lattice, with a resulting decrease in crystallinity also due to the presence of crystallites. This event follows the destruction of the original lattice and prompts the formation of more stable lattices, which in the end leads to the existence of other foreign phases ascertainable by X-ray analysis from 700 °C upward.

Above this temperature, the volume of the elementary cell appears to decrease slowly up to about 1000 °C in relation to a loss of CO<sub>2</sub> and H<sub>2</sub>O (if present). At around 1200 °C all the elementary-cell values coincide with and correspond to those considered canonical or stoichiometrically pure hydroxyapatite. The outcome is that a discharge of foreign ions allows the apatitic lattice to optimally rearrange the remaining fraction of atoms. While gaseous ions such as CO<sub>2</sub> and H<sub>2</sub>O leave the system, there may still persist some equilibria between the various phases formed. The trend is in fact toward a combination of phases thermodynamically stable at that temperature. This also applies to the equilibria relative to the quantities of existing phases and the equilibria between the lattice defects of one phase and those of other phases.

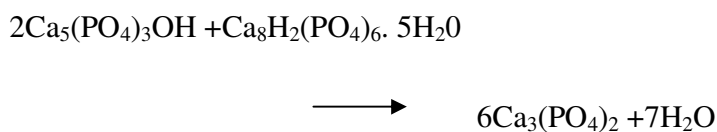
A report on stoichiometric reaction is complicated, but experience indicates some guidelines:

If OCP is present, at low temperatures there are reactions of the type:

HA (highly defective and low crystalline) + OCP



With stoichiometric hydroxyapatite, a reaction like that leads to:



At the highest temperatures, there are phase equilibrium reactions that lead to a decrease in the lattice defects of hydroxyapatite (especially in the presence of CaO). It must be stressed that if hydroxyapatite is stoichiometrically free from defects in terms of ionic impurities and free from the consequent defects due to vacancies, it would undergo no thermal transformation, apart from that of condensation to oxyapatite at a temperature of around 1400 °C.

All the transformation undergone by hydroxyapatite and leading to the formation of other compounds do not derive from stoichiometric hydroxyapatite, but from those apatitic/phosphatic compositions whose lattice hosts ions that, by their nature and for their complexity (in terms of distribution of charges, steric reasons, ionic/covalent ratio of the produced bond, etc.), differ from the canonical ones ( $\text{Ca}^{2+}$ ,  $\text{PO}_4^{3-}$ ,  $\text{OH}^-$ ) that they proceed to substitute. In general, the existence of impurities some influence not only on thermal stability but also on bio compatibility and biological resorption in in vivo implants.

The deposition of a hydroxyapatite layer on the substrate answers two purposes:

1. To preserve the substrate and prevent its contact with physiological fluids.
2. To enable an anchoring to tissue as natural as possible (just like what happens with the introduction of hydroxyapatite in-bulk devices).

Care must be taken to evaluate the kind of porosity and the existing pinholes. These defects may in fact be harmful, because they allow the physiological liquids that are on the outside of the coated prosthesis to come into contact with the substrate. Such a contact can induce corrosion phenomena below the coating layer that are not easy to identify and are more dangerous than corrosion phenomena that might have developed directly on the uncoated substrate. The reason is that such substrate is not under the protection of corrosion or passivation treatments, whose effects were in any case cancelled by the cleaning procedures (etching and sand-blasting) applied to prepare the surface for plasma-spray coating.

**(b). Foreign phases:** Depending on the method adopted to synthesize the apatitic powder, the powder may or may not be accompanied by other separated phases such as  $\text{CaHPO}_4$ ,  $\text{Ca}_8(\text{H}_2\text{PO}_4)_6 \cdot 5\text{H}_2\text{O}$ , and  $\text{Ca}_2\text{P}_2\text{O}_7$ . If present, these phases could be identified by X-ray diffractometry. The mentioned phases do not generally exceed just a few percent units in many commercial products, but are nonetheless noxious because they start a "story of reactions" with hydroxyapatite already at low temperatures (beyond  $600^\circ\text{C}$ ) and give rise to compounds in the ceramic body that are sufficiently soluble and consequently compromise in time the mechanical efficiency of an implanted device made with that ceramic.

It must be noted that a hydroxyapatite covering will bring the same biological benefits that would be brought by the introduction of an in-bulk hydroxyapatite ceramic. The use of hydroxyapatite as coating is evidently motivated by the fact that the substrate provides all the desired properties in terms of mechanical benefits. However, the minimum thickness of the deposited and properly evaluated layer should not be less than  $70\ \mu\text{m}$ . It was in fact observed that in animal and human implants there was in the phagocytic phase an average layer corrosion of around  $40\ \mu\text{m}$ . What was said above is valid provided that the deposited hydroxyapatite is crystalline, a condition ensuring greater physicochemical stability.

It may happen that a number of cells penetrate the porosity, affecting the walls of the ceramic pore. This event on the one hand vitalizes the covering hydroxyapatite layer but may, on the other hand, give rise to localized weakening that might in turn bring about a detachment from the substrate.

### **2.9.9. Transformations Induced at High Temperature by Plasma Spraying:**

Plasma spray application of hydroxyapatite on the substrate may give rise to a change (at least partial) in the nature of the latter.

The main transformations to be considered in producing a hydroxyapatite ceramic are:

Presence or possibility of formation of  $\text{CaO}$ .



Presence or possibility of formation of TCP whose  $\beta$ -phase undergoes a transformation of great importance in  $\alpha$ -TCP at 1290 °C

Powders must be precalcined to avoid any packing phenomenon. Grains must be rounded, possibly with a spherical shape, and carefully selected.

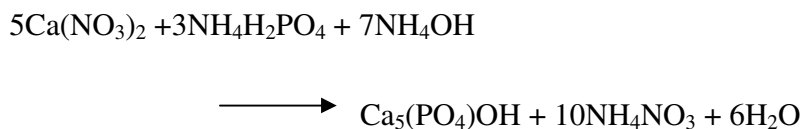
#### **2.9.10. A Survey on Different Methods for Synthesizing Hydroxyapatite:**

The nature of a hydroxyapatite crystal lattice allows easy replacement of a number of chemical groups with others, endowing the resulting compound characteristic slightly dissimilar to those of the theoretical hydroxyapatite. In a synthesis, it is simpler to obtain partially substituted apatites than stoichiometrically ones. The required formulation could be achieved through small chemical or operative adjustments of the previously proposed methods.

The quality of the obtained hydroxyapatite is commonly represented by values assumed by the theoretical stoichiometric ratio Ca/P=3/5 (or 1.6). Regarding the preparation of hydroxyapatite from an operative point of view, we shall discuss the following methods: (1) wet preparation, (2) sol-gel preparation, (3) mechanochemical preparation, (4) dry preparation, (5) preparation of hydroxyapatite as inorganic cement.

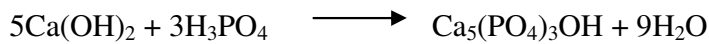
##### **2.9.10.1. Wet Preparation:**

Several methods of hydroxyapatite synthesis from an aqueous solution have been proposed since 1961 (Mooney and Aia, 1961). One of the commonest is under ammoniac-alkaline conditions according to Asada et al. (1987):



This process, however, though very simple, requires not only a great amount of ammonia for the reaction, but also repeated washing with water on the filtered precipitate to try to

eliminate any residual of it and of formed  $\text{NH}_4\text{NO}_3$ . An alternative method, the most widely adopted for small-scale productions, is that proposed by Akao et.al (1981):



The above reaction occurs when  $\text{H}_3\text{PO}_4$  is dropped in a  $\text{Ca}(\text{OH})_2$  aqueous suspension. Calcium hydroxide is in fact very weakly soluble in water, and consequently the reaction takes place between the  $\text{PO}_4^{3-}$  ions diffused from the drop plunged into the suspension and the surface of the colloidal particles, The alkaline pH of the aqueous environment, in which hydroxyapatite is stable, is maintained by the complete dissociation of the few dissolved molecules or  $\text{Ca}(\text{OH})_2$  which is a strong base. The hydroxyapatite forming reaction is therefore linked to the rate of: (1) diffusion the ionized phosphatic ionic groups ( $\text{PO}_4^{3-}$ ,  $\text{HPO}_4^{2-}$ ,  $\text{H}_2\text{PO}_4^-$  and  $\text{H}_3\text{PO}_4$  itself) connected to each other by well-known simultaneous equilibria, (2) dissolution of  $\text{Ca}(\text{OH})_2$  as well as that of diffusion of  $\text{Ca}^{2+}$  ions into the aqueous system, and (3) migration of the ionized phosphate groups within the colloidal grains of  $\text{Ca}(\text{OH})_2$ . The success of the transformation depends on the value of the local pH, even if the overall solution may remain alkaline. There develops in fact, all around the plunged drop, an environment resulting from the diffusion of  $\text{H}_3\text{PO}_4$  molecules and, according to the pH, the resulting ions are prevalently one of the above-cited allowed by the simultaneous equilibria. Therefore layers richer in  $\text{PO}_4^{3-}$ , or  $\text{HPO}_4^{2-}$ , Or  $\text{H}_2\text{PO}_4^-$ , or  $\text{H}_3\text{PO}_4$  will occur, starting from the periphery to the core of the drop. The hydroxyapatite-forming reaction is also linked to the concentration of  $\text{OH}^-$  ions, and through the formation of each molecule and the consequent trapping of an  $\text{OH}^-$  ions for each formed molecule the reaction contributes to a decrease in the local pH. In this way, unless the local pH is adequately checked, there is a risk that may give rise to a combination of residual  $\text{Ca}(\text{OH})_2$  in the core of the colloidal granules and to a certain quantity of phosphates of varying nature, such as dicalcium phosphate (DCP), tricalcium phosphate (TCP), and octacalcium phosphate (OCP).

Another factor to be considered is the presence of carbonate within the solution for all possible kinds of synthesis. It is in fact possible that  $\text{CO}_3^{2-}$  ions, even if not deliberately introduced as carbonate of some cation, are present in the solution at equilibrium with the

CO<sub>2</sub> of the atmosphere. The dissolved fraction of carbonic acid may replace the anionic component of the calcium compounds and give rise to more stable CaCO<sub>3</sub> by operating in an alkaline environment. This is a further component which may be involved in the production of other kinds of phosphates, including the carbonate apatites.

Such a presence of CO<sub>2</sub> can be avoided by promoting a reaction inside a reactor and cause gas not contaminated by CO<sub>2</sub> to gurgles in the solution. All the foreign ions present in the synthesis solution may lead to the formation of molecules different from the hydroxyapatite molecule. These molecules may aggregate (and eventually crystallize in foreign phases), or may induce the formation of other phases and hinder the formation of hydroxyapatite, or may associate in the precipitation of hydroxyapatite crystals and, by co-precipitating, replace one or other of the component groups in their regular group. In this way, for example, HPO<sub>4</sub><sup>2-</sup> and CO<sub>3</sub><sup>2-</sup> may replace PO<sub>4</sub><sup>3-</sup> in its site and CO<sub>3</sub><sup>2-</sup> may also replace the OH<sup>-</sup> group in its site.

If these replacements occur, defective hydroxyapatite is produced in which a number of empty sites are present inside the crystal lattice. Defective hydroxyapatites are always accompanied by lattice vacancies, which allow a rearrangement of the electro neutrality of the overall charge. The behavior during firing of these defective hydroxyapatite may cause alterations to the products, such as the formation by segregation of α- and β- TCP, free CaO, pyrophosphates, etc.

To favor the escape of foreign ions from the hydroxyapatite lattice and at the same time to increase the thickness and the rate of crystallization of synthesized hydroxyapatite, it is essential to allow a digestion of the solution once the synthesis has been completed, after the addition of the last drop which brings about the correct stoichiometric ratio between Ca<sup>2+</sup> and PO<sub>4</sub><sup>3-</sup> (in an atomic, or molar, ratio of 5/3).

The digestion consists in maintaining the solution at rest at a temperature of about 37 °C for at least 48 hours. It was ascertained that the highest degree of crystallinity was reached when the solution approached the boiling temperature (about 97 °C).

Another wet method for producing hydroxyapatite is to start from  $\text{Ca}^{2+}$  chelate complex [coming, e.g., from  $\text{Ca}(\text{NO}_3)_2$  or calcium acetate] ions with EDTA (ethylenediamine tetra-acetic acid). This method is generally adopted either to impregnate spongy bodies or clothes with hydroxyapatite or to coat fibrous materials with a hydroxyapatite film.

It consists in placing the body to be impregnated in an aqueous solution based on  $(\text{NH}_4)_2\text{HPO}_4$  with a pH brought to 7.5. A solution of  $\text{Ca}^{2+}$  with EDTA is then added to the previous one and the whole is mixed carefully. The strength in forming the complex with  $\text{Ca}^{2+}$  exerted by EDTA is so great that it prevents the capture of  $\text{Ca}^{2+}$  from it by the phosphate groups. Therefore, it is impossible to link  $\text{Ca}^{2+}$  and  $\text{PO}_4^{3-}$  partners to give rise to a precipitate. When the solution is suitably homogeneous,  $\text{H}_2\text{O}_2$  at 30 vol% is added. Oxygenated water oxidizes all the molecules of EDTA and thereby makes available the freed  $\text{Ca}^{2+}$  ions, which can now combine with the phosphate groups to form hydroxyapatite.

#### **2.9.10.2. Sol-gel preparation:**

The sol-gel method, which has attracted attention as a new synthesis method for glass and ceramic materials (Sakka, 1983, Maki and Sakka, 1986), is expected to produce fine granules at high purity at the highest stoichiometric obedience. This method is also pursued to obtain either bulk objects or thin coating films of hydroxyapatite directly without a powdering step (Masuda et al., 1990). Unlike what is commonly believed, the first paper concerning this method is very old, dating back to Ebelmen (1846), so belonging to history.

The procedure starts from molecular precursors dissolved in solutions that, unlike inorganic syntheses obtained by precipitation in aqueous solution, are organic solvents. The main conceptual difference comes just from the nature of such precursors. They are in fact organic molecules that include the inorganic atoms which will react afterward to give rise to the required chemical compound. This association of inorganic and organic parts is commonly called a metal-organic compound.

The name of the procedure originates from the constitution of a metal-organic component containing all the inorganic atoms in the correct stoichiometric proportion as required to obtain the required final inorganic compound, which is at first suspended as sol solution in the suitable solvent utilized for the organic reaction. This metal-organic component is obtained by a series of organic reactions starting from the precursors, in their turn each containing one of the different inorganic atoms to be associated. With the introduction of a further solvent in which the previous one is soluble, but which does not allow the solvability of the present sol, a flocculation of roundish colloidal gel particles is obtained which precipitate under gravity.

Although apparently different, this particular procedure (taken as a whole) is not substantially different from the common techniques of chemical synthesis already in use in industry, such as precipitation, co-precipitation, thermo hydrolysis, hydrothermy, etc. (Livage 994). Technologically speaking the adoption of this method is not easy as the procedures involved are very sensitive to many variables (far more so than with other methods).

Anyway, all the reactions can be described via the same chemical models. The only question is to expand the classical chemical interpretation of acid-base ratios by Arrhenius into the scheme followed by Bronsted and Lowry. The procedure consists in creating required inorganic compounds by a coupling process involving metal-organic components. Such a coupling process is in the first place a polymerization, and subsequently a colloidal condensation of gel micellae.

The polymerization step generally involves condensation coupling.

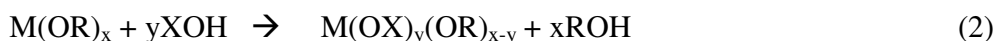
There can be many utilizable precursors, alkoxides, acetates, acethylacetonates, etc. Also, inorganic chemicals can be used provided they are soluble and/ or captured by complexatins agents in organic solvents, Mixtures of inorganic compounds as well as metal-organic precursors can be used too. All depends on the physiochemical operative conditions, on the ability to provide specific metal-organic precursors, and on the specificity of the required final compound.

The utilization of alkoxides is very popular owing to their easy availability in the market from many international companies. Generally speaking, their synthesis is carried out in various ways (Bradley *et al.*, 1978). The simplest method could be:



The chemical reactivity of alkoxides is connected to the impervious arrangement of the molecular structure of the metal-organic complex. This arrangement is conditioned by the inclination of the inorganic atom in a complex to assume a coordination with the largest number of molecules which produce *chelate* complexes, assuming its typical n-fold symmetry fashion. This depends on its external electronic configuration and on the consequent specific hybrid of coordination. However, the number of organic molecules coordinated in giving rise to the metal-organic complex depends not only on the maximum degree of coordination that is possible, but on the overall configuration arrangement induced by the steric situation, which occurs in connection with the dimensions and the stereoisometry of the organic molecule that is able to produce chelate complexes. Therefore, different complexes having very different molecular structures can be found for the same inorganic atom possessing extremely variable reactivity.

Most alkoxides are extremely reactive compared to nucleophilic compounds:



The chemistry of alkoxides applied by the sol-gel method is founded on this equation. Therefore, with a reaction of chemical condensation such as this, new molecular precursors are synthesized and, in their turn, are involved as they are formed, so giving rise to more and more modified molecules having new structural arrangement, chemical complexity, and different steric factors. In this way, during the polymerization a continuous modification of reactivity and functionality of the whole system in reaction is involved. This process of polymerization is consequently modifiable, so allowing intervention to chemically control the structure and morphology of the required final product. Needle-like structures of the final powders come more easily, e.g., from polymerization in linear chains, while micro crystals with axial/ basal ratio more prone to

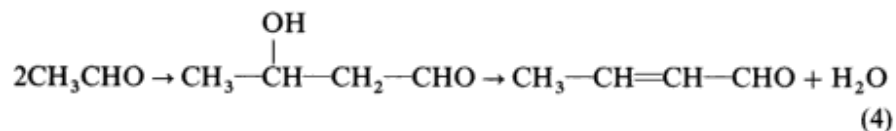
unity come more easily, e.g., from polymerization of clusters of multibranched polymers joined to each other.

A controller, or propagation stopper, of polymerization by polycondensation is acetylacetone ( $\text{CH}_3\text{-CO-CH}_2\text{-CO-CH}_3$ ) which, by formation of a chelate complex with its own carbonyl groups the reading sites of the head of propagation of the reacting polymeric molecules, stops the condensation process and so decreases the possibility of propagation of the polymerization process. The grain size of the powder of the required compound depends on when the condensation process is stopped.

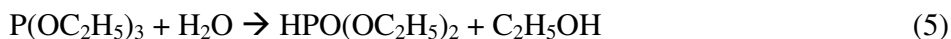
As concerns the sol-gel preparation of hydroxyapatite, a method was recently proposed (Masuda et al., 1990) which starts from calcium diethyl-oxide,  $\text{Ca}(\text{OC}_2\text{H}_5)_2$  and triethylphosphite,  $\text{P}(\text{OC}_2\text{H}_5)_3$ . The procedure continues by dissolving calcium diethyloxide in ethylene glycol and the triethylphosphite in ethanol. These nonaqueous solvents are carefully dried for 24 hours by molecular sieves before use. This is to avoid the reaction of the metal-organic component with the more acidic molecules of water present inside the solvent before they have been reacted in the useful way. The starting materials are allowed to react with each other in a completely dried  $\text{N}_2$ , atmosphere (to reach a good result,  $\text{N}_2$  must be dried by passing through a molecular sieve column). The ethylene glycol solution of  $\text{Ca}(\text{OC}_2\text{H}_5)_2$  is mixed with the ethanol solution of  $\text{P}(\text{OC}_2\text{H}_5)_3$  while stirring. When both solutions are well mixed to set the Ca/P molar ratio at 5/3, a mixture of water, ethanol, and acetic acid is in its turn added drop by drop (1 ml/min) always under stirring. The pH value will be maintained in a suitable range to favor gel flocculation and at the same time prevent possible reaction that may lead to a precipitate with a Ca/P ratio different from that theoretically required. In this manner the reagents undergo a number of reactions while the environmental solution changes its nature, favoring the formation of gel precipitates. The whole reactive process starts with the following dehydration of ethylene glycol by calcium diethyloxide:



The formed aldehyde is a source of problems. In the first place, it causes an aldolic condensation if the solution is under alkaline conditions:



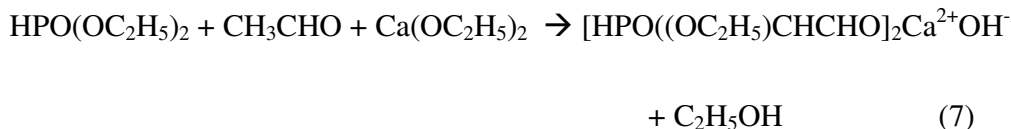
At the same time, the triethylphosphite reacts slowly with some of the added water to obtain



The phosphorylic ester so formed reacts with the aldehyde coming from reaction (3):



But this reaction is slow, while if  $\text{Ca}(\text{OC}_2\text{H}_5)_2$  is present the following faster reaction takes place:



In which the calcium ion compound undergoes the dissociation

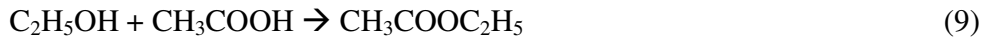


The calcium ion derivative turns into calcium hydroxide in the presence of a sufficient amount of water. Both hydroxyl calcium ion derivative

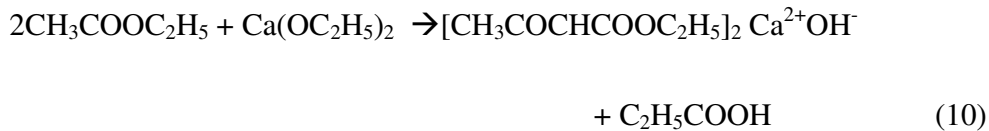
$[\text{HPO}(\text{OC}_2\text{H}_5)\text{CHCHO}]_2\text{Ca}^{2+}\text{OH}^-$  and calcium hydrate are substantially all precipitated as gel colloids, while the phosphoric ester is sufficiently soluble. Consequently the required correct stoichiometric proportion is not guaranteed.

To avoid this problem it is necessary to stop the action of aldehyde. An addition of acetic acid yields

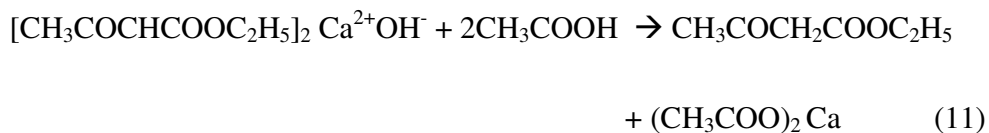




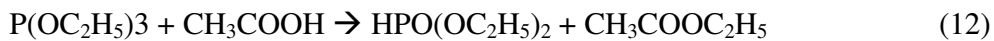
Ethyl acetate ester thus formed underwent an ester condensation in the presence of calcium diethyloxyde as calcium source. An alternative insoluble and relatively stable calcium derivative ion is formed:



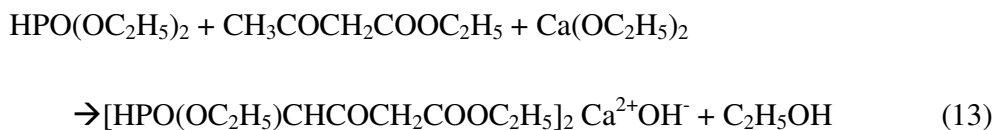
This derivative ion is partially converted to calcium acetate, depending on the pH and the amount of introduced acetic acid:



On the other hand, triethylphosphite would react with acetate to form phosphoric ester and ethyl acetate:



A phosphoric-calcium-containing ion derivative is obtained at this point by condensation of the products from reactions (5), (11), and (12):

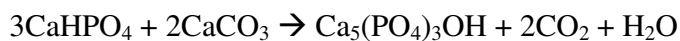


Since some amounts of phosphorus and calcium remain in the solution as soluble salts or organic compounds, a correct compromise to obtain a good Ca/P ratio of the gel precipitates to produce a high-purity hydroxyapatite is to balance all the existing reactions, both those with and without intervention of acetic acid. Such a compromise is reached when a relatively neutral environment (pH~ 7.5-8.5) is adopted, with a low concentration of acetic acid and no more than 20% ethanol.

The step that follows is to allow flocculation of the forming gel precipitate, possibly with the aid of a centrifugation process. The obtained gel mass is thus put in Pt crucibles and heated at 900<sup>0</sup>C in a kiln, possibly in a flux of air. During firing all the organic part is pyrolyzed, producing CO<sub>2</sub> and H<sub>2</sub>O, and the inorganic parts react together in giving rise to hydroxyapatite. Contamination of CO<sub>3</sub><sup>2-</sup> for PO<sub>4</sub><sup>3-</sup> can occur in the apatite lattice, depending on the amount of organic part and the rate of air flow. An enrichment of Ca<sup>2+</sup> can derive from a pH >8.5, which favors the lattice substitution of carbonate, while low values of the Ca/P ratio can derive from a pH < 6, which leads to formation of some calcium triphosphate.

### **2.9.10.3. Mechanochemical preparation:**

The mechanochemical method consists in subjecting powder mixtures of suitable composition to pressure by the use of grinding media. The reaction to produce hydroxyapatite is (Toriyama et al., 1995, 1996; Krajewski et al., 1995, 1996)



and can be activated by producing energy in the form of both heating and mechanical work . The reaction is generally promoted in large cylindrical jars filled with ZrO<sub>2</sub> balls of suitable dimensional distribution. Some have observed that Al<sub>2</sub>O<sub>3</sub> balls cannot produce sufficient activation of the reaction. The reason for this, apart from any unreliable catalytic influence on the substance constituting the balls, is the higher density of ZrO<sub>2</sub> balls. Such a higher density determines a higher pressure on the powders, especially those lying between the balls and the internal wall of the jar. This means that the equilibrium of the reaction is shifted toward the right, owing to the variation in the pressure of the reaction system. The provision of the obtained product is guaranteed by the outflow of CO<sub>2</sub> and H<sub>2</sub>O.

The best conditions were observed when use was made of a jar made from ZrO<sub>2</sub>, and the efficiency appeared to increase with increase in the diameter of the jar. This also agrees

with the thesis of pressure originating from both gravity and centrifugal forces of the column of balls incident on each point of the internal wall of the jar. On the basis of these observations, a threshold value of pressure will exist which is able to activate the reaction.

The operation consists in placing the powders to be reacted into the jar with a quantity of water ten times the overall weight of the powders. The overall weight of the balls must be at least five times as high as the amount of water. The best grinding conditions appeared to be at 24 hours and 280 rpm for the ZrO<sub>2</sub> based jar and at 48 hours, under the same reaction rate, for jars made from softer materials such as Teflon. The hydroxyapatite synthesized in a jar with softer walls was more defective and gave rise in the sintering phase to a considerable TCP fraction which, however, was almost absent in the synthesis performed inside ZrO<sub>2</sub> based jars.

#### **2.9.10.4. Other methods:**

Hydroxyapatite (Ca<sub>5</sub>(PO<sub>4</sub>)<sub>3</sub>(OH), HA) is similar with the mineral constituents of human bone and teeth. Due to its excellent biocompatibility and bioactivity, wide applications include bone fillers [198], surface coatings [199,200] and unloaded scaffolds [201,202]. It is the poor mechanical properties, such as fracture toughness and flexural strength that limit its medical applications of HA under load bearing conditions. These properties could be improved by using composites reinforced with HA or reducing crystalline size to nano scale [203,204].

Nano-sized HA particles could be prepared by a variety of techniques such as mechano chemical synthesis [205], combustion preparation [206] and various techniques of wet chemistry [207, 20]. Among the most reported precipitation process, chemical agents, such as citric acid [209,210], amino acid [211] and EDTA [212,213] were always used to mediate HA nucleation and crystal growth process. These modifiers would finally exert significant control on crystal morphology due to some form of affinity between modifying agent and HA crystal. However, less attention had been paid on precipitation kinetics of nucleation and growth, which was related with the degree of supersaturation.

Chengfeng Li [214] used  $\text{Ca}(\text{OH})_2$  and  $\text{H}_3\text{PO}_4$  to synthesize nano-sized hydroxyapatite. In the process of acid-base reaction, citric acid or sodium citrate was added to influence the crystallinity of hydroxyapatite. Formation of Ca-citrate complex resulted in variations of ionic concentrations and ionic activity products for solutions with different citrate additions. The degree of supersaturation was found higher for solutions with less citric acid or more sodium citrate addition. Consequently, hydroxyapatite particles with smaller size were gained. These crystalline behaviors were investigated and explained by mechanism of crystal nucleation and growth in solutions.

Hydroxyapatite has attracted much attention as a substitute material for damaged teeth or bones over the past several decades because of its crystallographical and chemical similarity with various calcified tissues of vertebrates [215-217]. The principal limitation of this material is that it is brittle and weak, which restricts the clinical orthopedic and dental applications [218,219].

There are several approaches for the improvement in mechanical properties of the HA. One is to fabricate HA reinforced with other ceramics. This approach has attracted much attention since the successful development of ceramic-matrix composite materials [220].

To be effective as a reinforcing agent for a ceramic-matrix composite material, the following conditions should be satisfied. First, the strength of the second phase must be higher than that of the matrix. Second, the interfacial strength between the matrix and the second phase should be neither too weak nor too strong. For an appropriate interfacial strength, no excessive reaction should occur between the matrix and second phase. In addition, the coefficient of thermal expansion (CTE) of the second phase should not differ too much from that of the matrix [221]. In the case of biomaterials, the biocompatibility of the reinforcing agent is another important factor that should be considered [222].

Zirconia has been commonly used as reinforcement for many ceramics because of its high strength and fracture toughness [223,224]. Bioinertness is another merit of the  $\text{ZrO}_2$

[225]. However, extensive reaction between the HAP and the  $ZrO_2$  to form TCP and fully stabilized  $ZrO_2$  is a serious disadvantage of this approach [226].

Alumina, which is also classified as a bioinert material, has been widely investigated as a reinforcing agent for HA [227]. Therefore, it is desirable to combine the advantages of both materials as reinforcements for the HA: the excellent mechanical properties of  $ZrO_2$  and the chemical inertness of  $Al_2O_3$  with respect to HA.  $ZrO_2$ - $Al_2O_3$  is one possible approach.

I. Mobasherpour et al. [228] synthesized nanocrystalline hydroxyapatite powder from a  $Ca(NO_3)_2 \cdot 4H_2O$  and  $(NH_4)_2HPO_4$  solution by the precipitation method. In the next step prepared  $ZrO_2$ - $Al_2O_3$  powder. After preparation, the powder was dried at  $80^\circ C$  and calcined at  $1200^\circ C$  for 1 h. Various amounts (HA-15 wt% ZA, HA-30 wt% ZA) of powder were mixed with the hydroxyapatite by ball milling. The powder mixtures were pressed and sintered at  $1000^\circ C$ ,  $1100^\circ C$  and  $1200^\circ C$  for 1 h. In order to study the structural evolution, X-ray diffraction (XRD) was used. Transmission electron microscopy (TEM) and scanning electron microscopy (SEM) were used to estimate the particle size of the powder and observe fracture surfaces. Results show that the bending strength of pressed nanocrystalline HA was improved significantly by the addition 15 wt% of  $ZrO_2$ - $Al_2O_3$  powders at  $1200^\circ C$ , but the fracture toughness was not changed, however when 30 wt% of ZA powders were added to nanocrystalline HA, the bending strength and fracture toughness of the specimens decreased at all sintering temperature.

The effect of fluoride additives on the mechanical properties of hydroxyapatite/alumina composites was investigated by Sung-Jin Kim et al. [229]. When  $MgF_2$  (5 vol%) was added to hydroxyapatite/alumina composites, the decomposition of hydroxyapatite was suppressed due to the substitution of F for  $OH^-$  in the crystal structure. Comparing two additives, such as  $MgF_2$  and  $CaF_2$ ,  $MgF_2$  showed much more effective for the suppression of phase decomposition in the hydroxyapatite/alumina composites due to the enhanced substitution of  $F^-$  for  $OH^-$ . In the case of  $MgF_2$  addition, a relatively high mechanical properties (flexural strength:  $\sim 170$  MPa; Vickers hardness:  $\sim 7$  GPa) was obtained compared to  $MgF_2$ -free composites.

The influence of equilibration conditions and hydroxyapatite (HAP) physico-chemical properties onto retention of  $\text{Cu}^{2+}$  ions was studied by M. Šljivić et al. [230] in batch conditions. The amount of cation removed from the solution increased with increasing pH, reaching almost 100% at pH 3, 4 and 7 for  $5 \times 10^{-4}$ ,  $10^{-3}$  and  $5 \times 10^{-3}$  mol/dm<sup>3</sup> solutions, respectively. Contact time necessary for reaching equilibrium was found to increase with the increase of  $\text{Cu}^{2+}$  concentration. Kinetic and equilibrium data were best described by pseudo-second-order kinetic model and Langmuir theoretical model. The calculated values of separation factors and Gibbs free energy change confirmed that the sorption was spontaneous and thermodynamically feasible at room temperature. The experiments conducted using HAP samples with different physico-chemical characteristics have revealed that the amounts of sorbed  $\text{Cu}^{2+}$  depended mainly on the specific surface area and crystallinity of the applied powders. Desorption of  $\text{Cu}^{2+}$  was more efficient in acidic conditions than in the solution of competing cation- $\text{Ca}^{2+}$ . The samples with higher sorption capacities also demonstrated higher stability; consequently, from the aspects of both higher sorption and lower desorption, utilization of low-crystalline HA samples with high specific surface area was superior for immobilization of  $\text{Cu}^{2+}$  ions. Taking into account molar Cu/Ca ratios, observed final pH changes, copper speciation in the function of pH and the results of X-ray diffraction analyses, conclusions about sorption mechanisms at different experimental conditions were derived.

The compressive strength of porous hydroxyapatite (HA) scaffolds was enhanced by Se-Won Yook et al. [231] by adding polystyrene (PS) polymer as a binder to hydroxyapatite (HA)/camphene slurries. As the PS content was increased from 0 to 20 vol% in relation to the HA content, the compressive strength was significantly increased from  $1.1 \pm 0.2$  to  $2.3 \pm 0.5$  MPa, while the pore size was decreased from  $277 \pm 47$  to  $170 \pm 29$  urn. The improvement in the compressive strength was mainly attributed to both the suppression of the cracking of the green sample during freeze drying and the mitigation of the formation of micro-pores in the HA walls.

M.I. Domínguez et al. [232] reports the synthesis, characterization and catalytic activity for CO oxidation of gold catalysts supported on calcium hydroxyapatite. On both the hydroxyapatite support and the gold-supported hydroxyapatite catalyst, the CO

conversion shows a peak near 100% of conversion at room temperature. The generation of structural vacancies by interaction of CO with the solid provokes the formation of peroxide species in the presence of gaseous oxygen, which seems to be responsible of this high conversion of CO at room temperature. Moreover, the influence of the pre-treatment temperature on the activity has been observed and related with the elimination of carbonate species and the generation of structural defects in the apatite structure, which are able to modify the gold oxidation state.

Ai-Juan Wang et al. [233] prepared hydroxyapatite microspheres by spray drying technology at different process parameters was investigated in this paper. The results indicated that the process parameters, such as the slurry concentration, compressed air flow rate, and liquid feed rate, played important roles in controlling the performance of hydroxyapatite microspheres, such as the specific surface area, the size distribution, etc., but had little influence on the micro morphology, phase composition and crystallinity. The spray dried particles were composed of low crystallinity and the scanning electron microscope results showed that they had good spherical structure with smooth surface. The results of the laser diffraction particle size analyzer indicated that the mean size increased with the increase of the slurry concentration and compressed air flow rate. Experimentally, most of the process parameters were crucial to the productive efficiency.

For immobilization technologies to be successful, the use of readily available and cost advantageous amendment is important when the remediation targets vast amounts of contaminated soils. Yohey Hashimoto et al. [234] investigate whether the byproduct-synthesized hydroxyapatite can be used as an immobilizing amendment for dissolved Pb from a shooting range soil, and to model the kinetic data collected from dissolution experiments. A soil-solution kinetic experiment was conducted under fixed pH conditions as a function of time. A Pb-contaminated soil was reacted with various hydroxyapatite amendments to determine the dissolution rate and mineral products of soil Pb. Three types of amendments used were pure hydroxyapatite (HA), and poorly crystalline hydroxyapatites synthesized from gypsum waste (CHA), and synthesized from incinerated poultry litter (PHA). The dissolved Pb concentration decreased with the addition of amendments at pH 3-7. Both CHA and PHA were more effective than HA for

attenuating Pb dissolution at pH 6 and above. According to the thermodynamic calculation at pH 6, the dissolved Pb concentration for CHA and PHA treatments was predicted to be 66% and 50% lower than that of HA treatment, respectively. A better Pb immobilization effect demonstrated by CHA and PHA resulted in their greater solubility at higher pH, which may promote the formation of chloropyromorphite precipitates. Dissolution kinetics of soil Pb was adequately explained by pseudo-first order and pseudo-second order equations in acid pH ranges. According to the ion exchange model, an adequate agreement between the experimental data and regression curves was shown in the initial 40 min of the reaction process, but the accuracy of model predictability decreased thereafter. According to kinetic models and dissolution phenomena, CHA and PHA amendments had better Pb sorption capacity with rapid kinetics than pure hydroxyapatite at weak acid to neutral pH.

Simone Sprio et al. [235] deals with the preparation of bioactive ceramic composites to be employed for the development of load-bearing bone substitutes, made of hydroxyapatite and bioactive dicalcium silicate ( $\text{Ca}_2\text{SiO}_4$ ,  $\text{C}_2\text{S}$ ) as a reinforcing phase. The composite materials were prepared by Fast Hot-Pressing (FHP), which allowed the rapid sintering of monolithic ceramics at temperatures up to 1500 °C, well above the commonly adopted temperatures for the consolidation of hydroxyapatite (1200-1300 °C). The purpose was to achieve the grain coalescence of both HA and the strengthening phase, so that to obtain a homogeneous ceramic material characterized by controlled phase composition and improved mechanical strength; the dwell time was reduced as much as possible to prevent HA decomposition and excessive grain growth. The most remarkable result, in terms of phase composition, was the absence of any secondary phases in the final ceramics other than HA and  $\text{C}_2\text{S}$ , even after sintering at 1500 °C. The flexure strength of the composite materials was found to be much higher than that of HA alone. Further mechanical characterization was also carried out on HA and composites, sintered in different conditions, to evaluate the elastic properties and fracture toughness, and properties close to those of mineral bone were found. These preliminary results confirmed that composites of HA and  $\text{Ca}_2\text{SiO}_4$  are promising for the development of bioactive load bearing ceramic bone substitutes with controlled phase composition.



Nano-hydroxyapatite reinforced poly(vinyl alcohol) gel (nano-HA/PVA gel) composite has been proposed by Yusong Pan et al. [236] as a promising biomaterial, especially used as an articular cartilage repair biomaterial. In this work, nano-HA/PVA gel composite was prepared by in situ synthesis method and incorporation with freeze-thaw cycle process. The effects of various factors on the friction coefficient of the gel composites and stainless steel ball counterpart were investigated by a ball-plate friction and wear tester. The variations of the friction coefficient with influence factors were explored by Hertzian contact theory and elastohydrodynamic lubrication theory. The results show that the friction coefficient of the gel composites is positively to the normal load and inversely proportional to the sliding speed and the diameter of stainless steel ball. Furthermore, the friction coefficient of the gel composites is obviously lower than that in distilled water or in physiological saline, whereas, friction coefficient has little difference between in distilled water and in physiological saline.

Adsorption kinetics and adsorption isotherms of Cu(II) onto a nanosized hydroxyapatite (HA) in the absence and presence of different low-molecular-weight organic acids are studied in batch experiments by Yu-Jun Wang et al. [237]. The results show that the adsorption kinetics of Cu(II) onto the HA are best described by pseudo-second order model, and the adsorption isotherms of Cu(II) onto the HA fit Dubinin-Radushkevich model very well with high correlation coefficient ( $R^2 = 0.97-0.99$ ). The amount adsorbed of Cu(II) onto the HA at pH 5.5 was much higher than that at pH 4.5. The presence of organic acids significantly decreased the adsorption quantity of Cu(II), clarifying the lower sorption affinities of Cu(II)-organic acid complexes onto the HA rather than Cu(II) ion. The decreased maximal adsorption quantity of Cu(II) onto the HA increased with the increasing logarithm of cumulative formation constants of Cu(II) and organic acids. The stronger coordination of organic acid with Cu(II), the more decreased Cu(II) adsorption quantity onto the HA.

Composites of hydroxyapatite with partially stabilized zirconia with MgO or MgF<sub>2</sub> were pressureless sintered by Zafer Evis et al. [238] between 1000 °C and 1300 DC. The reactions and transformations of phases were verified by X-ray diffraction. For the hydroxyapatite and zirconia composites with MgO, calcium from the hydroxyapatite

diffused into the zirconia phase, and the hydroxyapatite decomposed to tri-calcium phosphate at sintering temperatures higher than 1000 °C. Above about 1200 °C,  $\text{CaZrO}_3$  was formed. Composites containing the  $\text{MgF}_2$  decomposed slower than the composites with  $\text{MgO}$ , which was verified by the changes in the lattice volume of the hydroxyapatite left in these composites. Fluorine ions in  $\text{MgF}_2$  diffused into hydroxyapatite, which resulted in thermal stability at high sintering temperatures. Composites with  $\text{MgF}_2$  had higher hardness than those with  $\text{MgO}$ . The lowest porosity was found in a composite initially containing 10 wt% partially stabilized zirconia and 5 wt%  $\text{MgF}_2$ .

Micro-arc oxidation (MAO) is commonly used to modify the surface of Ti-based medical implants with a bioactive and porous titanium oxide ( $\text{TiO}_2$ ) layer. Dong-Yoon Kim et al. [239] reports a novel method of incorporating hydroxyapatite (HA) within the  $\text{TiO}_2$  layer by coupling MAO with an electrophoretic deposition (EPD) process. A HA-incorporated, porous  $\text{TiO}_2$  layer was produced successfully on the Ti substrate using the EPD-coupled MAO treatment, as confirmed by electron microscopy observations. Addition of ethanol to the electrolyte solution containing the fine HA particles was essential to reduce the level of gaseous emission on the anode, which obstructs the attachment of HA particles. In vitro cellular assays showed that the incorporation of HA significantly improved the osteoblastic activity on the coating layer.

R.M. Trommer et al. [240] reported the production of hydroxyapatite (HA) powder, one of the most studied calcium phosphates in the bioceramics field, using a cost-effective apparatus, composed by three major components: the atomization device, the pilot and main flames and finally the powder collector system. Calcium acetate and ammonium phosphate, diluted in ethanol and water, were used as salts in the precursor solution. The Ca/P molar ratio in the precursor solution was 1.65, equivalent to biological hydroxyapatite. After its production and collection, HA powder was calcined at 600 °C for 2 h. X-ray diffraction analysis pointed to the formation of crystalline hydroxyapatite powders. Carbonate was identified in the powders by Fourier-transform infrared (FTIR) spectroscopy. Scanning electronic microscopy (SEM) showed that the powders were composed of spherical primary particles and secondary aggregates, with the morphology unchanged after calcination. By transmission electronic microscopy (TEM), it was

observed that the crystallite size of the primary particles was  $24.8 \pm 5.8$  nm, for the calcined powder. The specific surface area was  $15.03 \pm 6.4$  and  $26.50 \pm 7.6$   $m^2/g$ , for the as-synthesized and calcined powder respectively.

## References:

- [1]. Phosphate Primer, website of the Florida Institute of Phosphate Research.
- [2]. "Figuring Out Phosphates," Food Product Design, June 2006, Lynn A. Kuntz .
- [3]. Campbell, Neil A.; Reece, Jane B. (2005). Biology (Seventh Edition ed.). San Francisco, California: Benjamin Cummings. pp.65. ISBN 0-8053-7171-0
- [4]. T. Kanazawa, Kagaku no Ryoiki, 24, 222 (1970) (in Japanese).
- [5]. W. Eitel, Silicate Science, vols. I-V, Academic Press (1964-1966).
- [6]. T. Kanazawa (ed.), Inorganic Phosphorus Chemistry, Kodansha (1985) (in Japanese).
- [7]. A.E.R. Westman, Topics in Phosphorus Chemistry, vol. 9 (Eds. E.J. Griffith and M. Grayson), p.300, Interscience (1977).
- [8]. J.R. Van Wazer and K.A. Holst, J. Am. Chem. Soc., 72, 639 (1950) .
- [9]. D.E.C. Corbridge, Phosphorus-An Outline of its Chemistry, Biochemistry and Technology (3rd Ed.), p.129, Elsevier (1985).
- [10]. A.D.F. Toy, Phosphorus Chemistry in Everyday Living, American Chemical Society (1977).
- [11]. J.R. Lehr et al., TVA DATA, Dec. 1976-FR, p.17-36, TVA, USA (1976) .  
R. Minami, Mineralogical Studies on Phosphate Rocks, Tokyo. University of Agriculture (1964).
- [12]. Elwell D, Scheel HJ (1975) Crystal Growth from High-Temperature Solutions. Academic Press.
- [13]. Nassau K. Nassau J (1980) The Growth of Synthetic and Imitation Gems. In: Freyhardt HC (ed) Crystals. Springer-Verlag, pp 1-50.
- [14]. Sunagawa I (1982) Gem Materials. Natural and Artificial. In: Kaldis E (ed) Current Topics in Materials Science, Vol 10. North Holland Publishing Company, pp 357-497.
- [15]. Frondel C: Mineralogy of the calcium phosphates in insular phosphate rock. Am Miner 1943;28:215-232.
- [16]. McConnell D: Apatite, Its Crystal Chemistry, Mineralogy, Utilization, and Geologic and Biologic Occurrences. New York, Springer-Verlag, 1973..

- [17]. Nriagu JO, Moore PB (eds): Phosphate Minerals, Berlin, Springer-Verlag, 1984.  
 Notholt AJG, Jarvis I (eds): Phosphorite Research and Development. London, Geological Society Special Publication No 52, 1990. .
- [18]. Dana JO, Dana ES: System of Mineralogy, 7th Ed Vol II, Rewritten by C Palache, H Berman. C Fronde!. New York, John Wiley and Sons, 1944.
- [19]. Eisenberger S, Lehrman A. Turner WD: The basic calcium phosphates and related systems, some theoretical and practical aspects. Chem Rev 1940;26:257-296.
- [20]. Bjerrum N: Calciumorthophosphate. I. Die Festen Calciumorthophosphate. II. Komplexbildung in Lösung von Calcium-und Phosphate-Ionen. Math.-fys Medd Kong Danske Viden Selskab 1958;31:1-79. (Translated by M H Rand, Atomic Energy Res Est, Harwell, UK, Trans 841, 1959).
- [21]. Newesely H: Kristallchemische und mikromorphologische Untersuchungen schwerlöslicher Calciumphosphate. Fortschr Chem Forsch 1966;5:688-746. Gmelins.
- [22]. Benard J: Combinaisons avec le phosphore; in Pascal P (ed): Nouveau Traite de Chimie Minerale, Tome IV, Le Calcium. Paris, Masson et C<sup>m</sup>, 1958, pp 455-4118
- [23]. Van Wazer JR: Phosphorus and its Compounds, Vol J, New York. Interscience Publishers, 1958.
- [24]. Mooney RW, Aia M: Alkaline earth phosphates. Chem Rev 1961;61:413-462.
- [25]. Young RA, Brown WE: Structures of biological minerals; in Nnncollll5 OU (ed): Biological Mineralization and Demineralization, Dahlem Konferenzen, 1981. Berlin, Springer-Verlag, 1982, pp 101-141.
- [26]. Brown EH, Lehr JR, Smith JP, Frazier A W: Preprnmlion lind chrnrcteri7.1ltion of some calcium pyrophosphates. J Agr Food Chem IC}6.1;11:214.222.
- [27]. Lehr JR, Brown EH, Frazier A W. Smith Jr, Thrasher Rf): Crystlllllographic Properties of Fertilizer Compound5. Chemical Englnr.rlng nulletin No 6, Muscle Shoals, Tennessee Valley Authority, 1967.
- [28]. H. Stockhorst and R. Bruckner, *J. de Phys*, (Paris), 43, C9-451 (1982).
- [29]. P.J. Miller, G.J. Exarhos and W.M. Risen Jr., *J. Chem. Phys.*, 59, 2796 (1973).
- [30]. D.E. Day and G.E. Rindone, *J. Am. Ceram. Soc.*, 45, 489 (1962)..
- [31] H. Kawazoe, *J. Non-Cryst, Sol.*, 42, 281 (1980)..
- [32]. N.J. Kreidl and W.A. Weyl, *J. Am. Ceram. Soc.*, 24, 372 (1941)..

- [33]. Y. Gohshi, H. Kamada, K. Kohra, T. Utaka and T. Arai, *Appl. Spectr.*, 36, 171 (1982)
- [34]. H. Kawazoe, *J. Non-Cryst. Sol.*, 42, 281 (1980).
- [35]. T. Kanazawa, *J. Non-Cryst. Sol.*, 52, 187 (1982).
- [36]. M.J. Weber, *J. Non-Cryst. Sol.*, 47, 117 (1982).
- [37]. J.A. Duffy and M.D. Ingram, *J. Non-Cryst. Sol.*, 21, 373 (1976).
- [38]. M.R. Reidmeyer and D.E. Day, *J. Am. Ceram. Soc.*, 68, C-188 (1985).
- [39]. Gutzow, S. Toshev, M. Marinov, and E. Popov, *Proc. Conf. Silic. Ind.* 9, 65(1968).
- [40]. G.E. Rindone and R.J. Ryder, *Glass Ind.*, 29, 51 (1957).
- [41]. Y. Abe, M. Nogami and H. Saito, *J. Ceram. Soc. Japan* 85, 163 (1977).
- [42]. J.C Elliott, *Structure and Chemistry of the Apatites and other Calcium Orthophosphates*, Elsevier Sci, The Netherlands (1994).
- [43]. G.Graham and P.W. Brown, Reactions of octacalcium phosphate to form hydroxyapatite, *J Crystal growth* 165:106 (1996).
- [44]. G.H. nancollas *Biological Mineralization and demineralization*, Dahlem Konferenzen, Springer-Verlag, Berlin (1982).
- [45]. R.A. Terpstra and P. Bennema, Crystal morphology of octacalcium phosphate, theory and observation. *J, Cryst. Growth* 82:416 (1987).
- [46]. M.U. Nylen, E.D Evans and K.A Omnel, Crystal growth in rat enamel, *J. Cell. Biol.* 18:109 (1963).
- [47]. P. Bodier-Houlle, P. Steuer, J.C. Voegel and F.J.C. Cuisinier, First experimental evidence for human dentine crystal formation involving conversion of octacalcium phosphate to hydroxyapatite, *Acta Cryst.* D54:1377 (1998).
- [48]. D.G.A. Nelson and J.C barry, High resolution electron microscopy of nonstoichiometric apatite crystals, *Anat. Rec.* 224:265 (1989).
- [49]. W.E. Brown, J.P. Smith, J.R. Lehr and A.W. Frazier, octacalcium phosphate and hydroxyapatite, *nature* 196: 1048 (1962).
- [50]. B.B. Tomazic, M.S. Tung, T.M. Gregory and W.E. Brown, Mechanism of hydrolysis of octacalcium phosphate, *Scanning Microsc* 3:119 (1989).
- [51]. J.Zhang and G.H. Nancollas, Kinetics and mechanisms of octacalcium phosphate dissolution at 37<sup>0</sup>C. *J. Phys. Chem* 96:5478 (1992).

- [52]. A. Bigi, M. Gazzano, A. Ripamonti and N. Roven, Thermal conversion of calcium phosphate into hydroxyapatite. *J. Inorg. Biochem* 32:251 (1988).
- [53]. R.Z. LeGeros, G. Daculsi, I. Orloy, T. Abergas and W. Torres, Solution-mediated transformation of octacalcium phosphate (OCP) to apatite, scanning Electron Microsc. 3:129 (1989).
- [54]. B.B. Tomazic, I. Mayer and W.E. Brown, Ion incorporation into octacalcium phosphate, *J. Cryst. Growth* 108:670 (1991).
- [55]. M.Iijima, K. Iijima, N. Wakamatsu, T. Goto, Y. Doi and Y. Moriwaki, Effects of  $\text{CO}_3^{2-}$  ion on the formation of octacalcium phosphate at pH 7.4 and  $37^\circ\text{C}$ , *J. Crystal Growth* 135:229 (1994).
- [56]. M.Iijima, K. Iijima, I. Moriwaki and Y. Kuboki, Oriented growth of octacalcium phosphate crystals on type I collagen fibrils under physiological conditions. *J. Crystal growth* 140:91 (1994).
- [57]. Y. Morowaki, Y.Do, T. Kani, T. Aoba, J. Takahasi, M. Okazaki, Synthesis of enamel-like apatite at physiological temperature and pH using ion selcting membranes, in *Mechanism of Tooth Enamel Formation*, S. Suga, ed, Quintessence Publishing Co, Tokyo (1983).
- [58]. M. Iijima, H. Tohda and Y. Moriwaki, Growth and lameller mixed crystals of octacalcium phosphate and apatite in a model system of enamel formation, *J.Crystal Growth* 116:319 (1992).
- [59]. V.K. Sharma, M. Johnsson, J.D. Sallis and G.H. nancollas, Influence of citrate and phosphocitrate on the crystallixation of octacalcium phosphate, *Langmuir* 8:676 (1992).
- [60]. M. Markovic, B. O. Fowler and W. E brown, *Octacalcium phosphate carboxylates*, CRC Press, Boca Raton (1994).
- [61]. R. Z. LeGeros, R. Kijkovska and J.P. LeGeros, Formation and transformation of octacalcium phosphate, OCP, a preliminary report, *Scanning electron Microscopy* 4:1771 (2984).
- [62]. M. H. salami, J. C. Heughebeart and J. H. nancollas, Crystal growth of calcium phosphates in the presence of magnesium ions, *Langmuir* 1:119 (1985).

- [63]. I.Y. Pieters. E. A. P. De Mayer and R. M. H. Verbeeck, Stoichiometry of  $K^+$  and  $CO_3^{2-}$  containing apatites prepared by the hydrolysis of octacalcium phosphate, *inorg. Chem*, 35:5791 (1996).
- [64]. R. Z. Le Geros, Variation in the crystalline components of human dental calculus: I. Crystallographic and spectroscopic methods of analysis. *J. Dent. Res* 53:45 (1974).
- [65]. D. W. Holcomb and R. A. Young, Thermal decomposition of human tooth enamel. *Calcif. Tissue Int.* 31:189 (1980).
- [66]. M. S. Tung and W. E. Brown, the role of octacalcium phosphate in subcutaneous heterotopic calcification, *Calcif, Tissue Int.* 37:329 (1985).
- [67]. H. A. Lowenstam and S. Weiner, *On Biomineralization*, Oxford University Press, Oxford (1989).
- [68]. L. Addadi, J. Moradian-Oldak, H. Furedi-Milhofer, S. Weiner and A. Veis, Stereochemical aspect of crystal regulation in calcium phosphate, Elsevier Science Publ, The Netherlands (1992).
- [69]. S. I. Stupp, G. W. Ciegler, *Organoapatites: materials for artificial bones. 1. Synthesis and microstructure*, *J. Biomed. Mater. Res* 26:169 (1992).
- [70]. E. Bertoni, A. Bigi, G. Falini, S. Panzavolta, an. Aroveri, Nanocrystals of magnesium and fluoride substituted hydroxyapatite. *J. Inorg. Biochem.* 72:29 (1998).
- [71]. E. Bertoni, A. Bigi, G. Falini, S. Panzavolta and N. Roveri, Hydroxyapatite/Polyacrylic acid composite nanocrystals. *J. Mater. Chem.* 9:779 (1999).
- [72]. D. N. Misra, Adsorption of polyacrylic acids and their sodium salts on hydroxyapatite: effect of their relative molar mass. *J. Colloid Interface Sci.* 181:289 (1996).
- [73] JL. Meyer and ED. Eanes, *CalcifTissue Res.*, 25 (1978) 209-216.
- [74] WE. Brown, M. Mathew and MS. Tung, *Progr Cryst Growth Char.*, 4 (1981) 59 87.
- [75] S. Mann, New York Oxford University Press., (2001) 38 67.
- [76] S. Kamakura, Y. Sasano, H. Homma, O. Suzuki, M. Kagayama and K. Motegi, *J Dent. Res.*, 78 (1999) 1682-1687.
- [77] O. Suzuki, M. Nakamura, Y. Miyasaka, M. Kagayama and M. Sakurai, *Tohoku J Exp Med.*, 164 (1991) 37 50.



- [78] O. Suzuki, M. Nakamura, Y. Miyasaka, M. Kagayama and M. Sakurai, *Bone Miner.*, 20 (1993) 151-166.
- [79] S. Ban, T. Jinde and I. Hasegawa, *Dent Mater J.*, 11 (1992) 130-140.
- [80] J.L. Meyer and E.D. Eanes, *CalcifTissue Res.*, 25 (1978) 209-216.
- [81] N. Eidelman, L.C. Chow and W.E. Brown, *CalcifTissue Int.*, 41 (1987) 18-26.
- [82] W.E. Brown, N. Eidelman and B. Tomazic, *Adv Dent Res.*, 1 (1987) 306-313.
- [83] S. Aoki, K. Sakamoto, S. Yamaguchi and A. Nakahira, *Journal of the Ceramic Society of Japan*, 108 (2000) 909-914.
- [84] A. Nakahira, S. Aoki, K. Sakamoto and S. Yamaguchi, *J Mater. Sci. Mater. Med.*, 12 (2001) 793-800.
- [85] B.O. Fowler, E.C. Moreno and W.E. Brown, *Arch Oral Bioi.*, 11 (1966) 477-492. 7
- [86] H. Monma, *Gypsum & Lime*, 229 (1990) 396-401.
- [87] A. Bigi, B. Bracci, F. Cuisinier, R. Elkaim, M. Fini, I. Mayer, I. N. Mihailescu, G. Socol, L. Sturba, P. Torricelli, *Biomaterials*, 26 (2005) 2381-2389.
- [88] S. Kamakura, K. Sasaki, Y. Honda, T. Anada, O. Suzuki, *Journal of Biomedical Materials Research - Part B Applied Biomaterials* 79 (2006) 210-217.
- [89] S. Ban, T. Jinde and J. Hasegawa, *Dent Mater J*, 11 (1992) 130-140.
- [90] Shiho Ishihara, Takuya Matsumoto, Takamasa Onoki, Taiji Sohmura and Atsushi Nakahira, New concept bioceramics composed of octacalcium phosphate (OCP) and dicarboxylic acid intercalated OCP via hydrothermal hot-pressing, *Materials Science & Engineering C* (2009), doi:10.1016/j.msec.2009.02.023
- [91] N. Yamasaki, T. Weiping, K. Jiajun and K. Hosoi, *J Mat. Sci. Lett.*, 14 (1995) 1268-1270.
- [92] A. Nakahira, S. Takezoe and Y. Yamasaki, *Chemistry Letters*, 33 (2004) 1400-1401.
- [93] T. Onoki, K. Hosoi and T. Hashida, *Scripta Materialia*, 52 (2005) 767-770.
- [94] A. Nakahira, T. Murakami, T. Onoki, K. Hosoi and T. Hashida, *JAm. Ceram. Soc.*, 88 (2005) 1334-1336.
- [95] A. Nakahira, S. Takezoe, Y. Yamasaki, Y. Sasaki, and Y. Ikuhara, *JAm. Ceram.Soc.*, 90 (2007) 2322-2326.
- [96] T. Kubo, Y. Yamasaki and A. Nakahira, *J Mater. Res.*, 22 (2007) 1286-1291.

- [97] H. Nagata, N. Hirao, T. Onoki, Y. Baba, Y. Yamasaki and A. Nakahira, *Journal of the Ceramic Society of Japan*, 116 (2008) 216-219.
- [98] M. Takimura, H. Nagata, Y. Yamasaki, Y. Ikuhara, T. Suzuki and A. Nakahira, *Journal of the Ceramic Society of Japan*, 114 (2006) 554-557.
- [99] H. Nagata, M. Takimura, Y. Yamasaki and A. Nakahira, *Materials Transaction*, 47 (2006) 2103-2105.
- [100] M. Takimura, H. Nagata, Y. Yamasaki and A. Nakahira, *Diffusion and Defect Data Pt. B: Solid State Phenomena*, 124-126 (2007) 1833-1836.
- [101] A. Nakahira, M. Takimura, and Y. Yamasaki, *J Non-Crystalline Solids*, 353 (2007) 4203-4207.
- [102] H. Nagata, T. Kubo and A. Nakahira, *The Journal of Ion Exchange*, 18 (2007) 594-597.
- [103] K. Yanagisawa, M. Nishioka, K. Ioku, N. Yamasaki, *Journal of Materials Science Letters*, 12 (1993) 1073-1075.
- [104] N. Yamasaki, T. Kai, M. Nishioka, K. Yanagisawa, K. Ioku, *Journal of Materials Science Letters*, 9 (1990) 1150-1151.
- [105] Suzuki O, Kamakura S, Katagiri T, Nakamura M, Zhao B, Honda Y, et al. Bone formation enhanced by implanted octacalcium phosphate involving conversion into Ca-deficient hydroxyapatite. *Biomaterials* 2006;27:2671-81.
- [106] Liu Y, Cooper PR, Barralet JE, Shelton RM. Influence of calcium phosphate crystal assemblies on the proliferation and osteogenic gene expression of rat bone marrow stromal cells. *Biomaterials* 2007;28:1393-403.
- [107] Shelton RM, Liu Y, Cooper PR, Gbureck U, German MJ, Barralet JE. Bone marrow cell gene expression and tissue construct assembly using octacalcium phosphate microscalfolds. *Biomaterials* 2006;27:2874-81.
- [108] Anada T, Kumagai T, Honda Y, Masuda T, Kamijo R, Kamakura S, et al. Dose-dependent osteogenic effect of octacalcium phosphate on mouse bone marrow stromal cells. *Tissue Eng Part A* 2008;14:965-78.
- [109] Sugihara F, Onishi H, Kushitani S, Iwaki N, Mandai K, Minamigawa K, et al. In: Wilson J, Hench L, Greenspan DC, editors. *Bone tissue reaction of octacalcium phosphate*. *Bioceramics*, 8. Pergman Press; 1995. p. 89-91.

- [110] Kamakura S, Sasano Y, Homma-Ohki H, Nakamura M, Suzuki O, Kagayama M, et al. Multinucleated giant cells recruited by implantation of octacalcium phosphate (OCP) in rat bone marrow share ultrastructural characteristics with osteoclasts. *J Electron Microscop* (Tokyo) 1997;46:397-403.
- [111] Barrere F, van der Valk CM, Dalmeijer RA, Meijer G, van Blitterswijk CA, de Groot K, et al. Osteogenicity of octacalcium phosphate coatings applied on porous metal implants. *J Biomed Mater Res A* 2003;66:779-88.
- [112] Imaizumi H, Sakurai M, Kashimoto O, Kikawa T, Suzuki O. Comparative study on osteoconductivity by synthetic octacalcium phosphate and sintered hydroxyapatite in rabbit bone marrow. *Calcif Tissue Int* 2006;78:45-54.
- [113] Barrere F, Layrolle P, van Blitterswijk CA, de Groot K. Biomimetic calcium phosphate coatings on Ti6Al4V: a crystal growth study of octacalcium phosphate and inhibition by  $Mg^{2+}$  and  $HCO_3^-$ . *Bone* 1999;25:107S-11S.
- [114] Bigi A, Bracci B, Cuisinier F, Elkaim R, Fini M, Mayer I, et al. Human osteoblast response to pulsed laser deposited calcium phosphate coatings. *Biomaterials* 2005 ;26:2381-9.
- [115] Habibovic P, van der Valk CM, van Blitterswijk CA, De Groot K, Meijer G. Influence of octacalcium phosphate coating on osteoinductive properties of biomaterials. *J Mater Sci Mater Med* 2004;15:373-80.
- [116] LeGeros RZ, Daculsi G, Orly I, Abergas T, Torres W. Solution-mediated transformation of octacalcium phosphate (OCP) to apatite. *Scanning Electr Microsc* 1989;3:129-38.
- [117] Tomazic BB, Etz ES, Brown WE. Nature and properties of cardiovascular deposits. *Scanning Microsc* 1987; 1 :95-105.
- [118] Meyer JL, Eanes ED. A thermodynamic analysis of the secondary transition in the spontaneous precipitation of calcium phosphate. *Calcif Tissue Res* 1978;25:209-16.
- [119] Tung MS, Brown WE. An intermediate state in hydrolysis of amorphous calcium phosphate. *CalcifTissue Int* 1983;35:783-90.
- [120] Brown WE, Mathew M, Tung MS. Crystal chemistry of octacalcium phosphate. *Prog Cryst Growth Charact* 1981 ;4:59-87.

- [121] Suzuki O, Kamakura S, Katagiri T. Surface chemistry and biological responses to synthetic octacalcium phosphate. *J Biomed Mater Res B Appl Biomater* 2006; 77:201-12.
- [122] Chickerur NS, Tung MS, Brown WE. A mechanism for incorporation of carbonate into apatite. *Calcif Tissue Int* 1980;32:55-62.
- [123] Tung MS, Tomazic B, Brown WE. The effects of magnesium and fluoride on the hydrolysis of octacalcium phosphate. *Arch Oral Biol* 1992;37:585-91.
- [124] Suzuki O, Yagishita H, Yamazaki M, Aoba T. Adsorption of bovine serum albumin onto octacalcium phosphate and its hydrolyzates. *Cells Mater* 1995;5:45-54.
- [125] Suzuki O, Yagishita H, Amano T, Aoba T. Reversible structural changes of octacalcium phosphate and labile acid phosphate. *J Dent Res* 1995;74:1764-9. [126] Siew C, Gruninger SE, Chow LC, Brown WE. Procedure for the study of acidic calcium phosphate precursor phases in enamel mineral formation. *Calcif Tissue Int* 1992;50:144-8.
- [127] Mathew M, Brown W, Schroeder L., Dickens B. Crystal structure of octacalcium bis(hydrogenphosphate) tetrakis(phosphate )pentahydrate,  $Cas(HP04h(P04)4' 5H20$ . *J Chern Crystallogr* 1988;18:235-50.
- [128] Nelson DG, Mclean JD. High-resolution electron microscopy of octacalcium phosphate and its hydrolysis products. *CalcifTissue Int* 1984;36:219-32.
- [129] Lu JX, Gallur A, Flautre B, Anselme K, Descamps M, Thierry B, et al. Comparative study of tissue reactions to calcium phosphate ceramics among cancellous, cortical, and medullar bone sites in rabbits. *J Biomed Mater Res* 1998;42:357-67.
- [130] Brown WE, Smith JP, Lehr JR, Frazier AW. Octacalcium phosphate and hydroxyapatite: crystallographic and chemical relations between octacalcium phosphate and hydroxyapatite. *Nature* 1962;196:1050-4.
- [131] Naohisa Miyatake, Koshi N. Kishimoto, Takahisa Anada, Hideki Imaizumi, Eiji Itoi and Osamu Suzuki, Effect of partial hydrolysis of octacalcium phosphate on its osteoconductive characteristics, *Biomaterials*, Volume 30, Pages 1005-1014 (2009).
- [132] Kondo N, Ogose A, Tokunaga K, Ito T, Arai K, Kudo N, et al. Bone formation and resorption of highly purified beta-tricalcium phosphate in the rat femoral condyle. *Biomaterials* 2005;26:5600-8.

- [133] M.J. Arellano-Jiménez, R. García-García and J. Reyes-Gasga, Synthesis and hydrolysis of octacalcium phosphate and its characterization by electron microscopy and X-ray diffraction, *Journal of Physics and Chemistry of Solids*, Volume 70, Pages 390-395 (2009).
- [134] R. Xin, Y. Leng, N. Wang, in situ TEM examinations of octacalcium phosphate to hydroxyapatite transformations. *J. Cryst. Growth* 289 (2006) 339-344.
- [135] Suzuki O, Nakamura M, Miyasaka Y, Kagayama M, Sakurai M. Bone formation on synthetic precursors of hydroxyapatite. *Tohoku J Exp Med* 1991;164:37-50.
- [136] Sugihara F, Onishi H, Kushitani S, Iwaki N, Mandai K, Minamigawa K, et al. Bone tissue reaction of octacalcium phosphate. In: Wilson J, Hench L, Greenspan DC, editors. *Bioceramics*, vol. 8. Pergman Press; 1995. p. 89-91.
- [137] Kamakura S, Sasano Y, Homma H, Suzuki O, Kagayama M, Motegi K. Implantation of octacalcium phosphate (OCP) in rat skull defects enhances bone repair. *J Dent Res* 1999;78:1682-7.
- [138] Barrere F, van der Valk CM, Dalmeijer RA, van Blitterswijk CA, de Groot K, Layrolle P. In vitro and in vivo degradation of biomimetic octacalcium phosphate and carbonate apatite coatings on titanium implants. *J Biomed Mater Res A* 2003;64:378-87.
- [139] Bigi A et al. Human osteoblast response to pulsed laser deposited calcium phosphate coatings. *Biomaterials* 2005;26:2381-9.
- [140] Habibovic P, van der Valk CM, van Blitterswijk CA, De Groot K, Meijer G. Influence of octacalcium phosphate coating on osteoinductive properties of biomaterials. *J Mater Sci Mater Med* 2004;15:373-80.
- [141] Suzuki O, Kamakura S, Katagiri T, Nakamura M, Zhao B, Honda Y, et al. Bone formation enhanced by implanted octacalcium phosphate involving conversion into Ca-deficient hydroxyapatite. *Biomaterials* 2006;27:2671-81.
- [142] Suzuki O, Nakamura M, Miyasaka Y, Kagayama M, Sakurai M. Maclura pomifera agglutinin-binding glycoconjugates on converted apatite from synthetic octacalcium phosphate implanted into subperiosteal region of mouse calvaria. *Bone Miner* 1993;20:151-66.

- [143] Dekker RJ, de Bruijn JD, Stigter M, Barrere F, Layrolle P, van Blitterswijk CA. Bone tissue engineering on amorphous carbonated apatite and crystalline octacalcium phosphate-coated titanium discs. *Biomaterials* 2005;26:5231-9.
- [144] Liu Y, Cooper PR, Barralet JE, Shelton RM. Influence of calcium phosphate crystal assemblies on the proliferation and osteogenic gene expression of rat bone marrow stromal cells. *Biomaterials* 2007;28:1393-403.
- [145] Shelton RM, Liu Y, Cooper PR, Gbureck D, German MJ, Barralet JE. Bone marrow cell gene expression and tissue construct assembly using octacalcium phosphate micro scaffolds. *Biomaterials* 2006;27:2874-81.
- [146] Imaizumi H, Sakurai M, Kashimoto O, Kikawa T, Suzuki O. Comparative study on osteoconductivity by synthetic octacalcium phosphate and sintered hydroxyapatite in rabbit bone marrow. *Calcif Tissue Int* 2006;78:45-54.
- [147] Anada T, Kumagai T, Honda Y, Masuda T, Karmijo R, Kamakura S, et al. Dose-dependent osteogenic effect of octacalcium phosphate on mouse bone marrow stromal cells. *Tissue Eng Part A* 2008;14:965-78.
- [148] Ban S, Jinde T, Hasegawa J. Phase transformation of octacalcium phosphate in vivo and in vitro. *Dent Mater J* 1992;11:130-40.
- [149] LeGeros RZ, Daculsi G, Orly I, Abergas T, Torres W. Solution-mediated transformation of octacalcium phosphate (OCP) to apatite. *Scanning Electron Microsc* 1989;3:129-37 [discussion 137-138].
- [150] Iijima M, Tohda H, Suzuki H, Yanagisawa T, Moriwaki Y. Effects of F<sup>-</sup> on apatite-octacalcium phosphate intergrowth and crystal morphology in a model system of tooth enamel formation. *Calcif Tissue Int* 1992;50:357-61.
- [151] Tung MS, Tomazic B, Brown WE. The effects of magnesium and fluoride on the hydrolysis of octacalcium phosphate. *Arch Oral Bioi* 1992;37:585-91.
- [152] Suzuki O, Yagishita H, Yamazaki M, Aoba T. Adsorption of bovine serum albumine onto octacalcium phosphate and its hydrolyzates. *Cells Mater* 1995;5:45-54.
- [153] Brown WE, Mathew M, Tung MS. Crystal chemistry of octacalcium phosphate. *Prog Crystal Growth Charact* 1981;4:59-87.
- [154] Suzuki O, Kamakura S, Katagiri T. Surface chemistry and biological responses to synthetic octacalcium phosphate. *J Biomed Mater Res B Appl Biomater* 2006;77:201-12.

- [155] Brown WE, Smith JP, Lehr JR, Frazier A W. Crystallographic and chemical relations between octacalcium phosphate and hydroxyapatite. *Nature* 1962;196:1050-5.
- [156] Tseng YH, Mou CY, Chan rc. Solid-state NMR study of the transformation of octacalcium phosphate to hydroxyapatite: a mechanistic model for central dark line formation. *J Am Chern Soc* 2006;128:6909-18.
- [157] Suzuki O, Imaizumi H, Kamakura S, Katagiri T. Bone regeneration by synthetic octacalcium phosphate and its role in biological mineralization. *Curr Med Chern* 2008;15:305-13.
- [158] Bucholz RW. Nonallograft osteoconductive bone graft substitutes. *Clin Orthop* 2002;395:44-52.
- [156] LeGeros RZ. Properties of osteoconductive biomaterials: calcium phosphates. *Clin Orthop* 2002;395:81-98.
- [160]Ogose A, Hotta T, Kawashima H, Kondo N, Gu W, Kamura T, et al. Comparison of hydroxyapatite and beta tricalcium phosphate as bone substitutes after excision of bone tumors. *J Biomed Mater Res B Appl Biomater* 2005;72:94-101.
- [161] Kamakura S, Sasano Y, Homma-Ohki H, Nakamura M, Suzuki O, Kagayama M, et al. Multinucleated giant cells recruited by implantation of octacalcium phosphate (OCP) in rat bone marrow share ultrastructural characteristics with osteoclasts. *J Electron Microsc* 1997;46:397-403.
- [162] Sugawara A, Fujikawa K, Kusama K, Nishiyama M, Murai S, Takagi S, et al. Histopathologic reaction of a calcium phosphate cement for alveolar ridge augmentation. *J Biomed Mater Res* 2002;61 :47-52.
- [163] T. Kikawa, O. Kashimoto, H. Imaizumi, S. Kokubun and O. Suzuki, Intramembranous bone tissue response to biodegradable octacalcium phosphate implant, *Acta Biomater* (2009), doi: 10.1 016/j.actbio.2008.12.008.
- [164]Suzuki O, Kamakura S, Katagiri T. Surface chemistry and biological responses to synthetic octacalcium phosphate. *J Biomed Mater Res B Appl Biomater* 2005; DOI:10.1002/jbm.b.30407.
- [165] Brown WE, Smith JP, Lehr JR, Frazier A W. Crystallographic and chemical relations between octacalcium phosphate and hydroxyapatite. *Nature* 1962;196:1050-5.

- [166] LeGeros RZ, Daculsi G, Orly I, Abergas T, Torres W. Solution-mediated transformation of octacalcium phosphate (OCP) to apatite. *Scanning Microsc* 1989;3:129-37 [discussion 137-138].
- [167] Tomazic BB, Tung MS, Gregory TM, Brown WE. Mechanism of hydrolysis of octacalcium phosphate. *Scanning Electron Microsc* 1989;3:119-27.
- [168] Bodier-Houlle P, Steuer P, Voegel JC, Cuisinier FJ. First experimental evidence for human dentine crystal formation involving conversion of octacalcium phosphate to hydroxyapatite. *Acta Crystallogr D Biol Crystallogr* 1998;54(Parts 6, 2):1377-81.
- [169] Elliot JC. The interpretation of the infrared absorption spectra of some carbonate-containing apatites. In: Fearnhead RW, Stack MV, editors. *Tooth Enamel*. Bristol: John Wright; 1965. p. 20-2.
- [170] Aoba T. Recent observations on enamel crystal formation during mammalian amelogenesis. *Anat Rec* 1996;245:208-18.
- [171] Kim HM, Rey C, Glimcher MJ. Isolation of calcium-phosphate crystals of bone by non-aqueous methods at low temperature. *J Bone Miner Res* 1995;10:1589-601.
- [172] Lu X, Leng Y. Theoretical analysis of calcium phosphate precipitation in simulated body fluid. *Biomaterials* 2005;26:1097-108.
- [173] Eidelman N, Chow LC, Brown WE. Calcium phosphate phase transformations in serum. *Calcif Tissue Int* 1987;41:18-26.
- [174] Suzuki O, Nakamura M, Miyasaka Y, Kagayama M, Sakurai M. Bone formation on synthetic precursors of hydroxyapatite. *Tohoku J Exp Med* 1991;164:37-50.
- [175] Suzuki O, Nakamura M, Miyasaka Y, Kagayama M, Sakurai M. Maclura pomifera agglutinin-binding glycoconjugates on converted apatite from synthetic octacalcium phosphate implanted into subperiosteal region of mouse calvaria. *Bone Miner* 1993;20:151-66.
- [176] Suzuki O, Yagishita H, Yamazaki M, Aoba T. Adsorption of bovine serum albumin onto octacalcium phosphate and its hydrolyzates. *Cells Mater* 1995;5:45-54.
- [177] Osamu Suzuki, Shinji Kamakura, Takenobu Katagiri, Masanori Nakamura, Baohong Zhao, Yoshitomo Honda and Ryutaro Kamijo, Bone formation enhanced by



implanted octacalcium phosphate involving conversion into Ca-deficient hydroxyapatite, *Biomaterials*, Volume 27, Pages 2671-2681(2006).

[178] Brown WE, Smith JP, Lehr JR, Frazier A W. Crystallographic and chemical relations between octacalcium phosphate and hydroxyapatite. *Nature* 1962;196:1050-5.

[179] LeGeros RZ, Daculsi G, Orly I, Abergas T, Torres W. Solution-mediated transformation of octacalcium phosphate (OCP) to apatite. *Scanning Microsc* 1989;3:129-37 [discussion 137-138].

[180] Tomazic BB, Tung MS, Gregory TM, Brown WE. Mechanism of hydrolysis of octacalcium phosphate. *Scanning Electron Microsc* 1989;3:119-27.

[181]. Verbeeck RMH, Devenyns JAH. The effect of the solution Ca/P ratio on the kinetics of dissolution of octacalcium phosphate at constant pH. *J Cryst Growth* 1990,102:647-657.

[182]. Zhang J, Nancollas GH. Kinetics and mechanisms of octacalcium phosphate dissolution at 37°C.. *J Phys Chem* 1992;96:5478-5483.

[183]. Cheng P-T: Formation of octacalcium phosphate and subsequent transformation to hydroxyapatite at low supersaturation: A model for cartilage calcification. *Calcif Tissue Int* 1987,40:339-343.

[184]. Tung MS, Eidelman N, Sieck B, Brown WE: Octacalcium phosphate solubility product from 4 to 37°C. *J Res Natl Bur Stands* 1988,93:613-624.

[185]. Chickerur NS, Tung MS, Brown WE: A mechanism for incorporation of carbonate into apatite. *Calcif Tissue Int* 1980,32:55-62.

[186]. Brown WE, Smith JP, Lehr JR, Franzier AW: Octacalcium phosphate and hydroxyapatite: Crystallographic and chemical relations between octacalcium phosphate and hydroxyapatite. *Nature* 1962,196:1050-1055.

[187]. Tomazic BB, Mayer I, Brown WE: Ion incorporation into octacalcium phosphate hydrolyzates. *J Cryst Growth* 1991,108:670-682.

[188]. Brown WE, Mathew M, Tung MS: Crystal chemistry of octacalcium phosphate. *Prog Crystal Growth Charact* 1981,4:59-87.

[189]. Brown WE, Tung MS, Chow LC: Role of octacalcium phosphate in the incorporation of impurities into apatite. *Proc. 2nd Int Congr Phosphorus Compounds*, Boston, 1980, Ed C. Eon, IMPHOS Pub., Paris, 1980, pp 59-71.

- [190]. LeGeros RZ, Daculsi G, Orly I, Abergas T, Torres W: Solution-mediated transformation of octacalcium phosphate (OCP) to apatite. *Scanning Microscopy* 1989,3:129-138.
- [191]. B.O. Fowler, E.C. Moreno and W.E Brown, *Arch. Oral Biol*, 11,477 (1966).
- [192]. L.C. Bell, A.S. Posner and J.P. Quirk, *J. Colloid Interface Sci.* 42, 250 (1973).
- [193]. H. Monma and S. Ueno, *gypsum and Lime*, No.172, 11 (1981).
- [194]. L.C. Bell and C.A. Black, *Soil. Sci. Soc. Amer. Proc*, 34, 583 (1970).
- [195]. H. Monma, *J. Catal*, 75, 200 (1982).
- [196]. Straub, D.A. (2007). "Calcium Supplementation in Clinical Practice: A Review of Forms, Doses, and Indications". *NCP- Nutrition in Clinical Practice* 22 (3): 286. doi:10.1177/0115426507022003286. PMID 17507729.
- [197] Tucker, L.A.; Nokes, N.; Adams, T. (2007). "Effect of a Dietary Supplement on Hip and Spine BMD: A Randomized, Double-blind, Placebo-controlled Trial: 1515: Board# 5 May 30 2: 00 PM-3: 30 PM". *Medicine & Science in Sports & Exercise* 39 (5): S230. doi:10.1249/01.mss.0000273874.34214.2e. <http://www.acsm-msse.org/pt/re/msse/fulltext.00005768-200705001-01696.htm>.
- [198] H. Oonishi, L.L. Hench. J. Wilson. F. Sugihara. E. Tsuji. S. Kushitani, H. Iwaki, Comparative bone growth behavior in granules of bioceramic materials of various sizes.], *Biomed. Mater. Res.* 44 (1999) 31-43.
- [199] G.jiang.J. Wen. D. Shi, In vitro bioactive behavior of hydroxylapatite-coated porous Ah03. *J. Biomed. Mater. Res.* B53 (2000) 457-466.
- [200] A. Montenero, G. Cnappi, F. Ferrari. M. Cesario E. Salvioli, L. Mattogno, S. Kaciulis, M. Fini, Sol-gel derived hydroxyapatite coatings on titanium substrate. *J. Mater. Sci.* 35 (2000) 2791-279Z
- [201] T. Tian, J.M. Tian, Preparation of porous hydroxyapatite. *J. Mater. Sci.* 36 (2001) 3061-3066.

- [202] K.A. Hing, S.M. Best, K.E. Tanner, W. Bonfield, P.A. Revell. Quantification of bone ingrowth within bone-derived porous hydroxyapatite implants of varying density. *J. Mater. Sci. Mater. Med.* 10 (1999) 663-670.
- [203] S. Liao, M. Ngiarn, F. watan, S. Ramakrishna, C.K. Chan. Systematic fabrication of nano-carbonated hydroxyapatite/collagen composites for biomimetic bone grafts. *Bioinspiration Biomimetics* 2 (2007) 37-41.
- [204] w. Suchanek, M. Yoshimura. Processing and properties of hydroxyapatite-based biomaterials for use as hard tissue replacement implants. *J. Mater. Res.* 13 (1998) 94-117.
- [205] C. Mochales, H.E. Briak-BenAbdeslam, M.P. Ginebra, A. Terol, J.A. Planell, P. Boudeville, Dry mechanochemical synthesis of hydroxyapatites from DCPD and CaO: influence of instrumental parameters on the reaction kinetics, *Biomaterials* 25 (2004) 1151-1158.
- [206] E.M. Rivera, M. Araiza, W Brostow, V.M. Castafio, R Diaz-Estrada, R Hernandez, j.k, Rodriguez, Synthesis of hydroxyapatite from eggshells, *Mater. Lett.* 41 (1999) 128-134.
- [207] M.s. Tung, T. O'Farrell, Effect of ethanol on the formation of calcium phosphates, *j Colloids Surf. A* 110 (1996) 191-198.
- [208] Y.X. Pang, X. Bao, Influence of temperature, ripening time and calcination on the morphology and crystallinity of hydroxyapatite nanoparticles, *J. Eur. Ceram. Soc.* 23 (2003) 1697-1704.
- [209] AL. Macipe, J.G. Morales, RR Clemente, Nanosized hydroxyapatite precipitation from homogeneous calcium/citrate/phosphate solutions using microwave and conventional heating, *Adv. Mater.* 10 (1998) 49-53.
- [210] M.A. Martins, C Santos, M.M. Almeida, M.E. Costa, Hydroxyapatite micro- and nanoparticles: nucleation and growth mechanisms in the presence of citrate species,]. *Colloid Interface Sci.*, 318 (2008) 210-216.

- [211] E. Boanini, M. Fini, M. Gazzano, A Bigi, Hydroxyapatite nanocrystals modified with acidic amino acids, *Euro. J. Inorg. Chem.* 23 (2006)4821-4826.
- [212] J. Zhang, X. Gao, B.c. Song, Z.F. Wang, WW Lu, A novel technique to synthesize hydroxyapatite whiskers, *Mater. Lett.* 62 (2008) 1162-1164.
- [213] J. Liu, K. Li, H. Wang, M. Zhu, H. Xu, H. Van, H. Wang, Self-assembly of hydroxyapatite nanostructures by microwave irradiation, *Nanotechnology* 16 (2005) 82-87.
- [214] Crystalline behaviors of hydroxyapatite in the neutralized reaction with different citrate additions. *Powder Technology*, Volume 192, Issue 1, 15 May 2009, Pages 1-5.
- [215] W. Suchanek, M. Yoshimura, Processing and properties of hydroxyapatite-based biomaterials for use as hard tissue replacement implants, *J. Mater. Res.* 13 (1.) (1998).
- [216] I. Mobasherpour, M. Soulati Heshajin, A. Kazemzadeh, M. Zakeri, Synthesis of nanocrystalline hydroxyapatite by using precipitation method, *J. Alloys Compd.* 430 (1-2) (2007) 330-333.
- [217] W.R. Rao, R.E Boehm, A study of sintered apatites, *J. Dent. Res.* 53 (1974) 1351.
- [218] G. De With, H.J.A. Van Dijck, N. Hattu, K. Prijs, Sintering of hydroxylapatite-zirconia composite materials, *J. Mater. Sci.* 16 (1981) 1592.
- [219] P. Ducheyne, M. Marcolongo, E. Schepers, in: L.L. Hench, J. Wilson (Eds.), *An Introduction to Bioceramic*, World Scientific Publishing Co., Singapore, 1993, pp. 281-297.
- [220] YM. Kong, S. Kim, H.E. Kim, Reinforcement of hydroxyapatite bioceramics by addition of ZrO<sub>2</sub> coated with Al<sub>2</sub>O<sub>3</sub>, *J. Am. Ceram. Soc.* 82 (11) (1999) 2963.
- [221] D.W. Richerson, *Modern Ceramic Engineering, Properties, Processing and use in Design*, Marcel Decker, New York, 1992, pp. 731-807.

- [222] K. Tsukuma, K. Veda, M. Shimada, High-temperature strength and fracture toughness of Y2O3-partially-stabilized ZrO2/Al2O3 composites, *J. Am. Ceram. Soc.* 68 (1.) (1985), c-4-c-5.
- [223] O.N. Grigoryev, S.A. Firstov, O.A. Babiy, G.E. Homenko, Effect of zirconia (3 mol% yttria) additive on mechanical properties and structure of alumina ceramics, *J. Mater. Sci.* 29 (1994) 4633.
- [224] S.P. Hulbert, in: L.L. Hench, J. Wilson (Eds.), *An Introduction to Bioceramic*, World Scientific Publishing Co., Singapore, 1993 pp. 25-40.
- [225] N. Tamari, M. Mouri, I. Kondo, Mechanical properties and existing phases of composite ceramics obtained by sintering of a mixture of hydroxyapatite and zirconia, *J. Ceram. Soc. Jpn.* 95 (8) (1987) 806-809.
- [226] J.M. Wu, T.S. Yeh, Sintering of hydroxylapatite-zirconia composite materials, *J. Mater. Sci.* 23 (1988) 3771.
- [227] E. Champion, S. Gautier, D. Bernache-Assollant, Characterization of hot pressed Al2O3-platelet reinforced hydroxyapatite composites (biomaterial for orthopedics), *J. Mater. Sci. Mater. Med.* 7 (1996) 125.
- [228]. I. Mobasherpour, M. Solati Hashjin, S.S. Razavi Toosi, R. Darvishi Kamachali, Effect of the addition ZrO<sub>2</sub>-Al<sub>2</sub>O<sub>3</sub> on nanocrystalline hydroxyapatite bending strength and fracture toughness, *Ceramics International*, Volume 35, Issue 4, May 2009, Pages 1569-1574.
- [229] Sung-Jin Kim, Hee-Gon Bang, Jun-Ho Song, Sang-Yeup Park, Effect of fluoride additive on the mechanical properties of hydroxyapatite/alumina composites, *Ceramics International*, Volume 35, Issue 4, May 2009, Pages 1647-1650.
- [230] M. Šljivić, I. Smičiklas, I. Plećaš, M. Mitrić, The influence of equilibration conditions and hydroxyapatite physico-chemical properties onto retention of Cu<sup>2+</sup> ions, *Chemical Engineering Journal*, Volume 148, Issue 1, 1 May 2009, Pages 80-88.

- [231] Se-Won Yook, Hyoun-Ee Kim, Byung-Ho Yoon, Young-Mi Soon, Young-Hag Koh, Improvement of compressive strength of porous hydroxyapatite scaffolds by adding polystyrene to camphene-based slurries, *Materials Letters*, Volume 63, Issue 11, 30 April 2009, Pages 955-958.
- [232] M.I. Domínguez, F. Romero-Sarria, M.A. Centeno, J.A. Odriozola, Gold/hydroxyapatite catalysts: Synthesis, characterization and catalytic activity to CO oxidation, *Applied Catalysis B: Environmental*, Volume 87, Issues 3-4, 7 April 2009, Pages 245-25.
- [233] Ai-juan Wang, Yu-peng Lu, Rui-fu Zhu, Shi-tong Li, Xiao-long Ma , Effect of process parameters on the performance of spray dried hydroxyapatite microspheres, *Powder Technology*, Volume 191, Issues 1-2, 4 April 2009, Pages 1-6.
- [234] Yohey Hashimoto, Tomohiro Taki, Takeshi Sato, Sorption of dissolved lead from shooting range soils using hydroxyapatite amendments synthesized from industrial byproducts as affected by varying pH conditions, *Journal of Environmental Management*, Volume 90, Issue 5, April 2009, Pages 1782-1789.
- [235] Simone Sprio, Anna Tampieri, Giancarlo Celotti, Elena Landi , Development of hydroxyapatite/calcium silicate composites addressed to the design of load-bearing bone scaffolds, *Journal of the Mechanical Behavior of Biomedical Materials*, Volume 2, Issue 2, April 2009, Pages 147-155.
- [236] Yusong Pan, Dangsheng Xiong , Friction properties of nano-hydroxyapatite reinforced poly(vinyl alcohol) gel composites as an articular cartilage *Wear*, Volume 266, Issues 7-8, 25 March 2009, Pages 699-703.
- [237] Yu-Jun Wang, Jie-Hua Chen, Yu-Xia Cui, Shen-Qiang Wang, Dong-Mei Zhou , Effects of low-molecular-weight organic acids on Cu(II) adsorption onto hydroxyapatite nanoparticles, *Journal of Hazardous Materials*, Volume 162, Issues 2-3, 15 March 2009, Pages 1135-1140.

[238] Zafer Evis, Metin Usta, Isil Kutbay , Improvement in sinterability and phase stability of hydroxyapatite and partially stabilized zirconia composites, *Journal of the European Ceramic Society*, Volume 29, Issue 4, March 2009, Pages 621-628.

[239] Dong-Yoon Kim, Miyoung Kim, Hyoun-Ee Kim, Young-Hag Koh, Hae-Won Kim, Jun-Hyeog Jang , Formation of hydroxyapatite within porous TiO<sub>2</sub> layer by micro-arc oxidation coupled with electrophoretic deposition, *Acta Biomaterialia*, In Press, Corrected Proof, (2009).

[240] R.M. Trommer, L.A. Santos, C.P. Bergmann , Nanostructured hydroxyapatite powders produced by a flame-based technique, *Materials Science and Engineering: C*, In Press, Corrected Proof, Available online 20 February 2009. doi: 10. 1016/j.mec.2009.02.006.

### **3. MATERIALS AND METHODS**



### 3.1. Reagents and solutions:

All experiments were performed with analytical reagent grade chemicals and solvents. All solutions were using distilled water from a borosilicate auto still (Jencons Ltd). The following reagents and solutions were used in the present investigations:

$\text{Ca}(\text{H}_2\text{PO}_4)_2 \cdot \text{H}_2\text{O}$  and  $\text{CaCl}_2$  used for the synthesis of phosphate materials, with Ca/P ratio of 1.67 and 1.33, and these are purchased from Sigma-Aldrich, 25%  $\text{NH}_4\text{OH}$  solution used to control pH, HCl and NaOH used for zeta-potential, purchased from Fluka.

### 3.2. Synthesis of Hydroxyapatite (HA):

The apparatus used consisted of a 1 L glass reactor vessel having a four neck cover (Fig.3.2 (1)). The dispersed element (Model G 45M, IKA-Works, Inc., Wilmington, NC) of the dispersing equipment (Model S 50 KG-HH, IKA-Works) was passed through the central neck (Fig.3.2 (2)). The reaction temperature was adjusted by a temperature controller (Fig.3.2 (4)), which was connected to a thermocouple (Fig.3.2 (3)) and heating mantle (Fig.3.2 (5)). A flowing stream of air was used to remove  $\text{CO}_2$  from the reactor. The air was passed through an absorption tube containing solid NaOH as a  $\text{CO}_2$  absorbent (Fig.3.2 (7)), and the flow rate was adjusted using a flow meter (Fig.3.2 (6)). A condenser (Fig.3.2 (9)) and a proper syringe containing concentrated  $\text{NH}_4\text{OH}$  solution (Fig.3.2 (8)) were connected to the one angled side neck.

An 800 mL solution of 0.0538 mol of  $\text{Ca}(\text{H}_2\text{PO}_4)_2 \cdot \text{H}_2\text{O}$  and 0.1254 mol  $\text{CaCl}_2$  with a Ca/P molar ratio of 1.67 (the stoichiometry of HA) was transferred into the reactor vessel and was heated to  $97^\circ \pm 1^\circ\text{C}$  using an airflow rate of 15 L/h for 30 minute. The rotation speed of the disperser was adjusted at 5000 rpm, and then 18 ml of concentrated  $\text{NH}_4\text{OH}$  solution (25% w/w) was added slowly (3 min). The pH of the solution increase to 8.90 and white slurry was produced. The modified precipitation method described above is called “pH shock wave method”. The slurry produced was aged under over night at room temperature, filtrated; washed using distilled water and dried at  $90^\circ\text{C}$  for 6 hours.

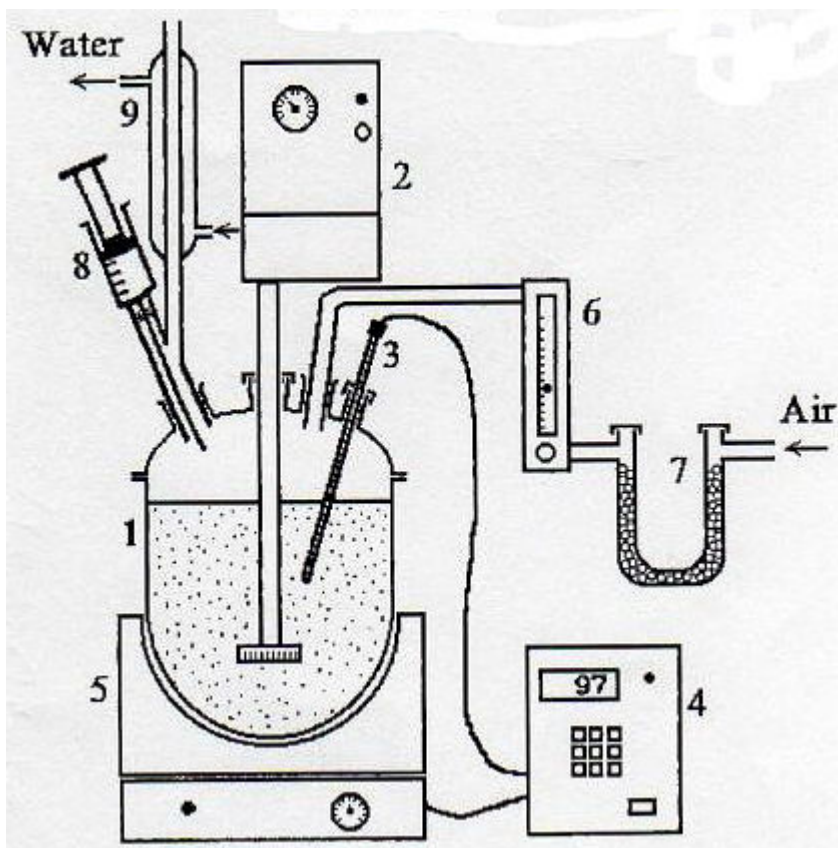


**Figure 3.2:** Schematic illustration of reaction apparatus for the synthesis of octacalcium phosphate: (1) reaction vessel, (2) dispersing instrument, (3) thermocouple, (4) temperature controller, (5) heating mantle, (6) flow meter, (7) U-shape adsorption tube, (8) syringe, and (9) condenser.

### 3.3 Synthesis of octacalcium phosphate (OCP):

The used apparatus was the same as for synthesis of hydroxyapatite. An 800 mL solution of 0.0538 mol of  $\text{Ca}(\text{H}_2\text{PO}_4)_2 \cdot \text{H}_2\text{O}$  and 0.0891 mol  $\text{CaCl}_2$  with a Ca/P molar ratio of 1.33 (the stoichiometry of OCP) was transferred into the reactor vessel and was heated to  $97^\circ \pm 1^\circ\text{C}$  using an airflow rate of 15 L/h for 30 minute. The rotation speed of the disperser was adjusted at 5000 rpm, and then 15 ml of concentrated  $\text{NH}_4\text{OH}$  solution (25% w/w) was added slowly (3 min). The pH of the solution increase to 8.90 and white slurry was produced. The modified precipitation method described above is called “pH shock wave method”. The slurry produced was aged under over night at room temperature, filtrated; washed using distilled water and dried at  $90^\circ\text{C}$  for 6 hours. The same procedure was

repeated using threonine concentration of 0.2mM/L, 0.4mM/L and 0.6mM/L. A portion of 1 g of the samples was subsequently calcined for 3 hours at 900 °C. The calcinations temperature was chosen with respect to thermal data derived from differential thermal analysis (DTA). Table 3.3 showed the experimental conditions, and composition of samples (uncalcined and calcined).

**Table 3.3:** Experimental conditions and composition of samples.

Name of samples	Ca/P Molar Ratio	Final Solution pH	Code of Samples	
			Raw	Calcined
Hydroxyapatite	1.67	8.9	HA	.....
Octacalcium Phosphate (OCP)	1.33	8.7	TH0	TH0C
OCP+Threonine 0.2mM/L	1.33	8.8	TH2	TH2C
OCP+Threonine 0.4mM/L	1.33	8.9	TH4	TH4C
OCP+Threonine 0.6mM/L	1.33	8.8	TH6	TH6C

### 3.4. Characterization :

The products obtained by these procedures were studied by powder X-ray diffractometry (XRD), Fourier Transform infrared spectrometry (FT-IR), scanning electron microscope (SEM), differential thermal analysis-thermogravimetric analysis (DTG-TG).

#### 3.4.1. XRD:

XRD technique was conducted using a diffractometer (Model D500, Siemens, Karlsruhe, Germany) with secondary graphite monochromator and CuK<sub>α</sub> radiation. The measurements were performed using the following combination of slits: 1.0<sup>0</sup>/1.0<sup>0</sup>/1.0<sup>0</sup> as aperture diaphragms, 0.15<sup>0</sup> as detector diaphragm and 0.15<sup>0</sup>

as diffracted beam monochromator diaphragm. The measured  $2\theta$  range was scanned in steps of  $0.03^\circ$  in 10s/step.

#### **3.4.2. FT-IR:**

FT-IR was performed using a spectrophotometer (Model Spectrum RX I FT-IR, Perkin-Elmer). The KBr disk technique was used with 2mg of sample powder in 200 mg of spectroscopic grade KBr (Merck), which has been dried at  $100^\circ\text{C}$ . Infrared spectra were recorded in the  $4000\text{-}400\text{ cm}^{-1}$  region, with resolution of  $4.00\text{ cm}^{-1}$ .

#### **3.4.3. SEM:**

The SEM samples were prepared as follows: (i) the powders were attached to aluminum stubs using carbon glue (Leit-C, Neubauer Chemikalren, Germany), (ii) the powders were coated with a 5-10 nm thick gold film to prevent electron-beam charging and (iii) the powders were examined using SEM with an acceleration electron-beam voltage of 25 kV.

#### **3.4.4. TG-DTG:**

TG and DTG analysis of the samples were performed using a NETZSCH simultaneous TG-DTG apparatus (Model STA 449C, Jupiter) from ambient temperature to  $1400^\circ\text{C}$  in nitrogen atmosphere (flow rate  $\sim 30\text{ mL/min}$ ) with heating rate of  $\beta=10^\circ\text{C min}^{-1}$ . The mass of the samples was about 50 mg.

#### **3.4.5. $\text{N}_2$ Porosimetry:**

All the materials were characterized by nitrogen adsorption-desorption isotherms at 77K using a commercial SORPTOMATIC/FISONS 1900 apparatus. Prior to each adsorption-desorption measurements the samples were degassed at  $T=473\text{K}$  under  $p=10^{-2}\text{ mbar}$  for 24h. The specific surface area (ssa) were determined on a routine basis using the linear part of BET equation at  $0.05 < (P/P_0) < 0.15\text{-}0.25$ .

## 4. Results and discussion:

### 4.1. XRD analysis of HA:

Figure 4.1 shows the XRD pattern of hydroxyapatite powder. The sample has been first indexed with X-Cell algorithm [1] and refined afterwards with Pawley fitting in order to find the best approximation for the unit cell parameters. Background has been subtracted using a 20 points polynomial function and a smoothing function has been applied using Savitsky-Golay filter. This pattern of XRD indicates both crystalline and amorphous powder of hydroxyapatite, because all the peaks are not strong and sharp and also not in the same labeled. There is no other extraneous peak detected in XRD pattern, which indicates the synthesized powder is single-phase hydroxyapatite. Peaks at  $25.898^{\circ}$  and  $32.923^{\circ}$  in  $2\theta$  assigned as major peaks of hydroxyapatite due to (002) and (300) planes [File No. PDF# 73-1731]. The lattice parameters calculated using the X-Cell algorithm software [1]. The calculated values of  $a= 9.427 \text{ \AA}$ ,  $c = 6.930 \text{ \AA}$  and volume=  $529.390 \text{ \AA}^3$ . These values are slightly different from standard data of hydroxyapatite [PDF# 73-1731], where  $a= 9.400 \text{ \AA}$ ,  $c=6.930 \text{ \AA}$  and volume=  $530.30 \text{ \AA}^3$ .

**Table 4.1:** Peak shift data compared with standard hydroxyapatite

Plane	d-space ( $\text{\AA}$ )		Shift
	PDF 73-1731	HA 1.67	
002	3.467	3.442	-0.025
210	3.079	3.144	+0.065
211	2.814	2.809	-0.005
112	2.791	2.775	-0.016
300	2.719	2.716	0.000
202	2.640	2.640	0.000
220	2.259	2.269	+0.010
222	1.946	1.945	-0.001
312	1.893	1.891	-0.002
213	1.848	1.839	-0.009

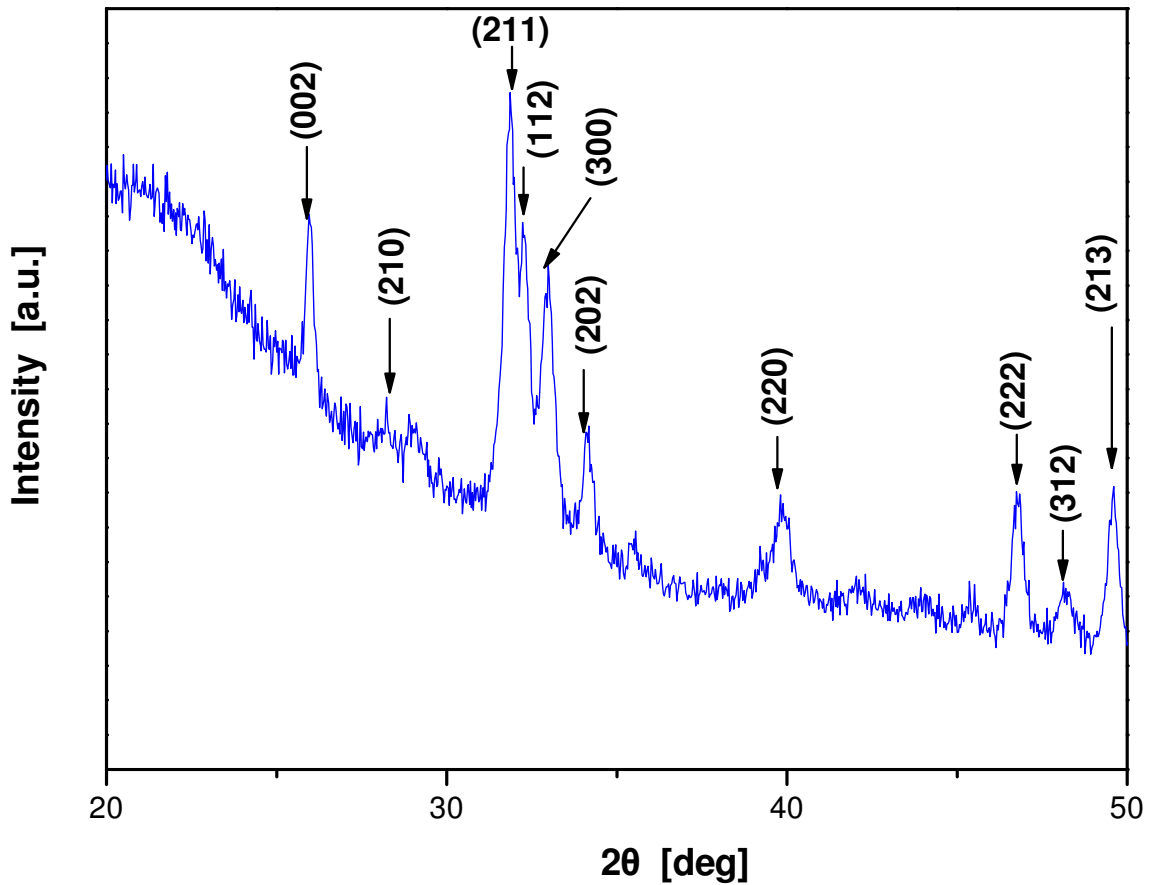


**Figure 4.1:** XRD pattern of hydroxyapatite.

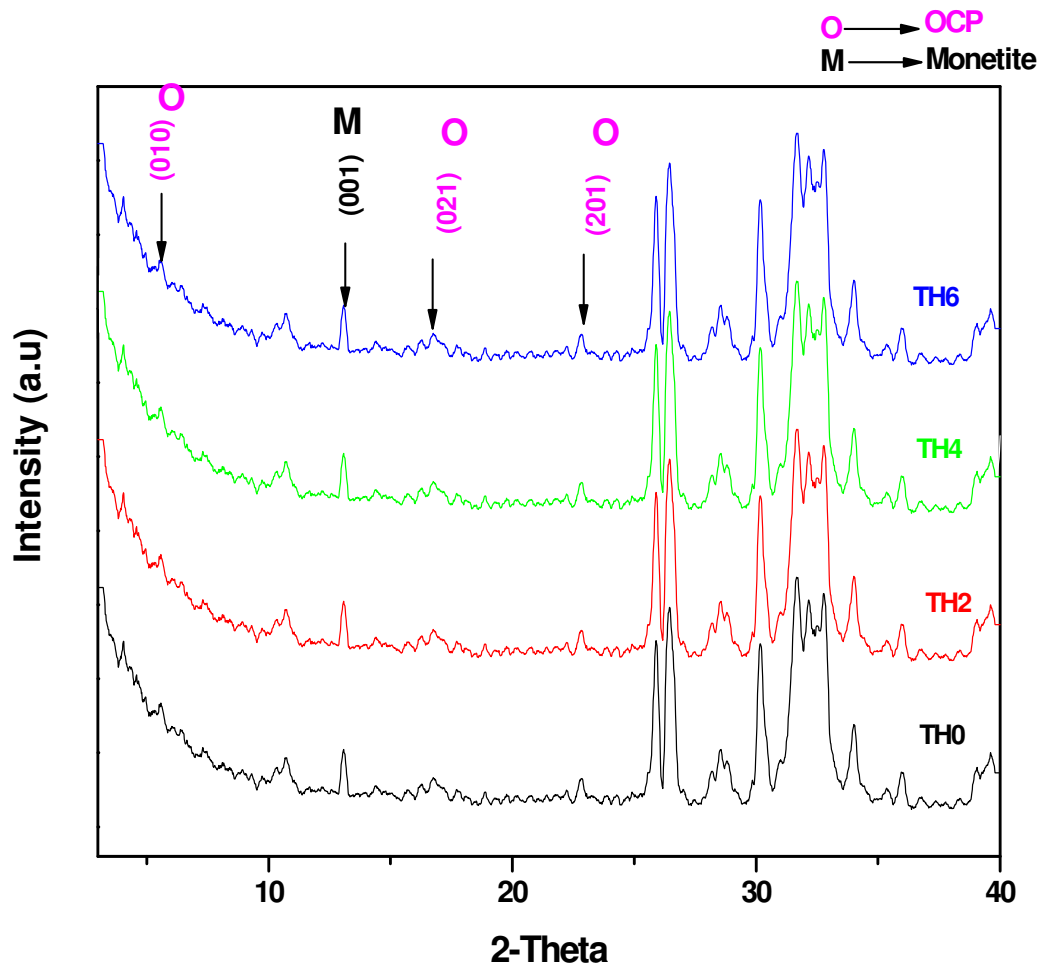
The difference of a axis is due to the replace of  $\text{PO}_4$  group by acid phosphate. From the literature [34] the presence of acid phosphate group results to increase of a and b axis , on the contrary not effect on c axis. In our results these behavior is different, that is, the distance of c axis is reduced, while a and b axis remain unchanged. This behavior attribute to low crystallinity of hydroxyapatite and presence of amorphous phase. Koumoulidis et al [2] also got slightly difference with standard data of hydroxyapatite. Furthermore, we can say that standard hexagonal hydroxyapatite is formed, with space group  $\text{P6}_3/\text{m}[173]$ . Table 4.1 showed the peak shift, which is calculated by Bragg equation [3] and compared with the standard XRD spectra of hydroxyapatite.

## 4.2. XRD analysis of OCP:

Figure 4.2(a), 4.2(b) and 4.2(c) showed the XRD patterns of uncalcination and calcination samples of OCP. All samples have been first indexed with X-Cell algorithm [1] and refined afterwards with Pawley fitting in order to find the best approximation for the unit cell parameters. Background has been subtracted using a 20 points polynomial function and a smoothing function has been applied using Savitsky-Golay filter. The total reflection pattern was similar to the know reflection pattern of synthesized OCP [PDF# 86-1407]. In the present study at first we try to fix our crystallic system as triclinic system and the calculated values of lattice parameters using X-Cell algorithm software [1] were  $a= 7.204\text{\AA}$ ,  $b= 6.087\text{\AA}$  and  $c= 4.333\text{\AA}$ . However, these values does not fix with the standard triclinic system [File No. PDF# 26-1056].

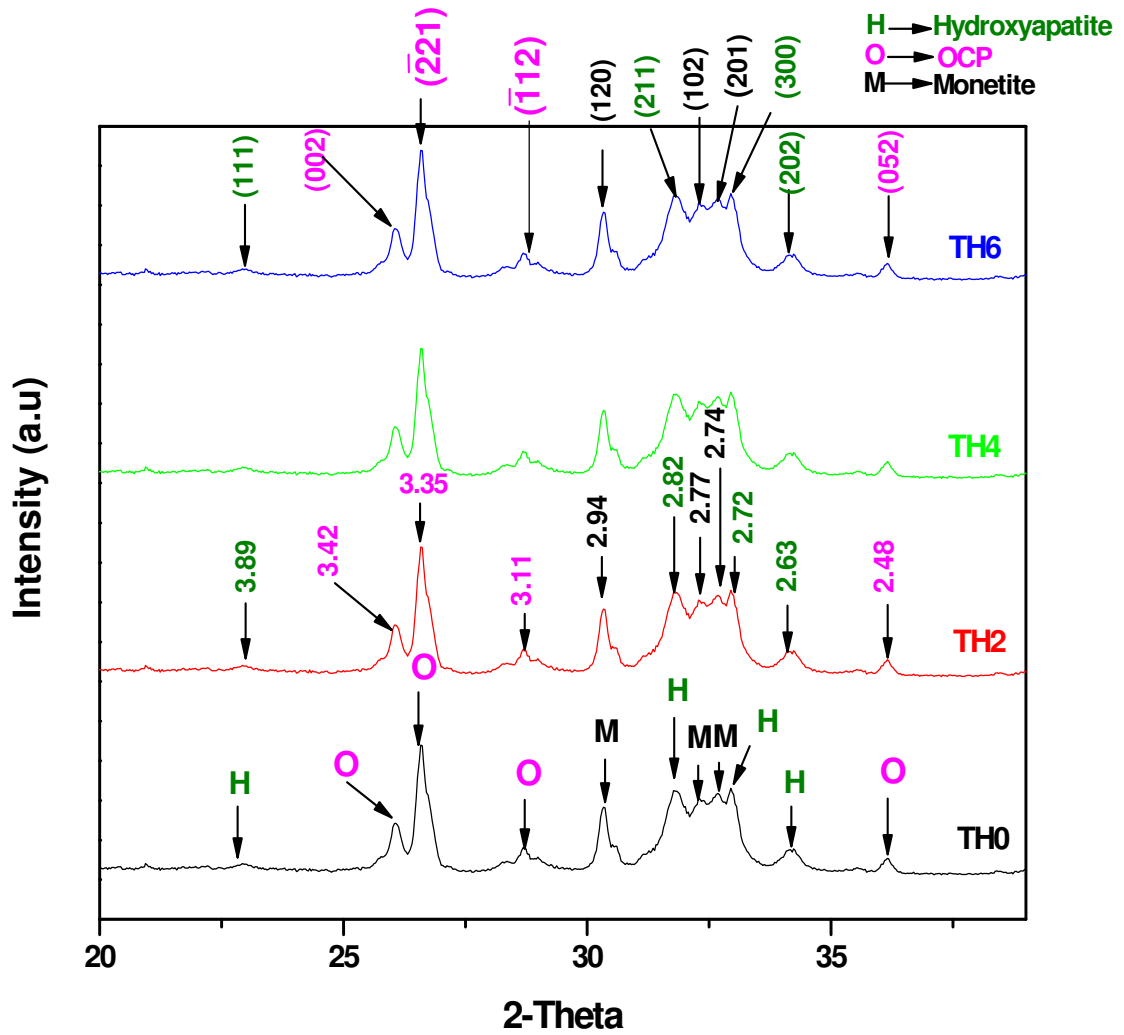
The second solution of this system has been indexed as orthorhombic and the calculated lattice parameters were  $a= 10.733\text{\AA}$ ,  $b= 13.753\text{\AA}$  and  $c= 5.832\text{\AA}$ . These values are more exact with standard orthorhombic OCP system [File No. PDF# 86-1407]. Still these values are slightly different with standard file. This is due to the presence of multiphase and the element content on unit cell.

Figure 4.2(a) and 4.2(b) showed the XRD pattern of uncalcination samples. After used different concentrations of threonine no change detected in the XRD pattern. The entire pattern showed the phases of OCP monetite ( $\text{CaHPO}_4$ ) and hydroxyapatite. To be well observation of phases, we separate the XRD pattern of uncalcination samples. One pattern showed  $2\theta$  ranges between  $3-40^\circ$  (figure 4.2(a)) and another  $2\theta$  ranges between  $20$  until  $40^\circ$  (figure 4.2(b)). In figure 4.2(b), on TH0 showed the phases, on TH2 indicate the values of d space ( $\text{\AA}$ ), calculated from Bragg equation [3] and on TH6, it is indicate the reflection planes for phases. The peaks at  $2\theta$  values  $4.8^\circ$ ,  $16.7^\circ$ ,  $22.7^\circ$ ,  $26.0^\circ$ ,  $26.5^\circ$ ,  $28.6^\circ$  and  $36.1^\circ$  derived from (010), (021), (201), (002), ( $\bar{2}21$ ), ( $\bar{1}\bar{1}2$ ) and (052) reflections indicate the phase of OCP. The peaks at  $2\theta$  values  $13.0^\circ$ ,  $30.3^\circ$ ,  $32.5^\circ$  and  $32.7^\circ$  derived from (001), (120), (102) and (201) planes indicate the phase of monetite [File No. PDF# 75-1520]. And the peaks at  $2\theta$  values  $22.80$ ,  $31.80$ ,  $32.90$  and  $34.10$  derived from (111), (211), (300) and (102) planes indicate the phase of hydroxyapatite [File No. PDF# 73-1731].



**Figure 4.2(a):** XRD pattern of uncalcination samples of OCP (2Theta 3-40)





**Figure 4.2(b):** XRD pattern of uncalcination samples of OCP (2Theta 20-40)

Figure 4.2(c) showed the XRD pattern of calcination samples of material. Calcination temperature used in the present study is 900 °C. All the peaks detected here are more sharp than uncalcined samples. The curve on TH0C indicates the phases of  $\beta$ -TCP and  $\beta$ -pyrophosphate. The curve on TH4C indicates the d space values, determined from Bragg equation [3] and curve on TH6C indicates the planes for  $\beta$ -TCP and  $\beta$ -Ca<sub>2</sub>P<sub>2</sub>O<sub>7</sub>. Two phases are observed here, one is  $\beta$ -tricalcium phosphate ( $\beta$ -TCP) [File No. PDF# 79-0700] and other is  $\beta$ -calcium pyrophosphate ( $\beta$ -Ca<sub>2</sub>P<sub>2</sub>O<sub>7</sub>). Some difference is detected here for sample TH4C, in which the intensity decreases and the peaks are more broad than other samples. Some shift is also observed after using different concentrations of threonine for

samples TH2C, TH4C and TH6C at  $2\theta$  values between  $30.99^{\circ}$  until  $34.72^{\circ}$ . This shift is due to the increase of  $2\theta$  values and decrease of  $d$  space, which do not affect the main phenomena of phases. All the peaks determined are according to the literature [File No. PDF# 79-0700]. The lattice parameter calculated for  $\beta$ -TCP, using X-cell algorithm software were,  $a=8.174 \text{ \AA}$ ,  $b=3.348 \text{ \AA}$  and  $c=11.394 \text{ \AA}$ . The system is monoclinic with the space group P2/C.

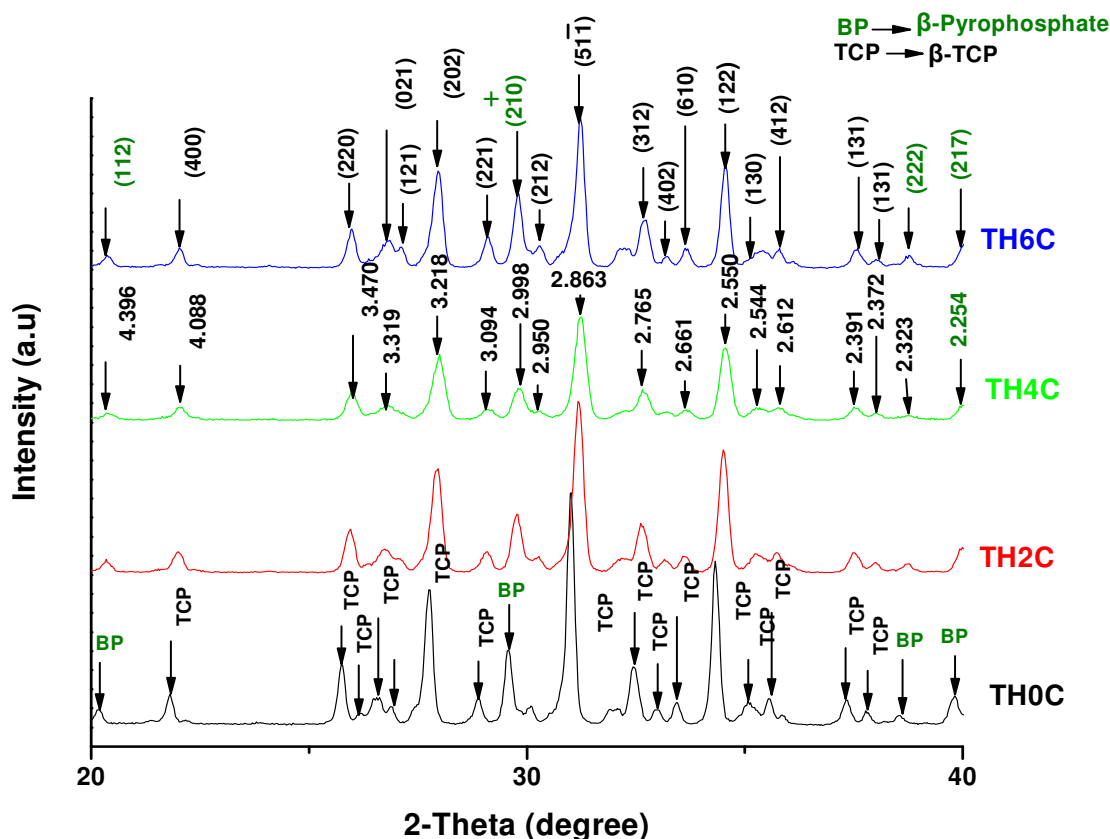


**Figure 4.2(c):** XRD pattern of calcination samples of OCP

### 4.3. FT-IR analysis of HA:

Fourier transform infrared spectroscopy (FT-IR) was used to determine the reaction chemistry of the synthesized hydroxyapatite. Figure 4.3 shows the FT-IR adsorption spectra of HA powders. According to the standard IR transmission spectra, peaks observed at  $3573$  and  $631 \text{ cm}^{-1}$  (present study  $3576$  and  $633 \text{ cm}^{-1}$ ) are assigned to OH band. Peaks around  $472$ ,  $563$ ,  $960$ ,  $1040$  and

1106  $\text{cm}^{-1}$  are phosphate groups ( $\text{PO}_4$ ), and peak at 873  $\text{cm}^{-1}$  assigned to P-O-H bond. The presence of P-O-H bond indicates the material is Ca-deficient hydroxyapatite.

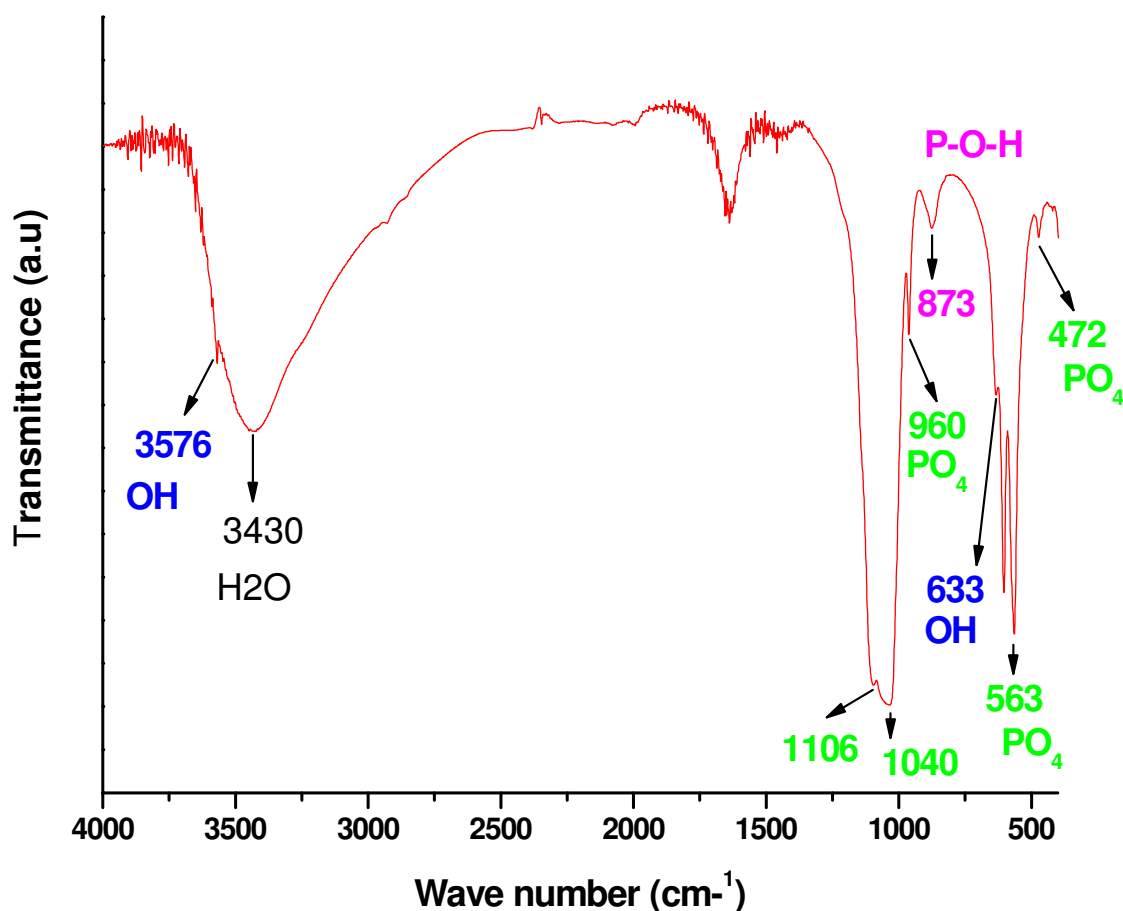


**Figure 4.3:** FT-IR spectra of hydroxyapatite.

#### 4.4. FT-IR analysis of OCP:

Figure 4.4(a) and 4.4(b) shows FT-IR spectra of ucalcination and calcination samples of material. After use the different concentrations of threonine, there is no change happen in the peaks band for samples TH0, TH2, TH4 and TH6. It is observed the same peaks in all samples. In figure 4.4(a) the three distinct bands origination from P-O in the orthophosphate stretch absorption around 1030- 1113  $\text{cm}^{-1}$  tended to obscure the central peak at 1070  $\text{cm}^{-1}$ . The band  $\text{HPO}_4^{2-}$  appeared at 960  $\text{cm}^{-1}$  come from OCP, monetite and Ca-deficient

hydroxyapatite. The two sharp adsorption bands of  $\text{PO}_4^{3-}$  appearing at 560 and 600  $\text{cm}^{-1}$  suggest that the particle has a crystallized OCP structure [4, 5], which is also confirmed by XRD analysis. Furthermore, there is a possibility of adsorption bands due to  $\text{COO}^-$  at 1600-1250  $\text{cm}^{-1}$  [6] for OCP, which is not found in the present study.

The FT-IR spectrum of the powders calcined at 900  $^\circ\text{C}$  (fig 4.4 (b)) become similar to that of  $\beta$ -TCP [33], which is confirmed by the previous XRD result. The characteristic peaks of  $\text{PO}_4$  ions which consistence the standard spectra of  $\beta$ -TCP, appeared at 942-1141 and 558-613  $\text{cm}^{-1}$ . This result is similar with Yan Zhang et al. [7]. After 900  $^\circ\text{C}$ , there is no more heat treatment in the present study for the samples that can further transform  $\beta$ -TCP to  $\alpha$ -TCP.

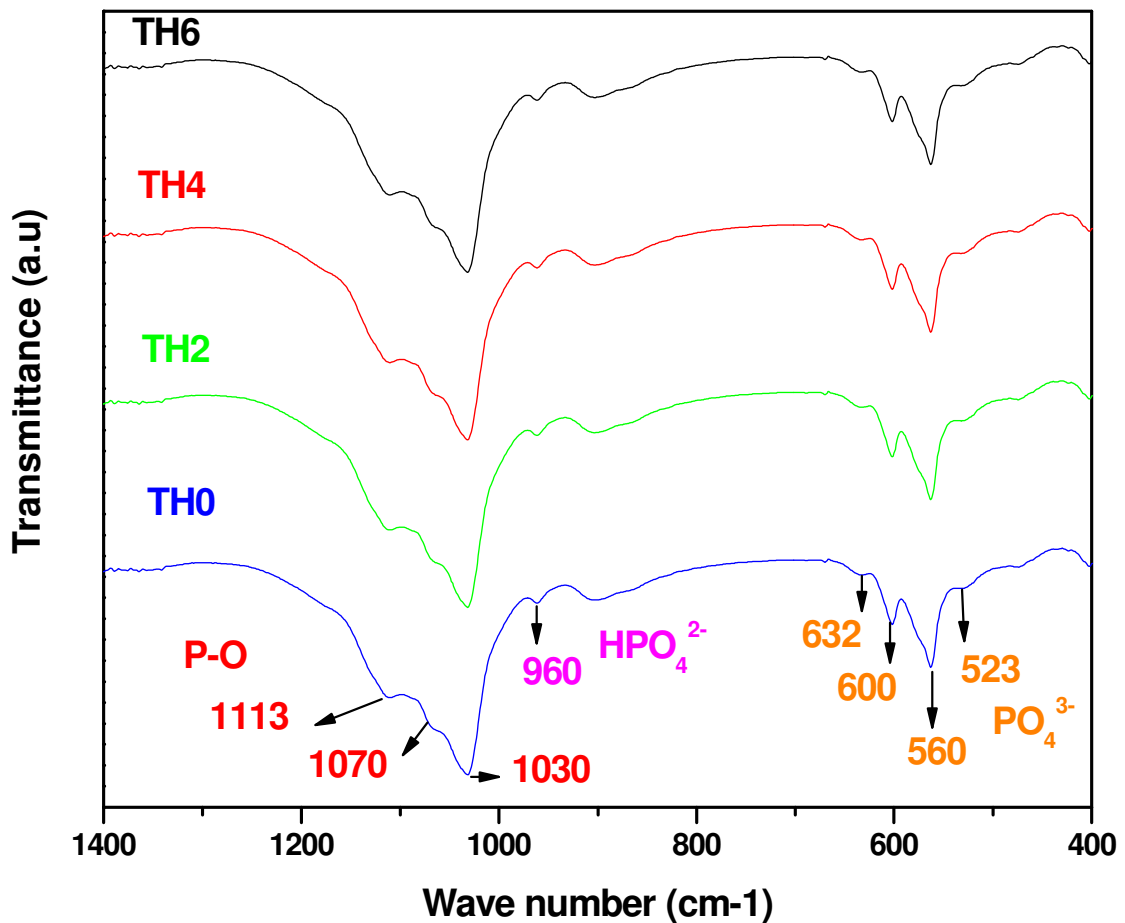


**Figure 4.4(a):** FT-IR spectra of uncalcination samples of OCP.

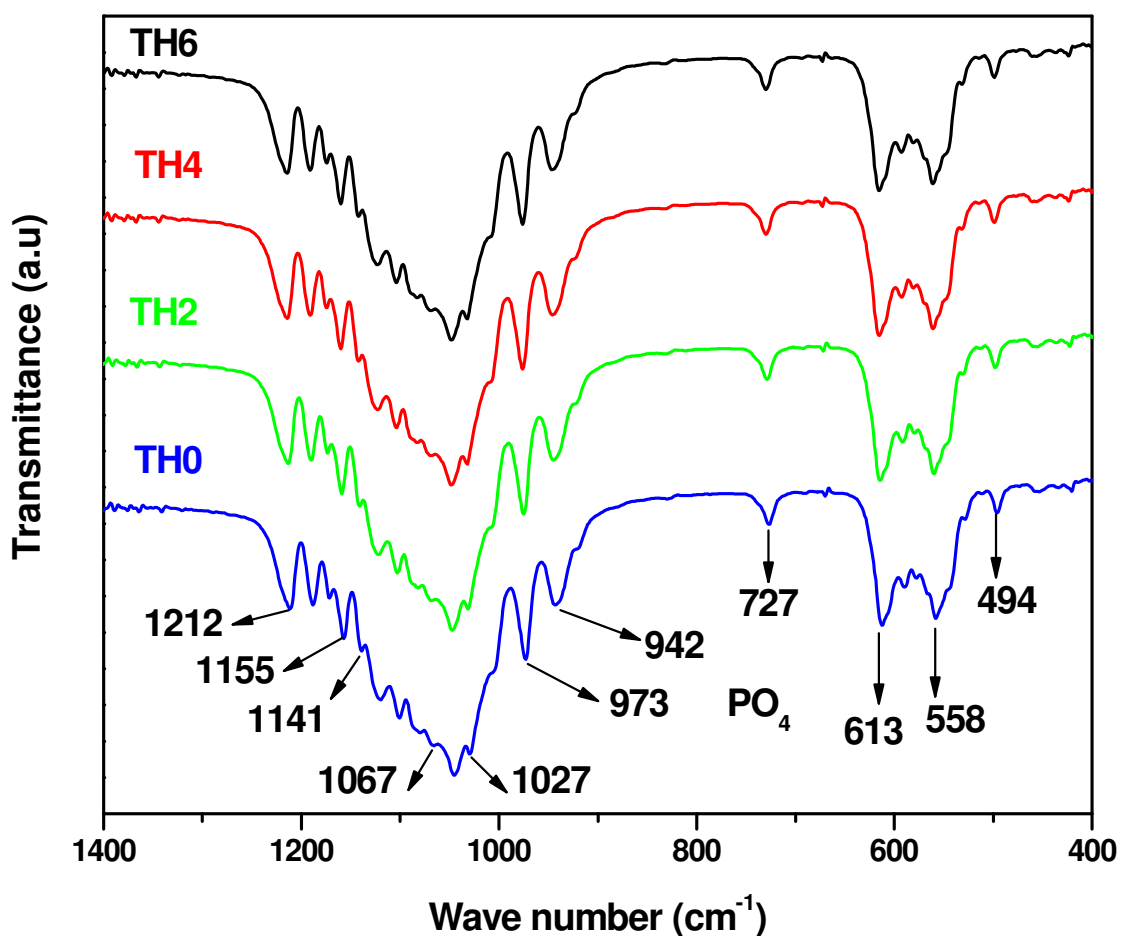
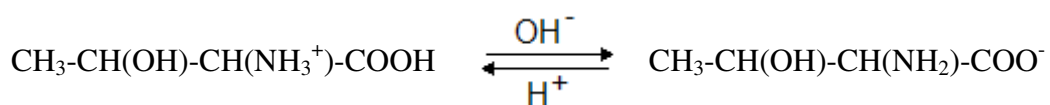


Figure 4.4(b): FT-IR spectra of calcination samples of OCP.

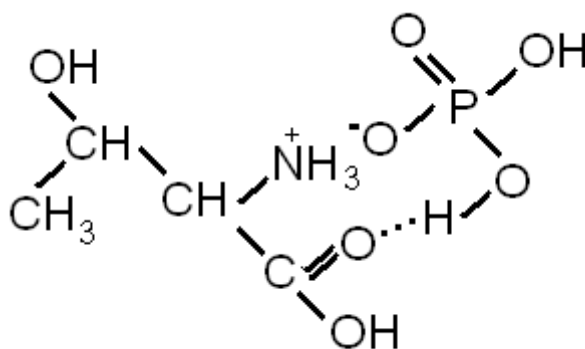
#### 4.5. Mechanism of OCP and monetite formation:

Threonine is an essential amino acid, serving as a carrier for phosphate in phosphoproteins [35, 36]. The chemical structure of threonine (2-amino 3-hydroxy butanoic acid) and the equilibrium for different pH, is shown in the following equation.



In our experimental conditions before add of ammonium solution, the initial solution of salts has pH ~3.3. The main forms of threonine and phosphates are  $\text{CH}_3\text{-CH(OH)-CH(NH}_3^+\text{)-COOH}$  and  $\text{H}_2\text{PO}_4^-$ , correspondingly, which create

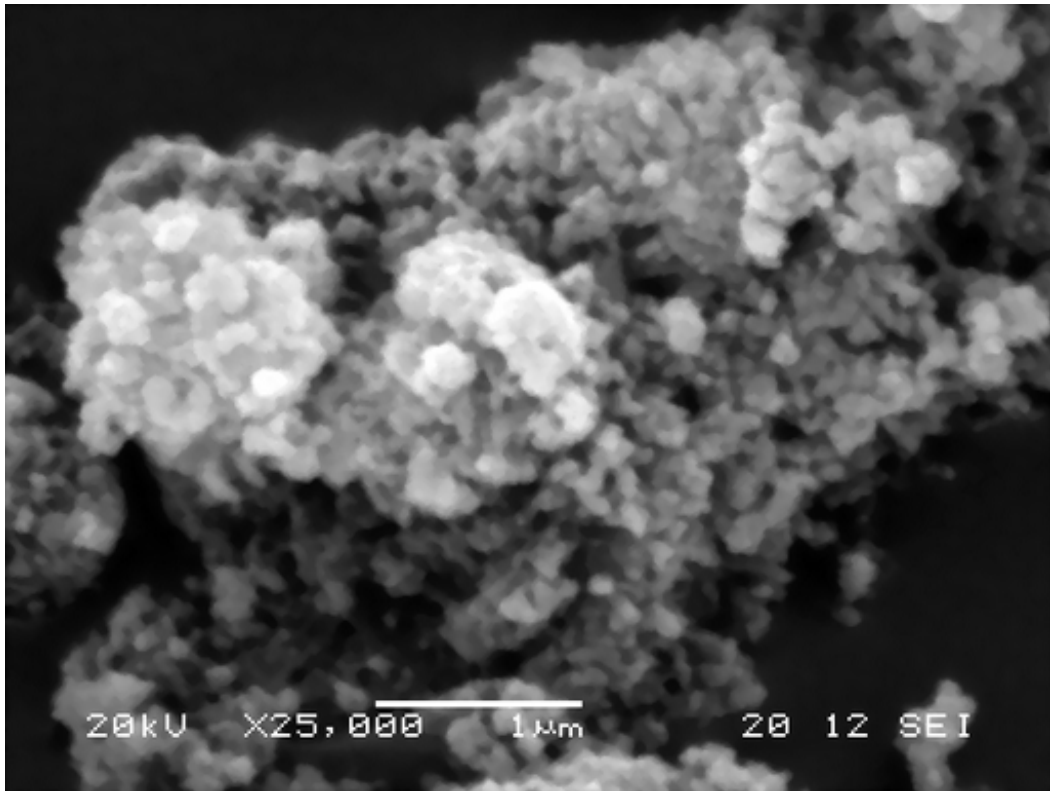
together the following complex.



In this complex, one hydroxyl group of phosphate is bonded with the threonine molecule by an hydrogen bond. By this way, it is inhibited to formation of HA and is remained as acid phosphate group, consequently it create OCP and monetite.

#### 4.6. SEM analysis of HA:

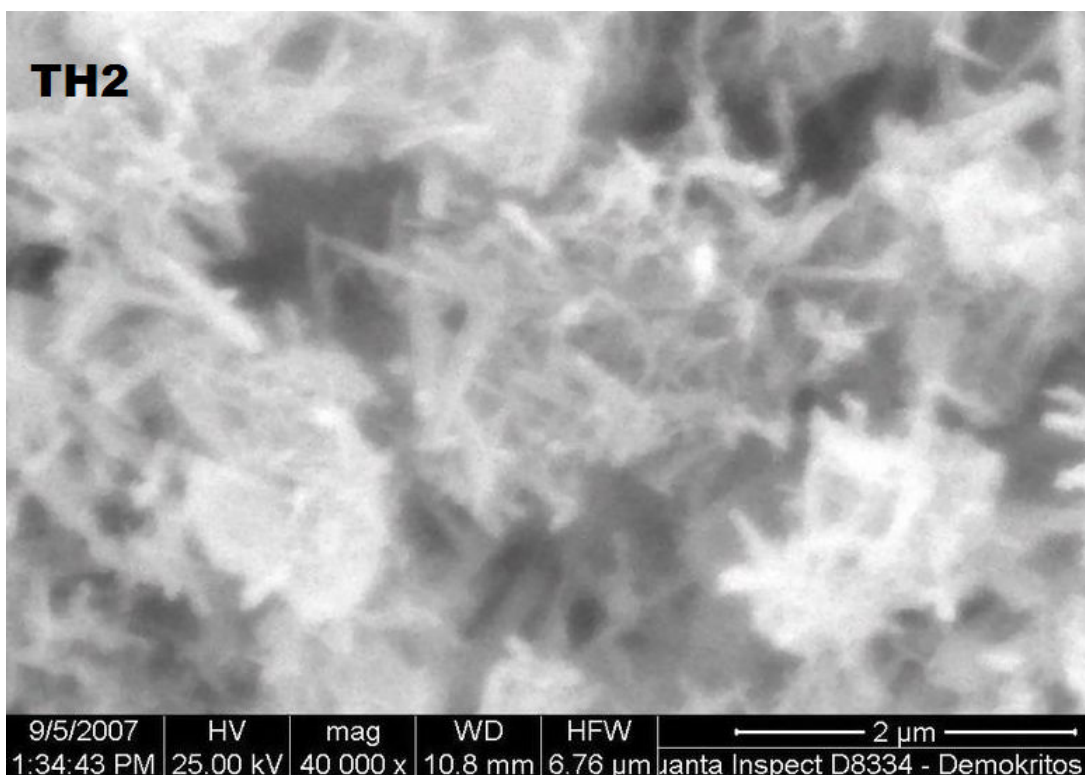
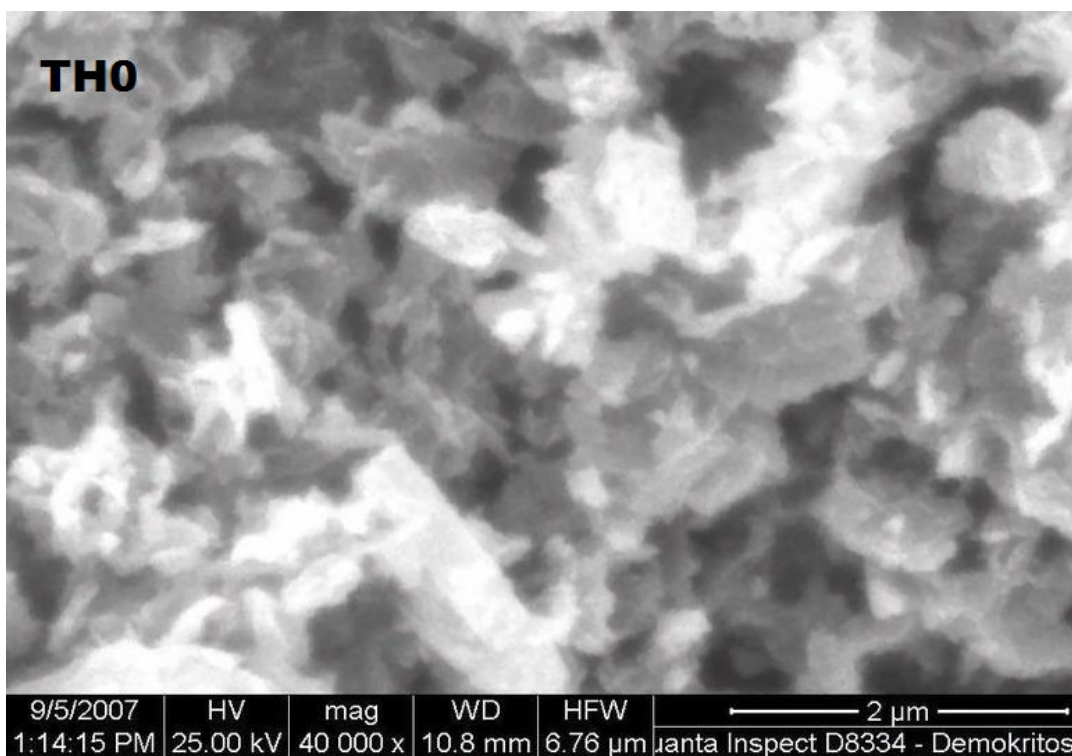
Figure 4.6 shows typical SEM micrograph of hydroxyapatite. The observed particles were spherical in shape and highly agglomerated. Numerous aggregates of isolated particles also observed in SEM image and the observed particle size was ~75 to ~150 nm.



**Figure 4.6:** SEM micrograph of hydroxyapatite.

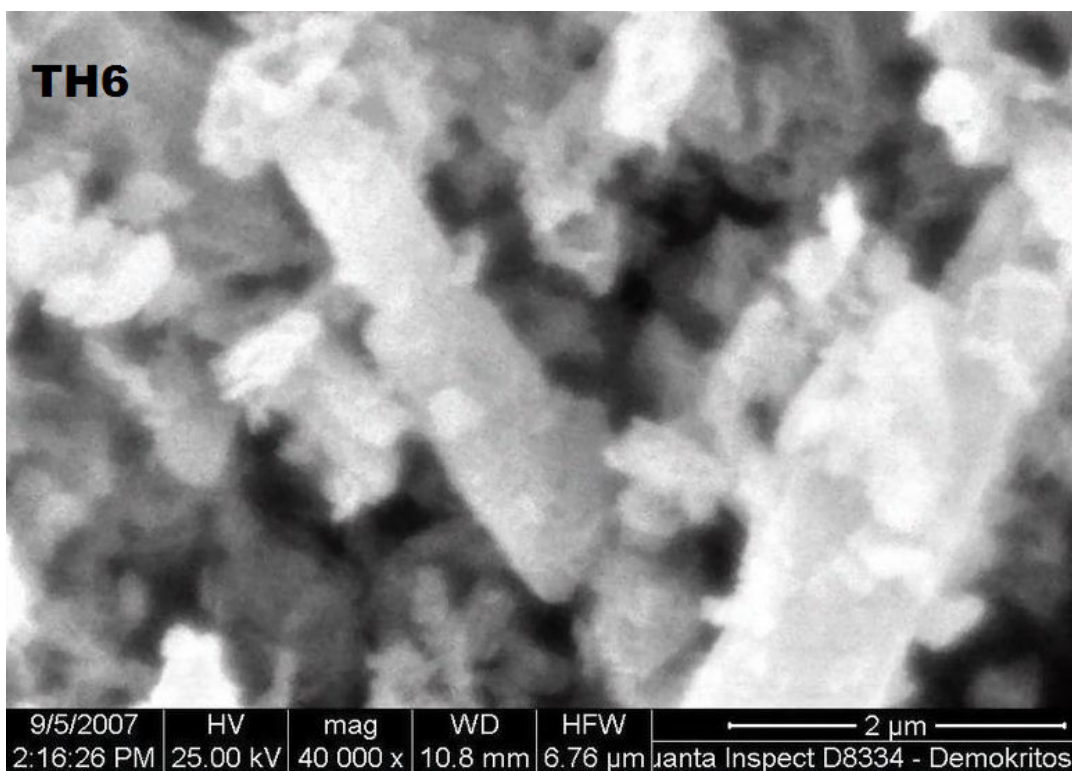
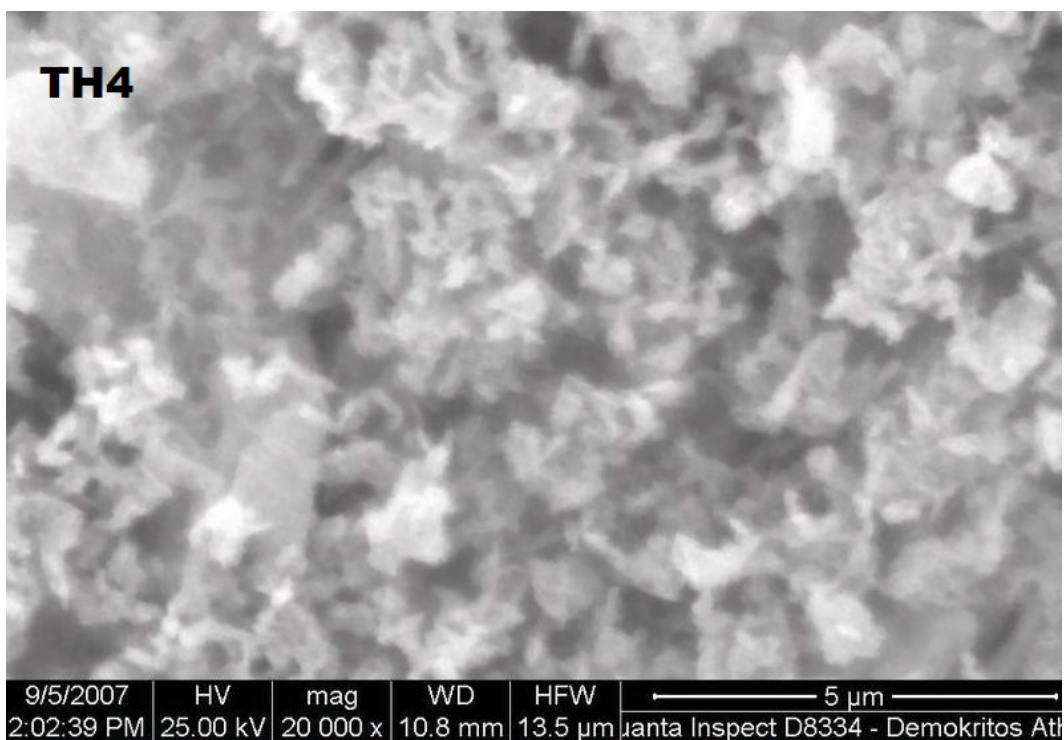
#### **4.7. SEM analysis of OCP:**

Figure 4.7(a) and 4.7(b) shows typical SEM micrographs of samples. It could be found that each particle contained a number of fine grains. The obtained powders appeared to weakly agglomerate particles after eliminating the absorbed water. SEM images of powders also showed numerous aggregates of much smaller and thinner images. The OCP granules of TH0 composed of aggregates of un-uniform particles. After use different concentration of threonine, change in shape and size is observed for all samples. By using small concentration of threonine, TH2 granules were composed of numerous isolated small needle-like particles without any agglomeration. The mean particle size is about 1 µm for



**Figure 4.7(a)** : SEM micrographs of uncalcination samples of OCP





**Figure 4.7(a) continued:** SEM micrographs of uncalcination samples of OCP

for sample TH2. TH4 granules aggregate of spheroidal particles and after increase threonine concentration, for TH6 granules, the synthesized particles were big

aggregates of round spherical shape and some particles get rod-shaped and their mean sizes were 150-300 nm.

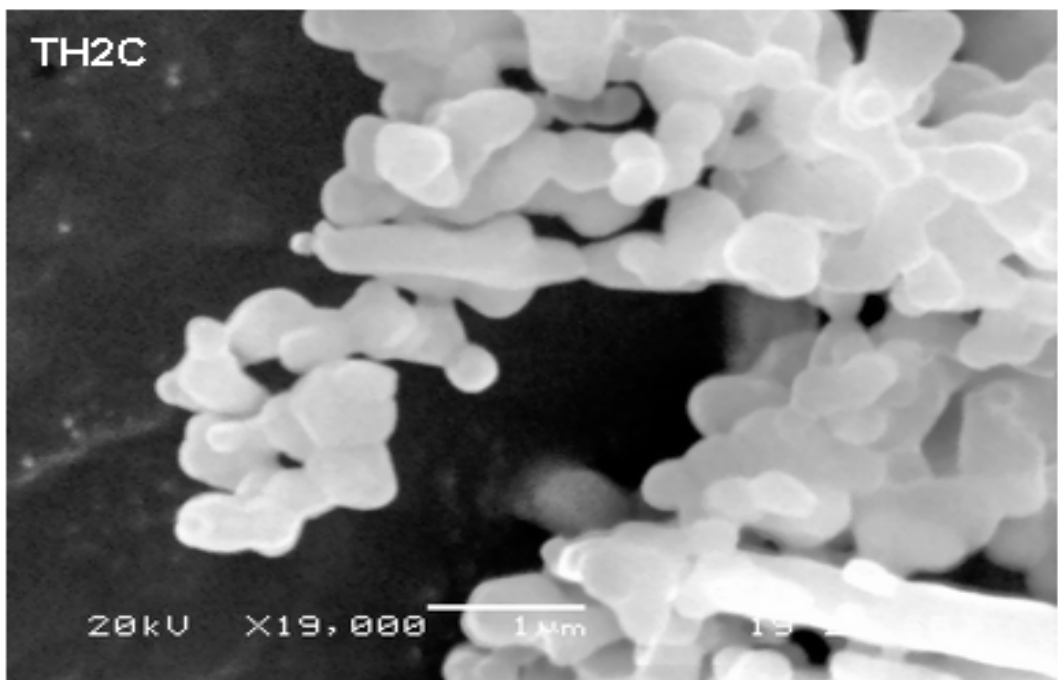
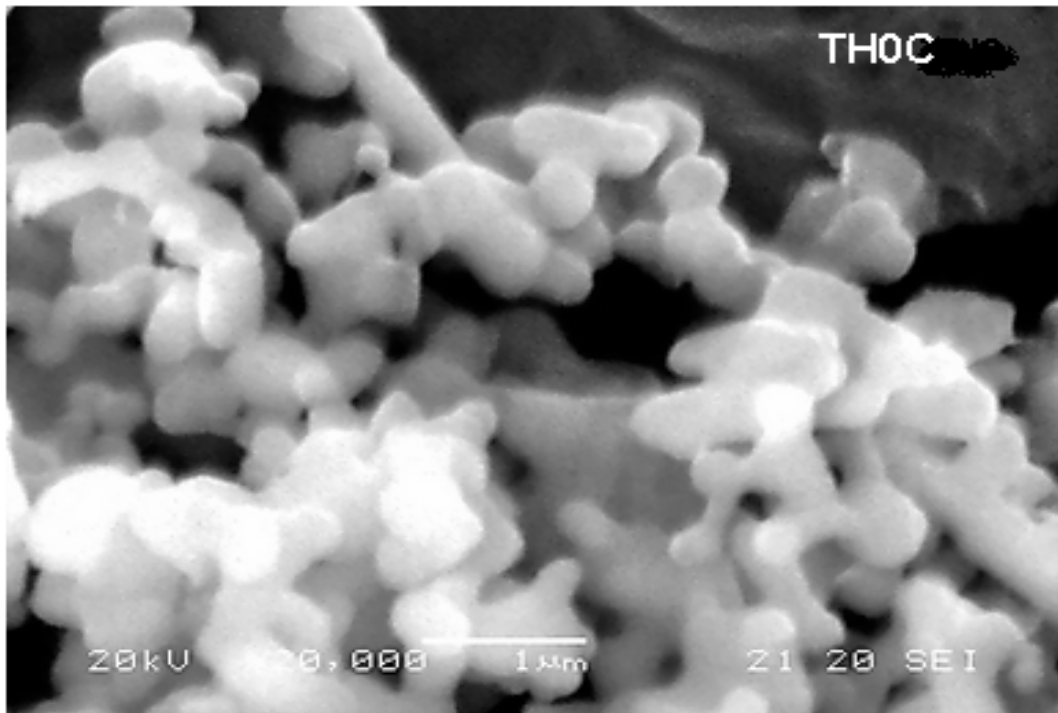


**Figure 4.7(b):** SEM micrographs of calcination samples of OCP.

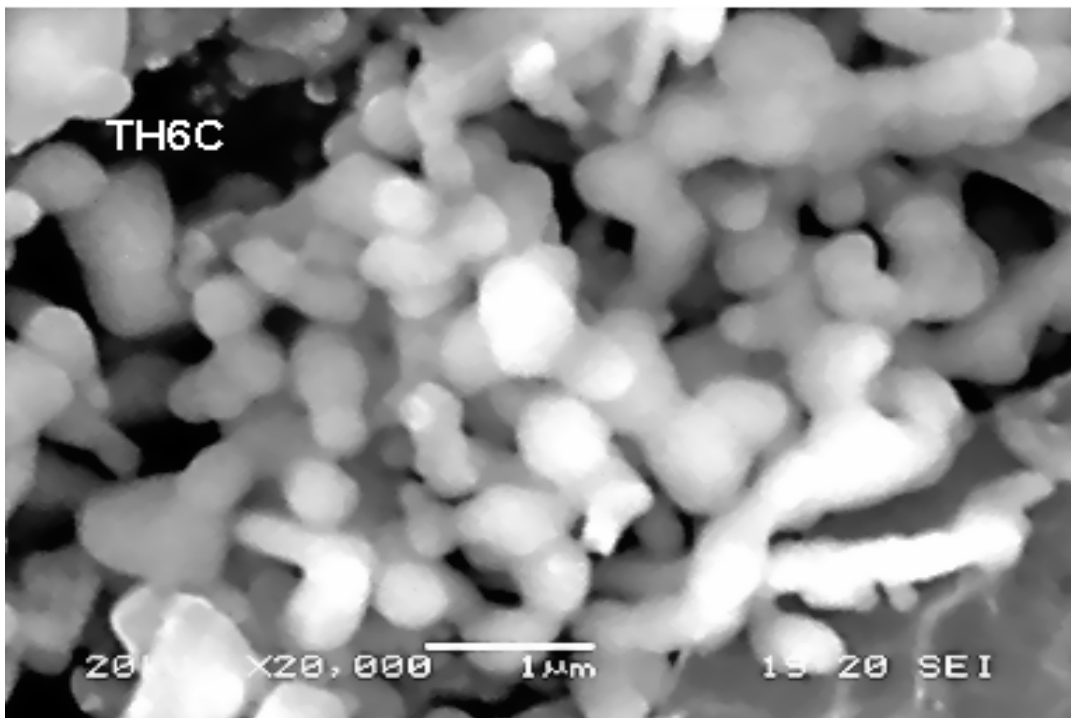
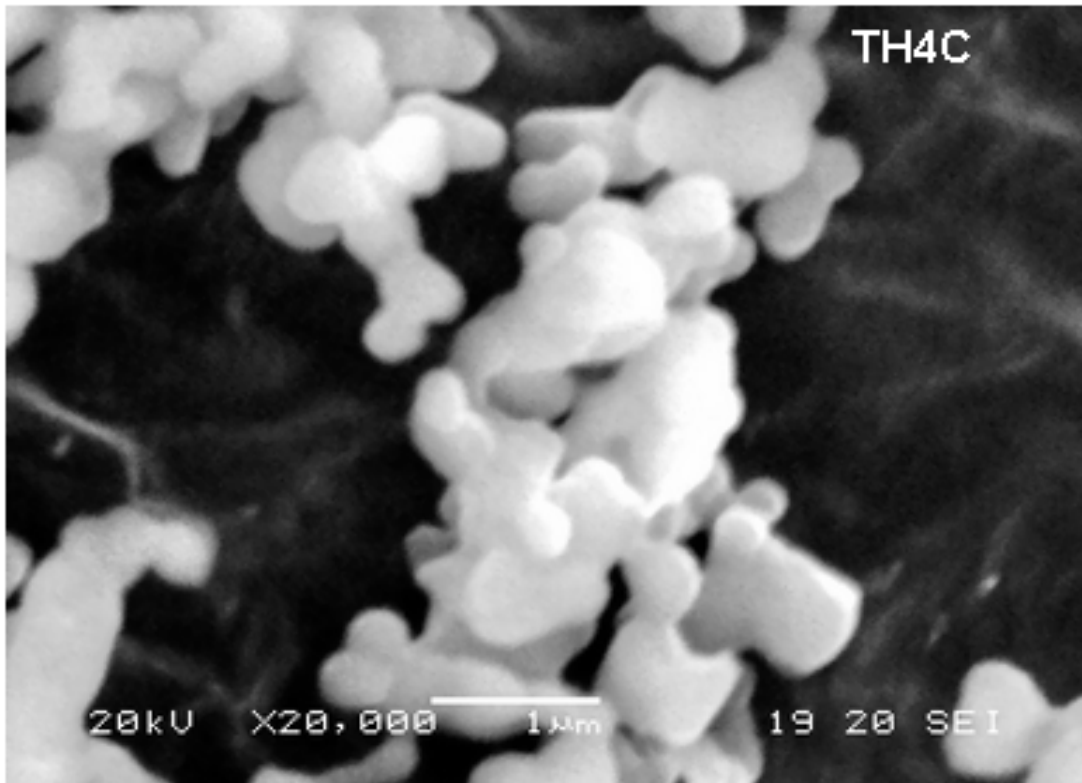


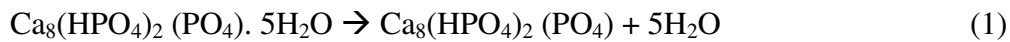
**Figure 4.7(b) continued:** SEM micrographs of calcination samples of OCP.

After calcined at  $900^{\circ}\text{C}$ , the primary particles of material were conglomerated tightly into secondary powders of botryoidal (resembling a cluster

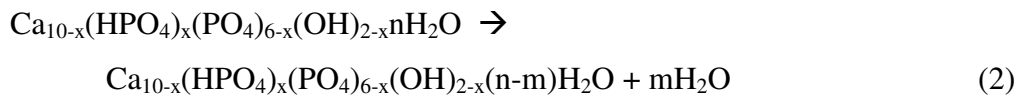
of grapes in form) shape (Fig 4.7(b)). Calcination did not cause a change in the particles morphology, and the OCP particles remain spherical geometry, and kept aggregated. All of these phenomena suggest that the material formed in this study incorporated organic compounds in the interlayer .

#### 4.8. Thermal analysis of material:

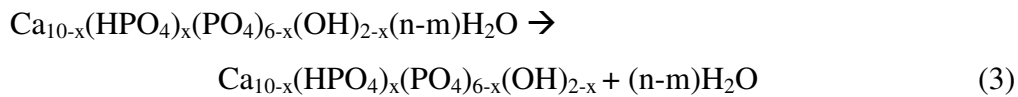
Figure 4.8(a) and 4.8(b) shows the TG and DSC curves of uncalcined samples of material (TH0, TH2, TH4 and TH6). The thermal decomposition takes place through four successive steps between the temperature ranges 20 until 1400 °C. The first step is exothermic, takes place between room temperature and about 400 °C. This step mainly assigned the removal of adsorbed and crystalline water. For octacalcium phosphate, the reaction is:



For hydroxyapatite the removal of water is:



This step suggests an increasing water adsorption tendency and the removal of residual crystalline water is:



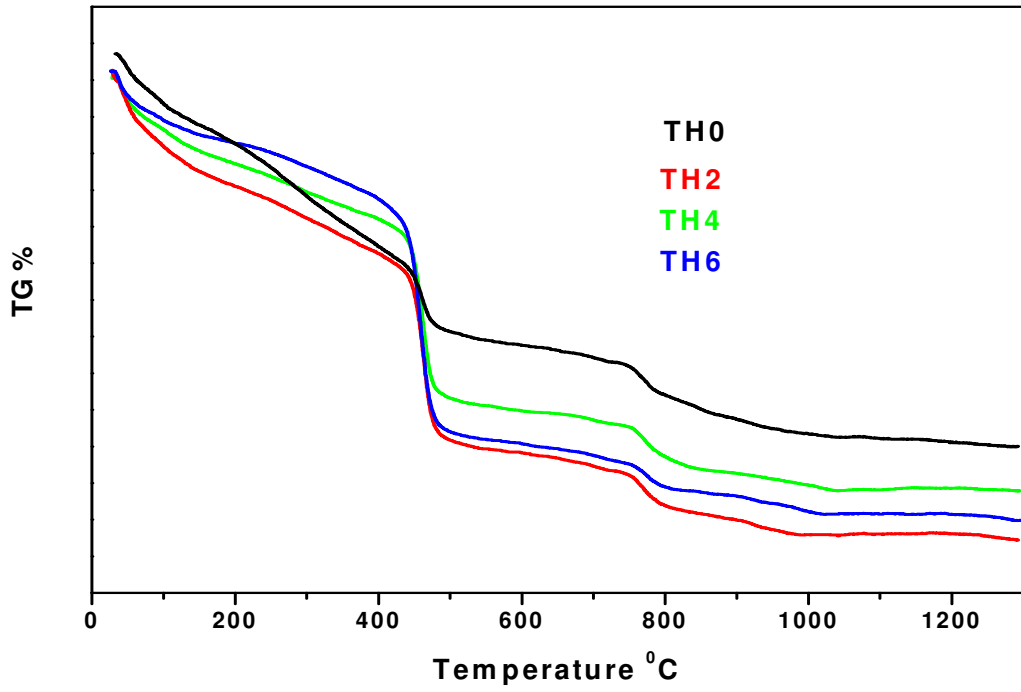


Figure 4.8(a): TG curve of uncalcination samples of OCP

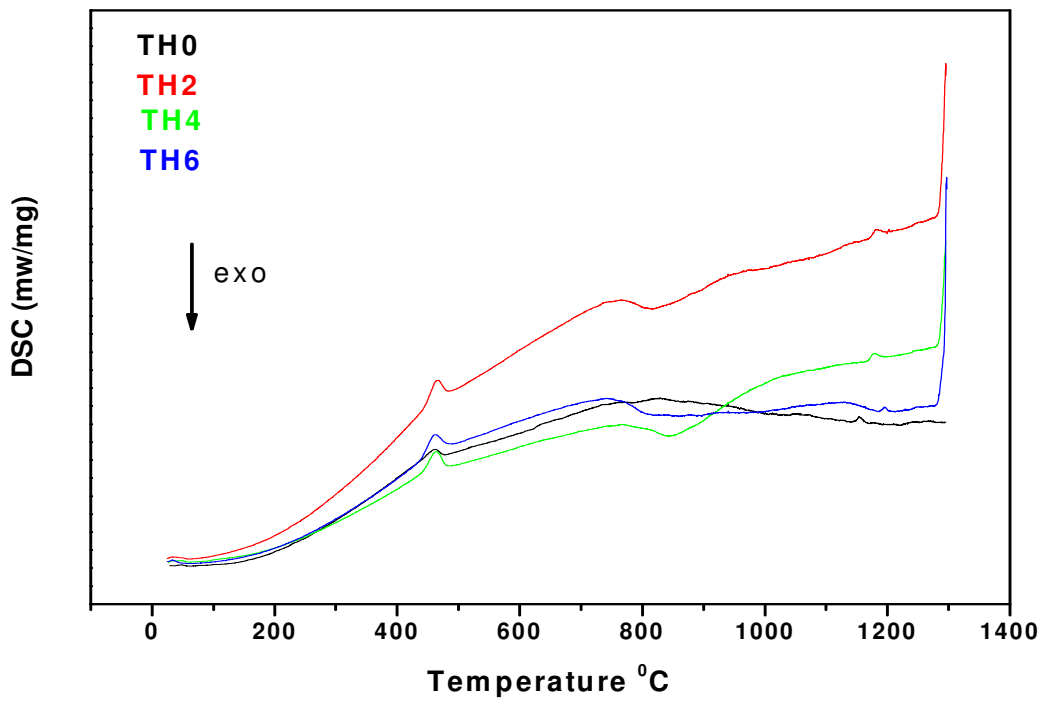
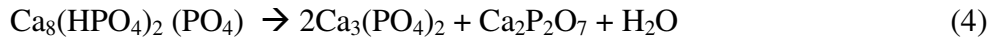


Figure 4.8(b): DSC curve of uncalcination samples of OCP.

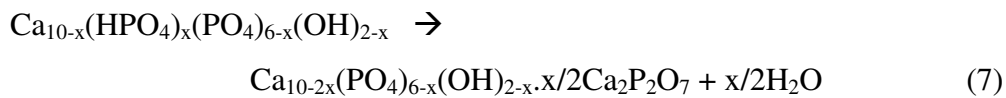
Second step is endothermic and occurred at temperature range between 400 and 750 °C. In this step very weak peak observed for sample TH0 on DSC curves, on the other hand, for samples TH2, TH4 and TH6 more sharp peaks than TH0 detected. Here mainly decomposition of octacalcium phosphate to pyrophosphate occurred under the following reaction:



In this step monetite also decompose to calcium pyrophosphate about 417-422 °C. Later between 519-530 °C the amorphous calcium pyrophosphate is crystallized to  $\gamma$ -  $\text{Ca}_2\text{P}_2\text{O}_7$ , which the peak is not observed in the present study. The reactions are:



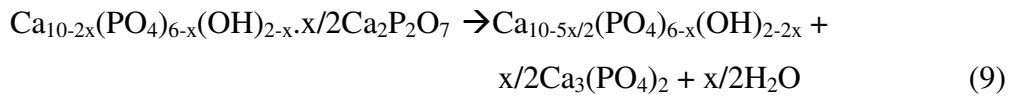
From equation (3) the transformation of acid phosphate to pyrophosphate take place under the following reaction:



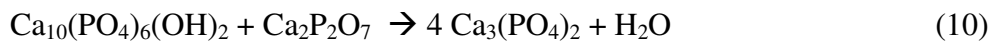
In the third exothermic step between temperatures 750-1100 °C, no peak detected for sample TH0 on DSC curves, while broad peaks observed for samples TH2, TH4 and TH6. In this step at about 854 °C the  $\gamma$ -  $\text{Ca}_2\text{P}_2\text{O}_7$  is transformed to  $\beta$ - $\text{Ca}_2\text{P}_2\text{O}_7$ , which is also detected in XRD results for calcination samples of 900 °C.



In this step the following reaction also take place:



In this step another reaction happen between hydroxyapatite and calcium pyrophosphate, to form  $\beta$ -TCP, which is the main phase of samples after calcination 900 °C, confirmed by XRD.



The fourth and final step occurs at temperature ranges 1100-1300 °C. Sharp endothermic peaks observed for all samples with some variation of temperatures on DSC curves. In this step the partial dehydration of hydroxyapatite happen from equation (9) under the following reaction:



Where  $V^{\text{OH}}$  denotes the lattice vacancies on OH sites. G.C. Koumoulidis et al. [8] have found the same result during the sintering of hydroxyapatite lath-like powders. The small and sharp peaks about 1200 °C on DSC curves indicate the transformation of  $\beta$ -TCP to  $\alpha$ -TCP.



About 1300 °C sharp peaks observed on DSC curves for samples TH2, TH4 and TH6, which indicates the melting of calcium pyrophosphate.



But for sample TH0 this peak is not detected due to the absent of pyrophosphate. This observation indicates the consumption of all the amount of pyrophosphate by the reaction (10). At the end of the experiment, we observed partial sintering of materials due to melting of pyrophosphates.

#### 4.9. Peak separation of material:

Figure 4.9(a), 4.9(b), 4.9(c) and 4.9(d) show the peak separation curves of uncalcination samples of material. These peak separation curves are calculated by using NETZSCH SEPARATION of PEAK software (SW/PKS/650.01A) from DTG curves. The mass loss (%) and peak temperature (°C) data are shown in Table 4.9(a) and Table 4.9(b), and depicted in figures 4.9(e) and 4.9(f), respectively. It is observe that for the first step (the removal of crystalline and adsorbed water), the main mass loss happen for sample TH0, it is the highest amount comparing other samples, which is 4.44%. After add different concentration of threonine the mass loss decreases and it is 3.92, 2.88 and 3.26% for samples TH2, TH4 and TH6, correspondingly.

For TH0, in the 1<sup>st</sup> stage of 1<sup>st</sup> step the presence of two phase of HA, and OCP cause the big mass loss but in 2<sup>nd</sup> stage it is remain only OCP. In the 2<sup>nd</sup> stage, the mass loss of samples TH2, TH4, TH6, which prepared by presence of threonine, were highest than sample TH0 and this indicate that the amount of produced OCP were highest in these samples. Also, the peak temperatures, that is, the temperature at the maximum rate transformation of the peak, of the second stage of first step increase as the threonine content increases.

In the second step of mass loss, it is opposite happen. The sample TH0, has the lowest mass loss (0.68 %) comparing other samples. The presence of threonine in the solution results to the increase of the mass loss about three times.

Take into account that in the second step mainly occurs the decomposition of acid-phosphate groups to pyrophosphates, we conclude that the presence of the threonine in the solution favors the preparation of monetite and OCP.

In the third step again highest mass loss observed for TH0, which is 0.86% and for TH2, TH4 and TH6, the mass loss is 0.56, 0.63 and 0.42%. Take into account that: i) in this step takes place the consumption of pyrophosphates by reaction of produced pyrophosphates species with the HA, (reaction 10) and ii) in the DSC curves of TH0 sample the melting of pyrophosphates don't observed, we conclude that the amount of HA are stoichiometric less than pyrophosphates, and some amount of pyrophosphates were remained unchanged.

A small and continuous mass loss observed in fourth step, which is 0.38, 0.35, 0.29 and 0.38% for samples TH0, TH2, TH4 and TH6.

In conclusion, that the presence of threonine in the initial solution inhibits the HA preparation and prevents the monetite and OCP phases formation.

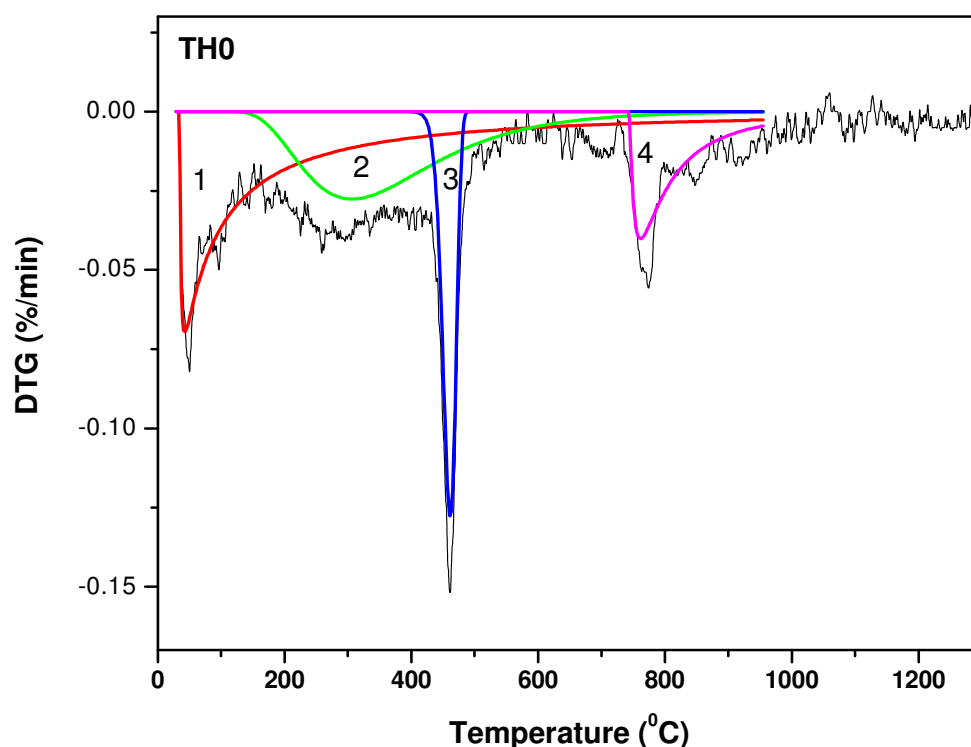


**Figure 4.9(a):** Peak separation curve of sample TH0.



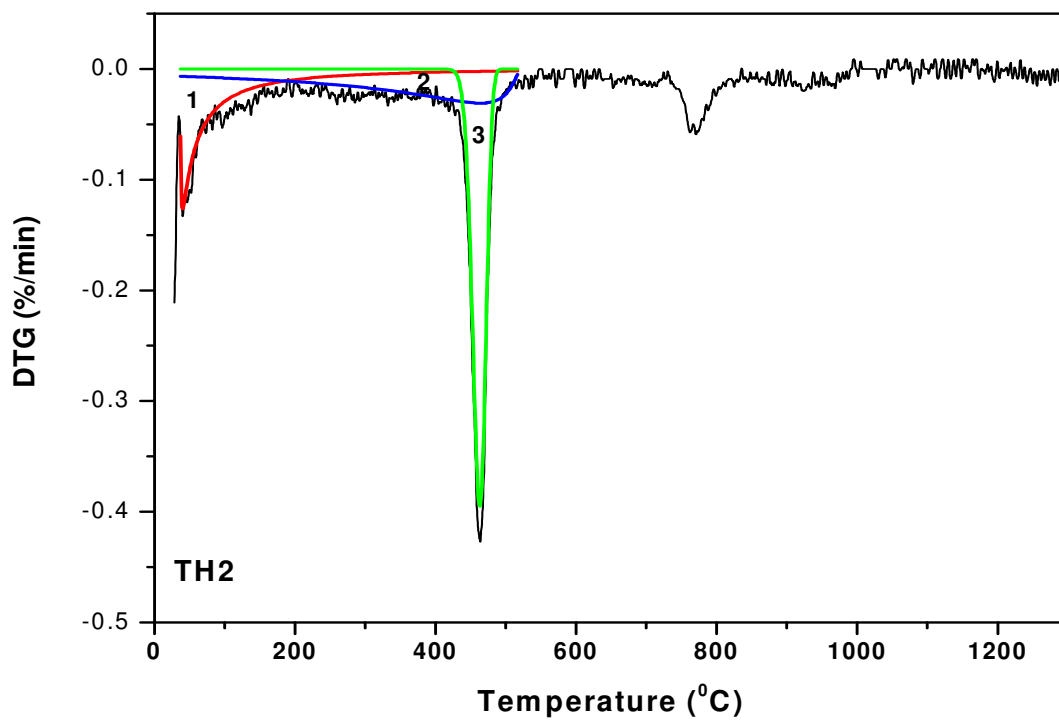


**Figure 4.9(b):** Peak separation curve of sample TH2.

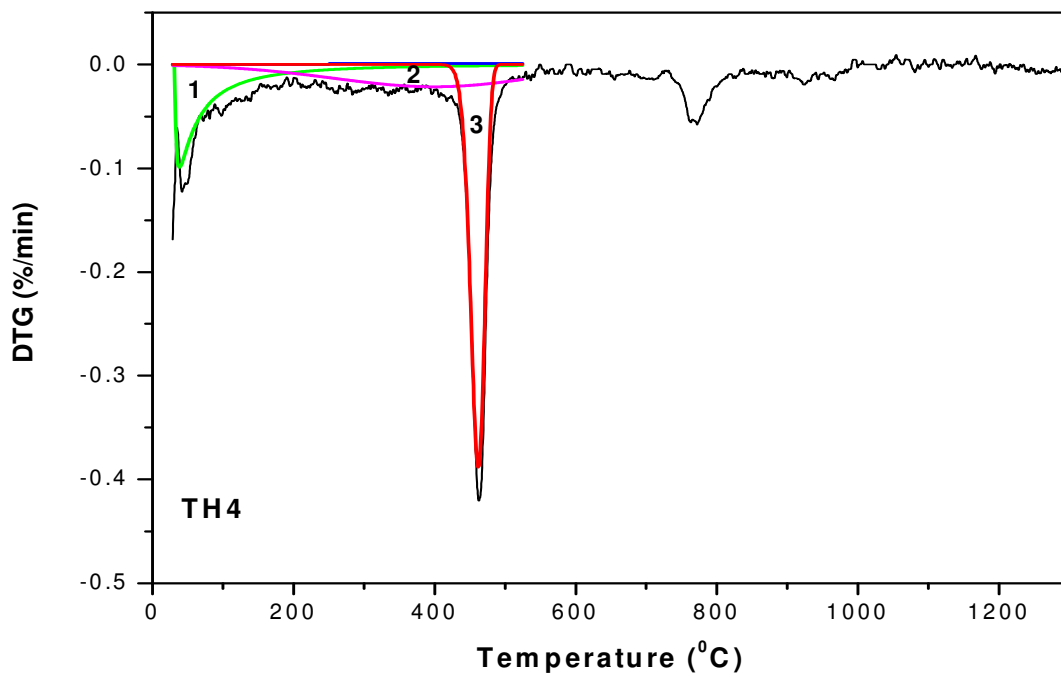


**Figure 4.9(c):** Peak separation curve of sample TH4.

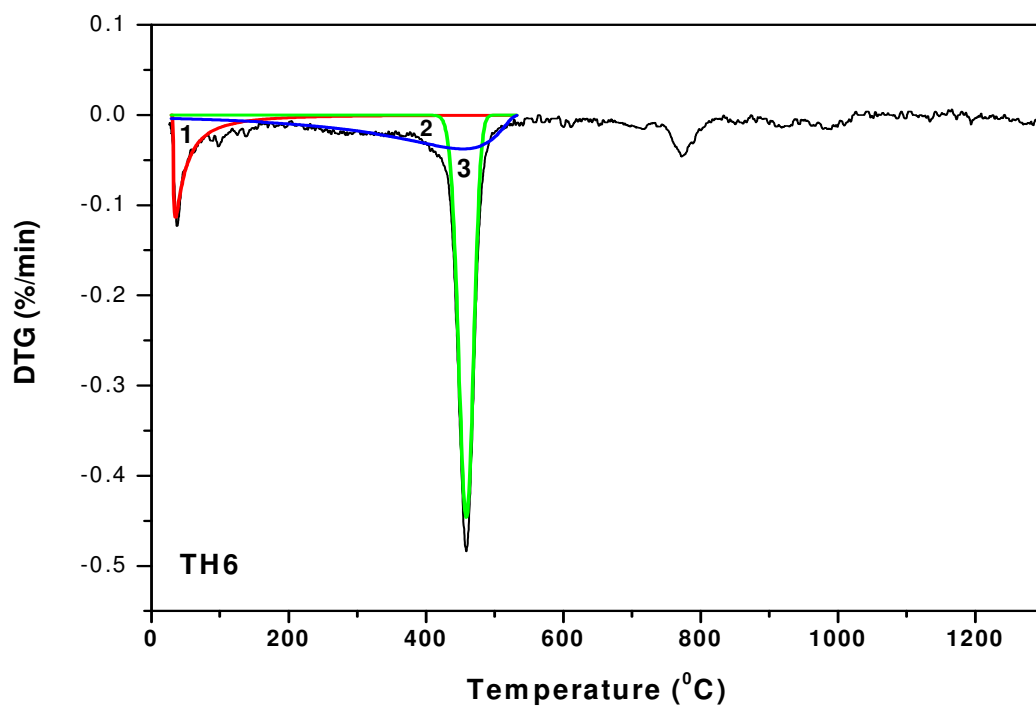


**Figure 4.9(d):** Peak separation curve of sample TH6.

**Table 4.9(a):** Mass loss (%) data of thermal analysis for uncalcination samples:

Sample code	Step					
	First			Second	Third	Fourth
	1 <sup>st</sup> stage	2 <sup>nd</sup> stage	Total			
TH0	2.90	1.54	4.44	0.68	0.86	0.38
TH2	1.60	2.32	3.92	1.89	0.56	0.35
TH4	1.33	1.55	2.88	1.97	0.63	0.29
TH6	0.83	2.43	3.26	1.93	0.42	0.38

**Table 4.9(b):** Peak Temperature ( $^{\circ}\text{C}$ ) of thermal analysis for uncalcination samples:

Sample code	Step			
	First		Second	Third
	1 <sup>st</sup> stage	2 <sup>nd</sup> stage		
TH0	35	306	454	762
TH2	38	357	461	769
TH4	40	379	462	772
TH6	42	399	463	776

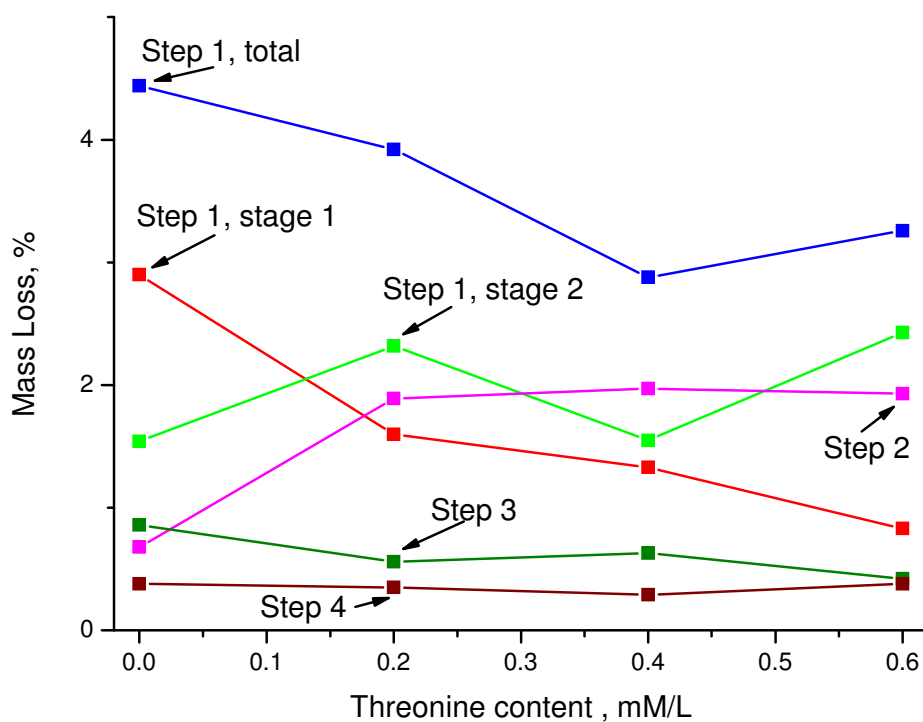


**Figure 4.9(e).** The mass loss of the steps-stages of samples for the peak separation

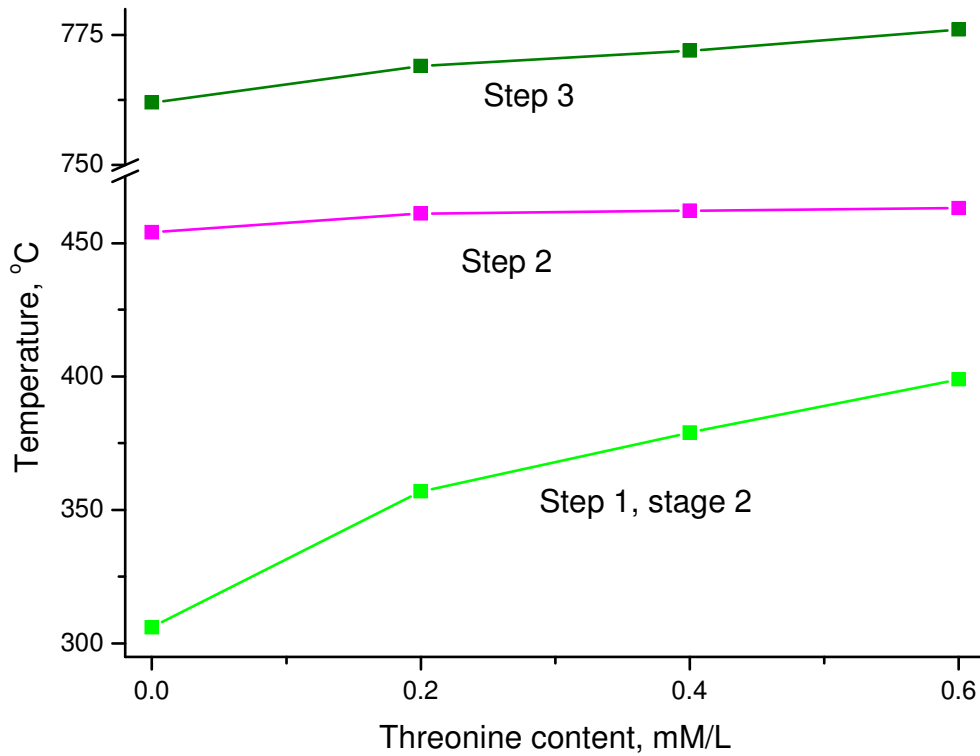


**Figure 4.9(f).** The peak temperatures of the steps-stages of samples for the peak separation

#### 4.10. BET analysis of HA:

The N<sub>2</sub> adsorption-desorption isotherms for the sample of hydroxyapatite is shown in figure 4.10. The most important morphological parameters can be calculated from analysis of the relationship between the volume adsorbed and the relative pressure of a physically adsorbing gas. The method is realized by rearranging the original BET equation [9].

$$\frac{V}{V_m} = \frac{C(P/P_0)}{[1 + (C-1)(P/P_0)][1 - (P/P_0)]} \quad (14)$$

In the form,

$$\frac{V[1 - (P/P_0)]}{(P/P_0)} = CV_m - (C-1)V[1 - (P/P_0)] \quad (15)$$

Plots of the form  $V [1-(P/P_0)] / (P/P_0)$  vs  $V[1-(P/P_0)]$  provide lines which have the shape of an inclined V, i.e. >, and variable slopes corresponding to (C-1) from

which the values of the C parameter can be determined for the whole range of partial pressures  $0 < (P/P_0) < 1$ . The inversion point of such plots, termed the I-point, projected on to the  $V [1-(P/P_0)]$  axis corresponds exactly to the volume of monolayer, i.e.  $V_m = V [1-(P/P_0)]$ , from which the values of the specific surface area (ssa  $\text{m}^2\text{g}^{-1}$ ) can be easily determined from the trivial relationship,  $\text{ssa} = 4.356 V_m$  [10,11]. In the present study  $V_m$  is calculated from BET isotherm instead of I-point.

Figure 4.10 show the adsorption-desorption isotherm of HA. The specific surface area (ssa) estimated according to the standard BET equation is  $53 \text{ m}^2 \text{ g}^{-1}$  and the corresponding  $V_m$  value is  $12 \text{ cm}^3 \text{ g}^{-1}$ .

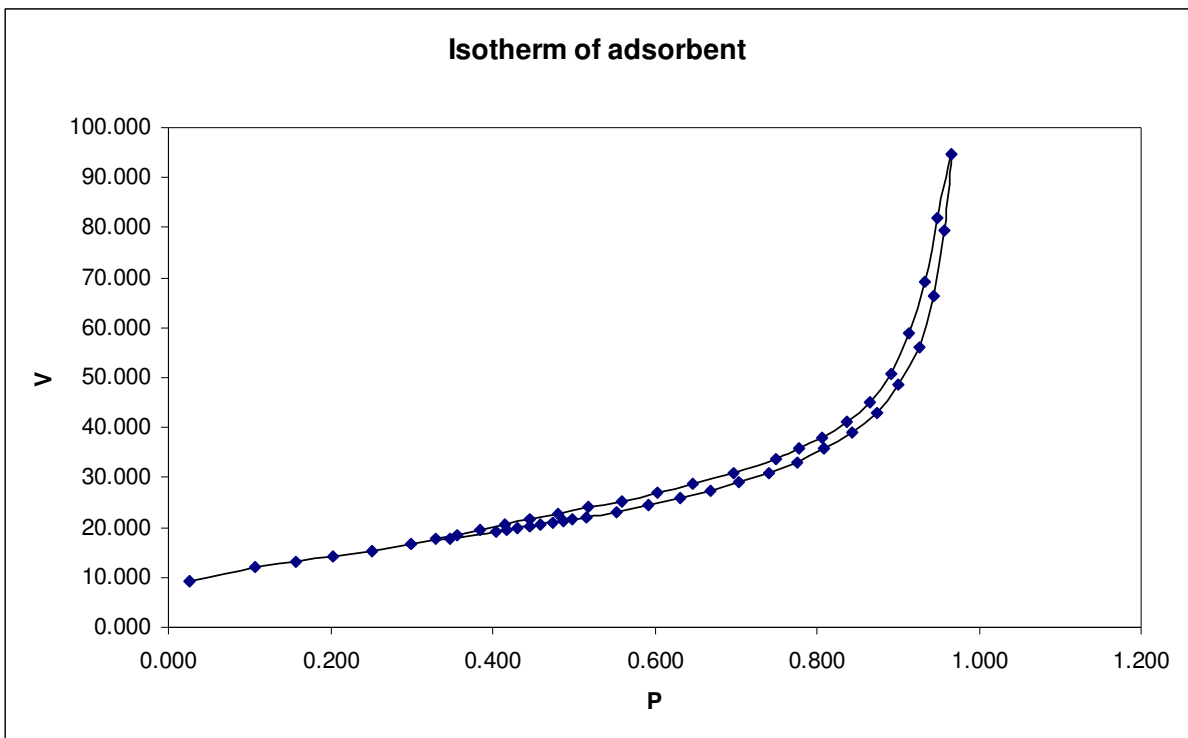


**Figure 4.10:** BET isotherm of hydroxyapatite.

#### 4.11 BET analysis of OCP:

The  $\text{N}_2$  adsorption-desorption isotherms for the uncalcined samples of OCP are shown in figure 4.11(a) and the calcined samples in figure 4.11(b). The specific surface area is determined by using the same BET method [9].

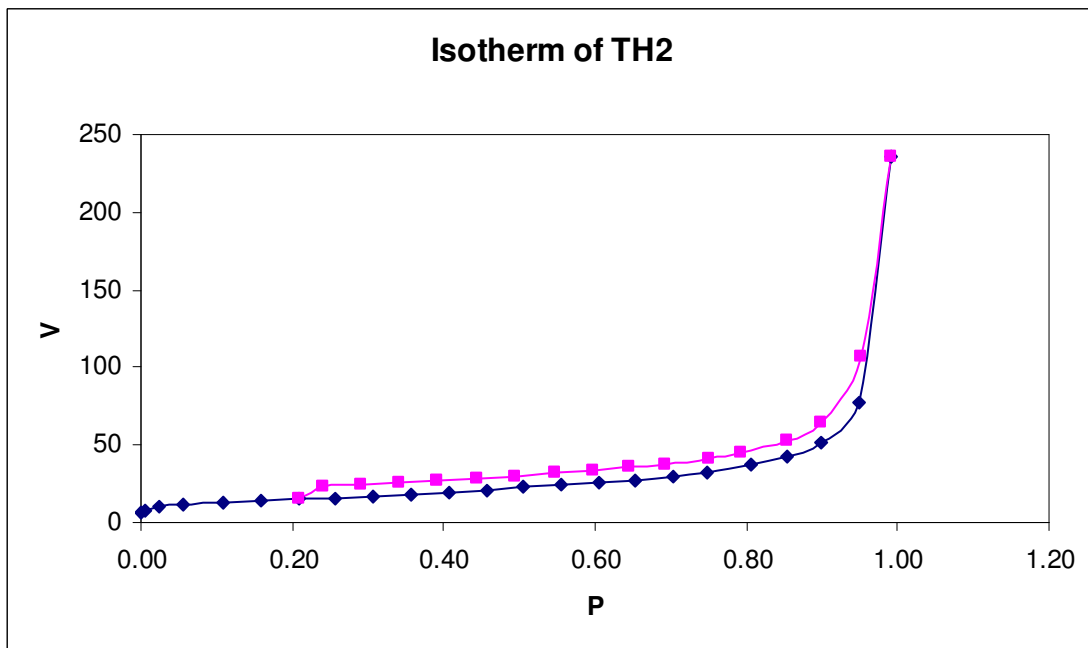
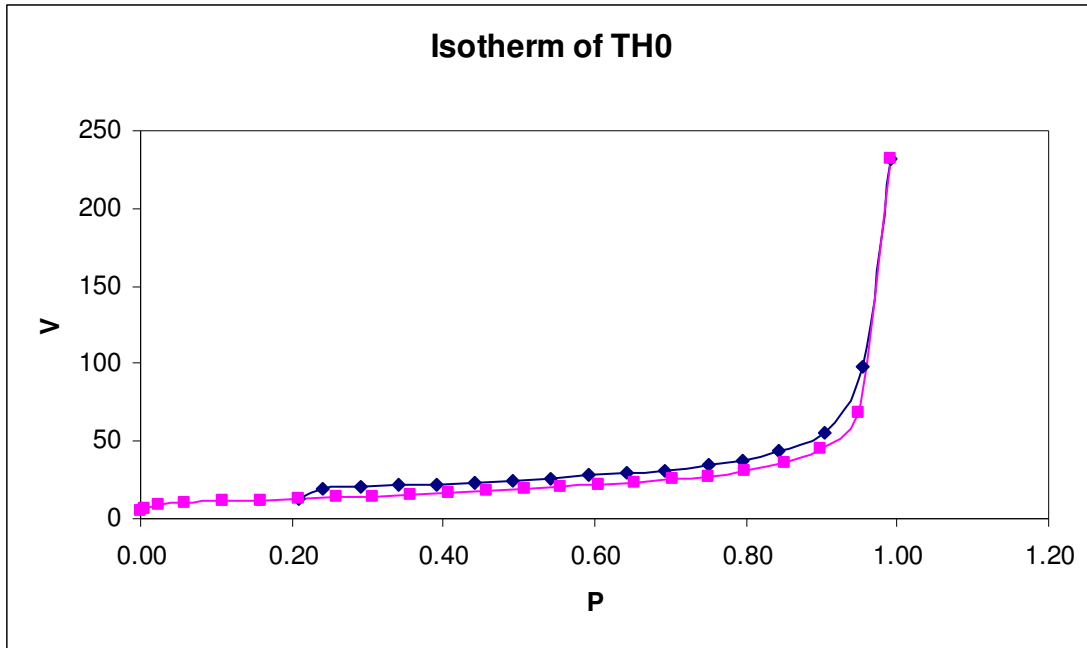


**Figure 4.11(a) :** BET isotherm curves of uncalcination samples of OCP.

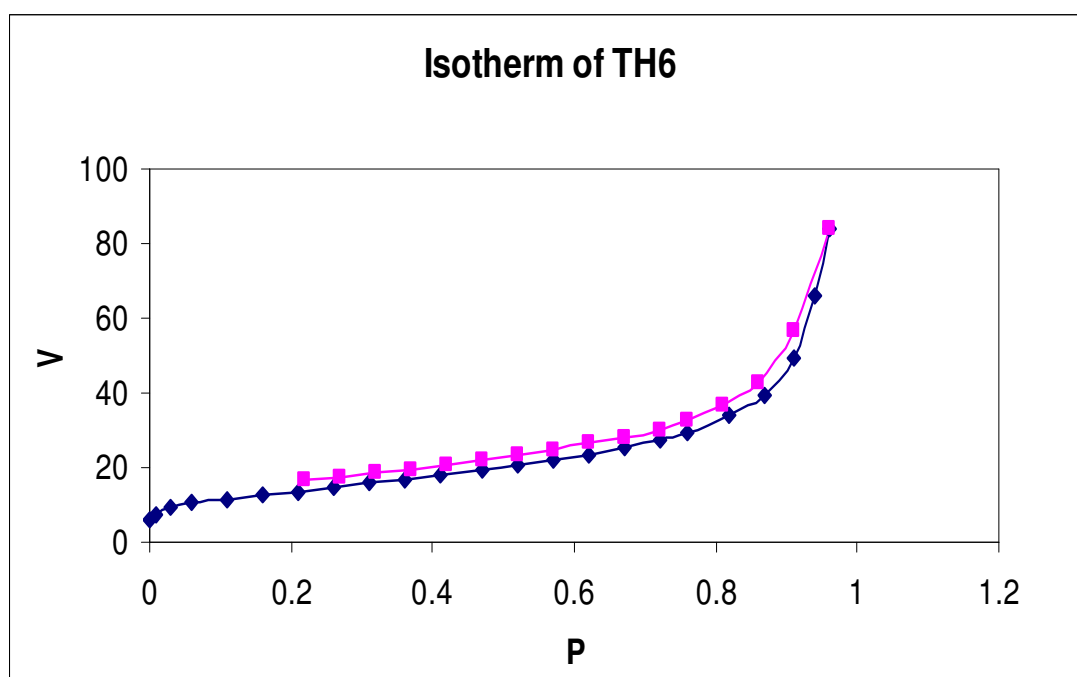
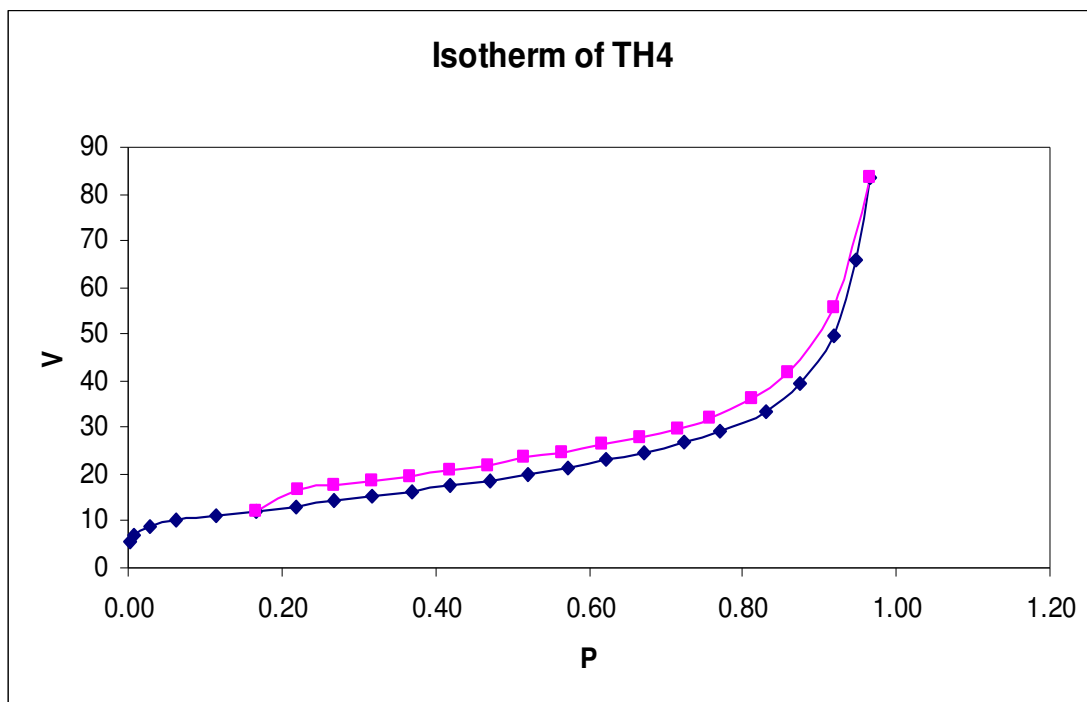


**Figure 4.11(a) continued:** BET isotherm curves of uncalcination samples of OCP.

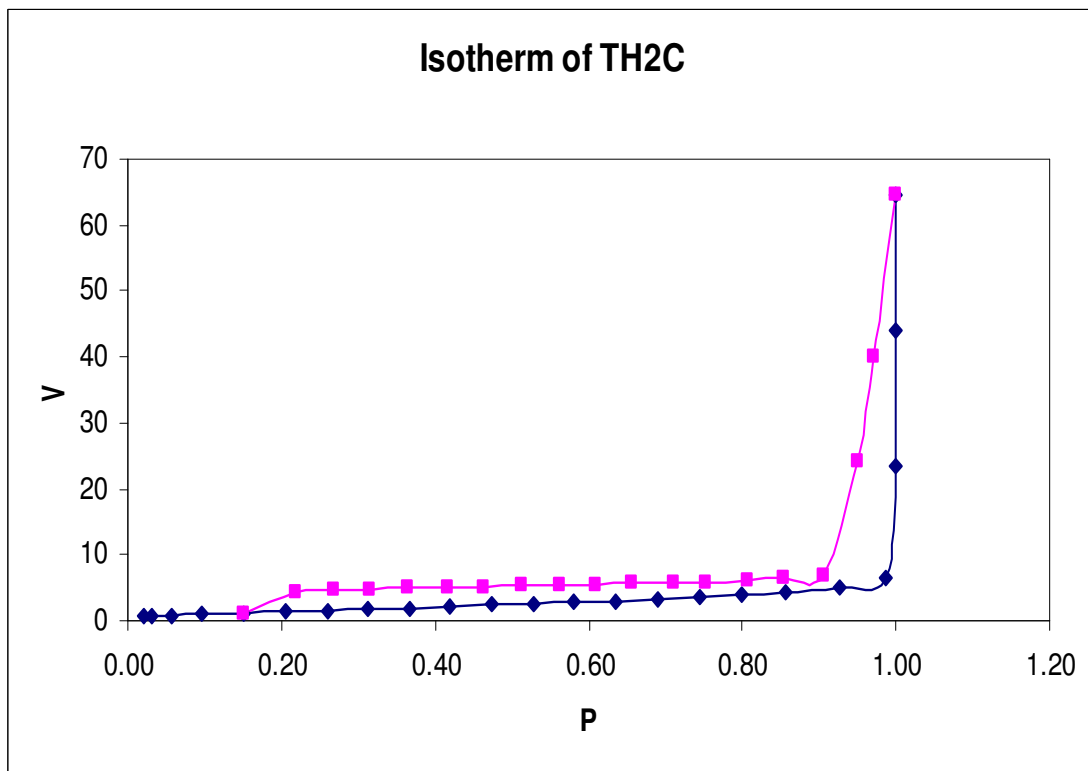
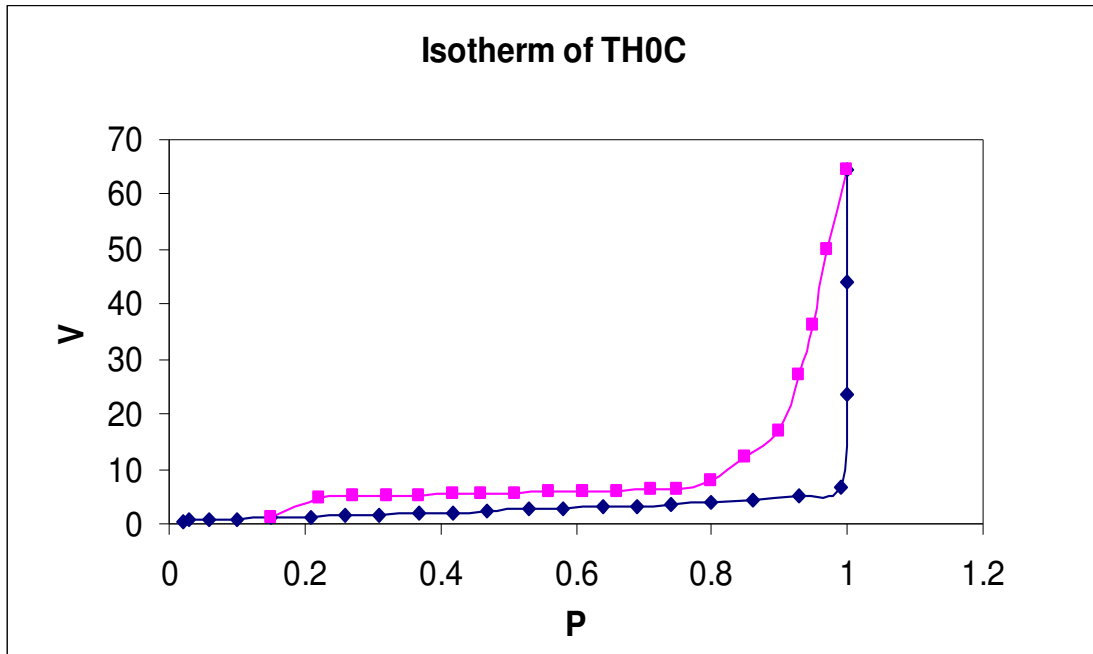


**Figure 4.11(b) :** BET isotherm curves of calcination samples of OCP.



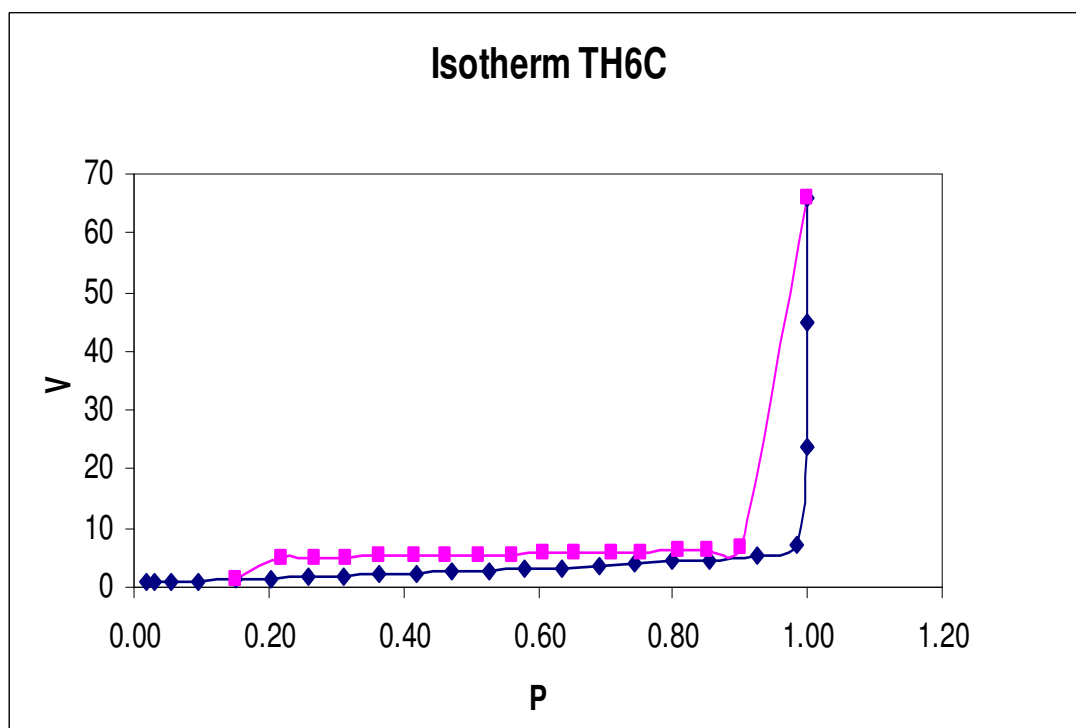
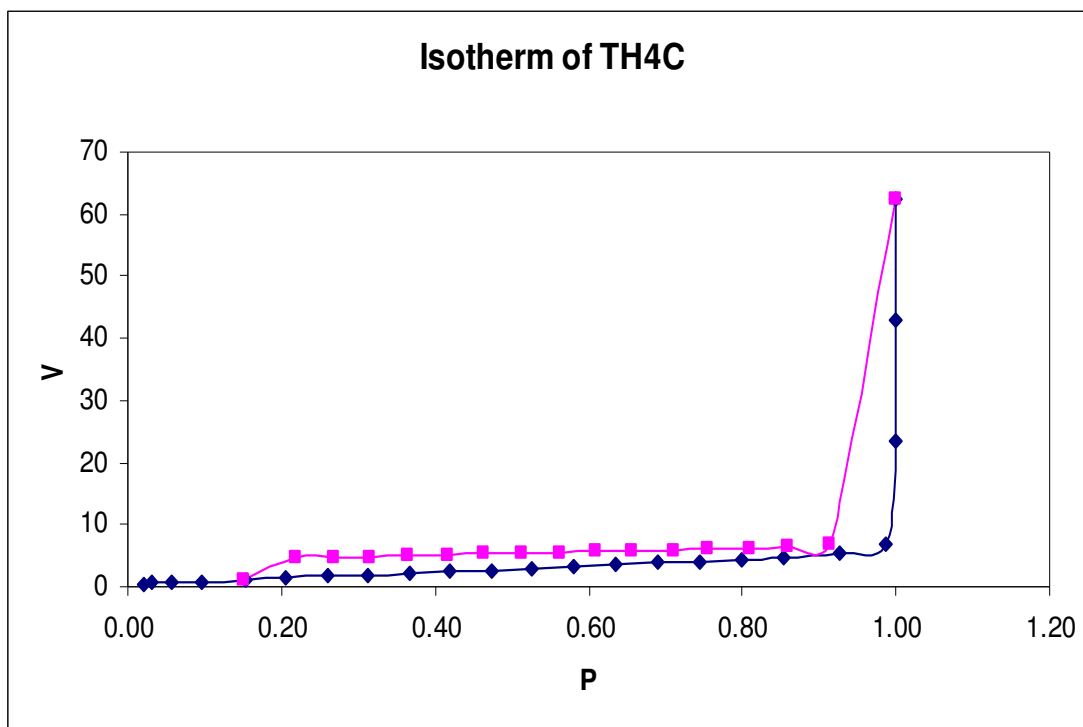


**Figure 4.11(b) continued:** BET isotherm curves of calcination samples of OCP

The initial part of the adsorption isotherm ( $P/P_0 < 0.2$ ) corresponded to monolayer and multilayer formation and followed the same path as that given by a

corresponding nonporous solid, which support the typical, type II isotherm (IUPAC) for samples TH0, TH2, TH4 and TH6. On reducing  $P/P_0$ , desorption occurs, resulting a hysteresis loops, which is occurred between 0.2-1.0 relative pressures, very close to type H3 (IUPAC).

Table 4.11 showed the specific surface area ( $ssa \text{ m}^2 \text{ g}^{-1}$ ) estimated according to the standard BET method and I-point method. Figure 4.11(c) showed the comparison between these two methods and it is observed that there is a very small difference between these two methods. It is observed from fig 4.11(a), that relative volume start between 0-10 and the specific surface are ( $ssa$ ) found from BET equation is between  $45\text{-}53 \text{ m}^2 \text{ g}^{-1}$  for uncalcination samples (TH0, TH2, TH4 and TH6) and  $5\text{-}6 \text{ m}^2 \text{ g}^{-1}$  for calcination samples (TH0C, TH2C, TH4C and TH6C), which indicates all the samples are nonporous.

**Table 4.11:** The specific surface area estimated from BET method and I-point method.

Sample code	$ssa \text{ (m}^2 \text{ g}^{-1}\text{)}$	
	BET method	I-Point method
TH0	45.32	44.45
TH2	53.12	52.09
TH4	46.38	45.38
TH6	48.83	47.18
TH0C	5.82	5.72
TH2C	5.76	5.49
TH4C	6.70	6.14
TH6C	6.66	6.19

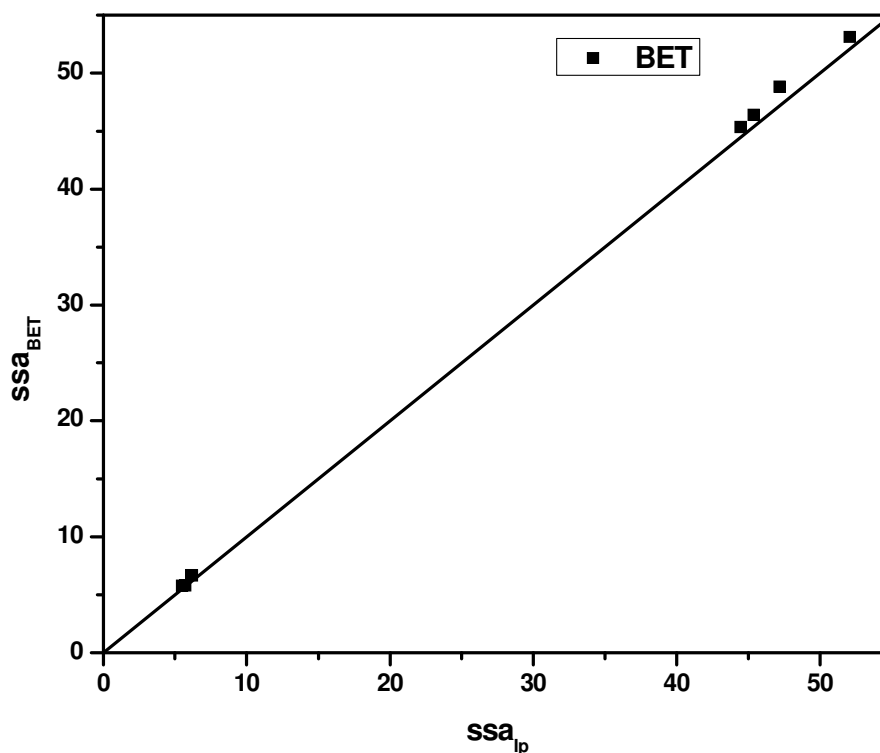


**Figure 4.11(c):** Comparison between the  $S_{BET}$  and  $S_I$  values.

#### 4.12. Determination of activation energy

In our present study, we also determine the activation energy,  $E$  and the pre-exponential factor. Activation energy may be defined, as the minimum energy required starting a chemical reaction. The Arrhenius equation gives the quantitative basis of the relationship between the activation energy and the rate at which a reaction proceeds. The study of reaction rate is termed as chemical kinetics. From the Arrhenius equation, the activation energy can be expressed as:

$$E_a = -RT \ln(K/A) \quad (16)$$

where  $A$  is the frequency factor for the reaction,  $R$  is the universal gas constant and  $T$  is the temperature (in Kelvin). While this equation suggests that the activation energy is dependent on temperature, in which the Arrhenius equation is valid this is cancelled by the temperature dependence of  $K$ . Thus,  $E_a$  can be

evaluated from the rate constant at any temperature (within the validity of the Arrhenius equation).

In our study we used Kissinger method [12], to determination of activation energy and pre-exponential factor, based on the following equation:

$$\ln (\beta / T_{\max }^2) = -E_a / R T_{\max } + \ln (A R / E_a) \quad (17)$$

where  $\beta$  is the heating rate ( $\text{K min}^{-1}$ ),  $T_{\max}$  is the maximum reaction rate temperature (K),  $E_a$  is the activation energy (kJ/mol),  $A$  is the pre-exponential factor ( $\text{min}^{-1}$ ) and  $R=8.314$  kJ/mol/K is the gas constant.

The plot of  $\ln (\beta / T_{\max }^2)$  against  $1000 / T_{\max}$  should be a straight line with a slope of  $-E_a / R$  and an intercept equal to  $\ln (A R / E_a)$ . The activation energy is calculated by multiply the slope with molar gas constant (8.314 kJ/mol/K).

Table 4.12 showed the activation energy  $E_a$  and pre-exponential factor  $A$  for different stages of DSC and DTG curves. Figure 4.12(a), 4.12(b), 4.12(c), 4.12(d) showed plot  $\beta / T_m^2$  vs  $1000 / T_m$  and figure 4.12(e), 4.12(f), 4.12(g), 4.12(h), 4.12(i), 4.12(j), 4.12(k), 4.12(l) showed DTG and DSC curves on different heating rate ( $\beta$  K/min) for the samples TH0, TH2, TH4 and TH6.

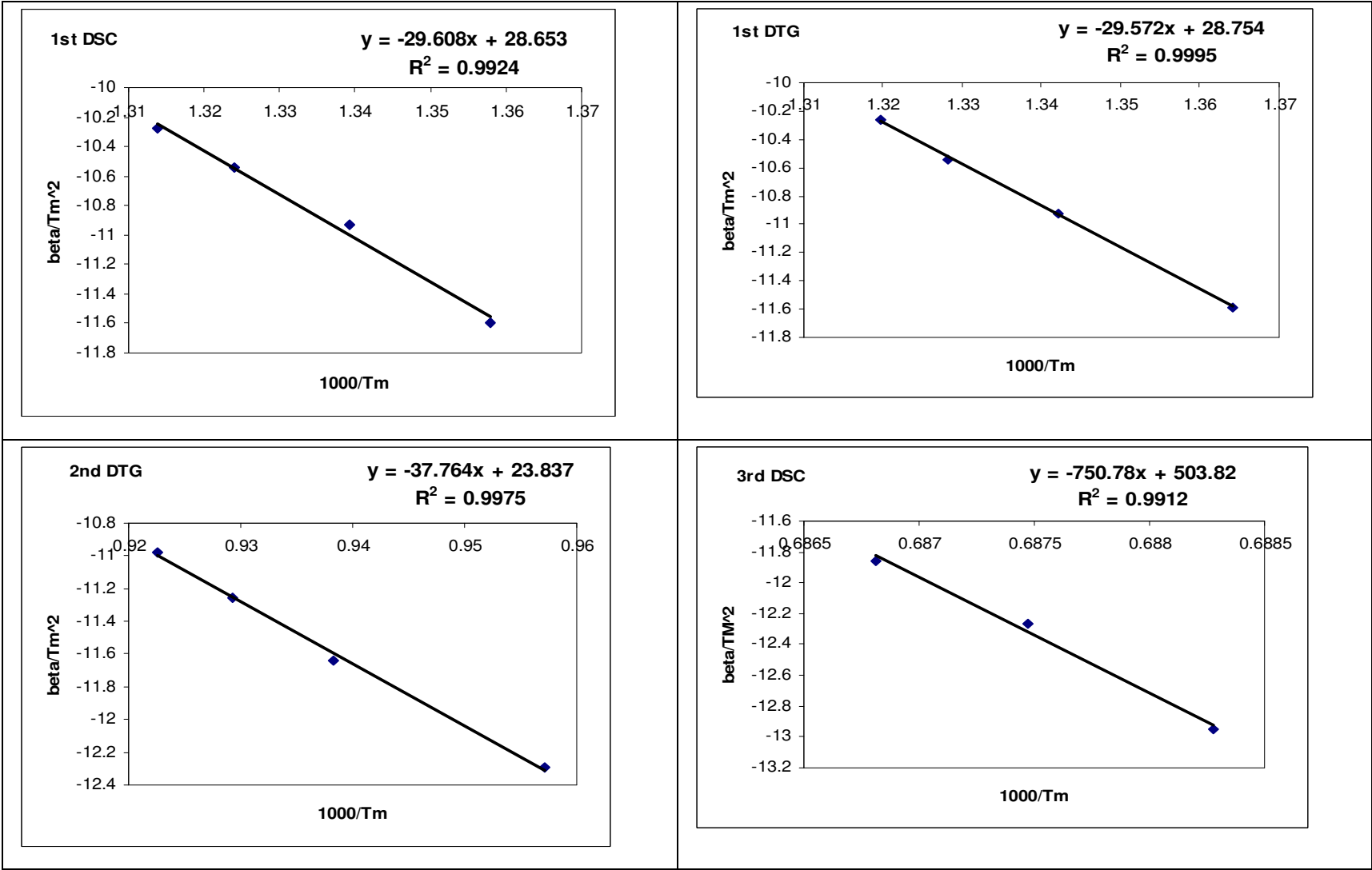


Figure 4.12(a): Plot  $\beta/T_m^2$  vs  $1000/T_m$  for sample TH0.

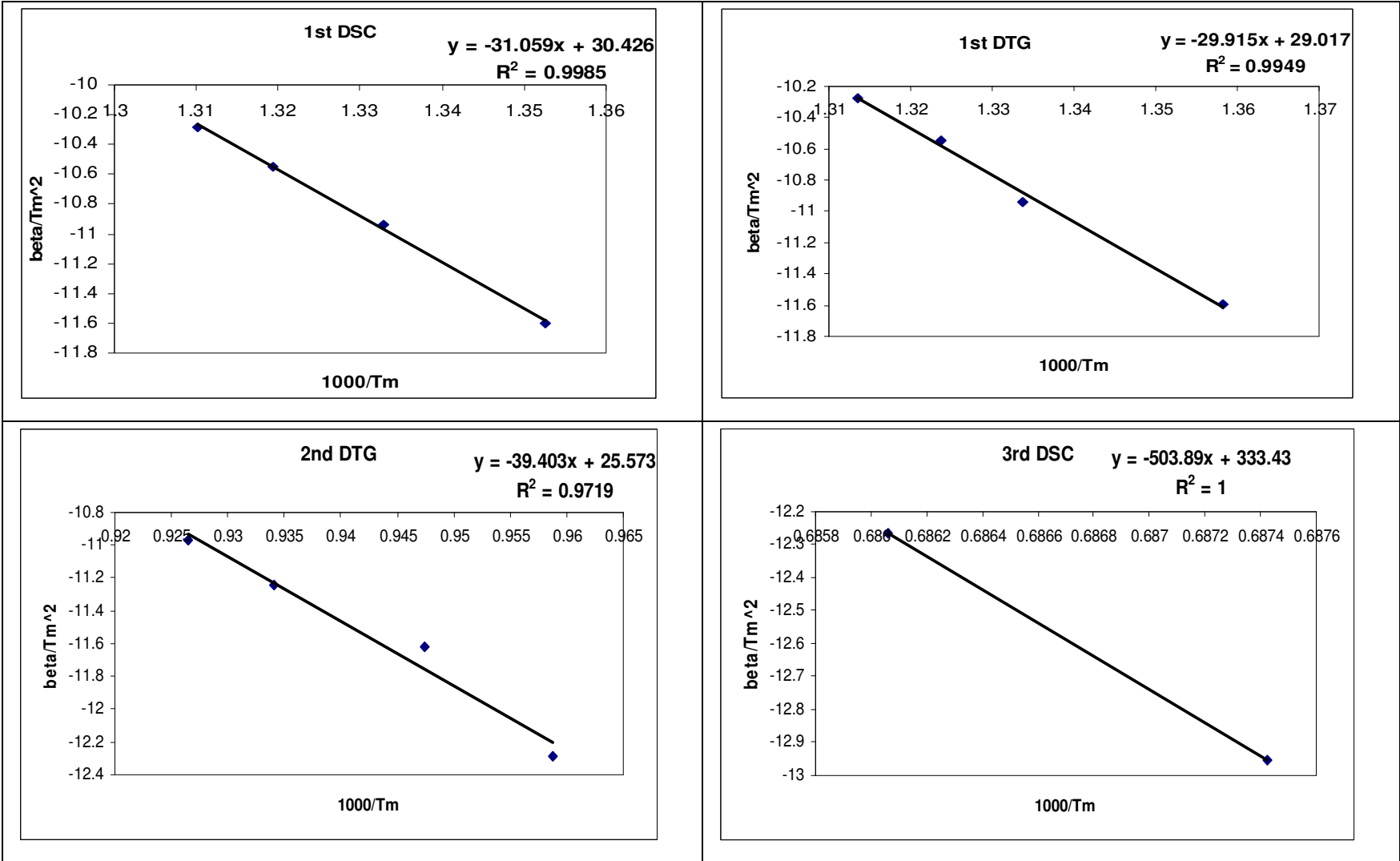


Figure 4.12(b): Plot  $\beta/T_m^2$  vs  $1000/T_m$  for sample TH2.

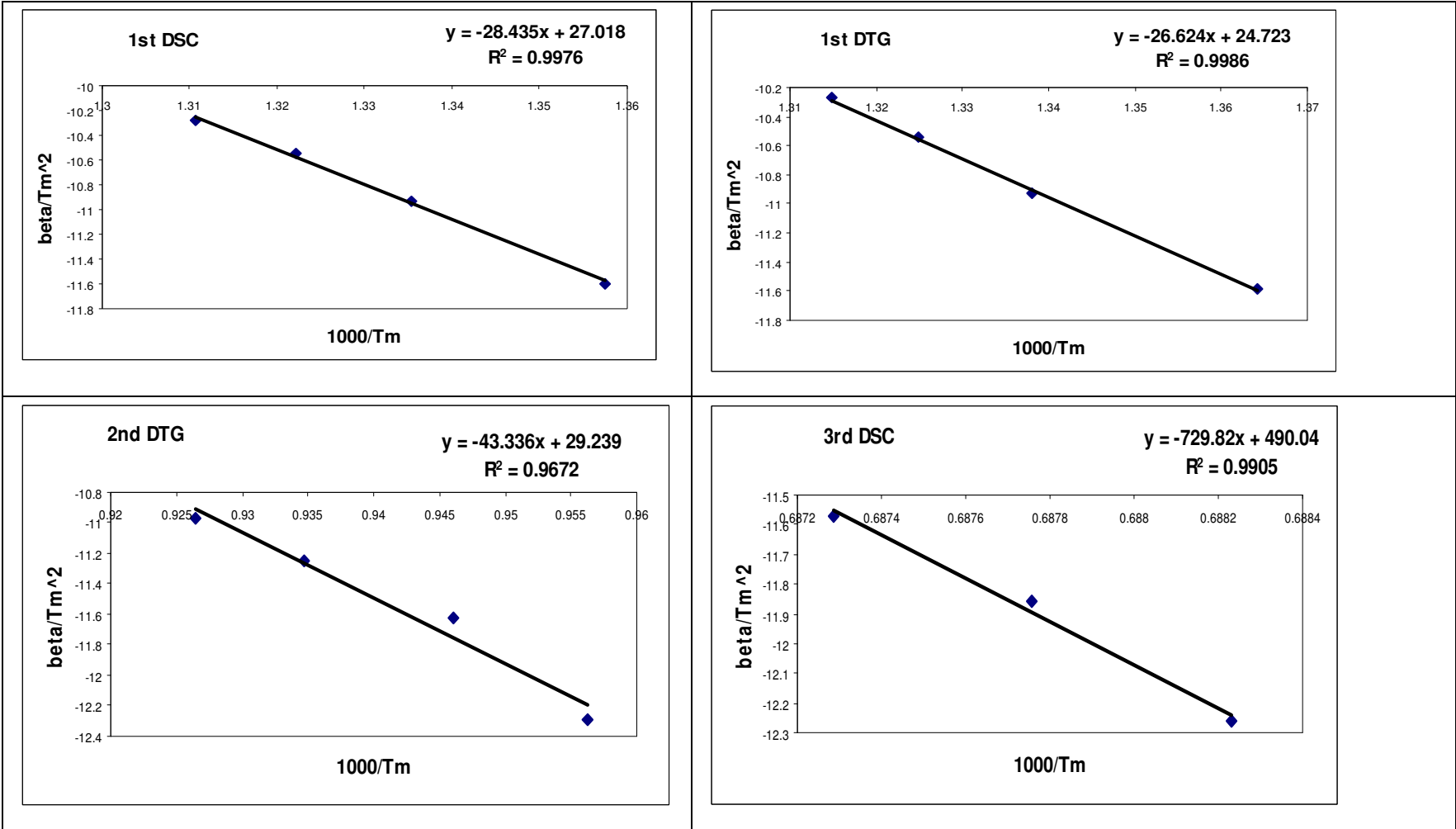


Figure 4.12(c): Plot  $\beta/T_m^2$  vs  $1000/T_m$  for sample TH4.

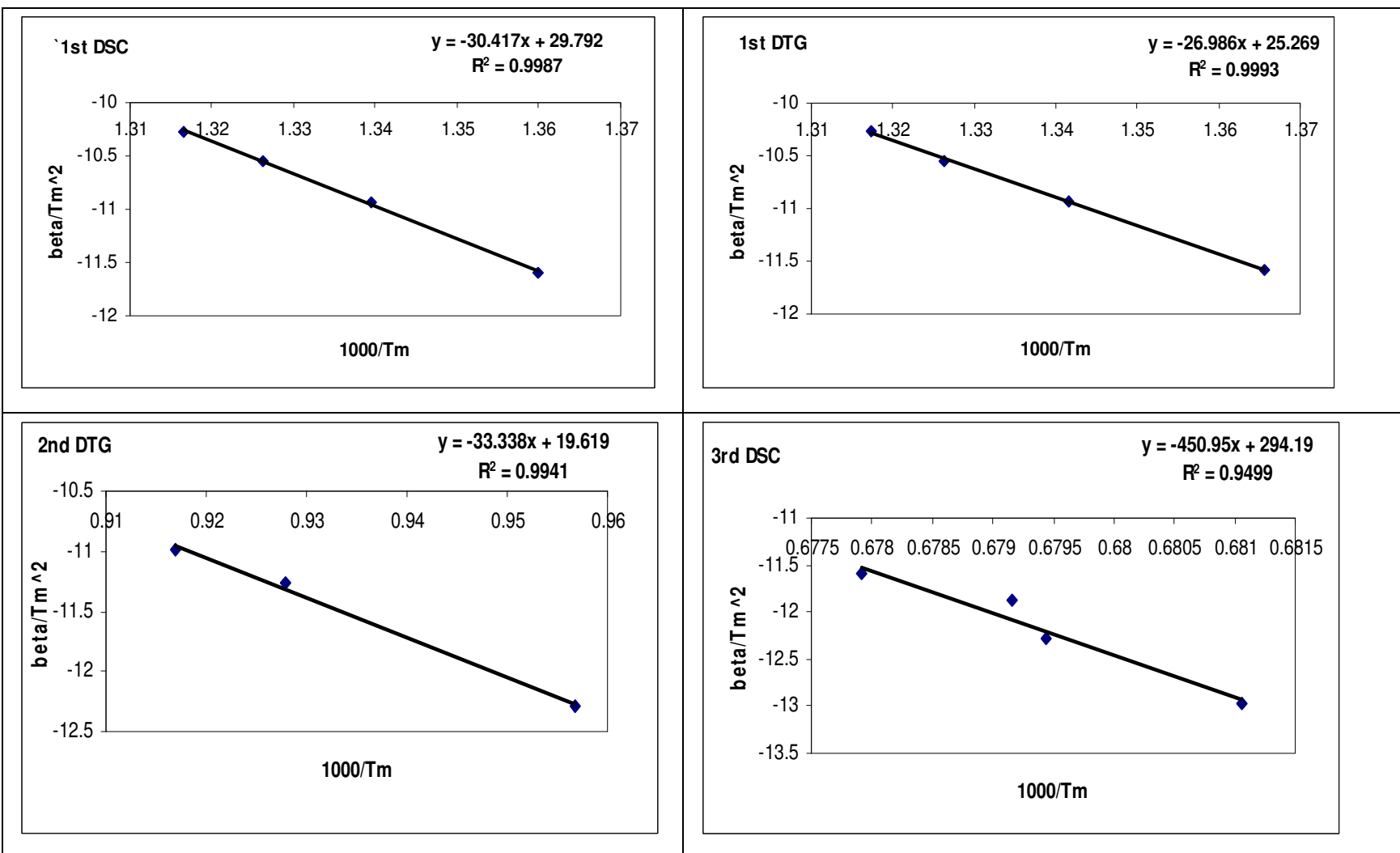


Figure 4.12(d): Plot  $\beta/T_m^2$  vs  $1000/T_m$  for sample TH6.



**Table 4.12:** The activation energy,  $E_a$  and the pre-exponential factor,  $A$  for different thermal decomposition steps, determined by Kissinger equation:

Sample code	Decomposition step						Transformation of $\beta$ -TCP $\rightarrow$ $\alpha$ -TCP	
	2 <sup>nd</sup> step				3 <sup>rd</sup> step			
	DSC		DTG		DTG		DSC	
	$E_a$ (kJ/mole)	$A$ (min <sup>-1</sup> )	$E_a$ (kJ/mole)	$A$ (min <sup>-1</sup> )	$E_a$ (kJ/mole)	$A$ (min <sup>-1</sup> )	$E_a$ (kJ/mole)	$A$ (min <sup>-1</sup> )
TH0	246	2.1 E+14	246	9.1 E+13	314	8.4 E+11	6242	4.8 E+221
TH2	258	5.1 E+14	249	1.2 E+14	328	5.0 E+12	4189	3.2 E+147
TH4	236	1.3 E+13	221	1.4 E+12	360	2.2 E+14	6068	4.8 E+215
TH6	253	2.6 E+14	224	2.5 E+12	277	1.1 E+10	3749	2.6 E+130

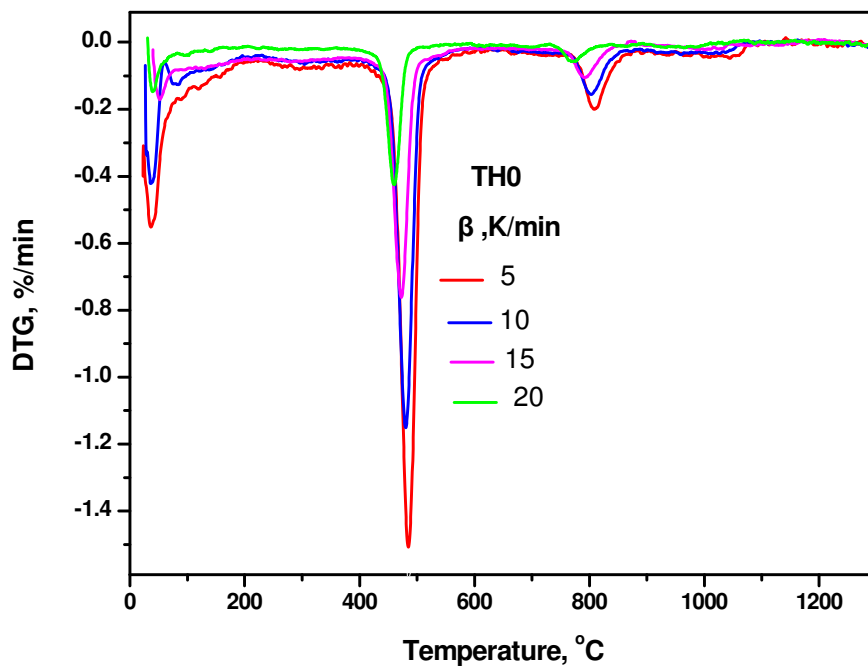


Figure 4.12(e): DTG curve of different heating rate for sample TH0.

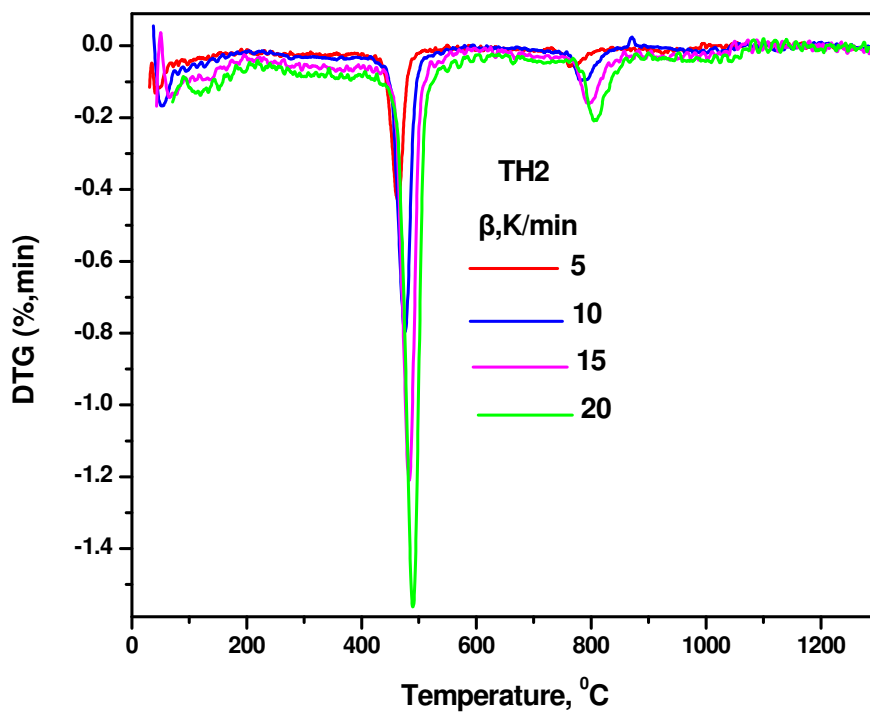


Figure 4.12(f): DTG curve of different heating rate for sample TH2.

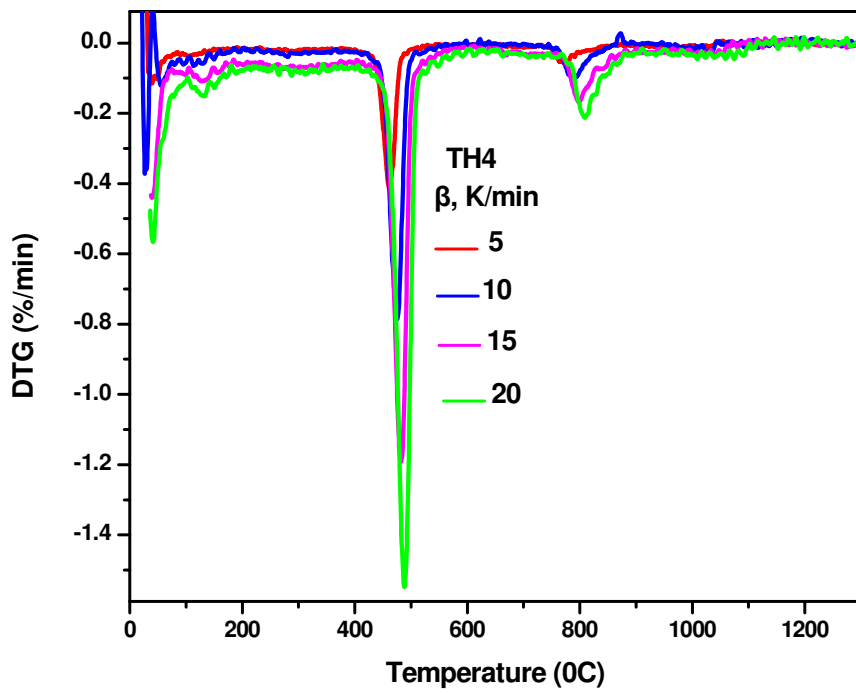


Figure 4.12(g): DTG curve of different heating rate for sample TH4.

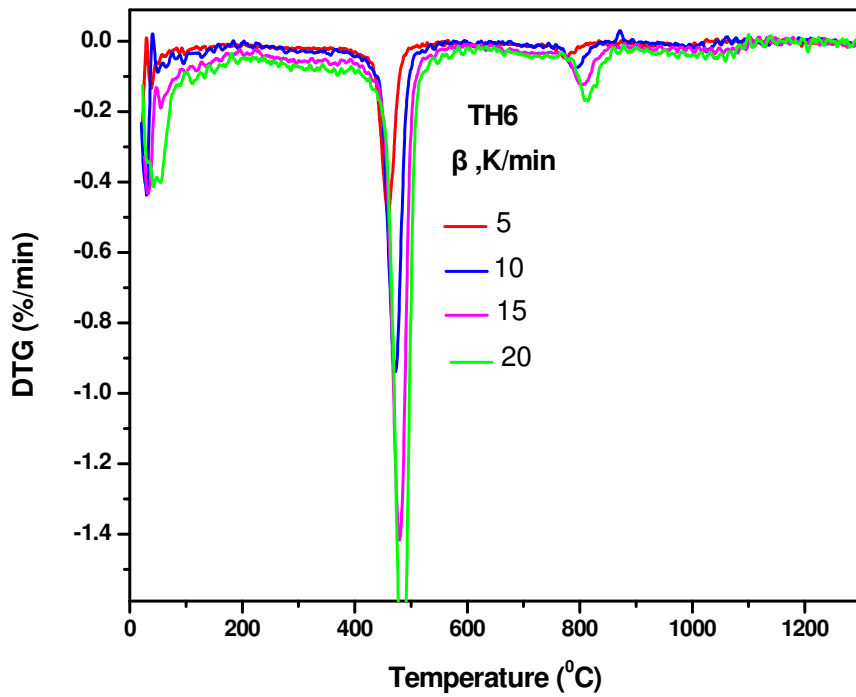


Figure 4.12(h): DTG curve of different heating rate for sample TH6.

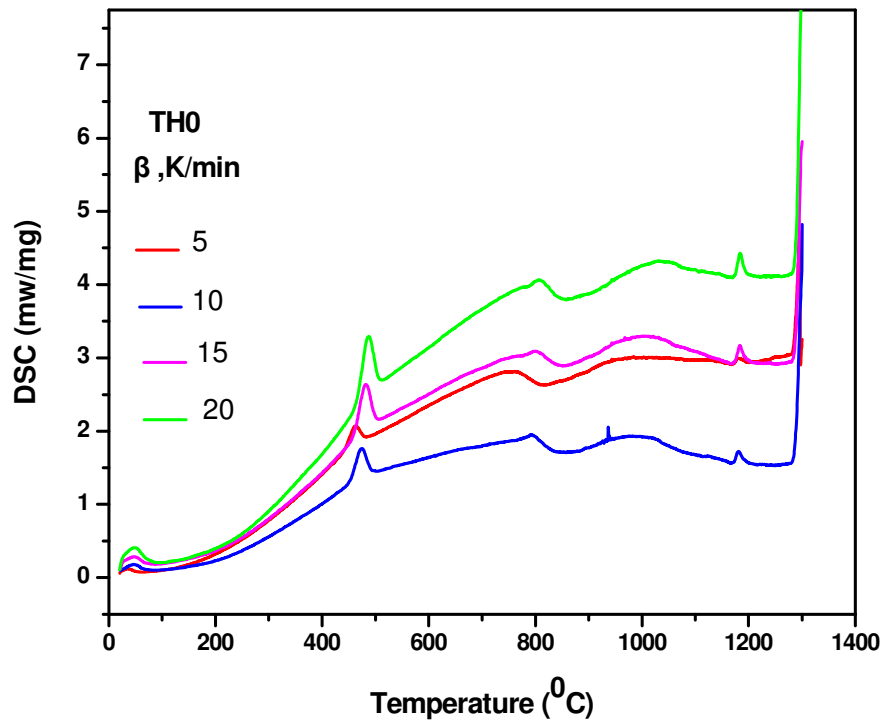


Figure 4.12(i): DSC curve of different heating rate for sample TH0.

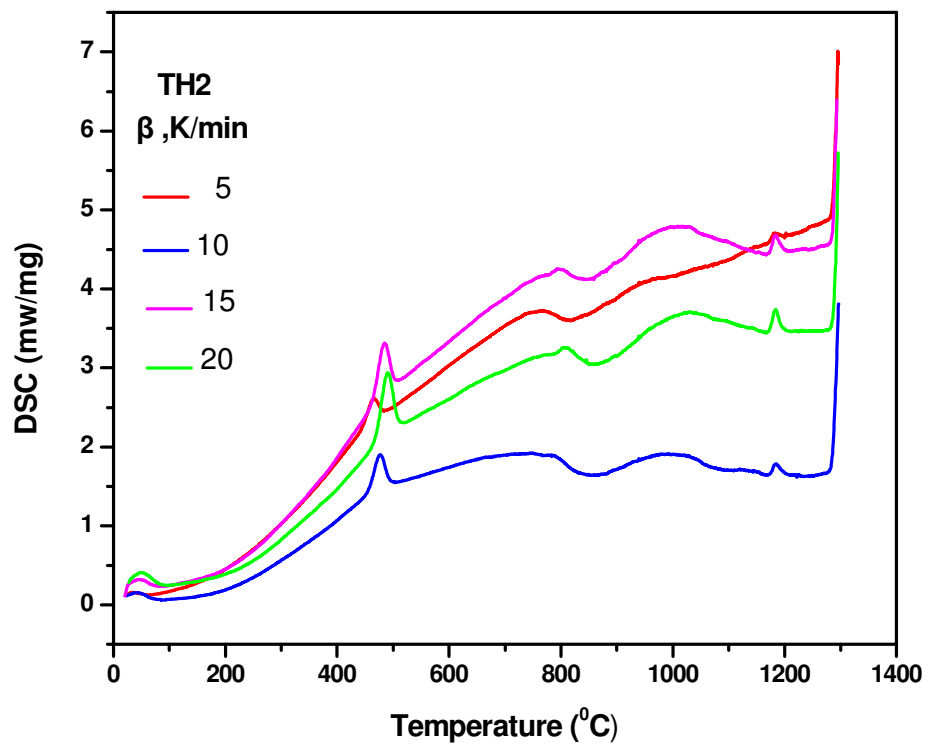


Figure 4.12(j): DSC curve of different heating rate for sample TH2.

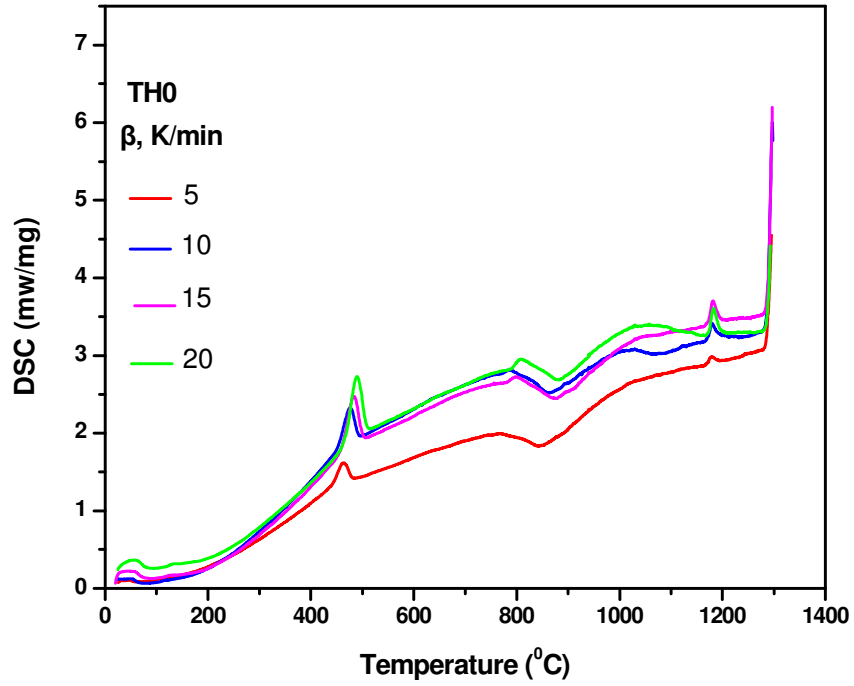


Figure 4.12(k): DSC curve of different heating rate for sample TH4

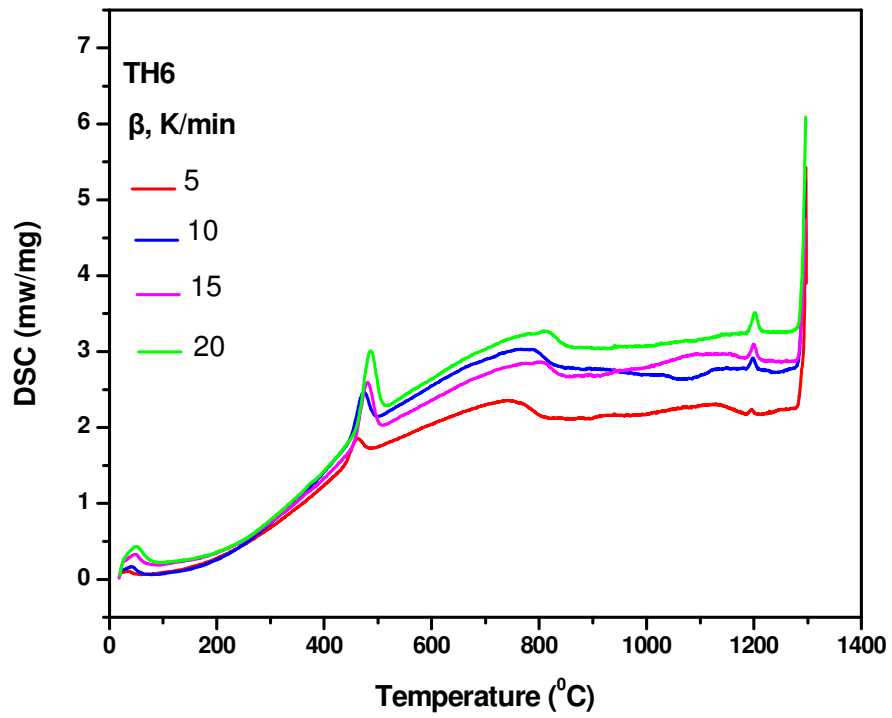


Figure 4.12(l): DSC curve of different heating rate for sample TH6.

#### 4.13. Compensation effect and isokinetic temperature:

Several terms have been employed essentially interchangeably to describe sympathetic relationships between the apparent activation energies and the preexponential factors for a series of processes, which is well known as compensation effect. Numerous series of catalytic studies have inferred that there is a compensation effect and have estimated a specific isokinetic temperature for individual series. Many theoretical analyses have offered explanations for this phenomena, although, the majority have focused on interpreting any isokinetic temperature that is evident or determining if compensation exists. However, there is no commonly accepted explanation for kinetic compensation. Many analyses suggest that there are several actual forms of kinetic compensation that may be evident in process depending on the nature of the series that are being compared. The compensation effect occurred in a group of related reactions for which the influence of changes in preexponential factor, A, on reaction rate is offset to a greater or lesser extent by a sympathetic variation in activation energy,  $E_a$ , often expressed as:

$$\log A = B + eE_a \quad (18)$$

Where B and e are constants. This effect has been observed in both heterogeneous and homogeneous rate processes.

As shown in figure 4.13(a), the activation parameters of the thermal degradation exhibit a compensation effect measured by second DSC, DTG and 3<sup>rd</sup> DTG steps. In the second DSC step  $\gamma$ - $\text{Ca}_2\text{P}_2\text{O}_7$  decomposed to  $\beta$ - $\text{Ca}_2\text{P}_2\text{O}_7$ . Second DTG step acid phosphate decompose to pyrophosphate and in the 3<sup>rd</sup> DTG step pyrophosphate decompose to hydroxyapatite, which is further react with calcium pyrophosphate to form  $\beta$ -TCP.

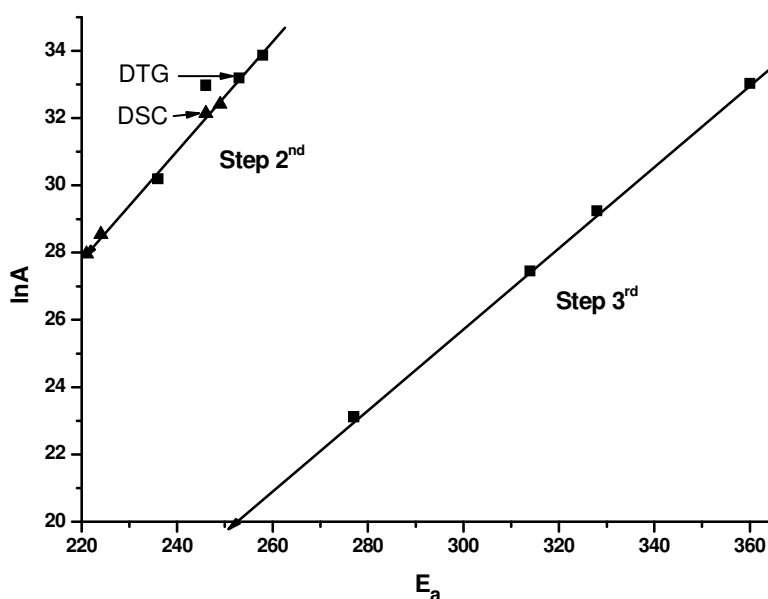


**Figure 4.13(a):** The compensation effect.

The isokinetic temperature is the temperature at which the rate coefficients for all the compounds are the same and hence the point through which all the Arrhenius plots must pass. It should be noted that this isokinetic plot is not a result of accidental compensation of errors, for if the given rate coefficients are modified such that all of the Arrhenius lines pass through a point, a perfect isokinetic relationship is obtained. The rate vs temperature curves for all the reactions pass through this single point. Comparisons are affected since the isokinetic temperature is a point of inversion of relative reactivity in the series. It is also a point of change in control of reaction rate by the energy of activation below it to control by the entropy of activation above it. The effect of changes in structure, solvent, e.t.c., will depend on the relation of the experimental temperature to the isokinetic temperature. The best mathematical explanation for the dependence of the rate constant on temperature is given by the Arrhenius equation:

$$K = A \exp(-E_a/RT) \quad (19)$$

Where  $E_a$  is the activation energy,  $A$  is the pre-exponential factor and  $T$  is the temperature. From equation(19),

$$\ln K = \ln A - E/RT \quad (20)$$

$$\ln A = \ln K + E/RT \quad (21)$$

Comparing equations (19) and (21),

$$B = \ln K_i$$

or,  $K_i = \exp(B)$

And,  $e = 1/RT_i$

or,  $T_i = 1/eR$

where  $K_i$  is the compensation constant and  $T_i$  is the isokinetic temperature.

**Table 4.13:** Values of parameters  $K_i$  and  $T_i$  determined from Arrhenius equation for different stages of DSC and DTG curves.

	e	B	$K_i$	$T_i$
2DSC	0.1604	-7.2597	0.0007033	477
2DTG	0.1607	-7.4849	0.0005615	475
3DTG	0.1195	-10.008	4.504E-05	734
4DSC	0.0841	-13.797	1.019E-06	1157

Table 4.13 showed the values of  $K_i$  and  $T_i$  determined from Arrhenius equation for different steps of DSC and DTG curves. Figure 4.13(b), 4.13(c) and 4.13(d) showed the linear plot of  $\ln A$  vs  $E$  for different stages of DSC and DTG.

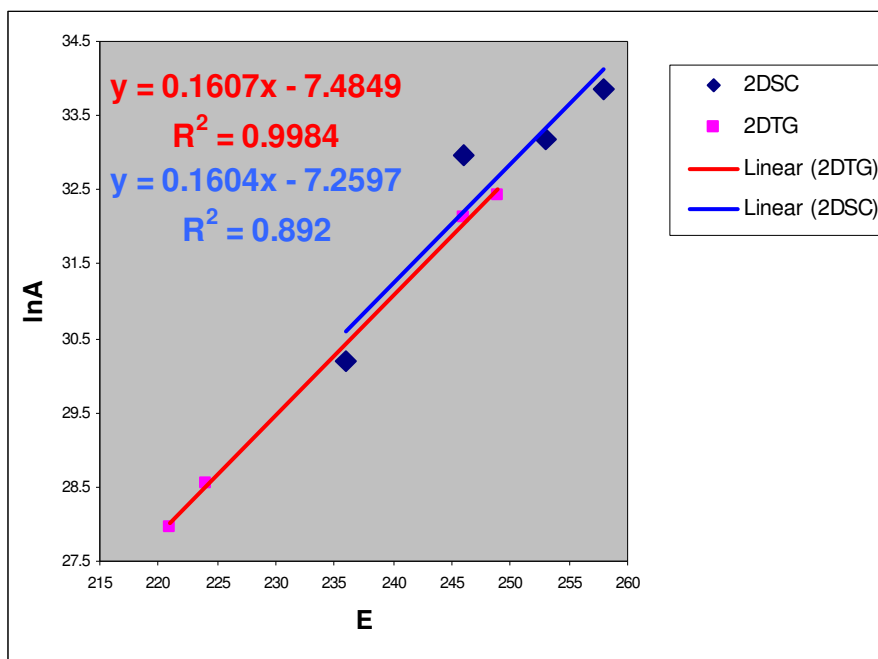


**Figure 4.13(b):** Plot  $\ln A$  vs  $E$  for 2<sup>nd</sup> DSC and 2<sup>nd</sup> DTG



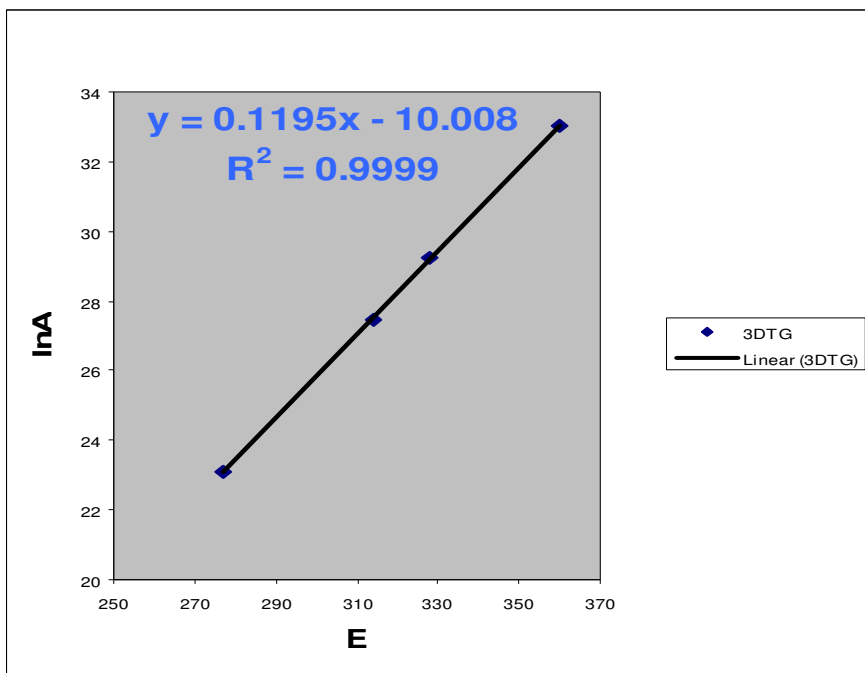


Figure 4.13(c): Plot  $\ln A$  vs  $E$  for 3<sup>rd</sup> DTG

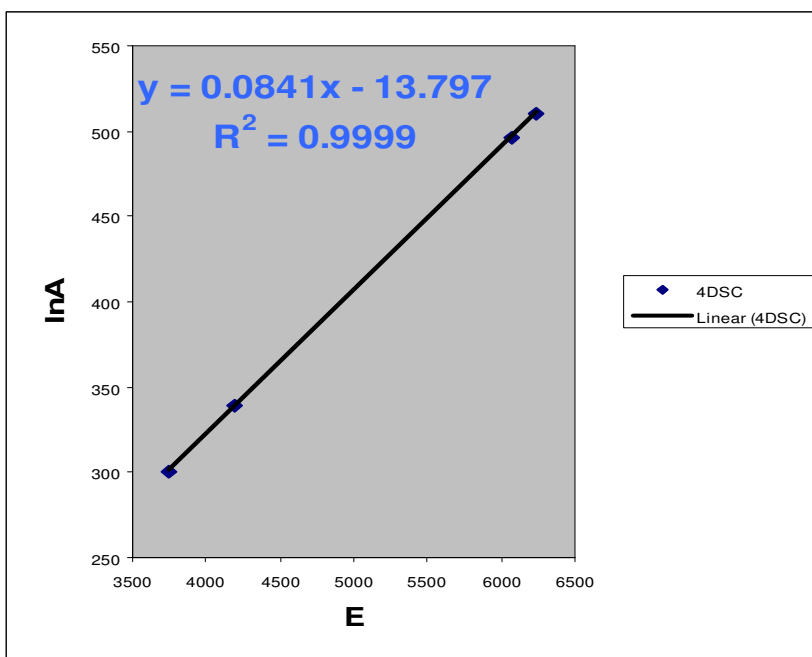


Figure 4.13(d): Plot  $\ln A$  vs  $E$  for 4<sup>th</sup> DSC

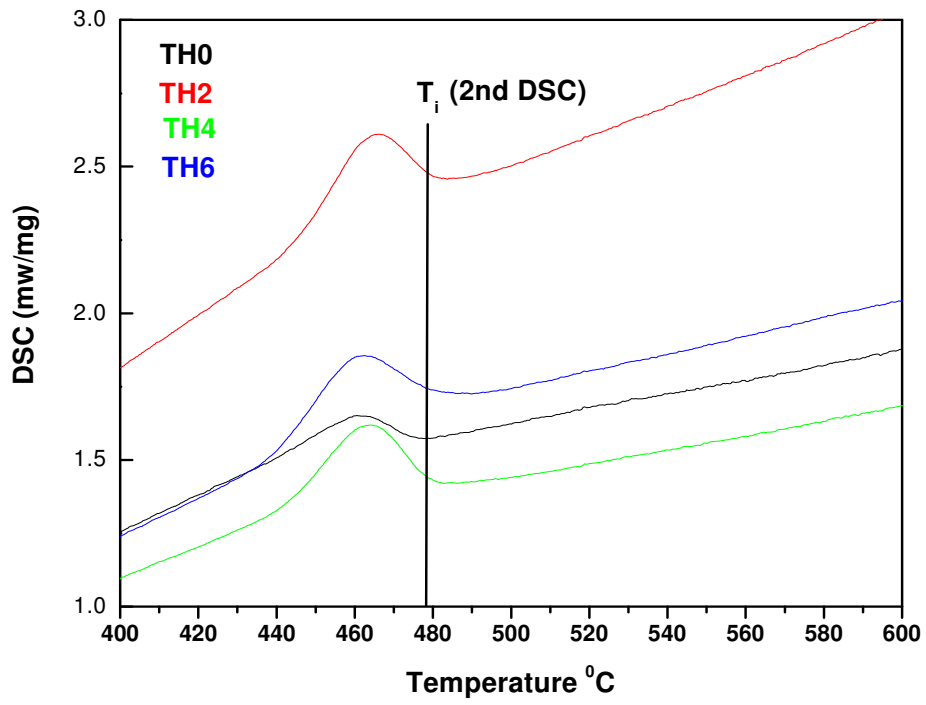


Figure: 4.13(e):  $T_i$  for 2<sup>nd</sup> DSC curve

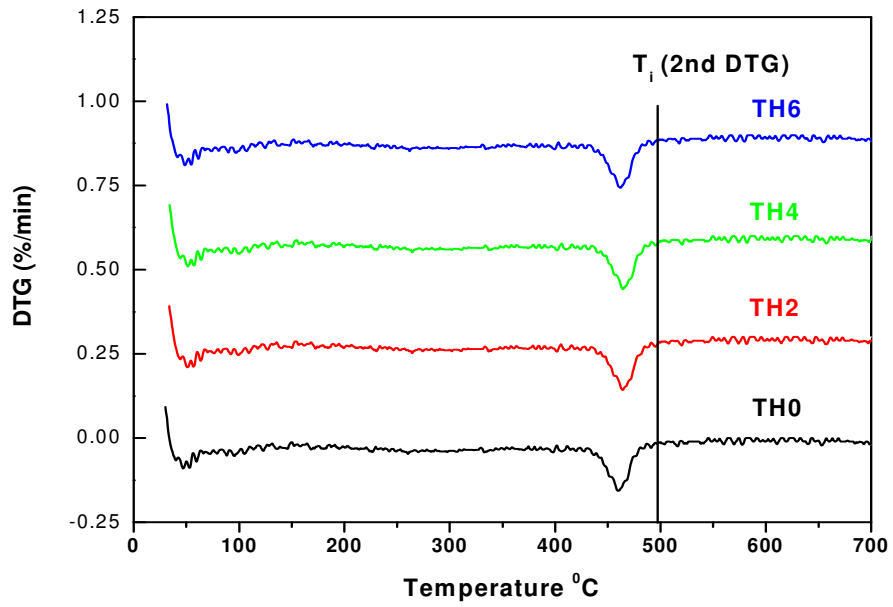


Figure: 4.13(f):  $T_i$  for 2<sup>nd</sup> DTG curve

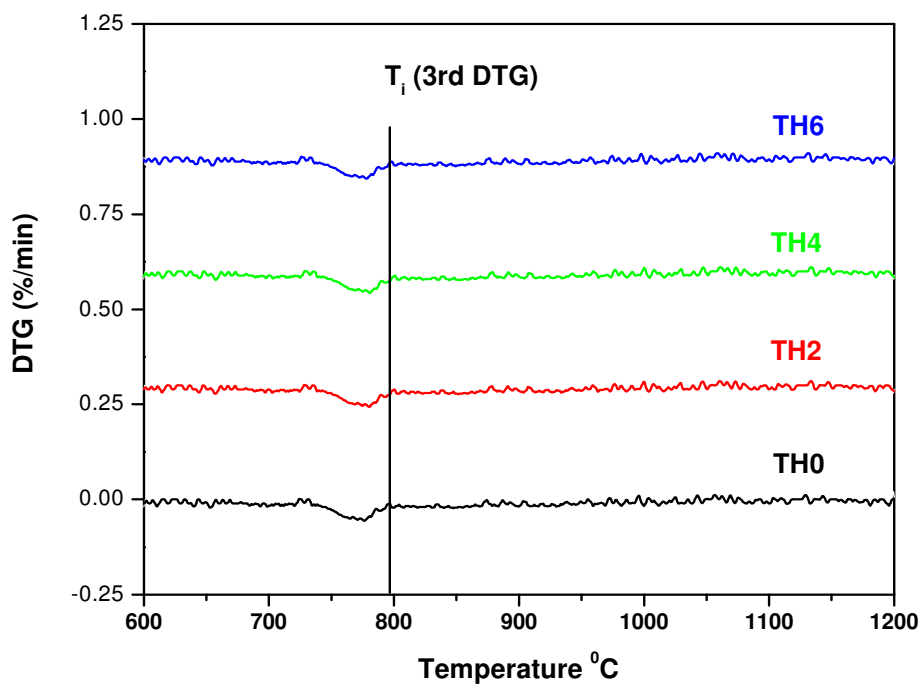


Figure: 4.13(g): Ti for 3<sup>rd</sup> DTG curve

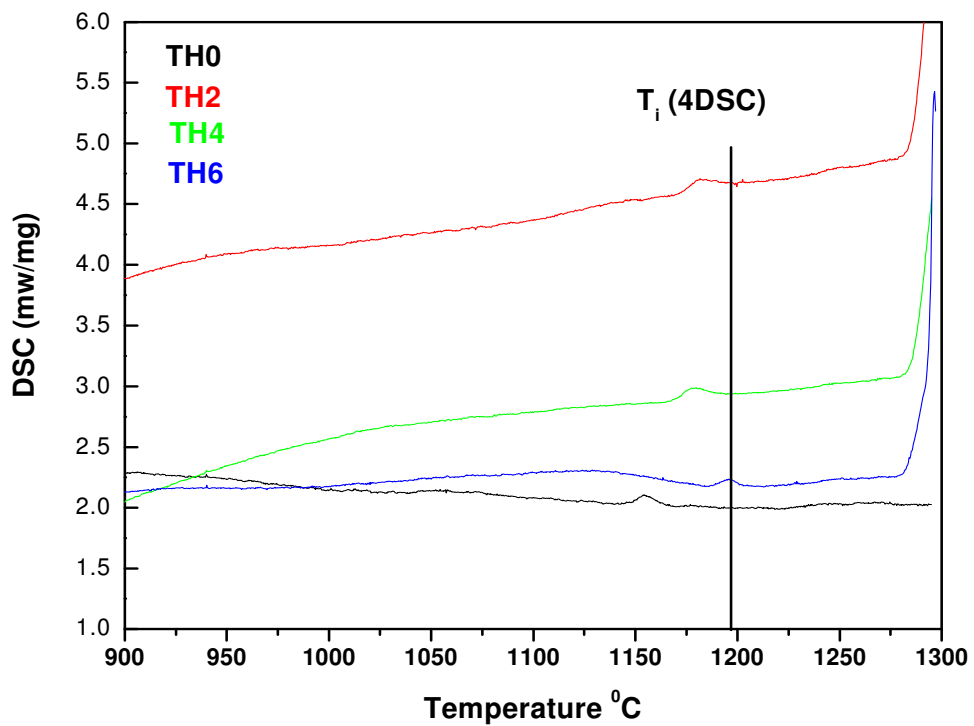


Figure: 4.13(h): Ti for 4<sup>th</sup> DSC curve

Figure 4.13(e), 4.13(f), 4.13(g) and 4.13(h) showed the isokinetic temperature (Ti) for different stages of DSC and DTG curves. All these values of Ti with in the range of thermal analysis result, which is 400-500 °C for 2<sup>nd</sup> DSC and measured Ti is 477 °C, for 2<sup>nd</sup> DTG, it is 400-500 °C and Ti for 2<sup>nd</sup> DTG 475 °C, for 3<sup>rd</sup> DTG, it is 700-800 °C and Ti for 3<sup>rd</sup> DTG 734 °C, for 4<sup>th</sup> DSC, it is 1100-1200 °C and Ti for 4<sup>th</sup> DSC 1157 °C.

#### 4.14. Conclusion:

We have successfully produced hydroxyapatite and octacalcium phosphate by using pH shock –wave method with high-speed dispersing equipment and the following observations are made:

- 1) From XRD pattern for the samples of Ca/P atomic ratio of 1.67, single phase of hydroxyapatite was detected. The calculated lattice parameters were  $a = 9.427 \text{ \AA}$ , and  $c = 6.930 \text{ \AA}$  (hexagonal  $P6_3/m$ ), while for the uncalcination samples of Ca/P atomic ratio 1.33, three phases of OCP, monetite and HA were detected and the lattice parameters were  $a = 10.733 \text{ \AA}$ ,  $b = 13.753 \text{ \AA}$  and  $c = 5.832 \text{ \AA}$  (orthorhombic  $Pna21$ ). For the calcination samples of the same ratio of Ca/P two phases of  $\beta$ -TCP and  $\beta$ - $\text{Ca}_2\text{P}_2\text{O}_7$  were detected and the lattice parameters were  $a = 8.174 \text{ \AA}$ ,  $b = 3.348 \text{ \AA}$  and  $c = 11.394 \text{ \AA}$ . The system is monoclinic with the space group  $P2_1/C$ .
- 2) FT-IR showed all the characteristics peaks for HA, OCP and  $\beta$ -TCP.
- 3) SEM analysis showed the different morphology of particles. For HA, it was spherical in shape and highly agglomerated. For uncalcination samples of OCP the particle shape was un-uniform and after used different concentration of threonine the shape changed to needle-like, spheroidal and big aggregate of round spherical. The calcination samples of OCP showed the botryoidal shape of particles.
- 4) The thermal analysis of OCP samples were studied between temperatures 0 and 1400 °C. The transformation takes place through four consecutive steps. At higher temperature, about 900 °C,  $\beta$ -TCP formed together with  $\beta$ - $\text{Ca}_2\text{P}_2\text{O}_7$ . At the end of the thermal experiment, we observed partial sintering of materials due to melting of pyrophosphate.
- 5) The  $\text{N}_2$  adsorption-desorption isotherms for the samples were measured by using BET equation and the observed specific surface areas (ssa) were 45-53  $\text{m}^2/\text{g}$  for uncalcination samples and 5-6  $\text{m}^2/\text{g}$  for calcination samples.

## References:

- [1] Neumann, M. "X-Cell - A Novel Indexing Algorithm for Routine Tasks and Difficult Cases", *J. Appl. Crystallogr.*, 36, 356-365 (2003).
- [2] George C. Koumoulidis, Tiberius C. Vaimakis and Antonios T. Sdoukos. Preparation of hydroxyapatite lath-like particles using high-speed dispersing equipment. *J. Am. Ceram. Soc.*, 84 [6] 1203-208 (2001).
- [3] W.L. Bragg, "The Diffraction of Short Electromagnetic Waves by a Crystal", *Proceedings of the Cambridge Philosophical Society*, 17, 43-57 (1913).
- [4] Dekker RJ, de Bruijn JD, Stigter M, Barrere F, Layrolle P, van Blitterswijk CA. Bone tissue engineering on amorphous carbonated apatite and crystalline octacalcium phosphate-coated titanium discs. *Biomaterials*;26:5231-5239 (2005).
- [5] Fowler BO, Markovic M, Brown WE. Octacalcium phosphate iii. Infrared and Raman vibrational spectra. *Chem Mater* 1993;5:1417-1423.
- [6] Hui Wang, Chang-Jian Lin, Ren Hu, Fan Zhang, Li-Wen Lin. A novel nano-micro structured octacalcium phosphate/protein composite coating on titanium by using an electrochemically induced deposition. Wiley Interscience 2007. DOI:10.1002/jbm.a.31653.
- [7] Yun Zhang, Guangfu Yin, Shifu Zhu, Dali Zhou, Yuehau Wang, Yong Li and Lin Luo, Preparation of  $\beta$ -Ca<sub>3</sub>(PO<sub>4</sub>)<sub>2</sub> bioceramic powder from calcium carbonate and phosphoric acid, *Current Applied Physics*, Vol 5 (2005), page 531-534.
- [8] G.C Koumoulidis, C.C. Trapalis and T.C. Vaimakis. Sintering of hydroxyapatite lath-like powders. *Journal of thermal analysis and calorimetry*, Vol. 84(2006) 1, 165-174.
- [9] S. Brunauer, H.P. Emmett, E. Teller, *J. Am. Chem. Soc.* 60 (1938) 309.
- [10] P.J. Pomonis, D.E. Petrakis, A.K. Ladavos, K.M. Kolonia, C.C. Pantazis, A.E. Giannakas, A. A. Leontiou. The I-point method for estimating the surface area of solid catalysts and the variation of C-term of the BET equation. *Catalysis Communications* 6 (2005) 93-96.
- [11] G. S. Armatas, D. E. Petrakis, P. J. Pomonis. A method of distinction between microporosity and mesoporosity using BET-Scatchard plots. *Microporous and Mesoporous Materials* 83 (2005) 151-161.
- [12] H. E. Kissinger, *J. Res. Nat. Bur. Std.*, 57 (1956) 217.

- [13] Hans E. Lundager Madsen, Influence of foreign metal ions on crystal growth and morphology of brushite ( $\text{CaHPO}_4 \cdot 2\text{H}_2\text{O}$ ) and its transformation to octacalcium phosphate and apatite, *Journal of Crystal Growth* 310 (2008) 2602–2612.
- [14] H.E. Lundager Madsen, *Acta Chem. Scand.* 24 (1970) 1677.
- [15] H.E. Lundager Madsen, *Acta Chem. Scand. A* 37 (1983) 25.
- [16] H.E. Lundager Madsen, *Acta Chem. Scand. A* 37 (1983) 25.
- [17] Xiong Lu, Zhanfeng Zhao, Yang Leng, Biomimetic calcium phosphate coatings on nitric-acid-treated titanium surfaces, *Materials Science and Engineering C* 27 (2007) 700–708.
- [18] Xiong Lu , Yang Leng , Qiyi Zhang, Electrochemical deposition of octacalcium phosphate micro-fiber/chitosan composite coatings on titanium substrates, *Surface & Coatings Technology* 202 (2008) 3142–3147.
- [19] S. Kamakura, Y. Sasano, T. Shimizu, K. Hatori, O. Suzuki, M. Kagayama, K. Motegi, *J. Biomed. Mater. Res.* 59 (2002) 29.
- [20] P. Habibovic, C.M. van der Valk, C.A. van Blitterswijk, K. de Groot, G. Meijer, *J. Mater. Sci. Mater. Med.* 15 (2004) 373.
- [21] Yang Liu, Paul R. Cooper, Jake E. Barralet, Richard M. Shelton, Influence of calcium phosphate crystal assemblies on the proliferation and osteogenic gene expression of rat bone marrow stromal cells, *Biomaterials* 28 (2007) 1393–1403.
- [22] Osamu Suzuki, Shinji Kamakura, Takenobu Katagiri, Masanori Nakamura, Baohong Zhao, Yoshitomo Honda, Ryutaro Kamijo, Bone formation enhanced by implanted octacalcium phosphate involving conversion into Ca-deficient hydroxyapatite, *Biomaterials* 27 (2006) 2671–2681.
- [23] Suzuki O, Kamakura S, Katagiri T. Surface chemistry and biological responses to synthetic octacalcium phosphate. *J Biomed Mater Res B Appl Biomater* 2005; DOI:10.1002/jbm.b.30407.
- [24] Suzuki O, Nakamura M, Miyasaka Y, Kagayama M, Sakurai M. Bone formation on synthetic precursors of hydroxyapatite. *Tohoku J Exp Med* 1991;164:37–50.
- [25] Kamakura S, Sasano Y, Shimizu T, Hatori K, Suzuki O, Kagayama M, Motegi K. Implanted octacalcium phosphate is more resorbable than beta-tricalcium phosphate and hydroxyapatite. *J Biomed Mater Res* 2002;59:29–34.

- [26] Chickerur NS, Tung MS, Brown WE. A mechanism for incorporation of carbonate into apatite. *Calcif Tissue Int* 1980;32:55–62.
- [27] Suzuki O, Nakamura M, Miyasaka Y, Kagayama M, Sakurai M. Maclura pomifera agglutinin-binding glycoconjugates on converted apatite from synthetic octacalcium phosphate implanted into subperiosteal region of mouse calvaria. *Bone Miner* 1993;20:151–66.
- [28] Suzuki O, Yagishita H, Yamazaki M, Aoba T. Adsorption of bovine serum albumin onto octacalcium phosphate and its hydrolyzates. *Cells Mater* 1995;5:45–54.
- [29] [13] Q.Y. Zhang, Y. Leng, *Biomaterials* 26 (2005) 3853.
- [30] [14] J. Wang, P. Layrolle, M. Stigter, K. de Groot, *Biomaterials* 25 (2004) 583.
- [32] Lj. Brecevic, V. Hlady, H. Furedi-Milhofer, *Colloid. Surf.* 28 (1987) 301.
- [33] S. H. Kwon, Y. K. Jun, S. H. Hong, H. Ee Kim, *Journal of European Ceramic Society.* 23, 1039 (2003).
- [34] R.Z. LeGeros, J.P. LeGeros, Dense hydroxyapatite, in L.L. Hench, J. Wilson, Editors, *An introduction to bioceramics*, World Scientific, Singapore, 1993, pp 144.
- [35] S. Hartshorne, D.M. Greenberg, *Arch. Biochem. Biophys.* 105, 173 (1964).
- [36] M.I. Bird, P.B. Nunn. *Biochem. J.* 214, 687 (1983)

## **5. Adsorption theory:**

Adsorption is a process that occurs when a gas or liquid solute accumulates on the surface of a solid or a liquid (adsorbent), forming a film of molecules or atoms (the adsorbate). It is different from absorption, in which a substance diffuses into a liquid or solid to form a solution. The term sorption encompasses both processes, while desorption is the reverse process.

Adsorption is present in many natural physical, biological, and chemical systems, and is widely used in industrial applications such as activated charcoal, synthetic resins, and water purification. Adsorption, ion exchange, and chromatography are sorption processes in which certain adsorbates are selectively transferred from the fluid phase to the surface of insoluble, rigid particles suspended in a vessel or packed in a column.

Similar to surface tension, adsorption is a consequence of surface energy. In a bulk material, all the bonding requirements (be they ionic, covalent, or metallic) of the constituent atoms of the material are filled by other atoms in the material. However, atoms on the surface of the adsorbent are not wholly surrounded by other adsorbent atoms and therefore can attract adsorbates. The exact nature of the bonding depends on the details of the species involved, but the adsorption process is generally classified as physisorption (characteristic of weak van der Waals forces) or chemisorption (characteristic of covalent bonding).

### **5.1. Isotherms:**

Adsorption is usually described through isotherms, that is, the amount of adsorbate on the adsorbent as a function of its pressure (if gas) or concentration (if liquid) at constant temperature. The quantity adsorbed is nearly always normalized by the mass of the adsorbent to allow comparison of different materials.

The first mathematical fit to an isotherm was published by Freundlich and Küster (1894) and is a purely empirical formula for gaseous adsorbates,



$$\frac{x}{m} = kP^{\frac{1}{n}}$$

where  $x$  is the quantity adsorbed,  $m$  is the mass of the adsorbent,  $P$  is the pressure of adsorbate and  $k$  and  $n$  are empirical constants for each adsorbent-adsorbate pair at a given temperature. The function has an asymptotic maximum as pressure increases without bound. As the temperature increases, the constants  $k$  and  $n$  change to reflect the empirical observation that the quantity adsorbed rises more slowly and higher pressures are required to saturate the surface.

## 5.2. Adsorbent Characteristics and general requirements:

Adsorbents are used usually in the form of spherical pellets, rods, moldings, or monoliths with hydrodynamic diameters between 0.5 and 10 mm. They must have high abrasion resistance, high thermal stability and small pore diameters, which results in higher exposed surface area and hence high surface capacity for adsorption. The adsorbents must also have a distinct pore structure which enables fast transport of the gaseous vapors.

Most industrial adsorbents fall into one of three classes:

- Oxygen-containing compounds – Are typically hydrophilic and polar, including materials such as silica gel and zeolites.
- Carbon-based compounds – Are typically hydrophobic and non-polar, including materials such as activated carbon and graphite.
- Polymer-based compounds - Are polar or non-polar functional groups in a porous polymer matrix.

## 5.3. Langmuir Adsorption Isotherm:

The Langmuir equation or Langmuir isotherm or Langmuir adsorption equation relates the coverage or adsorption of molecules on a solid surface to gas pressure or concentration of a medium above the solid surface at a fixed temperature. The equation was developed by Irving Langmuir in 1916 [1]. The equation is stated as:

$$\theta = \frac{\alpha \cdot P}{1 + \alpha \cdot P}$$

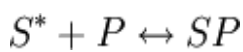
$\theta$  or theta is the fractional coverage of the surface,  $P$  is the gas pressure or concentration,  $\alpha$  (alpha) is a constant.

The constant  $\alpha$  is the Langmuir adsorption constant and increases with an increase in the binding energy of adsorption and with a decrease in temperature

### 5.3.1. Equation Derivation:

The equation is derived starting from the equilibrium between empty surface sites

( $S^*$ ), particles ( $P$ ) and filled particle sites ( $SP$ )



The Equilibrium constant  $K$  is thus given by the equation:

$$K = \frac{[SP]}{[S^*][P]}$$

Because the number of filled surface sites ( $SP$ ) is proportional to  $\theta$ , the number of unfilled sites ( $S^*$ ) is proportional to  $1-\theta$ , and the number of particles is proportional to the gas pressure or concentration ( $P$ ) the equation can be rewritten as:

$$\alpha = \frac{\theta}{(1 - \theta)P}$$

where  $\alpha$  is a constant

Rearranging this:

$$\theta = \alpha(1 - \theta)P$$

$$\theta = P\alpha - P\theta\alpha$$

$$\theta + P\theta\alpha = P\alpha$$

$$\theta(1 + P\alpha) = P\alpha$$

$$\theta = \frac{\alpha \cdot P}{1 + \alpha \cdot P}$$

Other equations relating to adsorption exist such as the Temkin equation or the Freundlich equation. The Langmuir equation (as a relationship between the

concentration of a compound adsorbing to binding sites and the fractional occupancy of the binding sites) is equivalent to the Hill equation.

### 5.3.2. Equation Fitting:

The Langmuir equation is expressed here as:

$$\Gamma = \frac{\Gamma_{max} Kc}{1 + Kc}$$

where  $K$  = Langmuir equilibrium constant,  $c$  = aqueous concentration (or gaseous partial pressure),  $\Gamma$  = amount adsorbed, and  $\Gamma_{max}$  = maximum amount adsorbed as  $c$  increases. The Langmuir equation can be fitted to data by linear regression and nonlinear regression methods. Commonly used linear regression methods are: Lineweaver-Burk, Eadie-Hofstee, Scatchard, and Langmuir.

The double reciprocal of the Langmuir equation yields the Lineweaver-Burk equation:

$$\frac{1}{\Gamma} = \frac{1}{\Gamma_{max}} + \frac{1}{\Gamma_{max} Kc}$$

A plot of  $(1/\Gamma)$  versus  $(1/c)$  yields a slope =  $1/(\Gamma_{max}K)$  and an intercept =  $1/\Gamma_{max}$ . The Lineweaver-Burk regression is very sensitive to data error and it is strongly biased toward fitting the data in the low concentration range. It was proposed in 1934. Another common linear form of the Langmuir equation is the Eadie-Hofstee equation:

$$\Gamma = \Gamma_{max} - \frac{\Gamma}{Kc}$$

A plot of  $(\Gamma)$  versus  $(\Gamma/c)$  yields a slope =  $-1/K$  and an intercept =  $\Gamma_{max}$ . The Eadie-Hofstee regression has some bias toward fitting the data in the low concentration range. It was proposed in 1942 and 1952. Another rearrangement yields the Scatchard regression:

$$\frac{\Gamma}{c} = K\Gamma_{max} - K\Gamma$$

A plot of  $(\Gamma/c)$  versus  $(\Gamma)$  yields a slope =  $-K$  and an intercept =  $K\Gamma_{max}$ . The Scatchard regression is biased toward fitting the data in the high concentration

range. It was proposed in 1949. The last linear regression commonly used is the Langmuir linear regression proposed by Langmuir himself in 1918:

$$\frac{c}{\Gamma} = \frac{c}{\Gamma_{max}} + \frac{1}{K\Gamma_{max}}$$

A plot of (c/Γ) versus (c) yields a slope = 1/Γ<sub>max</sub> and an intercept = 1/(KΓ<sub>max</sub>). This regression is often erroneously called the Hanes-Woolf regression.

#### 5.4. Freundlich equation:

The Freundlich equation or Freundlich adsorption isotherm is an adsorption isotherm, which is a curve relating the concentration of a solute on the surface of an adsorbent, to the concentration of the solute in the liquid with which it is in contact. There are basically two well established types of adsorption isotherm: the Freundlich adsorption isotherm and the Langmuir adsorption isotherm

##### 5.4.1. Freundlich adsorption isotherm:

The Freundlich Adsorption Isotherm is mathematically expressed as

$$x/m = Kp^{1/n}$$

or

$$x/m = Kc^{1/n}$$

where

x = mass of adsorbate

m = mass of adsorbent

p = Equilibrium pressure of adsorbate

c = Equilibrium concentration of adsorbate in solution.

K and 1/n are constants for a given adsorbate and adsorbent at a particular temperature.

#### 5.5. A survey on different methods of adsorption:

Albanis et al. [2] showed the adsorption and removal of commercial dyes by using fly ash mixtures with a sandy clay loam soil of low organic matter content. They have got by adsorption batch experiments in soil mixture with 20% fly ash

content were up to 53% for acid yellow 7, 44.9% for acid yellow 23, 99.2% for direct yellow 28, 96.8% for basic yellow 28 and 88.5% for disperse blue 79.

Azharul et al. [3] showed the multiple response optimization for the removal of organophosphorus pesticide quinalphos [QP: *O,O*-diethyl *O*-2-quinoxalinylyl phosphorothioate] from the aqueous solution onto low-cost material and tried to overcome the drawbacks of univariate optimization. Used tea leaves were used as low-cost adsorbent and batch equilibration method was followed for this study. A Box–Behnken design was used to develop response model and desirability function was then used for simultaneous optimization of all affecting parameters in order to achieve the highest removal% of quinalphos. The optimum conditions of factors predicted for quinalphos removal% were found to be: pH 8.83, concentration  $7 \text{ mg L}^{-1}$  and dose 0.40 g. Under these conditions, maximum removal% of quinalphos was obtained 96.31%. Considering the above optimum conditions, the adsorption isotherms were developed and provided adsorption capacity of  $196.07 \text{ } \mu\text{g g}^{-1}$  by using Langmuir equation, indicating that used tea leaves may be applied as a low-cost material for pesticides removal from aqueous matrices

Heavy metal contamination of waters and soils is particularly dangerous to the living organisms. Different studies have demonstrated that hydroxyapatite has a high removal capacity for divalent heavy metal ions in contaminated waters and soils. The removal of Cd from aqueous solutions by hydroxyapatite was investigated by A. Corami et al. [4] in batch conditions at  $25 \pm 2^\circ\text{C}$ . Cadmium was applied both as single or multi-metal (Cd + Pb + Zn + Cu) systems with initial concentrations from 0 to  $8 \text{ mmol L}^{-1}$ . The adsorption capacity of hydroxyapatite in single-metal system ranged from 0.058 to  $1.681 \text{ mmol of Cd/g of hydroxyapatite}$ . In the multi-metal system competitive metal sorption reduced the removal capacity by 63-83% compared to the single-metal system. The sorption of Cd by hydroxyapatite follows the Langmuir model. Cadmium immobilization occurs through a two-step mechanism: rapid surface complexation followed by partial dissolution of hydroxyapatite and ion exchange with Ca resulting in the formation of a cadmium-containing hydroxyapatite.

B. Nouredine et al. [5] has been undertaken to evaluate the adsorption in batch mode of a disperse dye (Disperse Blue SBL) by poorly crystalline hydroxyapatite synthesized by coprecipitation between  $\text{Ca}(\text{NO}_3)_2$  and  $(\text{NH}_4)_2\text{HPO}_4$  reagents in aqueous solution at room temperature. The adsorption experiments were carried out to investigate the factors that influence the dye uptake by the adsorbent, such as the contact time under agitation, adsorbent dosage, initial dye concentration, solution temperature, and pH. The experimental results show that the percentage of dye removal increases with increasing the amount of adsorbent, until the total discoloration. The adsorption isotherms follow the model of Langmuir with a high adsorption capacity. The adsorption was pH and temperature dependent.

Batch adsorption experiments were conducted by A. Bahdod et al. [6] to investigate the removal of phenol from wastewater by addition of three apatites (porous hydroxyapatite (PHAp) and crystalline hydroxyl- (HAp) and fluoroapatite (FAP)). The best performances were obtained with porous hydroxyapatite PHAp, which presented higher adsorption capacities (experimental:  $8.2 \text{ mg g}^{-1}$ , calculated  $9.2 \text{ mg g}^{-1}$ ) than HAp and FAp ( $3\text{-}4 \text{ mg g}^{-1}$ ). Different models of adsorption were used to describe the kinetics data, to calculate corresponding rate constants and to predict the theoretical capacities of apatite surfaces for phenol adsorption. A mechanism of phenol adsorption associating chemisorption and physisorption processes is presented allowing the discussion of the variations in adsorption behavior between these materials in terms of specific surface area and chemical composition. These data suggest that apatites are promising materials for phenol sorption.

Ronghai Zhu et al. [7] showed the removal of cadmium ions from aqueous solutions by synthetic hydroxyapatite ( $\text{Ca}_{10}(\text{PO}_4)_6(\text{OH})_2$ , HAP) with different morphologies was conducted in batch conditions. The influence of different sorption parameters, such as equilibration time, initial concentration of metal ion, the amount of HAP, pH value of solution and the specific surface area on the sorption amount of  $\text{Cd}^{2+}$  were studied and discussed. Experimental results are in agreement with pseudo-second-order kinetic equation. The Freundlich and Langmuir adsorption isotherms, often used to describe the sorption of solutes from a liquid phase, can be

applied to this experimental results. The Langmuir adsorption isotherm constant corresponding to adsorption capacity,  $X_m$ , was found to be 260.42 mg/g. The sorption amount of  $Cd^{2+}$  increased as the pH value enhanced from 5 to 8. The ion-exchange mechanism and surface complex mechanism may both exist in the adsorption process. Nearly linear dependence between  $Cd^{2+}$  sorption amount and specific surface area within a certain range has been confirmed.  $Cd^{2+}$  desorption amount decreased with the increasing pH value of the extracting solution.

## **6. MATERIALS AND METHODS**



## 6.1. Reagents and solutions:

All experiments were performed with analytical reagent grade chemicals and solvents. HCl and NaOH used for zeta-potential, purchased from Fluka. Direct yellow 27 [C.I. =10190-68-8, molecular formula =  $C_{25}H_{20}N_4Na_2O_9S_3$ , Molecular weight= 662.62,  $\lambda_{max} = 398$  nm], used for adsorption reaction got form Sigma-Aldrich. All solutions prepared using distilled water from a borosilicate auto still (Jencons Ltd).

## 6.2. Choice of dye:

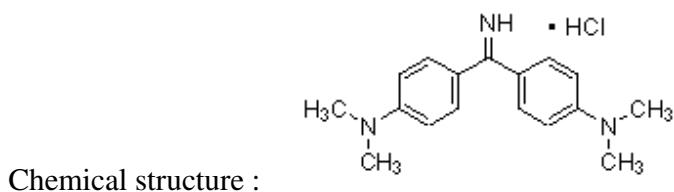
In the present study, we used five dyes in our adsorption experiment. The general information of these dyes are given below:

### 1. Auramine O

Molecular formula :  $C_{17}H_{21}N_3-HCl$

Molecular weight : 303.83

$\lambda_{max}$  : 432 nm

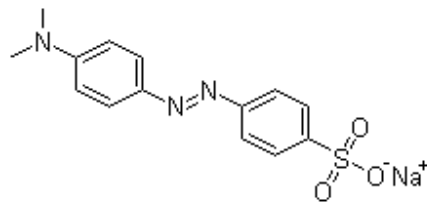


### 2. Methyl orange

Molecular formula:  $C_{14}H_{14}N_3NaO_3S$

Molecular weight: 327.33

$\lambda_{\text{max}}$  : 464 nm



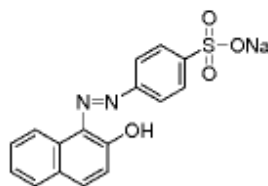
Chemical structure:

### 3. Acid orange 7

Molecular structure: C<sub>16</sub>H<sub>11</sub>N<sub>2</sub>NaO<sub>4</sub>S

Molecular weight: 350.32

$\lambda_{\text{max}}$  : 480 nm



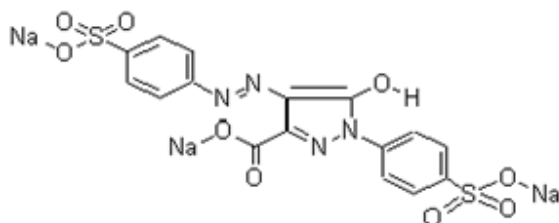
Chemical structure:

### 4. Acid yellow 23

Molecular structure: C<sub>26</sub>H<sub>29</sub>N<sub>3</sub>O<sub>2</sub>

Molecular weight: 415.53

$\lambda_{\text{max}}$  : 434 nm



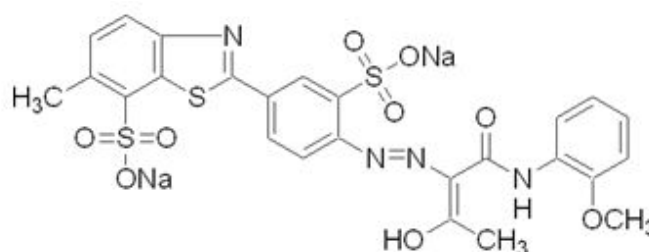
Chemical structure:

## 5. Direct yellow 27

Molecular formula:  $C_{25}H_{20}N_4Na_2O_9S_3$

Molecular weight: 662.62

$\lambda_{max}$  : 398 nm



Chemical structure:

But our synthesized materials can not remove the first 4 dyes from aqueous solution and these materials can remove only direct yellow 27 dye from aqueous solution. Some reasons that are involved not to have adsorption on these dyes are to be considered, the size of the dye, anionic or cationic character of dye, presence of functional groups etc. To find out the exact reason, it needs to work with more dyes with different groups and have broad research on it. As we worked only for five dyes so it is difficult to say the exact reason and we wish to continue this work with more dyes for our further research to find out a suitable reason on this matter. Therefore, we choose direct yellow 27 for our present adsorption study.

### 6.3. Choice of adsorbent:

In our present study, we synthesized mainly four samples of octacalcium phosphate (TH0, TH2, TH4 and TH6) and hydroxyapatite (HA). In order to choose an appropriate adsorbent we prepared 20 mg/L of 25 mL dye solution of direct yellow 27

and put 0.1 g of all the synthesized powder in it. Then shaken in a orbital shaker (rotator drive STR4 UK) with a constant speed of 10 (40 circle/min) for three hours, in order to reach equilibrium concentration.

Moreover, we have found the following dye removal percentage for our samples:

Sample	% Removal
TH0	79%
TH2	83%
TH4	80%
TH6	81%
HA	92%

As we can see that comparing all these materials, hydroxyapatite showed the highest dye removal percentage and the synthesis of all these materials had the same method and same reagents, which does not effect the synthesis cost. Comparing all these criteria, we choose hydroxyapatite as our adsorbent.

#### 6.4. Adsorption experiments:

The dye used in the present study, direct yellow 27 purchased from Sigma-Aldrich (CAS 10190-68-8). Some general information of direct yellow 27 is illustrated in table 6.4 and chemical structure in figure 6.4.

**Table 6.4:** General information of direct yellow 27

Direct yellow 27	
CAS number	10190-68-8
Molecular formula	C <sub>25</sub> H <sub>20</sub> N <sub>4</sub> Na <sub>2</sub> O <sub>9</sub> S <sub>3</sub>
Molecular weight	662.62
$\lambda_{max}$	398 nm

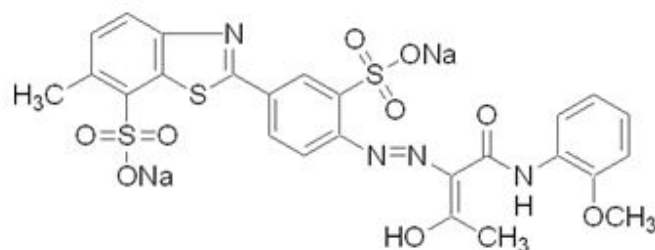


**Figure 6.4:** Chemical structure of direct yellow 27

An exact weighed quantity of dye was taken in a 500 ml flask and filled it with double distilled water until the mark, in order to make the stock solution of 500 mg/L (500 ppm). The dye solution is shaken well to dissolve completely and create a homogeneous solution. The stock solution was stored in dark place at room temperature.

All batch adsorption experiments were performed at room temperature and for this a fixed amount of HA adsorbent (0.025- 0.3g) was placed in a 50ml polypropylene centrifuge tube containing 25.0 ml of dye solution (20-60 mg/L) at pH ranging from 3.5 to 11.5. Then, the test tubes were shaken in a rotary orbital shaker (rotator drive STR4, UK) at 10 (40 circle/min) for three hours, in order to reach equilibrium concentration. At the end of the shaking, the samples were centrifuged at 4200 rpm for 5 min and the supernatant was collected and dye concentration were determined by using a UV-visible spectrophotometer (Jasco,V-530, Japan). The percentage removal of dye and amount adsorbed by the selected adsorbent was calculated by the following equation:

$$\text{Removal \%} = 100X \frac{(C_0 - C_e)}{C_0} \quad (1)$$

$$\text{Removal capacity (q}_e\text{)} = \frac{C_0 - C_e \cdot V}{m} \quad (2)$$

Where,  $q_e$  is the amount of dye up taken by the adsorbent (mg/g);  $C_0$ , the initial dye concentration (mg/L);  $C_e$ , the equilibrium concentration (mg/L);  $m$ , the mass of adsorbent (g) and  $V$  is the volume (L) of solution used for adsorption.

## 7. Results and discussion:

### 7.1. Zeta potential measurement:

To control the pH of the aqueous solution is an important parameter for adsorption process. In the present study Zeta-Meter System 3.0, New York, is used to determine the  $H^+$  and  $OH^-$  ion concentration at different pH. In aqueous solution the surface charge is positive (+) and negative (-) and zeta potential is the sum of all charges. When the

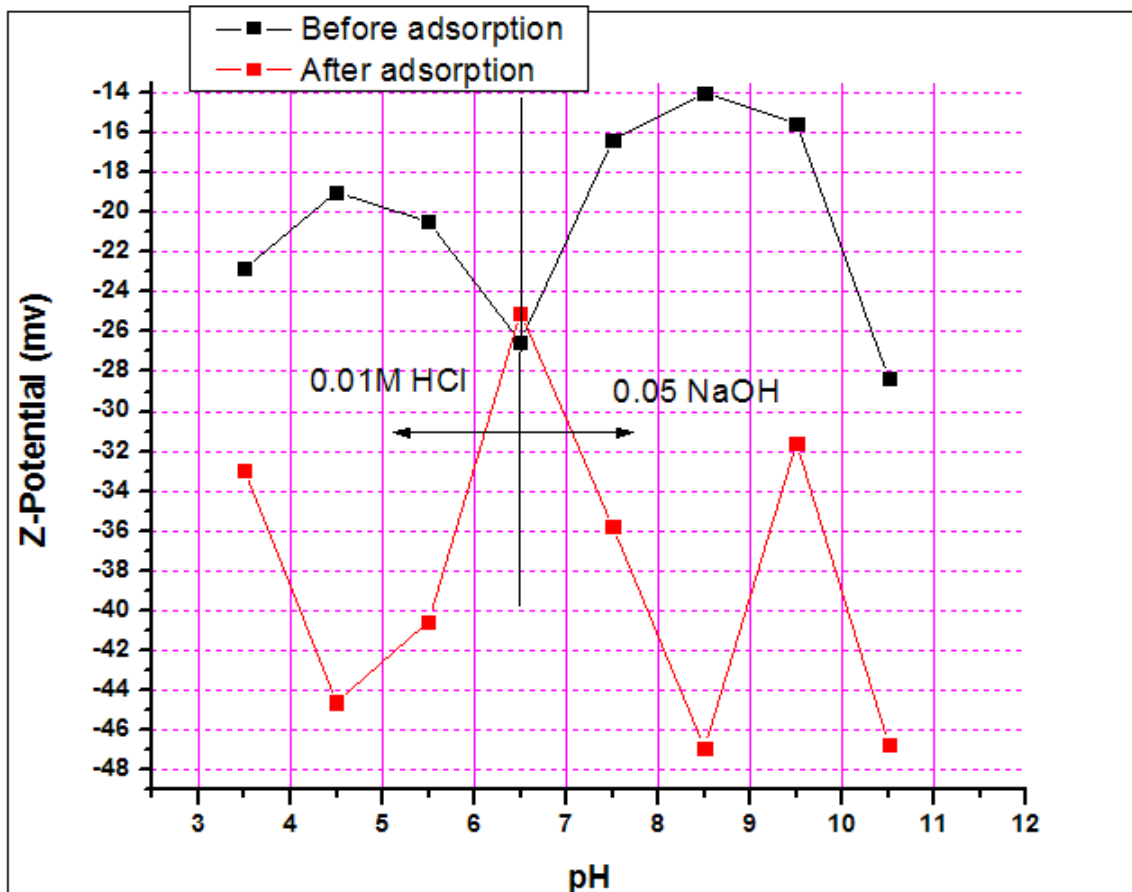
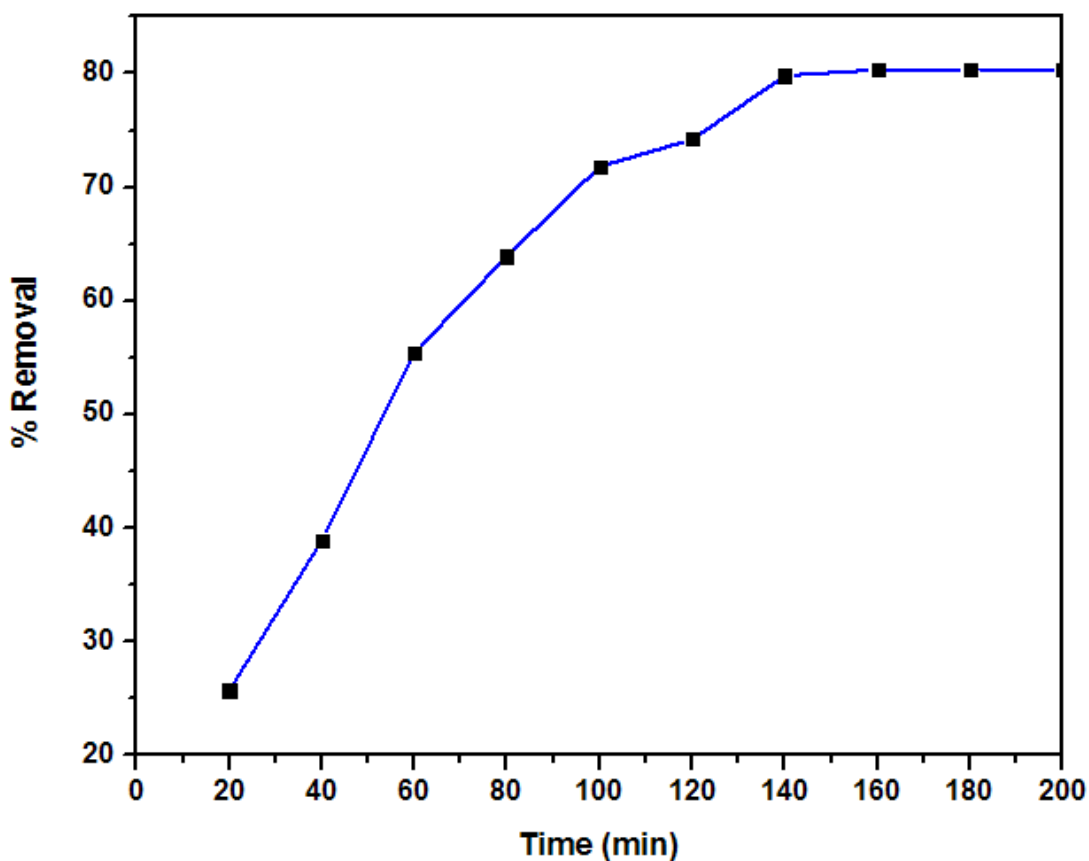


Figure 7.1: Zeta potential of adsorbent before and after adsorption.

positive and negative charges are same in solution, the sum is zero, which indicates the point of zero charge. To determine the point of zero charge of adsorbent in aqueous solution, pH parameter is used 3.5, 4.5, 5.5, 6.5, 7.5, 8.5, 9.5 and 10.5. It is not possible to use pH less than 3.5 as the adsorbent is dissolve in that value of pH.  $\text{KNO}_3$  is used as reference electrolyte, because  $\text{KNO}_3$  does not shift the zero point. In aqueous solution,  $\text{K}^+$  and  $\text{NO}_3^-$  ions come from  $\text{KNO}_3$ , which has no role to determine any surface potential. Figure 7.1 shows the pH vs Z-potential curve of adsorbent before and after adsorption. It is indicating that, there is no point of zero charge detected for the adsorbent, as all the values of zeta potential is negative. In addition, after adsorption the values of zeta potential increase rapidly.



**Figure 7.2:** Effect of contact time on removal of direct yellow 27 by hydroxyapatite (adsorbent amount 0.2g, solution concentration 40 mg/L, pH 6.5).

### 7.2. Effect of contact time:

The effect of contact time on the adsorption of direct yellow 27 is shown in Fig. 7.2. The removal percentage of dye increased with increase in contact time. During the adsorption of first 100 minutes, the color removal is fast and it was 71%. After that, the removal percentage was very slow and until 180 minute, it was 80% and reached equilibrium. At the beginning of the adsorption, large surface area of the adsorbent is vacant to have fast adsorption. After increasing time, the dye molecules are adsorbed by the adsorbent and are saturated with dye ions, which results the slowing down of the adsorption and reached equilibrium.

### 7.3. Effect of concentration:

The adsorption process is carried out at different initial dye concentration of 20, 30, 40, 50 and 60 mg/L. In figure 7.3 it is shown that at lower initial concentration dye removal percentage is high, almost 58%. However, after increase

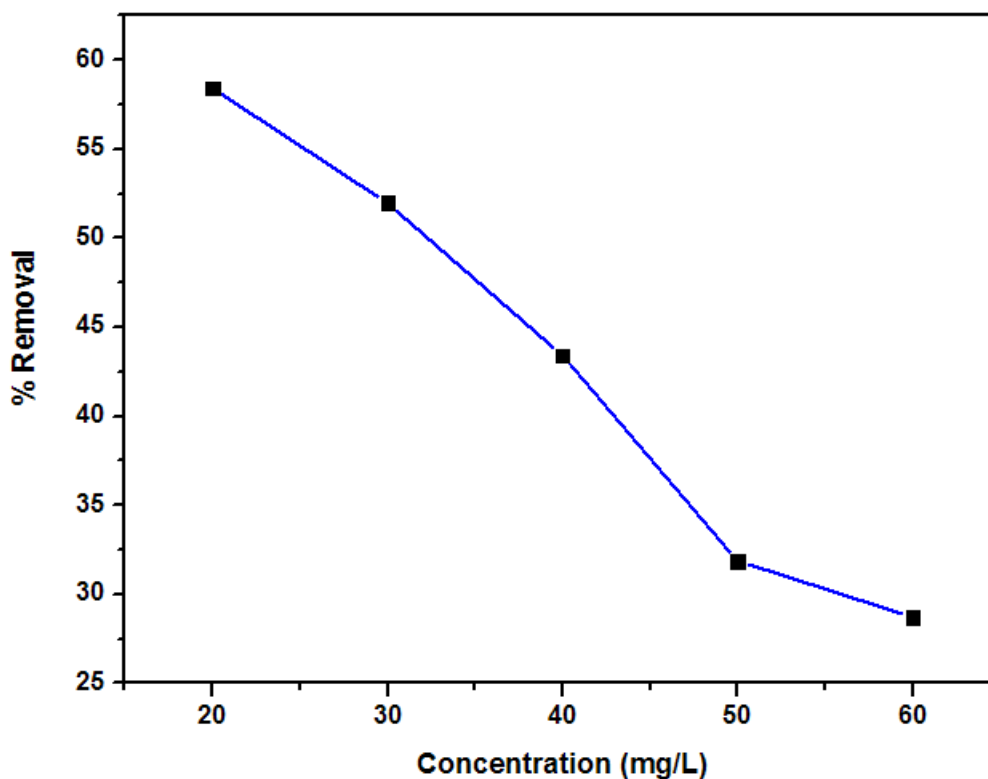


Figure 7.3: Effect of concentration (adsorbent amount 0.1g, solution pH 6.5).



the dye concentration under the same condition of pH and adsorbent amount, the color removal percentage of dye decrease to 28% for 60 mg/L of dye solution. It means that the adsorption process is highly dependent on initial concentration of dye. It is because of at lower concentration, the ratio of the initial number of dye molecules to the available surface area is low and subsequently the fractional adsorption becomes independent of initial concentration [8]. However, at higher concentration the available sites of adsorption becomes fewer and hence the percentage removal of dye is dependent upon initial concentration.

#### **7.4. Effect of adsorbent amount:**

The percentage of direct yellow 27 removal with varying amounts of hydroxyapatite is presented in figure 7.4. The amount of adsorbent used in the present study is 0.025, 0.05, 0.1, 0.2 and 0.3 gm. These amounts were used for 25 ml of dye solution with five different concentrations of 20, 30, 40, 50 and 60 mg/L. From figure 7.4, it is very clear that the dye removal percentage increased rapidly with the increasing of adsorbent dosage until the certain limit. An increase in the adsorption with the adsorbent dosage can attributed to a greater surface area and the availability of more adsorption capacity. It is observed that, for the adsorbent dosages of 0.025, 0.05, 0.1 and 0.2 gm of amount, the dye removal percentage increased for all concentrations of dye solution. Further more increase the amount of adsorbent, which is 0.3 gm, the dye removal percentage suddenly start to decrease. This is due to the large amount of adsorbent effectively reduces the unsaturation of the per unit mass, resulting in the great reduction of per unit mass adsorption at higher adsorbent amount [9]. Table 7.4 showed the adsorbent amount effect and removal percentage of dye for different dye concentrations.

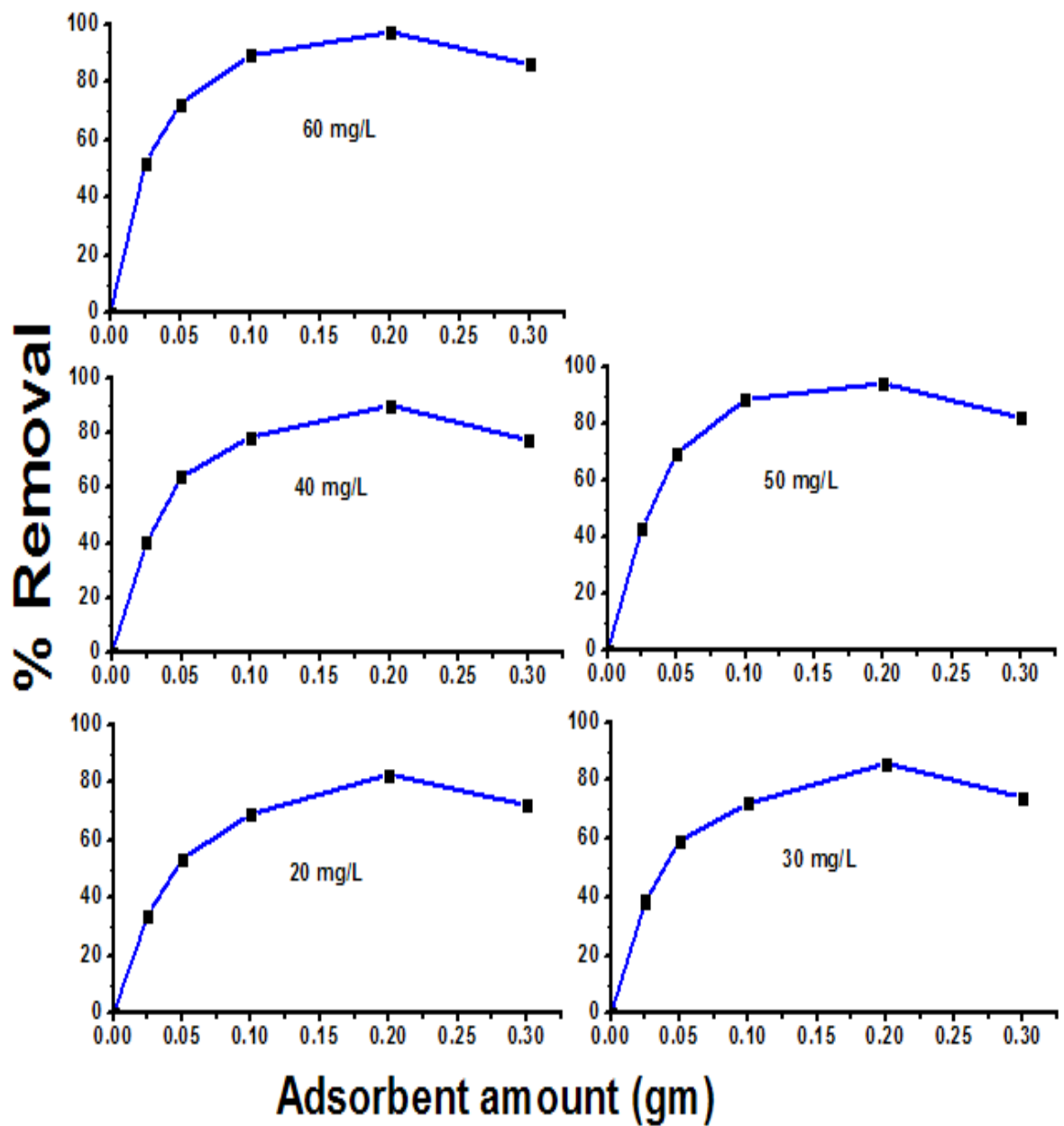


Figure 7.4: Effect of adsorbent amount (solution pH 5.5).

**Table 7.4:** The adsorbent amount effect and removal percentage of dye for different dye concentrations.

Dye concentration (mg/L)	Adsorbent dosage (gm)				
	0.025	0.05	0.1	0.2	0.3
20	34%	53%	68%	82%	72%
30	38%	59%	72%	85%	74%
40	40%	63%	78%	89%	77%
50	43%	69%	88%	94%	82%
60	52%	72%	89%	97%	86%

### 7.5. Effect of pH:

The pH of the aqueous solution is an important parameter in the adsorption process. Before describing the pH effect on adsorption mechanism, it is necessary to determine the point of zero charge ( $pH_0$ ) of the adsorbent. Adsorption of cations favored at pH higher than  $pH_0$ , while the adsorption of anions is favored at pH lower than  $pH_0$ . Both adsorbate and adsorbent may have functional groups, which are affected by the concentration of hydrogen ( $H^+$ ) and hydroxyl ( $OH^-$ ) ions that are involved in the adsorption process. In the present study it has been already showed that the highest zeta potential values of the adsorbent is detected at pH 6.5 and all zeta potential values were negative. The variation in the adsorption of dye was studied in pH ranged 3.5 to 11.5, with the regular pH difference of 1 and the results are shown in figure 7.5. The FTIR analysis revealed that the main active functional groups on hydroxyapatite surface were of alcohol groups ( $OH^-$ ) and mostly phosphate groups ( $PO_4^{3-}$ ). In aqueous solution phosphate exist four forms: at strong pH as aqueous

phosphoric acid ( $\text{H}_3\text{PO}_4$ ), at weak pH as dihydrogen phosphate ion ( $\text{H}_2\text{PO}_4^-$ ), at weak alkaline condition as hydrogen phosphate ion ( $\text{HPO}_4^{2-}$ ) and at strong alkaline condition

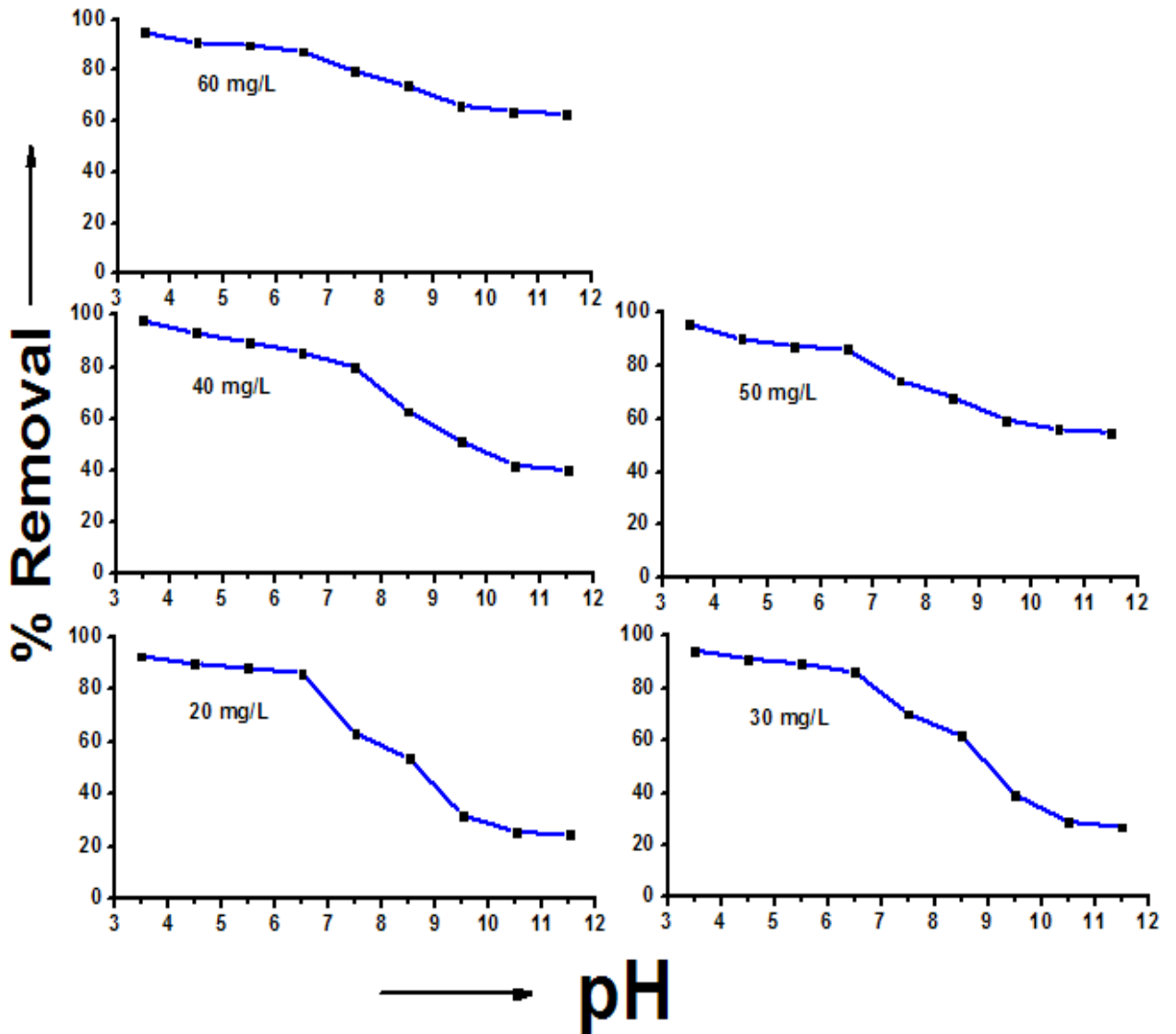


**Figure 7.5:** Effect of dye solution pH on removal percentage of dye (amount of adsorbent is 0.2g).

as phosphate ion ( $\text{PO}_4^{3-}$ ). As other direct dye, direct yellow 27 is an anionic dye chemically composed of sulfonated organic azo compounds which give sodium salts of sulfonic acids in aqueous solution [10]. At lower pH, and the association of dye anions with the less negative charged sites of the adsorbent could easily take place, thereby increasing the adsorption amount. On the other hand, at higher pH (basic pH), above mentioned active phosphate groups on the adsorbent surface become anionic in nature and not suitable for the adsorption of negatively charged dye (anionic) due to inter ionic repulsion between similar charged particle. Thus, the extent of dye adsorption on the surface of hydroxyapatite at basic pH is low. Therefore, the maximum adsorption observed at low pH that is pH 3.5 and. after increase the solution pH from 3.5 to 6.5, the percentage of solution decreases slowly from 92% to 86% for 20 mg/L dye concentration. Further increase of pH values from 6.5 until 11.5, adsorption removal decreases rapidly from 86% to 24% for the same concentration of dye solution.

#### 7.6. Kinetic study:

The Lagergren pseudo first order model can be represented by following the Eq. (3)

$$\log(q_e - q_t) = \log(q_e) - \frac{K_1 t}{2.303} \quad (3)$$

The pseudo second order can be expressed as

$$\frac{t}{q_t} = \frac{1}{K_2 q_e^2} + \frac{1}{q_e} t \quad (4)$$

where  $q_e$  the amount of dye adsorbed onto hydroxyapatite at equilibrium ( $\text{mg g}^{-1}$ ) and  $q_t$  is the amount ( $\text{mg g}^{-1}$ ) of dye adsorbed at any time  $t$  (min) and  $K_1$  and  $K_2$  are the rate constants of pseudo first order and second order model respectively.

Studied two kinetics models were developed by constructing linear plot of  $\log (q_e - q_t)$  vs.  $t$  for pseudo first order and  $t/q_t$  vs.  $t$  for pseudo second order model for initial concentration of 20mg/L. The rate constants  $K_1$ ,  $K_2$  measured from the slopes of corresponding linear plots. According to the regression coefficient ( $R^2$ ), the adsorption of direct yellow 27 on hydroxyapatite is best described by the pseudo second order kinetic model ( $R^2=0.982$ ) (Fig. 7.6(b)) than pseudo first order kinetic model ( $R^2=0.320$ ) (Fig. 7.6(a)). Besides, the calculated  $q_e$  (amount of dye adsorbed onto hydroxyapatite) values ( $q_e=2.041$  mg/g) for pseudo second order kinetic model is similar to experimental  $q_e$  value ( $q_e=2.002$  mg/g), indicating the best fitted model than pseudo first order model ( $q_e$  calculated=1.167,  $q_e$  experimental=2.002). These results indicated that the adsorption rate of direct yellow 27 dye depends on the concentration of dye at the adsorbent surface and the absorbance of these absorbed at equilibrium solution [11].

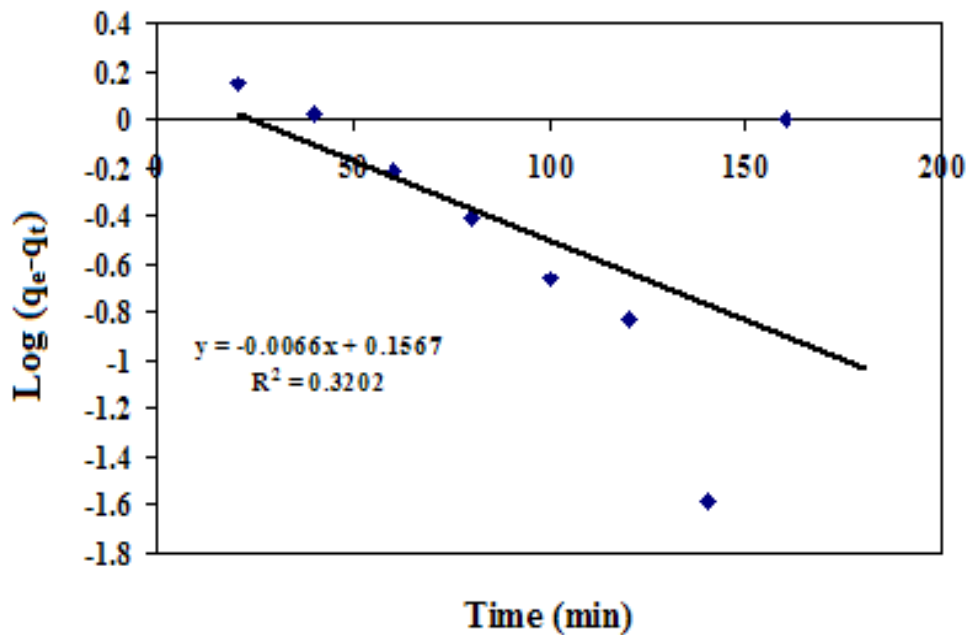


**Figure 7.6 (a):** First-order kinetics of adsorption process for direct yellow 27 dye (adsorbent amount 0.2g, solution concentration 40 mg/L, pH 6.5).

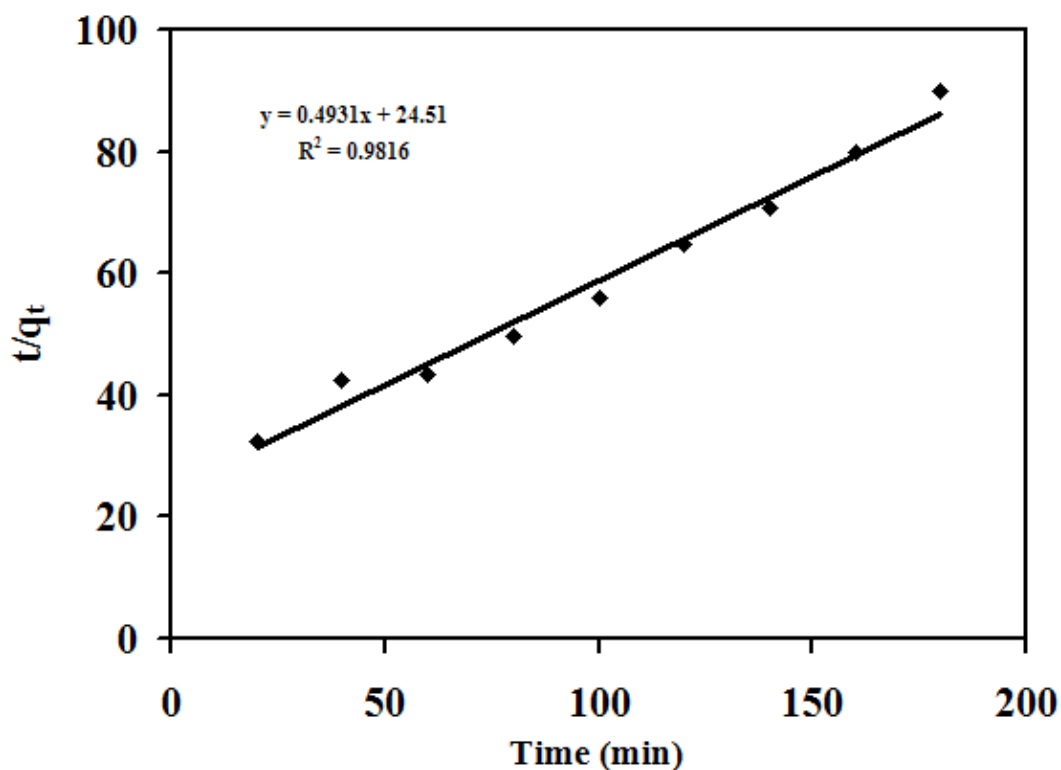


**Figure 7.6 (b):** Second-order kinetics of adsorption process for direct yellow 27 dye (adsorbent amount 0.2g, solution concentration 40 mg/L, pH 6.5).

### 7.7. Adsorption isotherms:

The adsorption equilibrium isotherm is important for describing how the adsorbate molecules distribute between the liquid and the solid phases when the adsorption process reaches an equilibrium state. Several isotherm equations are available for this purpose. The Langmuir [1] and Freundlich [112] models are commonly used to describe the adsorption isotherm, and their constants afford significant parameters for predicting adsorption capacities. The application of Langmuir isotherm suggests that the adsorption takes place at specific homogeneous sites within the adsorbent. Whereas, the Freundlich isotherm model assuming a heterogeneous surface in the adsorbent. The adsorption data of the dye is correlated with Freundlich and Langmuir models, which are represented by the following equations:

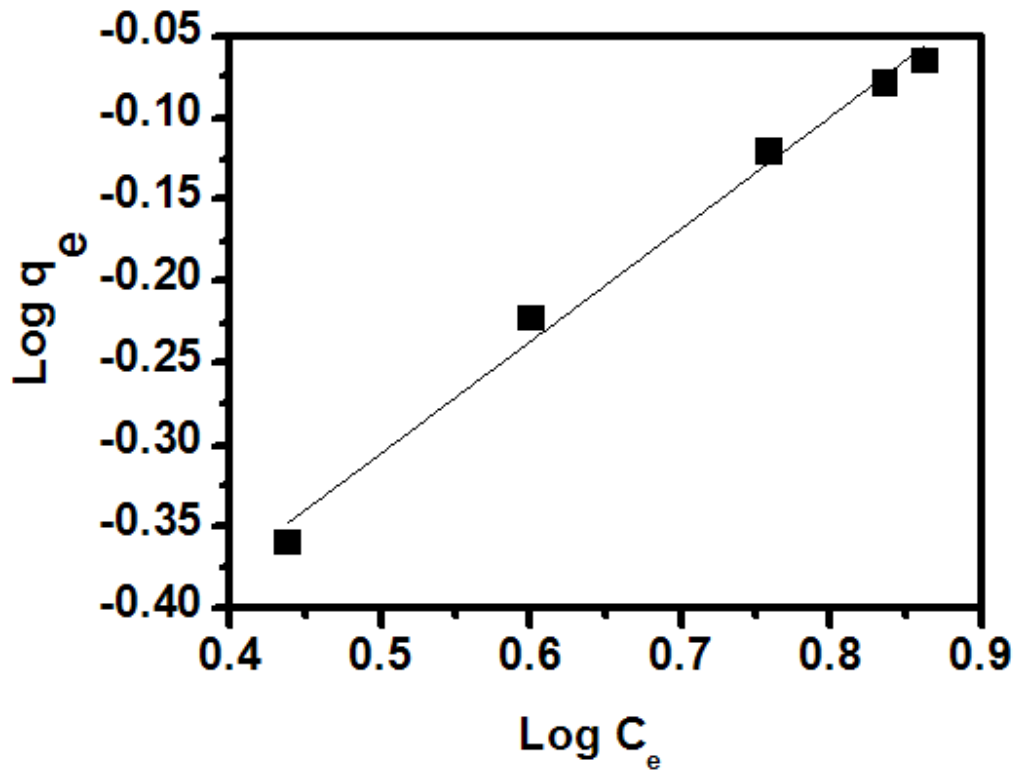


**Figure 7.7 (a):** Linear fit of experimental data obtained using Freundlich isotherm model (adsorbent amount is 0.2g and solution pH 6.5).

**Table 7.7:** The adsorption parameters of Freundlich and Langmuir model

Freundlich		Langmuir			
$K_F$	$1/n$	$R^2$	$q_m$ (mg g <sup>-1</sup> )	$K_a$ (l mg <sup>-1</sup> )	$R^2$
0.522	0.678	0.992	89.286	0.009	0.995



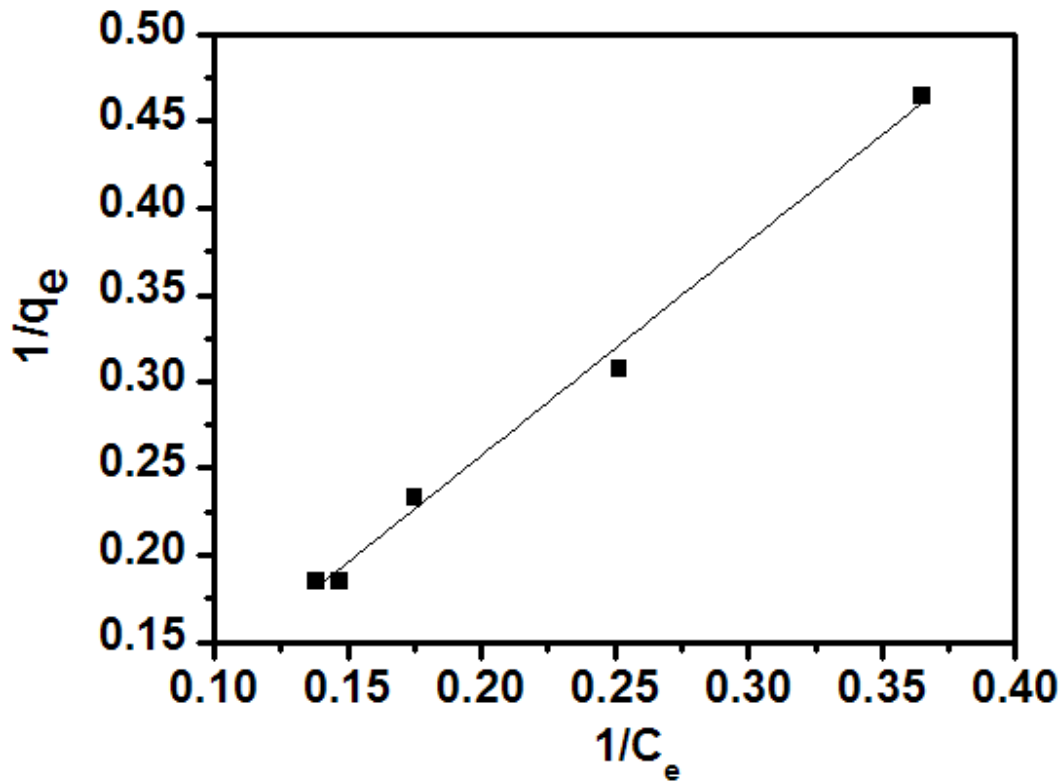


**Figure 7.7 (b):** Linear fit of experimental data obtained using Langmuir isotherm model (adsorbent amount is 0.2g and solution pH 6.5).

Freundlich isotherm:

$$q_e = K_F C_e^{1/n} \quad (5)$$

Langmuir isotherm:

$$q_e = \frac{q_m K_a C_e}{1 + K_a C_e} \quad (6)$$

All the adsorption isotherms were constructed for used hydroxyapatite using the linearized Freundlich (Eq.5) and Langmuir (Eq.6) isotherm equation by plotting  $\log(q_e)$  versus  $\log(C_e)$  and  $1/q_e$  versus  $1/C_e$ , respectively. From equation 5,

$$\log q_e = \log(K_F) + \frac{1}{n} \log(C_e) \quad (7)$$

$$\frac{1}{q_e} = \left( \frac{1}{K_a q_m} \right) \frac{1}{C_e} + \frac{1}{q_m} \quad (8)$$

where,  $q_e$  is the adsorbed amount ( $\text{mg g}^{-1}$ ),  $C_e$  is equilibrium concentration ( $\text{mg L}^{-1}$ ),  $K_F$  is the Freundlich coefficient that represents the degree or strength of adsorption.  $1/n$  is an exponential coefficient that reflects the curvature in the isotherm.  $q_m$  ( $\text{mg g}^{-1}$ ) is the maximum adsorption capacity of the adsorbent;  $K_a$  is the Langmuir's constant. A list of the obtained parameters together with  $R^2$  values are provided in Table 7.7. As seen, the equilibrium data is accommodated well by the Langmuir model (Fig.7.7 (b)), with high correlation coefficient than Freundlich model (Fig.7.7 (a)). Such coefficient indicate that the monolayer coverage of the adsorbate (dye) at outer surface of the adsorbent (hydroxyapatite) particles, and with maximum adsorption capacity of 89.29mg/g.

### **7.8. Conclusion:**

The present study showed that hydroxyapatite is an effective adsorbent for the removal of direct yellow 27 dye. The adsorption experiments were carried out to investigate the factors that influence the dye uptake by the adsorbent, such as adsorbent dosage and effect of pH. The experimental results showed that the percentage of dye removed increase with increasing adsorbent dosage, increase with increasing contact time, decrease with increasing initial dye concentration and decrease with increasing dye solution pH. The adsorption equilibrium was attained within 300 min. Kinetics data followed the pseudo second order model. The adsorption data followed the Langmuir model better than the Freundlich model and the adsorption equilibrium was describe well by the Langmuir isotherm model with maximum adsorption capacity 89.28 mg/g. Finally, we can say that, the utilization of hydroxyapatite as adsorbent for removal of direct yellow 27 dye is expected to be economical due to less production cost needed.

## References:

- [1] I. Langmuir, The constitution and fundamental properties of solids and liquids. part i. solids. J. Am. Chem. Soc. 38 (1916) 2221-95.
- [2] T.A. Albanis, D.G. Hela, T.M. Sakellarides and T.G. Danis, Removal of dyes from aqueous solutions by adsorption on mixtures of fly ash and soil in batch and column techniques. Global Nest: the int. J. 2(3) (2000) 237-244.
- [3] M. A. Islam, V. Sakkas, T. A. Albanis, Application of statistical design of experiment with desirability function for the removal of organophosphorus pesticide from aqueous solution by low-cost material, 170 (2009) 230-238.
- [4] A. Corami, S. Mignardi, V. Ferrini, Cadmium removal from single- and multi-metal (Cd + Pb + Zn + Cu) solutions by sorption on hydroxyapatite, J. Colloidal Interface Sci. 317 (2008) 402-408.
- [5] B. Nouredine, Q. Samir, A. Ali, N. Abederrahmarr, A. Yhya, Adsorption of disperse blue SBL dye by synthesized poorly crystalline hydroxyapatite, Journal of Environmental Science, 20 (2008) 1268-1272.
- [6] A. Bahdod, S. El Asri, A. Saoiabi, T. Coradin, A. Laghzizil, Adsorption of phenol from an aqueous solution by selected apatite adsorbents: Kinetic process and impact of the surface properties, Water Research, 43 (2009) 313-318.
- [7] R. Zhu, R. Yu, Jianxi Yao, D. Mao, C. Xing, D. Wang, Removal of Cd<sup>2+</sup> from aqueous solutions by hydroxyapatite, Catalysis Today, 139 (2008) 94-99.
- [8] V.V. Basava Rao, S. Ram Mohan Rao, Adsorption studies on treatment of textile dyeing industrial effluent by flyash, Chem. Eng. J. 116 (2006) 77-84.
- [9] K.G.Bhattacharyya, S.S. Gupta, Adsorptive accumulation of Cd(II), Co(II), Cu(II), Pb(II), and Ni(II) from water on montmorillonite: Influence of acid activation, . Colloid Interf. Sci. 310 (2007) 411.

- [10] C.P. Kaushik, Ravinder Tuteja, Namrata Kaushik, J.K. Sharma. Minimization of organic chemical load in direct dyes effluent using low cost adsorbents, Chem. Eng. J. (2009), doi:10.1016/j.cej.2009.07.042.
- [11] S. L. Sun, A. Q. Wang, Adsorption kinetics of Cu(II) ions using N,O-carboxymethyl-chitosan. J. Hazard. Mater. 131 (1–3) (2006) 103– 111.
- [12] H. Freundlich, Uber die adsorption in losungen. Z. Phys. Chem. 57 (1906) 385–470.